Spatial and temporal variations in the geometry and composition of the Permian Whitehill Formation South Africa

By: Mr Kenneth Chukwuma

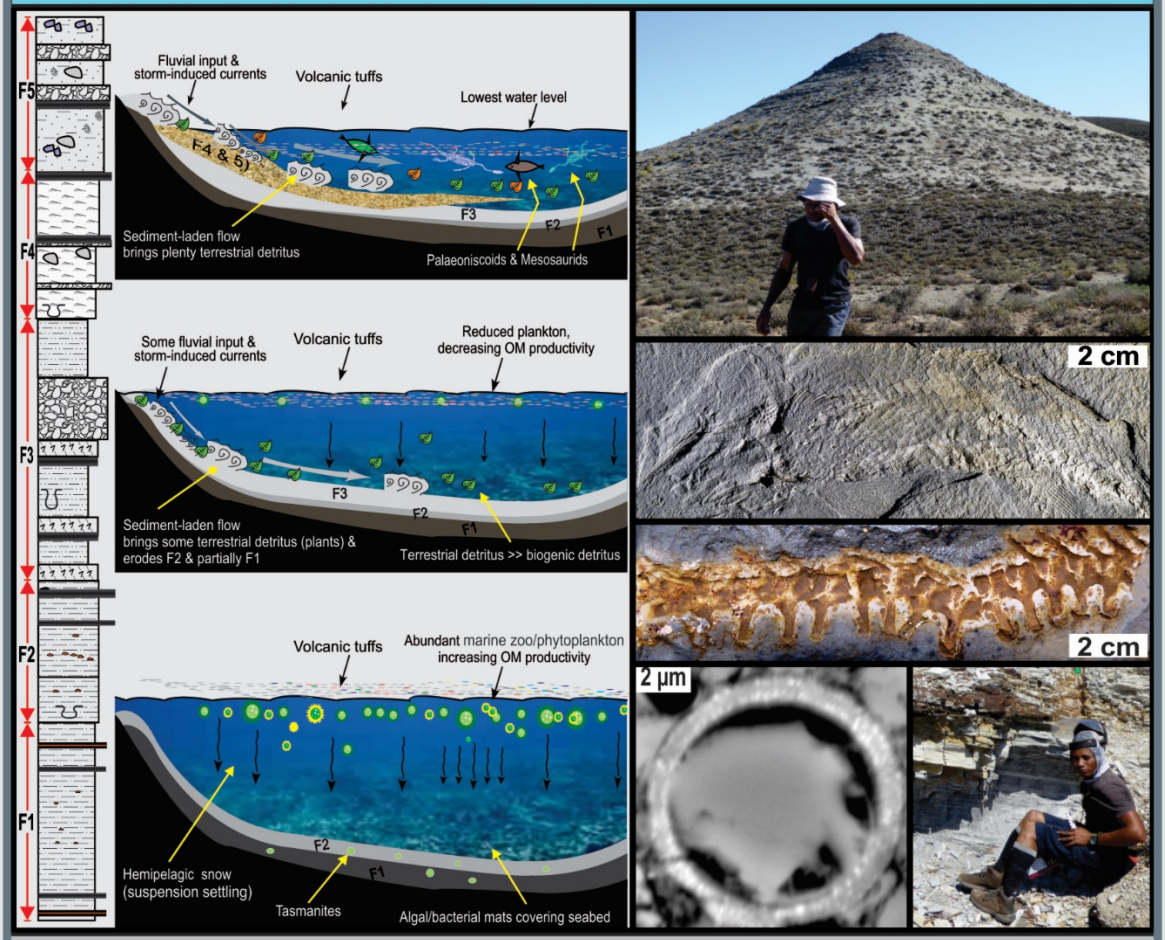

Supervisor: Dr E.M. Bordy

Thesis presented for the degree of
Doctor of Philosophy in Geology
in the Department of Geological Sciences
at the University of Cape Town

March, 2017

SPATIAL AND TEMPORAL VARIATIONS IN THE GEOMETRY AND COMPOSITION OF THE PERMIAN WHITEHILL FORMATION, SOUTH AFRICA

Kenneth Chukwuma

Thesis presented for the degree of
Doctor of Philosophy
in the Department of Geological Science
at the University of Cape Town

March, 2017

Plagiarism Declaration

"This thesis/dissertation has been submitted to the Turnitin module (or equivalent similarity and originality checking software) and I confirm that my supervisor has seen my report and any concerns revealed by such have been resolved with my supervisor."

Name: Chukwuma Kenneth

Student number: Chkken003

Signature: Signed by candidate

Signature removed

Date: 13/03/17

Acknowledgements

To be able to study for a PhD, although quite a task, is a privilege. In my case, the task was made much easier by my supervisor, Dr Emese M. Bordy. Apart from the unique way she introduced me to the wonderful world of shale, her support, guidance, encouragement and patience are out of this world.

I also wish to thank the following institutions and individuals without whose help this study would not have been possible. This study was primarily funded by the University of Cape Town's Science Faculty PhD Fellowship. The Society for Sedimentary Geology (SEPM), the International Association of Sedimentologists (IAS) and the Local Organizing Committee for the 35th International Geological Congress (35IGC) are heartily acknowledged for the student' travel grants availed to me.

A special word of thanks goes to my colleagues and friends at the University of Cape Town Sedimentary Geology and Paleontology Research Group (SGPRG-UCT) for all their support and assistance. I am sincerely grateful to Francisco Paiva, Sanda Spelman, and Claire Geel, for field assistance.

I am grateful to the staff at the Department of Geological Sciences. Prof Chris Harris Chris was very helpful in separating carbonates. My numerous discussions with Prof John Compton clarified some concepts and provided insights. Mention is also made of Dr Phil Janney for his assistance with stoichiometry, Dr Beth Kahle for system access and chairing various student's associations, Nicholas Laidler for lab assistance, David Wilson for thin section preparation, John Harrison for field logistics, and Denise Lesch for admin. Dr Takalani Theka of UCT Chemistry Department is also acknowledged for assistance with solvent extraction and Russel Williams (UCT Interlibrary) for resource supplies. Thank you to you all.

A special tribute goes to numerous Karoo farmers for allowing me to access the outcrops in their farms and for their traditional Afrikaans hospitality during my fieldwork, and to André Coetzee in particular for the base camp he provided.

A word of thanks also goes Dr Doug Cole (South African Council for Geoscience) for the well logs he provided and for our numerous discussions on this project. I am also grateful to Prof

Maarten de Wit (Nelson Mandela Metropolitan University, Port Elizabeth) for insightful discussions.

I also wish to convey my gratitude to Prof Asiwaju-Bello (HOD Geology, FUTA-Nigeria), Prof Anselm Igbafe (my Ms supervisor, now at Afe-Babalola University, Nigeria), Engr Emmanuel Nnebocha (West African Pumping Services, London), Tony Obioru (Chevron, Lagos), Chief Chris Odiete (Md, Shutman Nigeria Ltd), Hon. Eric Ebozele (MD, Glatrico Oil Services, Texas) and my friends, Maliphathwe Ndyoko and Julius Okiror for all their supports.

A final word of thanks goes to my family for boundless love.

Abstract

The Lower Permian Whitehill Formation (WHF) is an important hydrocarbon resource unit in the main Karoo Basin where it occurs in outcrops and up to 4 400 m in the subsurface and thus it is distributed over an area in excess of 260 000 km^2 in the southern half of South Africa. Although the formation is composed predominantly of black laminated carbonaceous shales, earlier studies detected significant spatiotemporal variability in its stratigraphy and composition, particularly the distribution of its organic carbon content across the basin. Because these stratigraphic variations and compositional heterogeneities remained largely uninvestigated, there are conflicting interpretations of not only the hydrocarbon potential of this resource unit but also the paleoenvironmental conditions that prevailed in the Karoo Basin during its accumulation. Following the recent global proliferation of unconventional hydrocarbon resources originating in organic-rich shale successions, the WHF is seriously being considered for gas shale exploitation in South Africa. Consequently, re-characterizing and explaining the spatiotemporal variations in its geometry and composition would be invaluable to the energy industry as well as the larger scientific community. With this aim, this study applied a combination of field descriptions, vintage borehole data, micro- to nano-scale petrographic observations, and multiple geochemical data so that a more critical understanding of the sedimentological controls responsible for the variability can be established.

Using this integrated approach, five primary sedimentary facies (F1-F5, i.e., stratigraphic subunits in the WHF) were identified, which show specific and systematic variations in nature and content of organic carbon, stable isotopic composition (of $\delta^{13}C_{org}$ and $\delta^{15}N$), C/N ratio, major and trace elemental enrichment, nature and content of iron sulfides, quartz texture, and CIA across the basin. The lower dark grey to black thinly laminated pyritic, carbonaceous fine shales (facies F1 and F2) contain up to 16.5 % TOC, $\delta^{13}C_{org}$ of -15.57‰, $\delta^{15}N$ of 12.49‰, C/N ratio of 1.50, average CIA of 68.11, Rb/K ($x10^{-3}$) and Sr/Ba ratios of 6.56 and 0.67, respectively. Relative to average shale, this unit is up to 6.27 and 3.11 times richer in Mo and Fe, respectively. The organic materials in this facies comprise Tasmanites cysts, colonial algae cells, and amorphous macerals and occur in well-defined laminae (lamalginites) as well as in discrete organic domains loosely associated with mineral grains (organo-minerallic aggregates). At least 25% of the silicate in this facies is of early

diagenetic origin, possibly derived from alteration of air-fall volcanic ash. Iron sulfides occur dominantly in form of framboidal aggregates of pyrite. Marcasite in form of lags cement and nodules is also reported. A binary mixture of organic matter and phosphorites with botryoidal textures is also abundant. The upper medium to light grey calcareous-siliceous silty lenticular shale (F3-F5) contain up to 2.04% TOC, $\delta^{13}C_{org}$ of -24.71‰, $\delta^{15}N$ of 4.93‰, C/N ratio of 17.62, average CIA of 74.33, Rb/K ($x10^{-3}$) and Sr/Ba ratios of 3.83 and 0.36, respectively. Relative to average shale, this unit was up to 2.65 and 0.43 times richer in Mo and Fe, respectively. Their organic macerals comprise disarticulated plant remains in disseminations with few amorphous macerals. At least 85% of the quartz content is of detrital origin likely sourced from the basin margins and transported to the basin by the action of bottom-hugging currents. Few iron sulfides occur dominantly in form of octa- and euhedral pyrite grains.

The data presented in this thesis suggest that the lower WHF (subunits F1 and F2) may have accumulated in a marine setting with high bioproductivity of organic carbon delivered in form of flocculated organo-minerallic aggregates (pelagic snow) onto an anoxic seabed overlain by dysoxic to oxic waters. Reduced terrigenous input, presence of phosphorites, increasing CIA and increasing $\delta^{13}C_{org}$ values with higher TOC point to a depositional setting that resulted from an interplay of sea-level highstand and climatic warm-ups. In contrast, the upper WHF (subunits F3-F5) was deposited largely under non-marine conditions with OM in the company of great detrital debris sourced from terrestrial settings, transported into the basin mainly in form of fluid mud flows and deposited above storm wave base. The presence various body and trace fossils, as well as the variations in bioturbation styles and intensities in subunits F3-F5, indicate that colonisation of the basin by invertebrate and vertebrate organisms is related to the different stages in the oxygenation of the sediment-water interface in an increasingly oxygenated setting.

Table of Contents

Final word count: 52,737

List of figures

List of Tables

Chapter 2: Spatiotemporal sedimentary facies variations in the Permian Whitehill Formation, main Karoo Basin

Chapter 3: Spatiotemporal geochemical variations and distribution of organic Carbon contents in the Permian Whitehill Formation of South Africa

Chapter 4: Evolution of porosity and pore geometry in the Permian Whitehill Formation Of South Africa – a FE-SEM image analysis study

List of equations

Chapter 3: Spatiotemporal geochemical variations and distribution of organic Carbon contents in the Permian Whitehill Formation of South Africa

List of appendices

Chapter 3: Spatiotemporal geochemical variations and distribution of organic Carbon contents in the Permian Whitehill Formation of South Africa

Chapter 1

Introduction and thesis outline

1.1. Introduction

Sedimentary rocks with dominant grain size up to 62.5 μm (1/16 mm) are collectively referred to as mudstones (sensu Lazar et al., 2015). Shales are laminated, fissile mudstones (Aplin et al., 1999). Because fissility can also develop with increased weathering, differentiating weathered mudstones from shales is often fraught with uncertainty (e.g., Wedepohl, 1971; Stow, 1981; Blatt, 1982; Macquaker and Gawthorpe, 1993; Macquaker and Adams, 2003; Aplin and Macquaker, 2010). In this work, the term shale is used in general sense to refer to mudstones with both primary or secondary fissility, whereas the term 'black shales' is used here to refer to those organic-rich shales that contain more than 0.5% total organic carbon (e.g., Tissot and Welte, 1984; Huyck, 1990) . Shales constitute approximately two-thirds of the Earth's sedimentary rock volume and had been deposited throughout the Earth's geological history in both terrestrial and marine environments (e.g., Ingram, 1953; Shepard, 1954; Tourtelot, 1960; Picard, 1971; Pettijohn et al., 1973; Blatt et al., 1980; Potter et al., 1980, 2005; Lundergard and Samuels, 1980; Macquaker and Adams, 2003; Aplin and Macquaker, 2010; Lazar et al., 2015). Therefore, shale-dominated successions can provide unparalleled insights into changes of Earth's surface in the geological past, as well on key controlling factors, which include climate changes, lateral and vertical movements of tectonic plates, and sea-level changes (e.g., Schieber and Zimmerle, 1998; Wright and Friedrichs, 2006; Hovikoski et al., 2008; Walsh and Nittrouer, 2009). As the depositories of the largest amounts of organic carbon, shales have been the source of more than 90% of global recoverable hydrocarbon (oil and gas) reserves and key reservoirs for unconventional hydrocarbon resources (Tissot and Welte, 1984; Klemme and Ulmisheck, 1991; Schieber, 1999, 2001; Durham, 2008). They may also act as natural barriers for the movement of fluids and gases in the Earth's

crust, and are relied upon as storage solutions for artificial carbon, and nuclear as well as other industrial waste (e.g., Fetter, 1994; Arnould, 2006; Blümling et al. 2007).

Because of their geological and economic importance, the study of shales had an early and encouraging beginnings (e.g., Sorby, 1908; Folk, 1951, 1962; Carozzi, 1960; Milner, 1962; Picard, 1971; Schiber and Zimmerle, 1998), however these were hampered by the challenges associated with the study of this sedimentary rock type (Potter et al., 1980, 2005; Schieber and Zimmerle, 1998; Bohacs, 1998; Wignall et al., 2005). The most obvious challenge to the study of shales is the very small size of their component grains, which makes discrimination of individual particles impossible, not only in hand specimen but even with a standard petrographic microscope (e.g., Folk 1980; Schieber and Zimmerle 1998; Macquaker and Adams, 2003). Therefore the study of these fine-grained sedimentary rocks lagged behind those of sandstones and carbonates, the positive outcomes that come from their analysis notwithstanding. However, the advent of field emission scanning electron microscope (FE-SEM; e.g., O'Brien and Slatt, 1990; Camp et al., 2013) and its auxiliary technology, particularly focused ion-beam milling (FIB; e.g., Loucks et al., 2009, 2012; Bernard et al., 2013; Schieber, 2013; Löhr et al., 2015), has largely overcome the problems associated with particle resolution and identification in shales. This development, which roughly coincided with the global proliferation of unconventional hydrocarbon resources originating in organic-rich shale successions, have resulted in a renewed interest in shale successions.

In the last two decades, a record number of studies focused on the sedimentology of shales (e.g., Schieber et al., 1998, 2000; Bohacs, 1998; Wignall and Newton, 1998; Werne et al., 2002; Sageman et al., 2003; Rimmer, 2004; Meyers and Bernasconi, 2006; Zonneveld et al., 2010; Ghadeer and Macquaker, 2012; Milliken et al., 2013; Lazar et al., 2015). These studies, which usually involved the integration of various sets of physical, chemical and biological observations, have shown that there are multiple pathways to the formation of shales, apart from continuous deposition of mud under quiet and low energy conditions as previously thought. In addition, multidisciplinary approach to study of shales unraveled a remarkable range of compositional and textural heterogeneity in shale successions, even in those that were previously described as "homogenous and isotropic", thus fulfilling Picard's 1971 (p. 179) prediction "In the future, '15 feet of gray shale' will no longer be an acceptable description of possibly a million years of

history". Variability in shale composition and texture, which result from a range of depositional, biologic, and diagenetic processes, occur in scales ranging from nanometer to decameter to kilometre. Understanding the sedimentological controls responsible for heterogeneities in shales is not only the key to the successful exploitation of their resource but is also a major pointer to environmental conditions prevalent during their deposition.

1.2. Research rationale

The Lower Permian Whitehill Formation (WHF) is a famous rock unit in the main Karoo Basin that occurs in outcrops and up to 4 400 m in the subsurface and thus it is distributed over an area in excess of 260 000 km^2 in the southern half of South Africa (e.g., Rogers and Schwarz, 1900; Schwarz, 1903; Rogers and Du Toit, 1909; McLachlan and Anderson, 1973; Anderson and McLachlan, 1979; SACS, 1980; Visser, 1990, 1992; Cole and Basson, 1991; Cole and McLachlan, 1991, 1994; Johnson et al., 2006). The formation has been the subject of several geological inquiries that date back to 1864 primarily because of its high organic carbon content, unique fossil assemblage, and landscape forming, white-weathering black shale (Rogers and Schwarz, 1900; Schwarz, 1903, 1912; Du Toit, 1927, 1937, 1954; Russel, 1939; Oelofsen, 1981; Cole and McLachlan, 1991, 1994; Visser, 1992; Faure and Cole, 1999; Geel et al., 2015). However, despite its long history of investigations, this rock unit remains poorly known from various geological aspects (e.g., Visser, 1992; Faure and Cole, 1999). For instance, whereas the formation is generally considered to formed largely from continuous deposition of carbonaceous mud into an essentially stratified, anoxic basin, such view is at odd with the abundance of erosion-related features, widespread presence of bioturbation (e.g. Oelofsen, 1981) and significant increase in silt to fine-sand grade materials present in some intervals in the northeastern basin margin (e.g., Cole and McLachlan, 1991, 1994; Visser, 1992). The type of environment under which the shale was deposited remains a subject of an active debate (e.g., Faure and Cole, 1999 vs Scheffler et al., 2006), with most workers suggesting a predominantly marine environment (e.g., Teichert, 1974; Kensley, 1975; McLachlan and Anderson, 1977; Anderson and McLachlan, 1979; Oelofsen, 1981, 1987; Oelofsen and Araujo, 1987; Christie, 1990; Visser, 1992, 1994; Scheffler et al., 2006), and others proposing a non-marine, homogenous, brackish to freshwater body with microbial shielded floor (e.g., Cole and McLachlan, 1991; Veevers et al., 1994; Pickford, 1995; Faure and Cole, 1999). The notable variations in its geometry (e.g., thinning from southwest to northeast; Cole and

McLachlan, 1991; Johnson et al., 2006) as well as the uneven distribution of organic carbon contents (e.g., Schwarz, 1903; Rogers and Du Toit, 1909; Cunningham-Craig, 1914; Du Toit, 1937; Botha, 1940; Potgieter, 1974; Rowsell and De Swardt, 1976; Cole, 1978; Anderson and McLachlan, 1979; Cole and McLachlan, 1991; 1994; Geel et al., 2015) both laterally across the basin and vertically within stratigraphic intervals are largely unquantified and unexplained. The syn- vs. post-depositional controls (e.g., structural deformation and metamorphism) on the distribution of organic carbon content in the WHF on a basinal scale are also lacking, with the exception of a few localities that were recently studied (e.g. Geel et al., 2015; Smithard et al., 2015) and need additional research. Moreover, the recent global proliferation of unconventional hydrocarbon resources originating in organic-rich shale successions has resulted in a renewed interest in the WHF, which is seriously being considered for gas shale exploitation in South Africa. Consequently, further insights into the origin of the rock constituents and the modifications these constituents went through following deposition are valuable not only for the scientific community but also for the energy industry.

1.3. Research aim and objectives

The aim of this research is to document, quantify, and explain the spatial-temporal variations in the geometry (stratigraphy) and internal composition (geochemistry) of the Lower Permian WHF in the main Karoo Basin using a combination of field descriptions, vintage borehole log data, micro- to nano-scale petrographic observations, and multiple geochemical data so that the sedimentological controls on the spatiotemporal variability of the WHF can be established. Specifically, this study aims to: a) document the spatial and temporal variations in the stratigraphy and geochemistry, particularly the nature and distribution of organic and inorganic shale constituents, of the WHF; b) investigate the mechanisms responsible for production, dispersal, and preservation of its shale constituents; and c) analyze the link between the spatiotemporal changes and the dynamics of sedimentation, particularly in a basin where depositional conditions varied from relatively deeper and anoxic during the sedimentation of the lower portion to shallower and oxygenated during the deposition of the upper and northerly portion of the formation.

In order to meet these aims the following four objectives, each of which forms a central chapter of this thesis, have been identified:

1. Capture the spatial and temporal facies variability in the WHF, particularly paying attention to the variations in grain texture (size and geometry), composition, micro- and macrofabrics, bedding styles, and bounding surfaces; and construct an overarching genetically-based stratigraphic model for the WHF.

2. Describe the provenance, mechanism of dispersal, and depositional conditions of the individual sedimentary components (organic/inorganic) of the shale and the sedimentological variables that controlled the production, dispersal and preservation of organic carbon, including the role played by clastic dilution, changing accommodation, sea-level, and climate conditions.

3. Describe and quantify the post-depositional/diagenetic changes in the primary shale constituents, particularly the developments of porosity and pore geometry, including the role played by thermal maturation (early vs late catagenesis) and other high-temperature structural deformation and metamorphism.

4. Describe the depositional environments and sources early diagenetic constituents in the shale matrix, particularly the deposition of silica in *Tasmanites* cysts and the development of fibrous chalcedony into single quartz grains.

1.4. Thesis organization

This thesis is divided into six chapters. The content of each chapter is as summarised below. The principal chapters (2-5) have been written in a format suitable for publication in ISI accredited journals, and as such the background information, methodologies, and references show some overlap in order to allow each chapter to be independent and organised for publication. This overlap is necessary for each chapter to be independent and ready to be submitted as manuscripts for publication following the examination of the thesis.

1. Chapter 1- Introduction: provides background information about shales, their importance and recent approaches used in their study. It also outlines the key aims and objectives of

this study, the outline of the thesis and the contribution of this research to general knowledge.

2. Chapter 2- is a published manuscript that is entitled “Spatiotemporal sedimentary facies variations in the Permian Whitehill Formation, main Karoo Basin”. It describes the spatial and temporal variations in the internal composition and geometry of the Whitehill Formation, including recognition and correlation of distinct shale packages and laterally extensive bounding surfaces; refines the lithostratigraphy of the WHF and proposes a unified stratigraphic framework for the WHF; c) constructs stratigraphic logs and thickness distribution map based recognition of five distinct lithofacies; d) analyses the link between spatiotemporal changes in the formation and the dynamics of sedimentation, including the predominant sediment source, transport, and depositional mechanisms in the Early Permian in the main Karoo Basin.

3. Chapter 3- Manuscript 2 is entitled: “Spatiotemporal geochemical variations and distribution of organic carbon contents in the Permian Whitehill Formation of South Africa”. It describes the spatial and temporal variations in the internal composition of the Whitehill Formation, including the nature and content of its organic and inorganic contents; b) assesses a variety of geochemical and petrographic provenance- and redox-proxies to evaluate the role played by organic carbon production and preservation and clastic dilution in accumulation of organic carbon in the WHF.

4. Chapter 4- Manuscript 3 is entitled: “Evolution of porosity and pore geometry in the Permian Whitehill Formation of South Africa- a FE-SEM image analysis study”. It assesses the outcome of processes that were active during deposition and diagenesis, including the effects of heat flow from the Cape Fold Belt on the size and geometry of pores and organic macerals.

5. Chapter 5- Manuscript 4 is entitled: “Fossil algal cysts and diagenetic quartz reveal a complex syn- and post-depositional history for the Permian carbonaceous shales of the Whitehill Formation (South Africa)”. It assesses the source, timing, and mechanisms of silica deposition in algal cysts and the implication on depositional and post-depositional conditions during the sedimentation of the WHF.

6. Chapter 6- Synthesis, conclusions, recommendations: summarises key findings of this thesis and explore potential avenues for further inquiry.

7. Appendix- This includes the details of the boreholes used in the construction of the thickness and depth distribution maps of the WHF as well as compilations of Rock-eval data from previous studies, e.g., by Rowsell and De Swardt (1976) and Cole and McLachlan (1994).

1.5. Thesis contribution

Using a combination of field descriptions, borehole logs, micro- to nanoscale petrographic observations, and multiple geochemical data, this study has, for the first time created a unified, genetically-based stratigraphic framework for the WHF. This stratigraphic model is based on combined lithologic, sedimentologic, paleontological, and geochemical data. It agrees with the earlier biostratigraphic model (e.g., Oelofsen, 1981) for the WHF. This all-encompassing model allows for more accurate delineation of the WHF as well as the correlation of distinct shale packages on a basinal scale. Previously, understanding of the vertical and lateral distribution of internal contents, particularly the distribution of organic carbon, of the WHF was limited the northern margin of the basin that has been studied by Cole and McLachlan (1991, 1994), to the localities studied during the historic post-II World War exploration of the Karoo Basin for oil in the 70's (e.g. Rowsell and De Swardt, 1976; Cole, 1978) and a handful of recent studies (e.g., Smithard et al., 2015; Geel et al., 2015).

This new study, for the first time, documents the occurrence of Tasmanites cysts in the WHF. Tasmanites cysts-a fossil algae with affinity to modern planktonic green algae-the prasinophyta-(Tappan, 1980; Schieber, 1996; Hoek et al., 1995; Telnova, 2012)-usually marks sedimentary intervals with maximum flooding due to sediment starvation (Lazar et al., 2015) in marine settings (Tappan, 1980; Baceta and Nunez-Betelu, 1994; Schieber, 1996; Telnova, 2012). The presence of Tasmanites cysts in the WHF is, thus, a strong evidence for marine incursion during the deposition of the WHF. Also, before now, it was generally argued that the absence of well-defined air-fall tuffaceous bed in the lower WHF and the presence of the same in the upper section is an indication

of variability in the level of ash concentrations in the atmosphere over the basin during the Lower Permian (e.g., Visser, 1992). This supposed variability has been interpreted as due to relative increase in volcanism in the source areas or a change to a drier and windier climate. This study demonstrates that the absence of air-fall ash beds in the lower WHF is likely the result of its dissolution and incorporation into the sediment body and not necessarily related to change in climatic conditions.

This thesis has also contributed towards a more critical understanding of the fate of organic carbon and transport and geochemical properties such as porosity and pore geometry during diagenesis and increasing thermal maturation. Specifically, this study, for the first time, demonstrated that with increasing thermal maturation, porosity and pore sizes generally show a linear increase until a threshold is reached when further increase in thermal maturation causes a dramatic infilling of earlier created pores. Precipitation of calcitic and phosphatic fibrous cement and veins created a unique form of architectural heterogeneity within the shales and an important one at that because it controls preferential flow of fluids across shale. An in-depth understanding of this shale component and its evolution is, therefore, fundamental in shale fracturing and in models that predict the response of shale to natural and induced physical and chemical changes.

The early diagenetic quartz grains reported in this study is also a novel observation. These intrabasinal quartz grains which differed markedly from their extrabasinal detrital equivalents likely represents early diagenetic silica deposition in algal cysts and other similar pore spaces and testify to an environment with bacterial sulfate reduction, reduction of iron oxides and hydroxides and increased pH. Furthermore, this observation coupled with detailed stable isotopic and elemental data have shown that the onset of the deposition of the WHF was analogous, on a reduced scale, to an oceanic anoxic event.

References

Anderson, A.M., and I.R. McLachlan, 1979, The oil-shale potential of the Early Permian White Band Formation in southern Africa, 83-89, *in*, A.M. Anderson and W.J. van Biljon, eds, Some sedimentary basin and associated ore deposits of South Africa: Special Publication of the Geological Society of South Africa, 6, 228p.

Aplin, A.C., and J.H.S Macquaker, 2010, Getting started in shales: AAAPG/Datapages, Getting Started Series, GS20.

Aplin, A.C., A.J. Fleet, and J.H.S Macquaker, 1999, Muds and mudstones: physical and fluid flow properties in mudstones at a basin scale, *in*, A. Aplin, A. Fleet,and J. Macquaker, eds, Muds and Mudstones: Physical and Fluid-Flow Properties: Geological Society of London, Special Publication, 1-7.

Arnould, M. 2006, Discontinuity networks in mudstones: a geological approach: Implications for radioactive wastes isolation in deep geological formations in Belgium, France, Switzerland: Bulletin of Engineering Geology and Environment, 65, 413-422.

Baceta, J.I., and L. Nunez-Betelu, 1994, Basics and Application of Rock- Eval/TOC Pyrolysis: an example from the uppermost Paleocene/lowermost Eocene, in, The Basque Basin, Western Pyrenees: Department of Geology and Geophysics, The University of Calgary, Ciencias Naturales-Natur Zientziak, 46, 43-62.

Bernard, S., R. Wirth, A. Schreiber, H-M., Schulz, and B. Horsfield, 2013, FIB-SEM and TEM investigation of organic-rich shale maturation series from the Lower Toarcian Posidonia Shale, Germany: Nanoscale pore system and fluid-rock interactions in Camp, W., Diaz, E., Wawak, B., eds., Electron Microscopy of Shale Hydrocarbon Reservoirs: AAPG Memoir, 102, 53-66.

Blatt, H., 1982, Sedimentary petrology: Freeman, New York, 564p.

Blatt H., G. Middleton, and R. Murray, 1980, Origin of Sedimentary Rocks: Prentice-Hall, Englewood Cliffs, 782p.

Blümling, P., F. Bernier, P. Lebon, and C. Derek Martin, 2007, The excavation-damaged zone in clay formations-time-dependent behavior and influence on performance assessment: Physics and Chemistry of the Earth, 32, 588-599.

Bohacs, K.M., 1998, Contrasting expressions of depositional sequences in mudrocks from marine to non-marine environs, *in*, J. Schieber, W. Zimmerle, and P. Sethi, eds., Shales

and Mudstones, Volume I: Basin Studies, Sedimentology, and Paleontology: Stuttgart, E. Schweizerbart'sche Verlagsbuchhandlung (Nagele u. Obermiller), 33-78.

Botha, P.R., 1940, Oil shale: Prezent Pan and Bultfontein, Boshoff district: Unpulished Rep. Geol. Surv. South Africa, 251p.

Camp, W., E. Diaz, and B. Wawak, 2013, Introduction, *in* Camp, W., Diaz, E., Wawak, B., eds., Electron Microscopy of Shale Hydrocarbon Reservoirs: AAPG Memoir, 102, ix-xi.

Carozzi, A.V., Microscopic sedimentary petrology, Wiley and Sons Inc., New York, 485p.

Christie, A.D.M., 1990, Origin, classification and utilization of oil shales in South Africa: South African Journal of Science, 86, 9-15.

Cole, D.I., 1978, Preliminary report on the oil potential of the Whitehill Formation between Strydenburg (Cape Province) and Hertzogville (Orange Free State): Report of the Geological Survey of South Africa, 1978-0304, (open file report).

Cole, D.I., and W.A. Basson, 1991, Whitehill Formation: Catalogue of South African Lithostratigraphic Units, M.R. Johnson, ed., 3, 3.51-3.52.

Cole, D.I. and McLachlan, I.R., 1991. Oil potential of the Permian WHF Shale Formation in the main Karoo Basin, South Africa. In: H. Ulbrich, and A.C. Rocha Campos, eds, Gondwana Seven Proceedings, 379-390.

Cole, D.I. and I.R. McLachlan, 1994, Oil shale potential and depositional environment of the Permian Whitehill Shale Formation in the main Karoo Basin: Open file report, Geological Survey of South Africa, 1994-0213, 1 & 2, 145p.

Cunningham-Craig, E.H., 1914, Report on the petroleum prospects in the Union of South Africa: The Government Printing and Stationery Office, Pretoria, 28p.

Demaison, G.J. and G.T. Moore, 1980, Anoxic environments and oil source bed genesis: AAPG Bulletin, 64, 1179-1209.

Durham, L., 2008, Prices, technology make shales hot: AAPG Explorer 11, 10-12.

Du Toit, A.L., 1927, A geological comparison of South America and South Africa: Publication No 381, Carnegie Institution, Washington, 158p.

Du Toit, A.L., 1937, Our wandering continents: An hypothesis of continental drifting: Oliver and Boyd, Edinburgh, 366p.

Du Toit, A.L., 1954, The geology of South Africa: 3rd Edition, S.H. Haughton, ed., Oliver and Boyd, Edinburgh, 611p.

Faure, K., and D.I. Cole, 1999, Geochemical evidence for lacustrine microbial blooms in the vast Permian main Karoo, Paraná, Falkland Islands and Huab basins of southwestern Gondwana: Palaeogeography, Palaeoclimatology, Palaeoecology, 152, 189-213.

Fetter, C. W., 1994, Applied hydrology: Macmillan, New York, 691p.

Folk, R.L., 1951, The distinction between grain size and mineral composition in sedimentary rock nomenclature: Journal of Geology, 62, 344-359.

Folk, R.L., 1962, Petrology and origin of the Silurian Rochester and McKenzie Shales, Morgan county, West Virginia, Journal of Sedimentary Petrology, 32, 539-578.

Folk, R. L., 1980, Petrology of sedimentary rocks: Hemphill Publishing Company, Austin, Texas, USA, 190p.

Geel, C., M. de Wit, P. Booth, H-M. Schulz, and B Horsfield, 2015, Palaeo-environment, diagenesis and characteristics of Permian black shales in the lower Karoo Supergroup flanking the Cape Fold Belt near Jansenville, Eastern Cape, South Africa: Implications for the shale gas potential of the Karoo Basin: South African Journal of Geology, 118, 248-274.

Ghadeer, S.G., and J.H.S. Macquaker, 2012, The role of event beds in the preservation of organic carbon in fine-grained sediments: analyses of the sedimentological processes operating during deposition of the Whitby Mudstone Formation (Toarcian, Lower Jurassic) preserved in northeast England: Marine and Petroleum Geology, 35, 309-320.

Hoek, C., D.G. Mann, and H.M. Jahns, 1995, Algae: An Introduction to Phycology: Cambridge University Press, Cambridge, 623p.

Hovikoski, J., R. Lemiski, M. Gingras, G. Pemberton, and J.A. Maceachern, 2008, Ichnology and sedimentology of a mud-dominated deltaic Coast: Upper Cretaceous Alderson Member (Lea Park Formation), Western Canada: Journal of Sedimentary Research, 78, 803-824.

Huyck, H.L.O, 1990, When is a metalliferous black shale not a black shale?, in, R.I. Grauh and H.L.O. Huyck, eds, Metalliferous black shales and related ore deposits: Proceesings, 1989 United State Working Group meeting, International Geological Correlation Program Project 254, U.S.G.S Circular, 1058, 42-56.

Ingram, R.L., 1953, Fissility in mudrocks: Geological Society of America Bulletin 65, 869-878.

Johnson, M. R., C.J. Van Vuuren, J.N.J. Visser, D.I. Cole, H. DeV Wickens, A.D.M Christie,

D.L. Roberts, and G. Brandl, 2006, Sedimentary rocks of the Karoo Supergroup, *in*, M.R. Johnson, C.R. Anhaeusser, and R.J. Thomas, eds., The Geology of South Africa: Geological Society of South Africa/Council for Geoscience, 461-499.

Kensley, B., 1975, Taxonomic status of the pygocephalomorphic crustacea from the Dwyka 'White Band' (Permo-Carboniferous) of South Africa: Annals of the South African Museum 67, 25-33.

Klemme, H.D., and G.F. Ulmisheck, 1991, Effective petroleum source rocks of the world: stratigraphic distribution and controlling factors: AAPG Bulletin, 75, 1809-1851.

Lazar, O.R., K.M. Bohacs, J. Schieber, J.H.S. Macquaker, and T.M. Demko, 2015, Mudstone Primer: Lithofacies variations, diagnostic criteria, and sedimentologic implications at lamina to bedset scale: nomenclature and description guidelines: SEPM Concepts in Sedimentology and Paleontology, 12, 198p.

Löhr, S.C., E.T. Baruch, P.A Hall, and M.J. Kennedy, 2015, Is organic pore development in gas shales influenced by primary porosity and structure of thermally immature organic matter?: Organic Geochemistry, 87, 119-132.

Loucks, R.G., R. M. Reed, S.C. Ruppel, and D.M. Jarvie, 2009, Morphology, genesis, and distribution of nanometerscale pores in mudstones of the Mississippian Barnett Shale: Journal of Sedimentary Research, 79, 848-861, doi:10.2110/jsr.2009.092.

Loucks, R.G., R.M. Reed, S.C. Ruppel, and U. Hammes, 2012, Spectrum of pore types and networks in mudrocks and a descriptive classification for matrix-related mudrock pores, AAPG Bulletin, 96, 1071-1098.

Lundergard, P.D. and N.D. Samuels, N.D., 1980, Field classification of fine-grained rocks: Journal of Sedimentary Petrology, 50, 781-786.

Macquaker, J.H.S., and R.L. Gawthorpe, 1993, Mudstone lithofacies in the Kimmeridge Clay Formation, Wessex Basin, southern England: implications for the origin and controls of distribution of mudstones. Journal of Sedimentary Petrology, 63, 1129-1143.

Macquaker, J.H.S., and A.E. Adams, 2003, Maximizing information from fine-grained sedimentary rocks: An inclusive nomenclature for Mudstones: Journal of Sedimentary Research 73, 735-744.

McLachlan, I. R., and A. Anderson, 1973, A review of the evidence for marine conditions in southern Africa during Dwyka times: Palaeontologica Africana, 15, 37-64.

McLachlan, I. R., and A. Anderson, 1977, Carbonates, "stromatolites" and tuffs in the Lower Permian White Band Formation: South African Journal of Science, 73, 92-94.

Meyers, P.A., and S.M. Bernasconi, 2006, Data report: organic carbon, total nitrogen, carbonate carbon, and carbonate oxygen isotopic compositions of Albian to Santonian black shales from Sites 1257-1261 on the Demerara Rise. In, D.C. Mosher, J. Erbacher, and M.J. Malone, eds, Proc. ODP, Sci. Results, 207, College Station, TX (Ocean Drilling Program), 1-13, doi:10.2973/ odp.proc.sr.207.106.2006.

Milliken, K.L., and R.J. Day-Stirrat, 2013, Cementation in mudrocks: brief review with examples from cratonic basin mudrocks, *in*, J.-Y. Chatellier, and D.M. Jarvie, eds., Critical Assessment of Shale Resource Plays: AAPG Memoir, 103, 133-150.

Milliken, K.L., M. Rudnicki, D.N. Awwiller, and T. Zhang, 2013, Organic matter-hosted pore system, Marcellus Formation (Devonian), Pennsylvania, AAPG Bulletin, 97, 177-200.

Milner, H.B., 1962, Sedimentary petrology, vol. 1: methods in sedimentary petrography, vol II: Principles and applications, Allen Unwin Ltd, London, 643p.

O'Brien, N.R., and R.M. Slatt, 1990, Argillaceous Rock Atlas: Springer- Verlag, New York, 141p.

Oelofsen, B.W., 1981, An anatomical and systematic study of the Family Mesosauridae (Reptilia: Proganosauria) with special reference to its associated fauna and palaeoecological environment in the WHF Sea: Unpublished PhD thesis, University of Stellenbosch, South Africa, 259p.

Oelofsen, B.W. and D.C. Araújo, 1987, Palaeoecological implications of the distribution of mesosaurid reptiles in the Permian Irati sea (Paraná Basin), South America: Rev. Bras. Geociêc., 13, 1-6.

Pettijohn, F.E., P.E. Potter, and R. Siever, 1973, Sand and Sandstones: Springer-Verlag, New York, 618p.

Picard, M.D., 1971, Classification of fine-grained sedimentary rocks: Journal of Sedimentary Petrology, 41, 179-195.

Pickford, M., 1995, Karoo Supergroup palaeontology of Namibia and brief description of a the conodont from Omingonde: Palaeontolology Africana, 32, 51-66.

Potter, P.E., J.B. Maynard, and W.A. Pryor, 1980, Sedimentology of Shale, Study Guide and Reference Source: Springer- Verlag, New York, 306p.

Potter, P.E., J.B. Maynard, and P.J. Depetris, 2005, Mud and Mudstones: Introduction and Overview: Springer-Verlag, Berlin, 297p.

Potgieter, G.J.A., 1974, The geology of an area south of Kimberley: Unpublished M.Sc. thesis, Univ. Orange Free State, 9lp.

Rimmer, S.M., 2004, Geochemical paleoredox indicators in Devonian- Mississippian black shales, Central Appalachian Basin (USA): Journal of Chemical Geology, 206, 373-391.

Rogers, A.W. and E.H.L Schwarz, 1900, Report on the survey of parts of the Clanwilliam, Van Ryn'sdorp and Calvinia Divisions: Rep. Geol. Comm. Cape Good Hope, 19-54.

Rogers, A. W. and A. L. Du Toit, 1909, An introduction to the Geology of Cape Colony: Longmans, Green and Co. New York, 491p.

Rowsell, D.M., and A.M.J. De Swart, 1976, Diagenesis in Cape and Karroo sediments, South Africa, and its bearing on their hydrocarbon potential: Transactions of the Geology Society of South Africa, 79, 81-145.

Russel, W.L., 1939, The stratigraphy of the Upper Witteberg, Dwyka, Ecca and Beaufort Formations in the Laingsburg region, Cape Province Union of South Africa: Unpubl. Rep. Geol. Surv. South Africa, 56p.

SACS (South African Committee for Stratigraphy), 1980, Stratigraphy of South Africa, Part 1, L.E. Kent, compiler: Handbook Geological Survey of South Africa, Pretoria, 8, 690p.

Sageman, B.B., Murphy, A.E., Werne, J.P., VER Straeten, C.A., Hollander, D.J., and Lyons, T.W., 2003. A tale of shales: the relative roles of production, decomposition, and dilution in the accumulation of organic-rich strata, Middle– Upper Devonian, Appalachian Basin: Chemical Geology, 195, 229-273.

Scheffler, K., D. Bühmann, and L. Schwark, 2006, Analysis of late Palaeozoic glacial to postglacial sedimentary succession in South Africa by geochemical proxies-Response to climate evolution and sedimentary environment: Palaeogeography, Palaeoclimatology, Palaeoecology, 240, 184-203.

Schieber, J., 1996, Early diagenetic silica deposition in algal cysts and spores: A source of sand in black shales?: Journal of Sedimentary Research, 66, 175-183.

Schieber, J., 1999, Distribution and deposition of mudstone facies in the Upper Devonian Sonyea Group of New York: Journal of Sedimentary Research, 69, 909-925.

Schieber, J., 2013, SEM Observations on ion-milled samples of Devonian Black Shales from

Indiana and New York: the petrographic context of multiple pore types, *in* Camp, W., Diaz, E., Wawak, B., eds., Electron Microscopy of Shale Hydrocarbon Reservoirs: AAPG Memoir, 102, pp. 153-171.

Schieber, J., and W. Zimmerle, 1998, Introduction and overview: the history and promise of shale research, in J. Schieber, W. Zimmerle, and P. Sethi, eds., Shales and Mudstones, Volume I. Basin Studies, Sedimentology, and Paleontology: Stuttgart, E. Schweizerbart'sche Verlagsbuchhandlung (Nagele u. Obermiller), 1-10.

Schieber, J, W. Zimmerle, and P. Sethi, 1998, Shales and Mudstones: Stuttgart, E. Schweizerbart'sche Verlagsbuchhandlung (Nagele u. Obermiller), 680p.

Shieber, J., D. Krinsley, and L. Riciputi, 2000, Diagenetic origin of quartz silt in mudstone and implication for silica cycling: Nature, 406, 981-985.

Schwarz, E. H. L., 1903, Geological survey of parts of Prince Albert, Willomore and Uniondale: Rep. Geol. Comm., Cape Good Hope, 72-137.

Schwarz, E. H. L., 1912, South African Geology: Blackie and Son Ltd, London, 200p.

Shepard, F.P., 1954, Nomenclature based on sand-silt-clay ratios: Journal of Sedimentary Petrology, 24, 151-158.

Smithard, T., E.M. Bordy, and D. Reid, 2015, The effect of dolerite intrusions on the hydrocarbon potential of the lower Permian WHF Formation (Karoo Supergroup) in South Africa and southern Namibia: A preliminary study: South African Journal of Geology, 118, 489-510.

Sorby, H.C., 1908, On the application of quantitative methods to the study of the structure and history of rocks: Geological Society of London, Quarterly Journal, 64, 171-232.

Stow, D.A.V., 1981, Fine-grained sediments: Terminology: Enginneering Geology, Quarterly Journal, 14, 243-244.

Tappan, H., 1980, The paleobiology of plant protists, San Francisco, W.H. Freeman and co., 1028p.

Teichert, C., 1974, Marine sedimentary environments and their faunas in Gondwana area: AAPG Memoir 23, 43-145.

Telnova, O.P., 2012, Morphology and ultrastructure of Devonian prasinophycean algae (Chlorophyta): Paleontological Journal, 46, 543-548.

Tissot, B.P., and D.H. Welte, 1984, Petroleum Formation and Occurrence: Springer-Verlag,

Berlin-Heidelberg, Germany, 699p.

Tourtelot, H.A., 1960, Origin and use of the word ‘‘shale’’: American Journal of Sciences, 258-A, 335-343.

Veevers, J.J., D.I. Cole, and E.J. Cowan, 1994, Southern Africa: Karoo Basin and Cape Fold Belt, *in*, J.J. Veevers, C. Powell, and McA, eds, Permian-Triassic Pangean Basins and Foldbelts along the Panthalassan Margin of Gondwanaland: Memoir of the Geological Society of America, 184, 223-278.

Visser, J.N.J., 1990, The age of the late Palaeozoic glacigene deposits in southern Africa: South Africa Journal of Geology, 93, 366-375.

Visser, J.N.J., 1992. Deposition of the Early to Late Permian Whitehill Formation during a sea-level highstand in a juvenile foreland basin. South African Journal of Geology, 95, 181-193.

Walsh, J.P.,and C.A. Nittrouer, 2009, Understanding fine-grained river-sediment dispersal on continental margins: Marine Geology 263, 34-45.

Wedepohl, K.H., 1971, Environmental influences on the chemical composition of shales and clays: Physics and Chemistry of the Earth, 8, 307-333.

Werne, J.P., B.B. Sageman, T.W. Lyons, and D.J. Hollander, 2002, An integrated assessment of a ‘‘type euxinic’’ deposit: evidence for multiple controls on black shale deposition in the Middle Devonian Oatka Creek formation: American Journal of Science, 302, 110-143.

Wignall, P.B., and R. Newton, 1998, Pyrite framboid diameter as a measure of oxygen deficiency in ancient mudrocks: America Journal of Science, 298, 537-552.

Wignall, P.B., R.J. Newton, and C.T.S. Little, 2005, The timing of paleoenvironmental change and cause-and-effect relationships during the Early Jurassic mass extinction in Europe: American Journal of Science, 305, 1014-1032.

Wright, L.D., and C.T. Friedrichs, 2006, Gravity-driven sediment transport on continental shelves: A status report: Continental Shelf Research 26, 2092-2107.

Zonneveld, K.A.F., G.M.J. Versteegh, S. Kasten, T.I. Eglinton, K.-C. Emeis, C. Huguet, B.P. Koch, G.J. de Lange, J.W. de Leeuw, J.J. Middelburg, G. Mollenhauer, F.G. Prahl, J. Rethemeyer, and S.G. Wakeham, 2010, Selective preservation of organic matter in marine environments: processes and impact on the sedimentary record: Biogeosciences 7, 483-511.

Chapter 2

Spatiotemporal sedimentary facies variations in the Permian Whitehill Formation, main Karoo Basin

Kenneth CHUKWUMA and Emese M. BORDY
Department of Geological Sciences, University of Cape Town, 7701, South Africa

This chapter includes a manuscript that is published as a book chapter in "Origin and evolution of the Cape Mountains and Karoo Basin'. The full reference of this publication is: "Chukwuma, K., and E.M. Bordy, 2016, Spatiotemporal sedimentary facies variations in the Permian Whitehill Formation, main Karoo Basin. In: Linol B and de Wit M (eds) Origin and Evolution of the Cape Mountains and Karoo Basin: Geo-biohistory in a terrain with shale gas resources and need for conservation, part of the series Regional Geology Reviews 8643: Springer Verlag, 101-110. DOI: 10.1007/978-3-319-40859-0_10". I am solely responsible for the collecting of the field data, writing the first draft of the manuscript, and drafting of the original figures. My co-author, which is my PhD supervisor, has helped to improve both the content and figures.

2.1. Abstract

The Lower Permian Whitehill Formation in the Karoo Basin is a potential gas shale unit in South Africa. Recharacterizing this heterogeneous formation and explaining the spatiotemporal variations in its variations in its geometry, texture, bedding features, composition and distribution of organic carbon content is necessary, because gas recovery can be strongly influenced by these characteristics of the host rock. Here, we report on these rock property variations and their sedimentological controls in light of recent advances in shale sedimentology by combining field descriptions, petrographic observations, and geochemical proxies. We distinguished five sedimentary facies (F1-F5) that suggest changes in the Lower Permian depositional conditions from overall low energy in F1 and F2, allowing pelagic snow aggregates to cover the basin floor, to higher energy in F3, F4, and F5, bringing terrestrial detritus via hyperpycnal and diluted mud flows, which possibly originated from summer melting of mountain glaciers in the Cargonian Highlands flanking the northern margin of the Karoo Basin.

Keywords: Karoo Basin, shale gas, Permian, mud depositional setting, sedimentary facies

2.2. Introduction

The Lower Permian Whitehill Formation (WHF) has attracted attention from geologists for over a century (e.g., Rogers and Du Toit, 1909; Schwarz, 1912; Cunningham-Craig, 1914)) due to the oil shale potential, abundant but low diversity fossil biota, and conspicuous white-weathering characteristics of the black, carbonaceous shale unit. Currently, renewed interest in the WHF is due to its perceived shale gas potential (e.g., Decker and Marot, 2012; Geel et al., 2013, 2015; Smithard et al., 2015). However, despite a large number of publications on its lithology (e.g., Cole and McLachlan, 1991; Visser, 1992), sedimentology (e.g., Visser, 1992), palaeontology (e.g., Oelofsen, 1981, 1987) and hydrocarbon potential (e.g., Rowsell and De Swardt, 1976; Cole and McLachlan, 1991; Geel et al., 2013; Smithard et al., 2015), the WHF remains poorly understood. For instance, while reference is often made to this black, thinly laminated, carbonaceous formation as a typical anoxic facies, no consensus exists on the palaeo-water depths (e.g., Oelofsen, 1981, p. 21, 143; Cole and McLachlan, 1991, p. 381) or salinity levels (e.g., Faure and Cole, 1999 vs, Scheffler et al., 2006). Furthermore, the widely accepted anoxic facies model requires refinement to explain why the WHF contains more siltstone and very fine-grained sandstone than 'black shale' in the northeastern part of the basin (e.g., Cole and McLachlan, 1991; Werner, 2006). Its regional geometry (e.g., thinning from SW to NE) and style of mud sedimentation (e.g., Visser, 1992; Werner, 2006) also need additional research. The distribution of organic carbon in the formation is uneven, both laterally across the basin and vertically within stratigraphic sections (Cole and McLachlan, 1991; Geel et al., 2013; Smithard et al., 2015). While some areas are enriched in organic carbon (up to 17% TOC); e.g., Cole and McLachlan, 1991), others are organic carbon-lean with less than 1% TOC. Quantifying the interplay of syn- vs. post-depositional controls (e.g., structural deformation and metamorphism) on the TOC distribution in the WHF on a basinal scale is lacking, with the exception of a few localities that were studied in recent publications (e.g., Geel et al., 2013; Smithard et al., 2015).

Recently, significant hydrocarbon reserves have been associated with 'black shale' globally. This, together with developments in horizontal drilling and multistage fracture stimulation technology have triggered an unprecedented interest in the sedimentology and stratigraphy of these 'black shales' worldwide (e.g., Bohacs et al., 2005; Macquaker et al., 2010; Lazar et al., 2015; Wilson and Schieber, 2015), and nationally in the WHF, the singular rock unit with ambient qualities for shale gas exploitation in South Africa. This study aims to: document the

variations in the internal composition and primary sedimentary features of the WHF, and analyse the link between the facies changes and the dynamics of sedimentation in time and space.

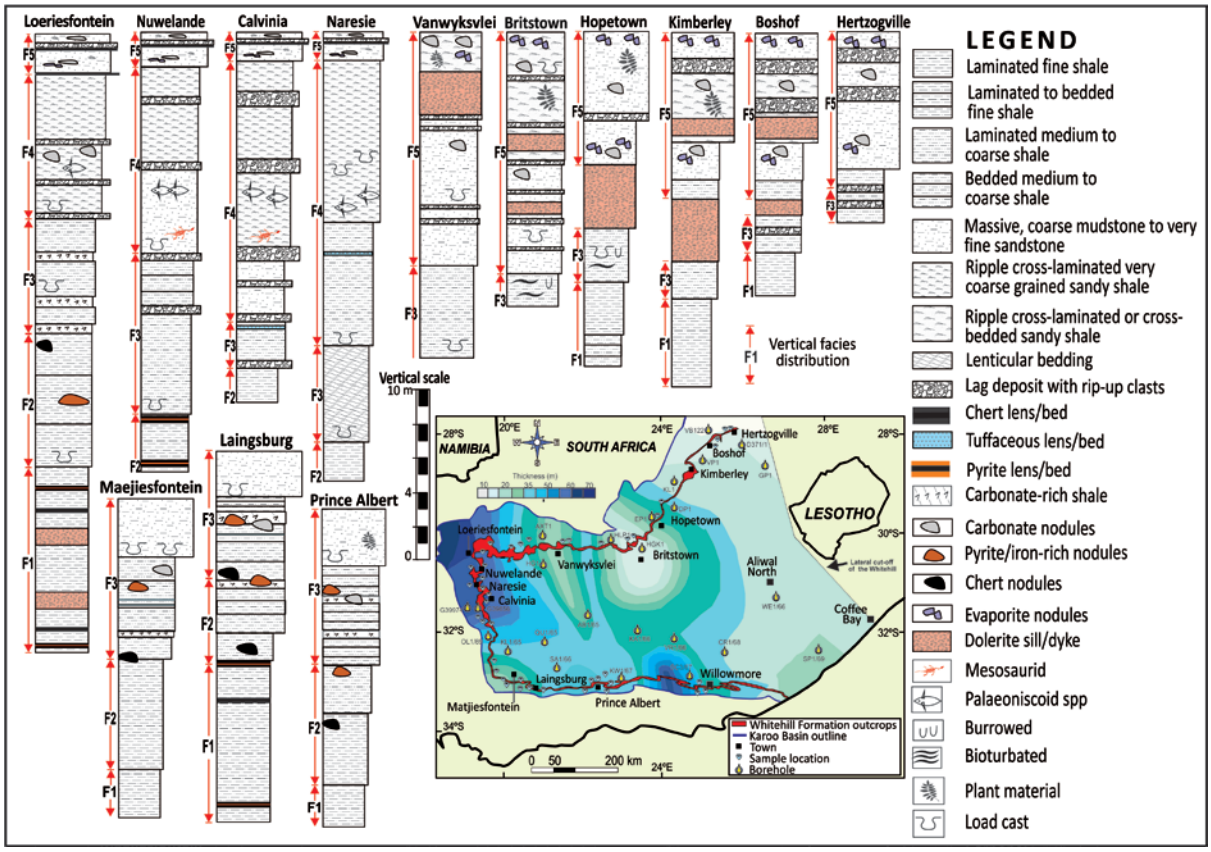

Fig. 2.1. Simplified sedimentological logs of the Whitehill Formation (WHF) measured at selected outcrop sites in the main Karoo Basin. Thickness reported are not the maximum thickness of the formation in those localities, but the maximum exposed section. For log locations and areal distribution of the WHF refer to inset map which also shows the thickness of the formation at each locality as constructed from borehole data. Note that F4 and F5 are only found at locations north of latitude 32°12' S.

2.3. Geological background

The WHF is part of the Permian Ecca Group, which in turn is part of the Upper Carboniferous to Lower Jurassic Karoo Supergroup. With an estimated thickness ranging between 30 to no more than 100 m, the WHF forms an outcrop belt along the western and southern portion of the Karoo Basin. It has been identified in the subsurface, where it ranges in depth from 1600 to 4400 m below the subsurface, and thus the formation covers an area of ~235,000 km2 in the southern half of the basin (inset Fig. 2.1; Visser, 1992; Tankard et al., 2012). Stratigraphically, the WHF occurs between the Prince Albert and Collingham Formations in the south and

between the Prince Albert and Tierberg Formations in the west. It is correlated with the upper part of the coal-bearing Vryheid Formation in the northeastern part of the basin (Cole and McLachlan, 1991; Visser, 1992). Based on palynology, litho- and biostratigraphy, the WHF is also correlated with the Irati Formation in the Paranà Basin of southwestern Brazil (Oelofsen, 1987). In spite of its tuffaceous beds, radiometric dates are not available for the WHF in South Africa. Absolute dates from the WHF correlative units are 280.5 ± 2.1 Ma in Namibia (Werner, 2006) and 278.4 ± 2.2 Ma in Brazil (Santos et al., 2006), and therefore the WHF in South Africa is inferred to be Kungurian in age.

At outcrop scale, the white-weathering formation is distinguished from the dark to olive grey lithologies of the under- and overlying Prince Albert and Collingham/Tierberg Formations. When freshly exposed, the WHF is predominantly black (Fig. 2.2), thinly laminated shale with vertical and lateral variations in silt content (Oelofsen, 1981; Cole and McLachlan, 1991; Visser, 1992). Nodules of carbonate, pyrite/marcasite and chert, evaporates (e.g., gypsum, halite) as well as pale grey to yellowish thin tuffaceous beds are also present (e.g., McLachlan and Anderson, 1977, 1979; Oelofsen, 1981, 1987; Cole and McLachlan, 1991; Visser, 1992; Faure and Cole, 1999; Werner, 2006). Visser (1992) subdivide the WHF in SW deep- and NE shallower-water facies mainly based on the distribution of post-depositional, diagenetic sedimentary features (e.g., chert) and not based on the primary characteristics of the sedimentary facies, such as lithology, texture, and suite of sedimentary strictures, geometry, and fossils (e.g., Tucker, 2011).

The lower part of the WHF is largely unfossiliferous, whereas the upper half hosts a highly diverse fossil assemblages comprising aquatic mesosaurid reptiles, palaeoonicid fish, crustaceans, insects, as well as terrestrial plant debris (e.g., palynomorphs, gymnsoerms wood, Glossopteris sp. leaves, club mosses; e.g., McLachlan and Anderson, 1973, 1977; Oelofsen, 1981; Cole and McLachlan, 1991). Ichnofossils, in addition to unidentified bioturbation, including arthropod tracks, fish swimming traces and coprolites (Oelofsen, 1981, 1987). The stratigraphic distribution of the fossils as well as carbon and pyrite prompted McLachlan and Anderson (1977) and Oelofsen (1981, 1987) to argue for a stratified Early Permian water body in the Karoo Basin, where the anoxic (reducing) bottom conditions contrasted the oxygenated surface conditions that supported free swimming, benthonic and planktonic organisms. Palaeontological evidence for a marine affinity is lacking (e.g., McLachlan and Anderson, 1973, 1979; Faure and Cole, 1999).

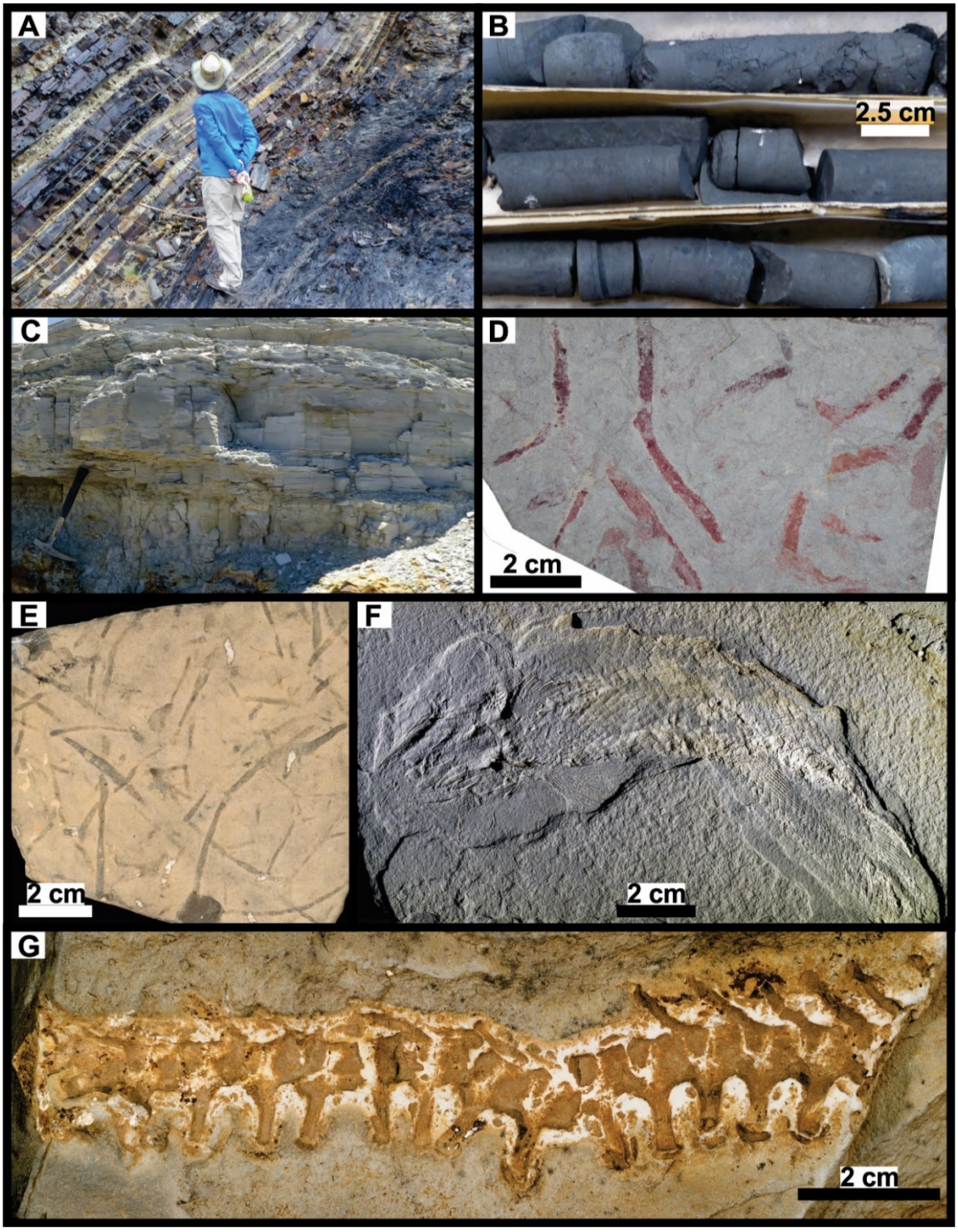

Fig. 2.2. **a**: Outcrop image of the crisp contact between the Whitehill and Collingham Formation (on the right and left, respectively) near Laingsburg. **b**: Freshly drilled outcrop samples obtained with a STIHL E-Z Core Rock Drill fitted with a Pomeroy 40x2.5 cm core barrel. **c**: Sharp-based and normally graded light grey to white shales and very fine-grained sandstones are common in the northern outcrop area (F5). Geopick is 31.3 cm long. **d**: Plant fragments in the upper Whitehill Formation (near Prince Albert; F3). **e**: Trace fossils are common in the middle Whitehill Formation (near Nuwelande; F3). **f**: Body fossil of palaeoniscoid fish found in F4 near Nuwelande. **g**: Body fossil of mesosaurid reptile (dorsal spine) found in F4 near Calvinia. Mseosaurids were endemic to SW Gondwana in the Early Permian.

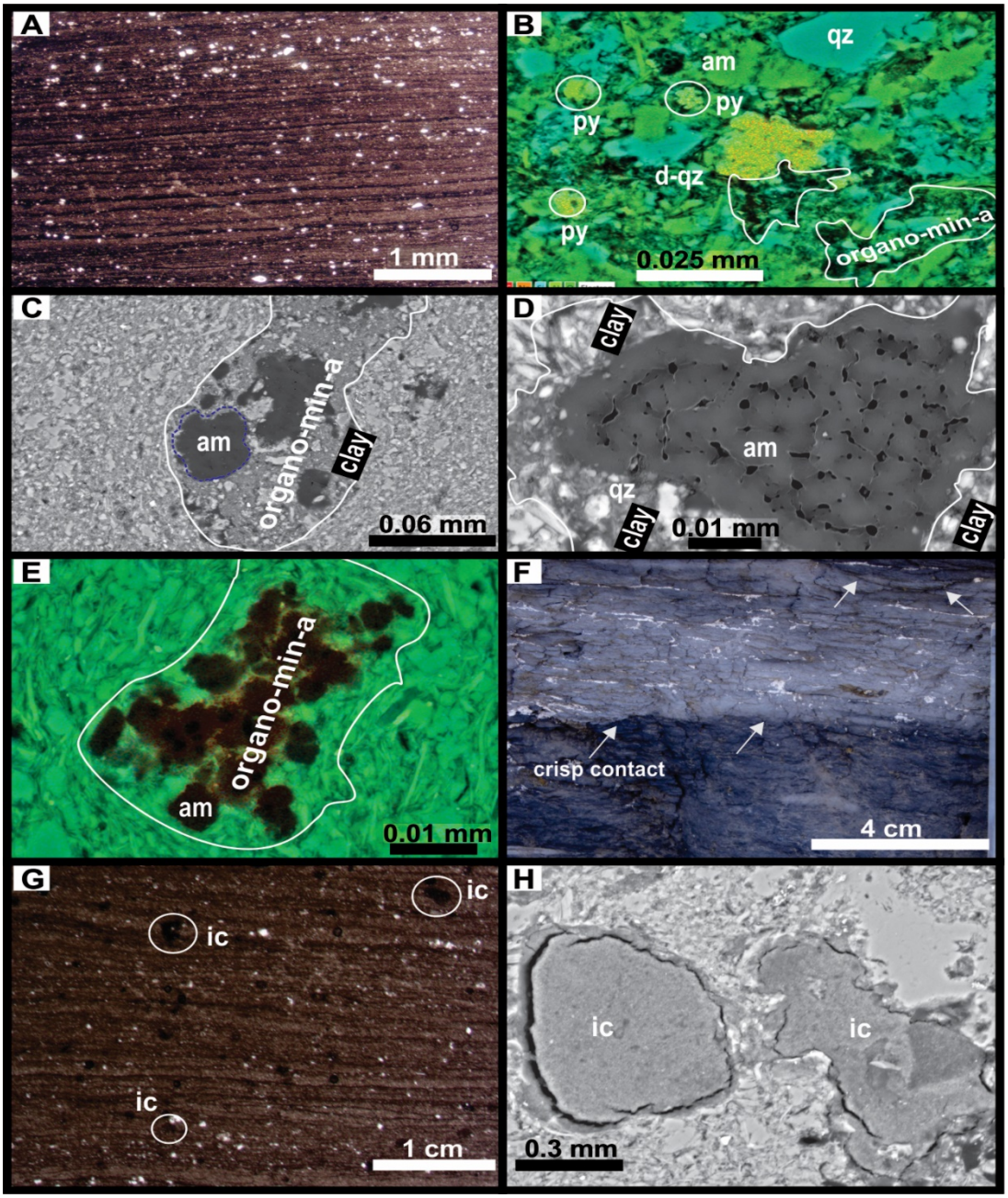

Fig. 2.3. Micro-sedimentary features (structure, fabric, texture) of F1, F2, and F3 in the Whitehill Formation (WHF). **F1 a:** Optical micrograph of uniform, continuous, horizontal laminations. **b**: Back-scattered electron image of shale matrix showing disseminated pyrite (py) and association of algal macerals (am), pellet-like materials, and clays that form organo-minerallic aggregates ('organo-min-a'—white outlines). Diagenetic quartz (d-qz) infills intergranular pores. Organic carbon, pre-compaction microcrystalline carbonates and pyrite cement indicate that pore waters controlled microbial reduction. The sulfate, likely derived from the water column, infilled the sediment pores prior to significant compaction and/or during very low to zero rate of sediment accumulation (e.g., Dean and McArthur, 1989; Macquaker and Gawthorpe, 1993). **F2 c**: Back-scattered electron image showing close knitting between algal macerals and clays ('organo-min-a'—white outlines). **d**: Close-up of features in the algal macerals shown in **c**. The 'organo-min-a' are larger in F2 compared to F1. Pores are partly filled with residual kerogen, quartz, and clay. **e**: Close-up of the algal maceral (am) and organo-minerallic aggregates ('organo-min-a'—white outlines). **F3 f**: Horizontally laminated to bedded, medium shales with crisp contact (arrows). **g**: Optical micrographs of intraclasts (ic) and vertical variability in lamina thickness. **h**: Back-scattered electron image of G showing the close-up of the subrounded to subangular intraclasts (ic), which are interpreted as rip-up shale particles with diameter up to 1.1 mm.

2.4. Methods

WHF outcrops were studied to capture the facies heterogeneity, which can be detected in the texture, fabric, and bedding features as well as composition. The exposed WHF strata we logged sedimentologically, photographed, and sampled along the entire outcrop belt, except in the easternmost part of the Eastern Cape, where the WHF is very poorly exposed (Fig. 2.1). The microtexture, mineralogy of the matrix fraction and cement were established using standard petrographic investigations and Zeiss MERLIN and EVO high-resolution field emission scanning electron microscope (FE-SEM) with nanoscale and cryo-EDS detectors operated mainly in back-scatter and cathodoluminescence modes between 20 and 30 kV at 9-11 mm working distance at Stellenbosch University Central Analytical Facilities. Total organic carbon content was measured with LECO CS244 carbon analyser at the Indian Institute of Technology in Bombay.

2.5. Observations

Five distinctive facies (F1-F5) of the WHF can be recognized (Table 2.1) that include fine- to coarse-grained shales (sensu Lazar et al., 2015) with a variety of primary sedimentary features, which are mainly laminations, very-thin to thin (1-5 cm) beds in F1 and F2 that give way to an upward increasing abundance of horizontal- to low-angle cross-laminations, internal scours, sharp bedding planes, diffused bedding, as well as normal graded beds (from coarse silt to clay) in F3, F4 and F5 (Fig. 2.4; Table 2.1). Ripple cross-laminations with foreset dip directions ranging between 44^{o} and 78^{o} (E-NE) were measured in F4 and F5 between Calvinia and Loeriesfontein (Fig. 2.1 and 2.2). The southern Karoo Basin outcrops only yielded some poorly preserved plant fragments in F3 (e.g., east of Prince Albert; Fig. 2.2). In contrast, the facies contain variable quantities of organic carbon that ranges from less than 1 to 16.5 wt.% in F4 and F4, respectively. Dark colored chert and dolomite nodules (up to 3 m in diameter) and beds (up to 1.4 m thick) are common in the lower part of the formation, particularly in F2, and light grey to yellowish carbonate and evaporate-rich concretions are mainly present in F4 and F5. Yellowish-weathering thin tuffaceous beds occur in the upper subunits of the formation and increase in thickness (up to 8 cm) and abundance in the central part of the basin (Fig. 2.1). Primary fabrics were occasionally overprinted by secondary alteration features (e.g., mineral-filled cracks). In Tanqua area, the shales are gently deformed and dip southward between 2^{o} and 6^{o}, whereas between Calvinia and Loeriesfontein, the shales dip 2-3^{o} northward. Between Vanwyksvlei and Hopetown, the shales dip southward at 2^{o} and 7^{o}. In contrast to the northern

study sites, bed thickness and orientation are harder to define than in the south due to structural deformations associated with the Cape orogeny (Fig 2.1).

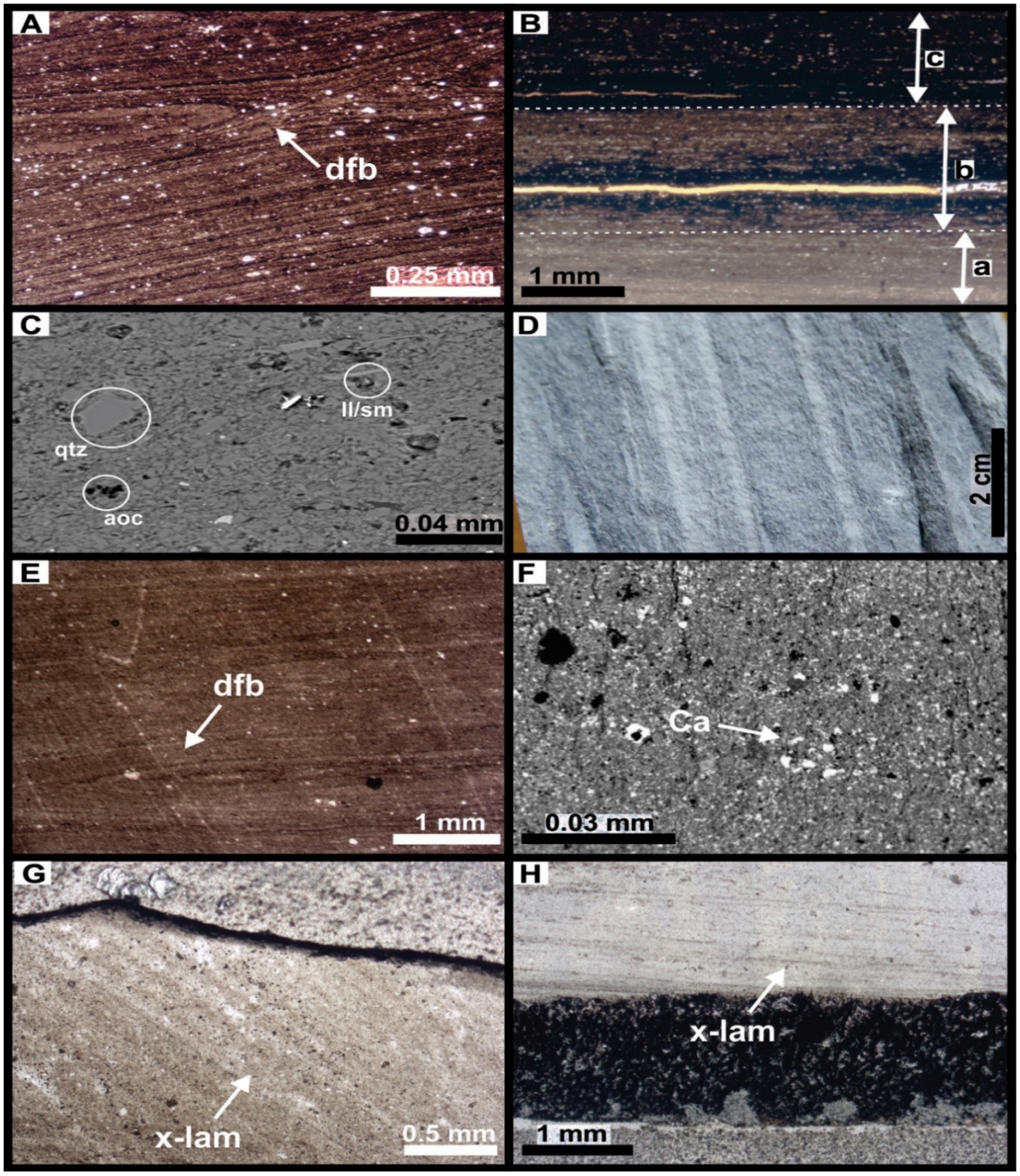

Fig. 2.4. Micro-sedimentary features (structure, fabric, texture) of F4 and F5 in the Whitehill Formation (WHF). **F4 a:** Optical micrograph of diffused bedding (dfb) and concave upward geometries. **b**: Optical micrograph of triplet feature. Note the gradual increase clay content (darker laminae). **c**: Back-scattered electron image illustrating the dominance of clay and quartz particles. **F5 d**: Horizontal interlaminations of clay- and silt-rich layers in shale hand specimen. **e**: Optical micrograph of diffused bedding (dfb) and concave upward geometries. **f**: Back-scattered electron image illustrating the grain size and mineral composition (mainly clay and quartz) in **c**. **g**: Optical micrograph of ripple cross-lamination (x-lam). Note the steep dip angle of the foresets, truncated by and erosional surface. **h**: Optical micrograph of low-angle cross-lamination (x-lam) in tangential contact with bedding plane.

2.6. Discussion

2.6.1. Depositional processes

Dominance of biogenic detritus, thin laminations, and close association between clay fraction and organic matter (OM- e.g., flattened algal macerals; Fig. 2.2) packaged as organo-minerallic aggregates ('org-min-a') in F1 and F2 indicate that these sediments were: (1) produced in an overall low energy water body away from the reach of coarse clastic sedimentary detritus; and (2) settled out of buoyant suspensions in form of pelagic snow aggregates (e.g., Fowler and Knauer, 1986; Bohacs et al., 2005; Macquaker et al., 2010). Mud-size particles do not only settle out of suspension individually but often clump together due to physical coagulation and/or zooplankton-mediated aggregation (e.g., Nittrouer et al., 1986; Alldredge and Gotschalk, 1990). In the latter, the organo-minerallic aggregates are glued together by extra-cellular mucopolysaccharides and exopolymeric secretions of plankton (e.g., Fowler and Knauer, 1986; Faure and Cole, 1999).

The disseminated fine-grained (<5 μm) pyrite framboids in F1 (Fig. 2.2) suggests that this facies may have been deposited on the basin floor with bacterial sulfate reduction and where sulfidic and anoxic condition existed (e.g., Demaison and Moore, 1980; Wignall and Newton, 1998; Lazar et al., 2015). In contrast, larger pyrite framboids and euhedral grains aligned along bedding planes in upper F2 indicate the presence of free oxygen at the sediment-water interface (e.g., Wilkin et al., 1997; Schieber, 2011; Lazar et al., 2015). The intergranular pore-filling clays and quartz in F1 and F2 (Fig. 2.2) indicate diagenetic origin (e.g., Macquaker et al., 2014; Lazar et al., 2015). The diagenetic nodules with well-developed carbonate cement and pre-compaction microcrystalline pyrite cement in F2 (Fig. 2.2) further attests that the pore water contained microbial reduced sulfate whose solutes filled the pores prior to significant compaction and initiate the growth of nodules, following a pause (i.e., zero or very low rate) in sedimentation (e.g., Dean and McArthur, 1989; Macquaker and Gawthorpe, 1993). Furthermore, the change from thin lamination of F1 to alternation of laminated and non-laminated (very thin beds) in F2 (Fig. 2.3) suggest disruption to anoxia that was persistent during the deposition of F1.

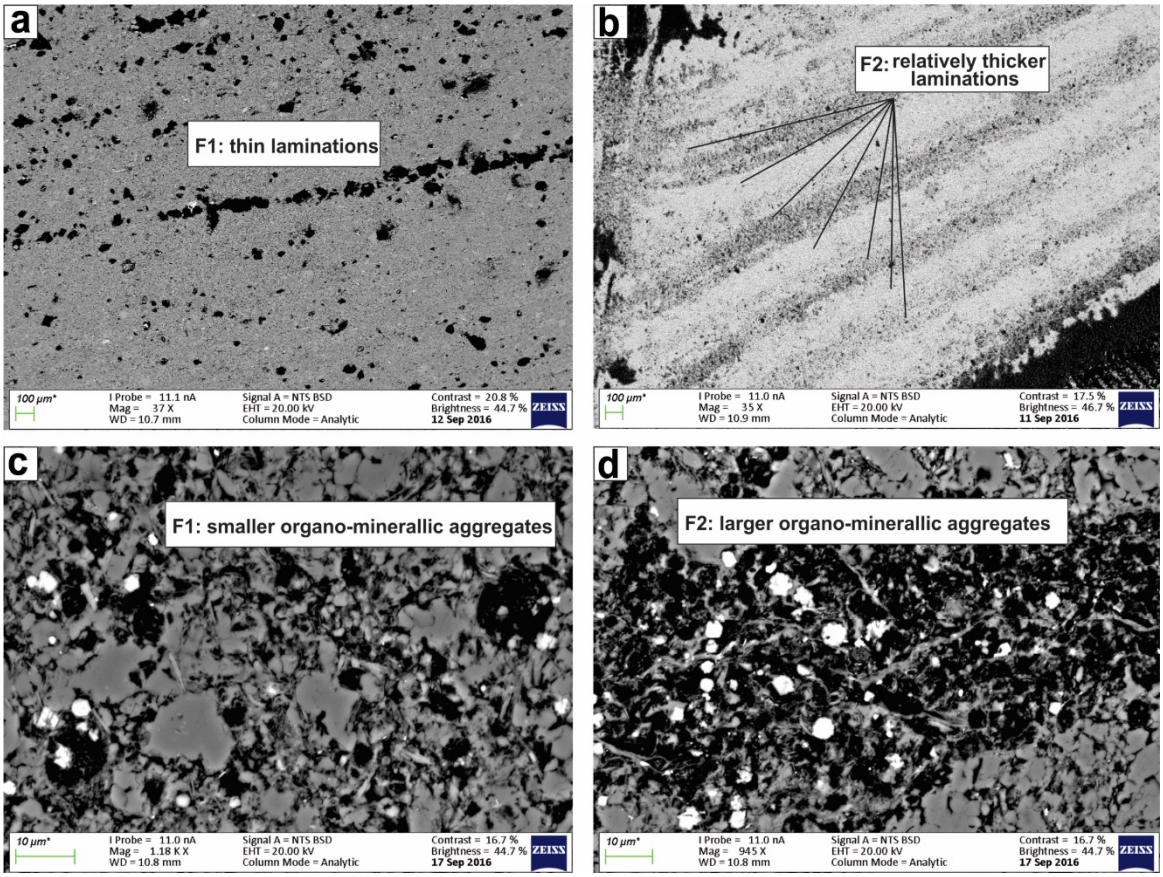

Fig. 2.5. Electron images of F1 and F2 captured under similar setting to show the primary diagnostic features used to distinguish the two facies. See text for details.

The marked increase in the quantity of coarse-grained silt and very-fine sand particles from F3 to F5, together with an upward increasing abundance of horizontal- to cross-laminations, internal scours, sharp bedding planes, diffused bedding, as well as normal graded beds (Figs. 2.1, 2.2, 2.3, 2.4; Table 2.1) are interpreted as products of sustained lateral sediment transport by turbulent flows with waxing and waning current energies (Macquaker et al., 2010; Wilson and Schieber, 2015). The increasingly higher energy levels during the deposition of F3-F5 are also attested by several shale layers with subrounded to subangular rip up particles with diameters of up to 1.1 mm (Fig. 2.3). These intraformational shale particles (Fig. 2.3g-h) may also be used as an indirect evidence for the above postulated pause in sedimentation that might have contributed to the consolidation of previously deposited mud (F1 and F2). The medium to coarse shale beds with sharp bases, horizontal and ripple cross-laminations, diminutive normal grading and diffused bedding in F3-F5 (Figs. 2.1, 2.2, 2.3, 2.4, Table 2.1), coupled with the higher abundance of trace and body fossils, suggest increasing oxygenation levels of the pore waters and higher influx of detrital clastics into the basin. These indicate significant changes in the sedimentary conditions relative to the inferred low energy and more anoxic

conditions prevalent during the sedimentation of F1-F2. These interpretations are also supported by the northeast-southwest aligned fossils in F4-F5 and very low amplitude oscillation ripple marks found by Oelofsen (1981, p. 24) near Hopetown, Loeriesfontein, and Calvinia. These symmetrical ripple marks recovered by Oelofsen occur with a facies that could correspond to the transition of F3 and F4. The overall facies descriptions and interpretations presented here are also in line with the sedimentological results of Cole and McLachlan (1991).

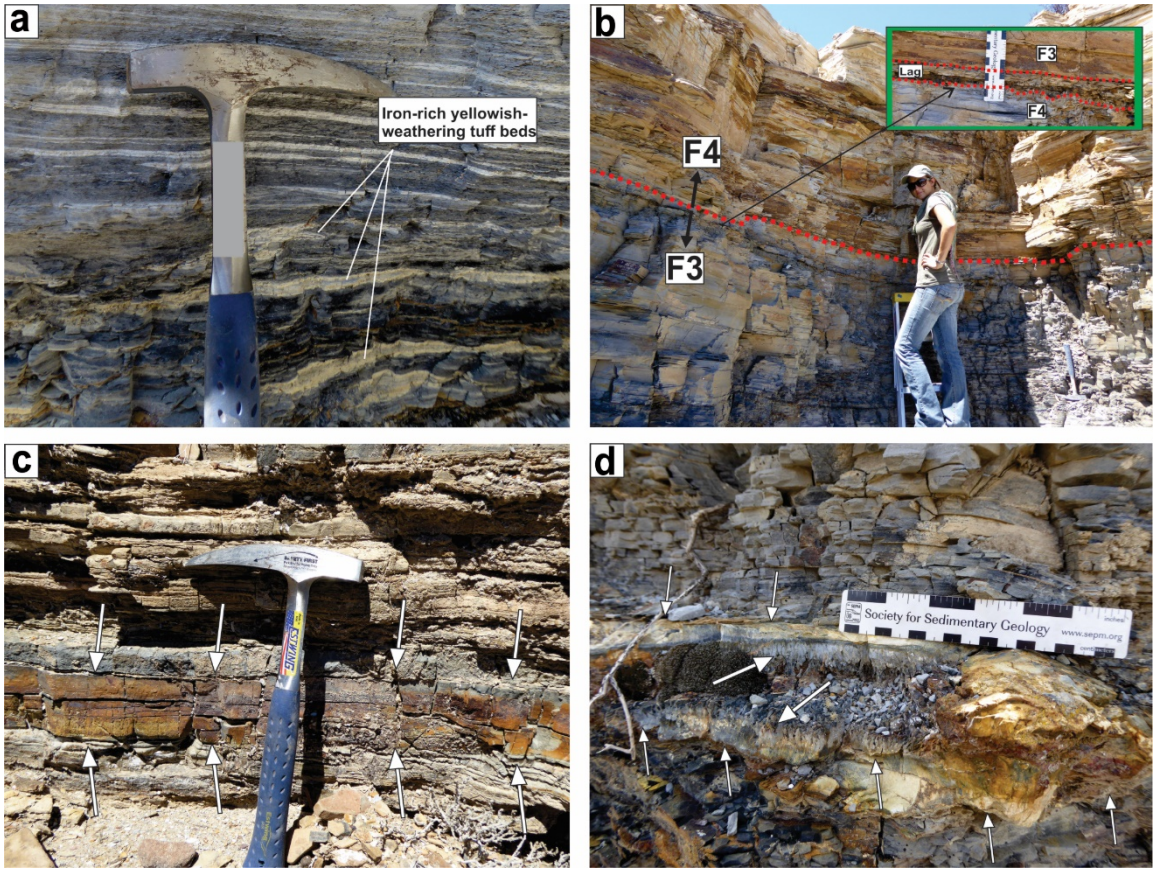

Fig. 2.6. Outcrop images of primary sedimentary features that marked the contacts between facies. **a**: Well-defined yellowish weathering tuffaceous bed in the upper Whitehill Formation (F3-F5). **b**: The contact between F3 and F4 is marked by a lag of about 2-5 cm thick and occasional erosional surface with a relief of about 5-10 mm. **c**: Iron sulfide bearing sequence lag (between arrows) that marked the F2-F3 boundary. From FE-SEM analyses, the lag is cemented by marcasite. **d**: A stratiform horizon of marcasite nodules that marked the F2-F3 boundary. The broken nodule (smaller arrows) shows rims of radiating-bladed marcasite (larger arrows). Observe differential compaction indicating that nodule formation was during early diagenesis, prior to significant reduction in pore spaces. These large amounts of iron sulfide that marked the F2-F3 boundary suggests that the redox interface stayed at this level for a relatively long period, which further testifies to zero and very low sedimentation.

Table 2.1. Summary of the sedimentary facies in the Whitehill Formation (also see Figures 2-4)

Facies code	Facies description	Sedimentary process interpretation
F1	Thinly and horizontally laminated (~5 mm-thick), black, carbonaceous (4.4-5.6 TOC wt.%), fine shale with an average TOC of 4.4-7.8 wt.%; Contains flattened organo-minerallic aggregates ('organo-min-a'), amorphous organic matter, fecal pellet-like materials, disseminated fine-grained (<5 μm) pyrite framboids/concretions, Tasmanites cysts and colonial algal cells, and minor silt-size quartz with some pyrite-filled hair cracks, few grains of barite. The matrix is composed of clay (illite-smectite), amorphous organic carbon (aoc), chert/quartz. Fossil Tasmanites cysts and colonial algae cells reported for the first time in the facies.	High bioproductivity, suspension settling of pelagic snow at the basin floor with anoxic and sulfidic water-sediment interface
F2	Laminated to thin bedded, black, splintery fine shale with a maximum TOC of ~16.5 wt.%. Contains silt-size quartz, clay, aoc, Tasmanites cysts, colonial algal cells, fecal pellets, algal maceral and pyrite along bedding planes; Few mm to 10 m diameter diagenetic nodules common in upper section; Matrix: clay, carbonates, aoc, quartz. Fossil Tasmanites cysts and colonial algae cells reported for the first time in the facies.	Suspension settling of pelagic snow under intermittent anoxic conditions. Highest rates of bioproductivity and subsequent interruption of the same, resulting in early cementation and remineralizations.
F3	Sharp-based, horizontally laminated to bedded, occasionally burrowed, diminutive normally graded, dark grey siliceous-argillaceous medium shale; Contains silt-size quartz, clay, fewer aoc and fecal pellets and lags of rip-up shale particules, with average TOC of 1.6 wt.%; Matrix: clay, quartz, carbonates Trace fossils are common and include fish swimming traces, arthropod tracks, horizontal and interconnecting burrows, and fragmentary plant fossil reported at east of Prince Albert.	Erosion and redeposition of muddy substrate by currents in sustained bed-load transport; incipient oxic bottom waters
F4	Horizontal and ripple cross-lamination, diffused bedding, internal scouring, grey siliceous medium shale with continuous nonparallel down-lapping (concave-up) geometries and triplet features; Average TOC of 1.01 wt.% Matrix: quartz, carbonate, clay Mesosaurid reptiles and palaeoniscoid fish are abundant in the lower part of F4.	Progressive dominance of waning wave-enhanced sediment gravity flows and bed-load dominated currents; often transient oxic bottom waters, especially in the upper part of F4
F5	Horizontal and ripple cross-lamination to massive, diffused bedding in light grey siliceous coarse-grained shale with continuous nonparallel down-lapping (concave-up) geometries and triplet features; thicker beds than in F4; Average TOC: 0.58 wt.% Matrix: quartz and carbonate Palaeoniscoid fish, and in the upper part, pygocephalomorphic crustaceans (e.g., *Notocaris tapscotti*) are abundant.	Rapid, *en masse* deposition of sand and silt in hyperpycnal flows and bed-load dominated currents; Often fully oxygenated water body

2.6.2. Basinal distribution of facies

Figs. 2.1 and 2.7 illustrate the basinal distribution of the five facies (F1-F5) of the WHF in the main Karoo Basin. F1 occurs in the entire area of the basin where WHF is documented. It is remarkable marked by its prominent dark color and lamination, although samples from localities closer to the Cape Fold Belt show progressive obliteration of these primary sedimentary features. The F1-F2 contact is gradational and marked by an increase in thickness of laminae and thin layers composed of predominantly organic macerals, interpreted here as lamalginites. The thickness of F1 in more or less uniform across the entire basin, except in the northern margin areas between Hopetown and Hertzogville where it shows a progressive decrease and grades into the underlying unit. F2 occurs in the southern part of the basin to the Brandvlei. It is thickest in Loerisefontein and decreased sharply thereafter until it disappeared in Brandvlei. F3 occurs in the entire basin but with sharp variation in thickness. The contact between F2 and F3 is marked by marcasite cemented lags and nodules of both marcasite and carbonates (majorly dolomite). In the southern part of the basin, up to latitude 32°12' S, the WHF is comprised only F1-F3, however, north of this latitude, F4 and F5 were detected. It was observed that this latitude roughly coincides with the location in the basin (north of latitude 32°30' S; Viljoen, 1994) where the formation overlying the WHF changed from the Collingham Formation to Tierberg Formation. The contact between F3 and F4 is marked by thin (<2 cm) calcitic/dolomitic lag and in places by an erosional surface, indicating a possibly winnowing (Fig. 2.6). The contact between F4 and F5 is transitional and sometimes marked by a change from thickly laminated/bedded F4 to massive-looking F5. The thickness of F4 and F5 increases northward up to the area between Vanwykvlei and Hopetown and then decrease sharply further north. The distribution of the facies, as well as primary sedimentary features observed, suggest that the much WHF north of Hopetown was eroded, transported further south, and redeposited in the Loeriesfontein locality (Fig. 2.1, 2.7).

2.6.3. Orientation of basinal palaeo-slope

Palaeo-slope of the basin at the time of the deposition if the WHF is difficult to establish, because of the monotony of finely laminated shales with palaeocurrent indicators limited to rare cross-laminations, ripple marks, and orientation of fossils (i.e., 47 mesosaurid and 138 pygocephalomorphic crustaceans specimens reported in Oelofsen, 1098; his Figs. 9 and 10).

Sedimentological and taphonomic evidence suggest that the ripples and the northeast-southwest aligned fossils were generated by weak, localised oscillatory flows rather than strong, unidirectional, basinal bottom currents (Oelofsen, 1981). These localised flow indicators are unsuitable to infer the Early Permian basinal palaeo-slope orientation (cf. Tucker, 2011). Notwithstanding the lack of reliable primary palaeocurrent indicator in the WHF, the basinal orientation of F3-F5 (Fig. 2.1) may be linked to a south-southwest dipping WHF palaeo-slope.

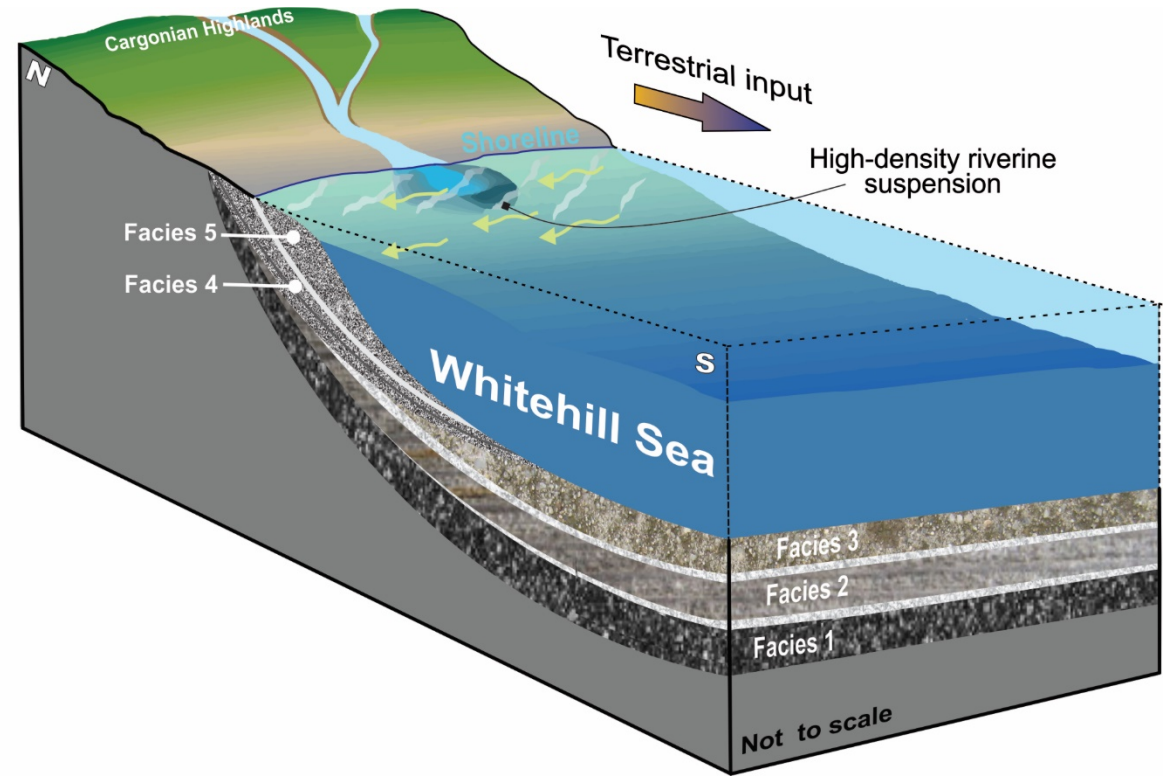

Fig. 2.7. Summary of the depositional model for the WHF showing the spatial distribution of the five facies (F1–F5) deposited by diverse sedimentary processes. The near-uniform and basinal extent as well as predominant fine-grained nature of F1 and F2 point to a low energy shelfal setting, away from coarse clastic inputs, in the distal parts of a large water body. Increase in grain-size and detrital fractions in F3–F5 indicate progradation in a regressing waterbody. Compositional and textural differences of the facies (Figs. 2.1-2.4; Table 2.1) attest to variable provenance and complex sediment dispersal histories.

2.6.4. Depositional setting interpretations

Our results are in line with previous interpretations that suggest a stratified and anoxic to brackish water body across south-west Gondwana during the Kungurian (e.g. McLachlan and Anderson, 1973; Faure and Cole, 1999; Werner, 2006; Flint et al., 2011). During the deposition of the lower unfossiliferous and higher organic carbon and pyrite contents (F1 and F2), we interpret that the surface water contained more nutrients (e.g., N, Si, P, Fe) that enabled higher primary productivity of OM, which was preserved together with fine-grained sediments on the basin floor under reducing (oxygen-depleted) conditions. Sediment-laden underflows subsequently entered the basin along its northern margin, possibly from summer melting of mountain glaciers north of the Karoo Basin (Cargonian Highlands). Consequently, the biogenic constituents produced were diluted by progressively higher input of terrestrial detritus. The contrast between the anoxic-brackish and freshwater fluids possibly triggered thermohaline currents as the hyperpycnal riverine discharge plunged into the basin floor, eroding and resuspending the muddy substrate. Considering the basinal extent of F3 (Fig. 2.1), bottom hugging currents (diluted mudflows) probably moved the sediments over large distances on relatively low gradients slopes (<0.7^{o}-e.g., Mulder et al., 2003; Bhattacharya and MacEachern, 2009). Similar processes and features were observed on modern muddy shelves near river mouths (Friedrichs and Wright, 2004), for example, at the mouths of Yellow (Wright et al., 2001) and Amazon (Kineke et al., 1996) Rivers, along the northern California coast (Eel River; e.g., Nittrouer et al., 1986; Wright et al., 2001), and in laboratory experiments (e.g., Schieber and Yawar, 2009). Our depositional model (Fig. 2.7), which proposes an overall shallowing upwards trend and basinward migration of the shoreline along the southward-dipping WHF palaeo-slope, is supported by: (1) upsection increase in grain size, thickness, sharp bedding planes, graded intervals, layers with rip-up particles; (2) the spatiotemporal distribution of the facies-i.e., the basinal extent of F1-F3 versus the restricted nature of F4 and F5 along the northern margin of the basin (Fig. 2.1, 2.5); and (3) reduced TOC in F4 and F5.

2.7 Conclusion

Five distinctive sedimentary facies in the WHF reveal that in addition to quiet setting of suspended mud particles, more energetic depositional processes were also present in the Karoo Basin during the Early Permian. The WHF facies and their basinal distribution are linked to (1) primary sediment production within the basin, (2) terrestrial clastic input from the Cargonian Highlands in the north of the basin, and (3) post-depositional alterations. F1 and F2 are interpreted as biologically produced pelagic snow aggregates that were deposited on the basin floor, remote from coarse sediment sources and under anoxic to dysoxic conditions, favorable to the preservation of organic carbon, especially in the lower part of F2. Terrestrial detritus is increasingly more dominant from F3 to F5, and this upward increase in clastic grains is interpreted to be linked to underflows from summer melting of mountain glaciers north of the Karoo Basin that fed the sediment-laden hyperpycnal currents along the northern margin of the basin and mud flows further to the south. In summary, the temporal and spatial variations in the internal composition, primary sedimentary structures, and distribution of organic carbon in the WHF reflect the diversity of sedimentary conditions (e.g., sediment supply, energy levels, mode of transport) in time and space within the Early Permian main Karoo Basin.

References

Alldredge, A.L., and C.C. Gotschalk, 1990, The relative contribution of marine snow of different origins to biological processes in coastal waters: Continental Shelf Research, 10, 41-58.

Bhattacharya, J.P., and J.A. MacEachern, 2009, Hyperpycnal rivers and prodeltaic shelves in the Cretaceous seaway of North America: Journal of Sedimentary Research, 79, 184-209.

Bohacs, K.M., G.J Grabowski, A.R. Carroll, P.J. Mankiewicz, K.J. Miskellgerhardt, J. R. Schwalbach, M.B. Wegner, and J.A. Simo, 2005, Production, destruction, and dilution: the many paths to source-rock development, *in*, Harris, N.B., ed., The Deposition of Organic Carbon-Rich Sediments: SEPM, Special Publication, 82, 61-101.

Cole, D.I., and I.R. McLachlan, 1991, Oil potential of the Permian WHF Shale Formation in the main Karoo Basin, South Africa. In: H. Ulbrich, and A.C. Rocha Campos (Editors), Gondwana Seven Proceedings, 379-390.

Cunningham-Craig, E.H., 1914, Report on the petroleum prospects in the Union of South Africa: The Government Printing and Stationery Office, Pretoria, 28p.

Dean, W.E., and M.A. McArthur, 1989, Iron-sulfur-carbon relationships in organic-carbon-rich sequences: Cretaceous western seaway: American Journal of Science 289, 708-743.

Decker, J., and J. Marot, 2012, Investigation of hydraulic fracturing in the Karoo of South Africa: Annexure A, Resource Assessment, Petroleum Agency SA, Available at: <http://www.dmr.gov.za/publications/ viewdownload/ 182/854.html> (last viewed 07-02-17).

Demaison, G.J., and G.T. Moore, 1980, Anoxic environments and oil source bed genesis, AAPG Bulletin, 64, 1179–1209.

Faure, K., and D.I. Cole, 1999, Geochemical evidence for lacustrine microbial blooms in the vast Permian main Karoo, Paraná, Falkland Islands and Huab basins of southwestern Gondwana: Palaeogeography, Palaeoclimatology, Palaeoecology, 152, 189-213.

Flint, K., D. Hodgson, A.R. Sprague, R.L. Brunt, W.C. Van der Marwe, J. Figuredo, A. Prèlat, D. Box, C. Di Celma, and J.P. Kavanagh, 2011, Depositional architecture and sequence stratigraphy of the Karoo Basin floor to shelf succession, Laingsburg depocentre, South Africa: Marine and Petroleum Geology, 28, 658-674.

Fowler, S.W., and G.A. Knauer, 1986, Role of large particles in the transport of elements and

organic compounds through the oceanic water column: Progress in Oceanography 16, 147-194.

Friedrichs, C.T., and L.D. Wright, 2004, Gravity-driven sediment transport on the continental shelf: implications for equilibrium profiles near river mouths: Coastal Engineering, 51, 795-811.

Geel, C., H-M Schulz, P. Booth, M. De Wit, and B. Horsfield, 2013, Shale gas characteristics of Permian black shales in South Africa: results from recent drilling in the Ecca Group Eastern Cape: Energy Procedia, 40, 256-265.

Geel, C., M. de Wit, P. Booth, H-M. Schulz, and B Horsfield, 2015, Palaeo-environment, diagenesis and characteristics of Permian black shales in the lower Karoo Supergroup flanking the Cape Fold Belt near Jansenville, Eastern Cape, South Africa: Implications for the shale gas potential of the Karoo Basin: South African Journal of Geology, 118, 248-274.

Kineke, G.C., R.W. Sternberg, J.H. Trowbridge, and W.R.Geyser, 1996, Fluidmud processes on the Amazon continental shelf: Continental Shelf Research, 16, 667-696.

Lazar, O.R., K.M. Bohacs, J. Schieber, J.H.S. Macquaker, and T.M. Demko, 2015, Mudstone Primer: Lithofacies variations, diagnostic criteria, and sedimentologic implications at lamina to bedset scale: nomenclature and description guidelines: SEPM Concepts in Sedimentology and Paleontology, 12, 198p.

Macquaker, J.H.S., and R.L. Gawthorpe, 1993, Mudstone lithofacies in the Kimmeridge Clay Formation, Wessex Basin, southern England: implications for the origin and controls of distribution of mudstones. Journal of Sedimentary Petrology, 63, 1129-1143.

Macquaker, J.H.S., M.A. Keller, and S.J. Davies, 2010, Algal blooms and “marine snow”: mechanisms that enhance preservation of organic carbon in ancient fine-grained sediments: Journal of Sedimentary Research, 80, 934-942.

Macquaker, J.H.S., K.G. Taylor, M.A. Keller, and D.A. Polya, 2014, Compositional controls on early diagenetic pathways in fine-grained sedimentary rock: Implications for predicting unconventional reservoir attributes of mudstones: AAPG Bulletin, 98, 587-603.

McLachlan, I. R., and A. Anderson, 1973, A review of the evidence for marine conditions in southern Africa during Dwyka times: Palaeontologica Africana, 15, 37-64.

McLachlan, I.R., and A.M. Anderson, 1977, Carbonates, "stromatolites" and tuffs in the lower Permian White Band Formation: South African Journal of Geology, 73, 92-94.

McLachlan, I.R., and A.M. Anderson, 1979, The oil potential of the Early Permian White Band

Formation in South Africa: Geological Society of South Africa Special Publication, 6, 83-86.

Mulder, T., J.P.M. Syvitski, S. Migeon, J.C. Fauge´res, and B. Savoye, 2003, Marine hyperpycnal flows: initiation, behavior and related deposits-A review: Marine and Petroleum Geology, 20, 861-882.

Nittrouer, C.A., T.B. Curtin, and D.J. DeMaster, 1986, Concentration and flux of suspended sediment on the Amazon continental shelf: Continental Shelf Research, 6, 151-174.

Oelofsen, B.W., 1981, An anatomical and systematic study of the Family Mesosauridae (Reptilia: *Proganosauria*) with special reference to its associated fauna and palaeoecological environment in the WHF Sea: Unpublished PhD thesis, University of Stellenbosch, South Africa, 259p.

Oelofsen, B.W., 1987, The biostratigraphy and fossils of the Whitehill and Iratí Shale Formations of the Karoo and Paraná Basins, in, C.D. McKenzie, ed., Gondwana Six: stratigraphy, sedimentology and paleontology: Geophysical Monograph, American Geophysical Union, 41,131-138.

Oelofsen, B.W. and D.C. Araújo, 1987, Palaeoecological implications of the distribution of mesosaurid reptiles in the Permian Irati Sea (Paraná Basin), South America: Revista Brasileira de Geociências, 13, 1-6.

Potter P.E., J.B. Maynard, and P.J. Depetris, 2005, Mud and Mudstones: Introduction and Overview: Springer-Verlag, New York, 297p.

Rogers, A. W., and A.L Du Toit, 1909, An introduction to the Geology of Cape Colony: Longmans, Green and Co. New York, 491p.

Rowsell, D.M. and A.M.J. de Swardt, 1976, Diagenesis in Cape and Karroo sediments, South Africa, and its bearing on their hydrocarbon potential: Transactions of the Geological Society of South Africa, 79, 81-145.

Santos, R.V., P.A. Souza, C.J. Sauza de Alvarenga, E.L. Dantas, M.M. Pimentel, C. Gouveia de Oliveira, and L. Medeiros de Araújo, 2006, Shrimp U-Pb zircon dating and palynology of bentonitic layers from the Permian Irati Formation, Paranà Basin, Brazil: Gondwana Research, 9, 456-463.

Schieber, J, 2011, Iron sulfide formation, in, J. Reitner and V. Thiel, eds, Encyclopedia of Geobiology: Springer-Verlag, 486-502.

Schieber, J., and Z. Yawar, 2009, A new twist on mud deposition: mud ripples in experiment and rock record: The Sedimentary Record, 7, 4-8.

Scheffler, K., D. Bühmann, and L. Schwark, 2006, Analysis of late Palaeozoic glacial to

postglacial sedimentary succession in South Africa by geochemical proxies-Response to climate evolution and sedimentary environment: Palaeogeography, Palaeoclimatology, Palaeoecology, 240, 184-203.

Smithard, T., E.M. Bordy, and D. Reid, 2015, The effect of dolerite intrusions on the hydrocarbon potential of the lower Permian WHF Formation (Karoo Supergroup) in South Africa and southern Namibia: A preliminary study: South African Journal of Geology, 118, 489-510.

Schwarz, E. H. L., 1912, South African Geology: Blackie and Son Ltd, London, 200p

Tankard, A., H. Welsink, P. Aukes, R. Neweighton, and E. Stettler, 2012, Geodynamic interpretation of the Cape and Karoo basins, South Africa, in, D.G. Roberts, A.W. Bally, eds, Regional Geology and Tectonics: Phanerozoic Passive Margins, Cratonic Basins and Global Tectonic Maps: Elsevier, U.K., 869-945.

Tucker, M.E., 2011, Sedimentary rocks in the field: A practical guide: Blackwell, Oxford, 275p.

Viljoen, J.H.A, 1994, Sedimentology of the Collingham Formation, Karoo Supergroup: South African Journal of Geology, 97, 167-183.

Visser, J.N.J., 1992, Deposition of the Early to Late Permian Whitehill Formation during a sea-level highstand in a juvenile foreland basin: South African Journal of Geology, 95, 181-193.

Visser, J.N.J., 1994, A Permian argillaceous syn- to post-glacial foreland sequence in the Karoo Basin, South Africa, M. Deynoux, J.M.G. Miller, E.W. Domack, N. Eyles, I.J. Fairchild, and G.M. Young, eds, Earth´s glacial record: Cambridge University Press, Cambridge, 193-203.

Werner, M., 2006, The stratigraphy, sedimentology and age of the Late Palaeozoic Mesosaurus Inland Sea, SW-Gondwana: new implications from studies on sediments and altered pyroclastic layers of the Dwyka and Ecca Group (lower Karoo Supergroup) in southern Namibia: Unpublished PhD Thesis, University of Würzburg, Germany, 428p.

Wignall, P.B., and R. Newton, 1998, Pyrite framboid diameter as a measure of oxygen deficiency in ancient mudrocks: America Journal of Science, 298, 537-552.

Wilkin, R.T., M.A. Arthur, and W.E. Dean, 1997, History of water-column anoxia in the Black Sea indicated by pyrite framboid size distributions: Earth and Planetary Science Letters, 148, 517-525.

Wilson, R.D., and J. Schieber, J., 2015, Sedimentary Facies and Depositional Environment of the Middle Devonian Geneseo Formation of New York, USA: Journal of Sedimentary

Research, 85, 1393-1415.

Wright, L.D., C.T. Friedrichs, S.C. Kim, and M.E. Scully, 2001, Effects of ambient currents and waves on gravity-driven sediment transport on continental shelves: Marine Geology, 175, 25-45.

Chapter 3

Spatiotemporal geochemical variation and distribution of organic carbon content in the Permian Whitehill Formation of South Africa

3.1. Abstract

The Lower Permian Whitehill Formation (WHF) in the main Karoo Basin of South Africa is an important hydrocarbon resource unit currently being considered for gas shale exploitation. However, significant variability in the geometry and composition (particularly in the distribution of organic carbon content) of this shale unit detected in earlier studies remain largely unquantified and unexplained. This has resulted in conflicting interpretations of not only the hydrocarbon potential of this resource unit but also the paleoenvironmental conditions that prevailed in the Karoo Basin in the Early Permian. Further insights into the sedimentological controls responsible for the stratigraphic and compositional variations in the formation are, therefore, valuable to the energy industry as it is to the larger scientific community. Our aim was to capture, quantify, and explain the heterogeneities in the WHF, especially the distribution of organic carbon content, using a combination of field descriptions, vintage borehole data, micro- to nano-scale petrographic observations, and multiple geochemical data so that a more critical understanding of the sedimentological controls responsible for the variability can be established.

Using this integrated approach, five primary sedimentary facies (F1-F5, i.e., stratigraphic subunits in the WHF) were identified, which show specific and systematic variations in nature and content of organic carbon, stable isotopic composition (of $\delta^{13}C_{org}$ and $\delta^{15}N$), C/N ratio, major and trace elemental enrichment, nature and content of iron sulfides, quartz texture, and CIA across the basin. The lower dark grey to black thinly laminated pyritic, carbonaceous fine shales (facies F1 and F2) contain up to 16.5 % TOC, $\delta^{13}C_{org}$ of -15.57‰, $\delta^{15}N$ of 12.49‰, C/N ratio of 1.50, average CIA of 68.11, Rb/K ($x10^{-3}$) and Sr/Ba ratios of 6.56 and 0.67, respectively. Relative to average shale, this unit is up to 6.27 and 3.11 times richer in Mo and Fe, respectively. This facies is dominated by organic matter produced in the water column and comprise two recognizable structured macerals (Tasmanites cysts and colonial algae cells). At least 25% of the silicate in this facies is

of early diagenetic origin, possibly derived from alteration of air-fall volcanic ash. Iron sulfides occur dominantly in form of framboidal aggregates of pyrite and as marcasite in form of lags cement and nodules. A binary mixture of OM and phosphorites with botryoidal textures is also abundant. The upper medium to light grey calcareous-siliceous silty lenticular shale (F3-F5) contain up to 2.04% TOC, $\delta^{13}C_{org}$ of -24.71‰, $\delta^{15}N$ of 4.93‰, C/N ratio of 17.62, average CIA of 74.33, Rb/K ($x10^{-3}$) and Sr/Ba ratios of 3.83 and 0.36, respectively. Relative to average shale, this unit was up to 2.65 and 0.43 times richer in Mo and Fe, respectively. The organic materials comprise disarticulated plant remains in disseminations with few amorphous macerals. At least 85% of the quartz content is of detrital origin likely sourced from the basin margins and transported to the basin by the action of bottom-hugging currents. Few iron sulfides occur predominantly in form of octa- and euhedral pyrite grains.

The data presented here suggest that the lower WHF (subunits F1 and F2) may have accumulated in a marine setting with high bioproductivity of organic carbon delivered in form of flocculated organo-minerallic aggregates (pelagic snow) onto an anoxic seabed overlain by dysoxic to oxic waters. Reduced terrigenous input, presence of phosphorites, increasing CIA and increasing $\delta^{13}C_{org}$ values with higher TOC point to a depositional setting that resulted from an interplay of sea-level highstand and climatic warm-ups. In contrast, the upper WHF (subunits F3-F5) was deposited largely under non-marine conditions with OM in company of great detrital debris sourced from terrestrial settings and transported into the basin mainly in form of fluid mud flows deposited above storm wave base. The presence various body and trace fossils, as well as the variations in bioturbation styles and intensities in subunits F3-F5, indicate that colonisation of the basin by invertebrate and vertebrate organisms is related to the different stages in the oxygenation of the sediment-water interface in an increasingly oxygenated setting.

Keywords: stable isotopic compositions, redox proxies, Rock-Eval pyrolysis, eutrophication, sea-level highstand

3.2. Introduction

This study is part of a research program on the spatial and temporal variations in the geometry and composition of the organic-rich Permian WHF in the main Karoo Basin of South Africa. As part of the overall research program, Chukwuma and Bordy (2016) investigated the variations in the geometry of the sedimentary facies in the WHF by mapping and quantifying the lithologic and sedimentologic heterogeneities within the formation. Five distinctive lithofacies were identified and differentiated. The present study examines the spatial and temporal variations in the composition of the formation. It is focused primarily on geochemical aspects, such the nature and distribution of organic carbon, isotopic compositions, and inorganic constituents, both laterally across the basin and vertically within stratigraphic sections. The objectives of the current inquiry are: (1) to quantify the variations in the distribution of organic carbon contents in the WHF in relation to its gas shale potential; and (2) to resolve the conflicting interpretations of palaeoenvironment and depositional condition, in particular, whether marine or nonmarine.

The Lower Permian WHF is one of the foremost and extensively researched rock units in the Karoo Basin (e.g., Gervais, 1864; Roger and Schwarz 1901; Broom, 1913; Du Toit, 1927; Russel, 1939), however, its lithostratigraphy (Roger and Du Toit, 1903; Du Toit, 1927; McLachlan and Anderson, 1973, 1977; Cole and Basson, 1991; Visser, 1992, 1994; Johnson et al., 1997, 2006), tectonics (Gervais, 1864; Roger and Schwarz 1901; Du Toit; 1927; Visser, 1990, 1992), and environmental conditions present at the time of its sedimentation (Russel, 1939; Visser, 1990, 1992; Anderson and McLachlan, 1979; Cole and McLachlan, 1991; 1994; Faure and Cole, 1999; Geel et al., 2015) remained an unremitting matter of controversy, with most researchers proposing a predominantly marine environment (e.g., Teichert, 1974; Kensley, 1975; McLachlan and Anderson, 1977; Anderson and McLachlan, 1979; Oelofsen, 1981, 1987; Oelofsen and Araujo, 1987; Christie, 1990; Visser, 1992, 1994), and others suggesting a non-marine, fresh- to brackish water body with no connection to the ocean (e.g., Cole and McLachlan, 1991; Veevers et al., 1994; Pickford, 1995; Faure and Cole, 1999). In particular, the reasons for production and preservation of organic matter (OM) in this rock unit have been debated in the literature and at professional gatherings. Cole and McLachlan (1991, 1994) and Faure and Cole (1999) are of the view that the presence of extensive bacterial mat provided the mechanism that generated and maintained anoxia during the deposition of the mud and OM. Anderson and McLachlan (1979), and Oelofsen (1981) postulated a stratified

water body, whereas in the view of Visser (1990, 1992) the high organic content of WHF relative to its over- and underlying strata was in response to basinal subsidence associated with phases of tectonic activity in the Cape Fold Belt (CFB), which is generally considered to be orogen to the south of the Karoo foreland basin. The latter author suggested that deepening of the Karoo foreland basin and sea-level highstand generated a unique condition for the deposition of organic-rich mud (Visser, 1992). Similarly, different studies have used elemental concentrations and ratios to establish depositional conditions during the formation of the WHF (e.g., Visser and Young, 1990; Faure and Cole, 1990; Scheffler, 2006; Geel et al., 2015) but with different interpretations. The main areas of disagreement have been whether the basin was marine or non-marine, anoxic or oxic. In this study, geochemical heterogeneities within the shale were evaluated, specifically examining parameters that have been used elsewhere (e.g., Berner and Raiswell, 1983; Dean and Arthur, 1989; Jones and Manning, 1994; Tribovillard et al., 1994; Rimmer, 2004; Jia et al., 2013) to provide insight into the environmental depositional conditions.

In spite of conflicting interpretations of its paleoenvironmental depositional conditions, most authors are unanimous in their view that the WHF is a distinctive rock unit in the overall Karoo succession, formally referred to as the Karoo Supergroup (e.g., Teichert, 1974; Visser, 1992; Faure and Cole, 1999). Apart from a notable increase in organic carbon contents of the formation with respect to the under- and overlying formations (e.g., Cole and McLachlan, 1991; Visser, 1992), other unique chemical characteristics of the WHF are: (1) white-weathering black shales; and (2) high pyrite (and other iron sulfides) and diagenetic quartz contents (e.g., Du Toit, 1927; McLachlan and Anderson, 1978; Cole and McLachlan 1991; Visser, 1992).

The recent global proliferation of unconventional hydrocarbon resources originating in organic-rich shale successions has resulted in renewed interest in the WHF- the singular rock unit with ambient qualities for gas shale exploitation in South Africa (e.g., Decker and Marot, 2012; Cole, 2014). According to US EIA (2011), over 495 trillion cubic feet (tcf) of recoverable shale gas are stacked away beneath the Karoo Basin of South Africa, with the major plays within the WHF. As a result of these developments, there is an acute need for a thorough mapping of the geochemical heterogeneity within the WHF. The characterization of spatial and temporal geochemical variability is necessitated because gas content and recovery are largely related to small-scale

changes in organic and inorganic compositions and textural properties of the reservoir units (e.g., Passey et al., 2010; Konitzer et al., 2014).

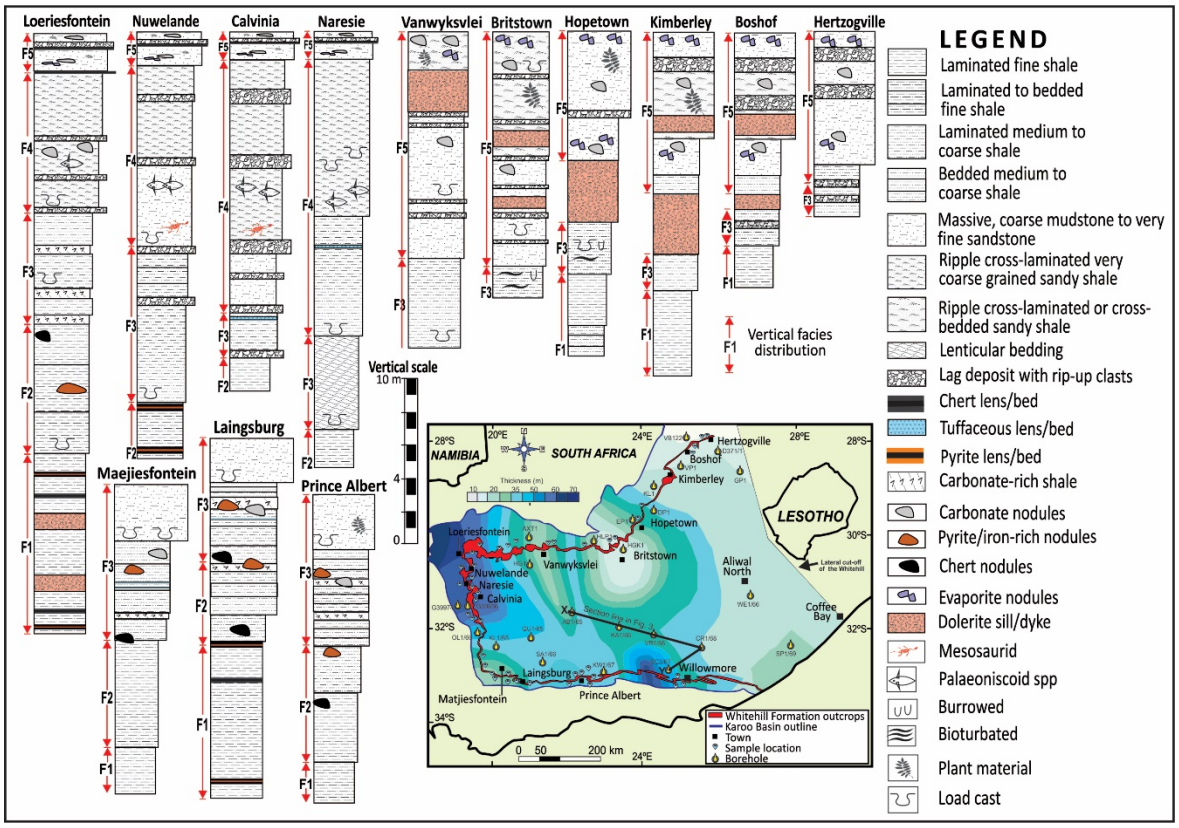

Fig. 3.1. Simplified sedimentological logs of the Whitehill Formation (WHF) measured at selected outcrop sites in the main Karoo Basin. Thickness reported are not the maximum thickness of the formation in those localities, but the maximum exposed section. For log locations and areal distribution of the WHF refer to inset map which also shows the thickness of the formation as constructed from borehole data

3.3. Samples and methods

3.3.1. Samples

The materials analysed in this study include more than 600 pieces of shale samples, field data (e.g., photographs, lithologic and geographic measurements and sketches), and over 50 borehole logs. The shale samples examined come from twelve localities along the semi-continuous exposure belt of the WHF in the main Karoo Basin (Fig. 3.1). Most the samples were recovered largely unweathered using a STIHL E-Z Core Rock Drill fitted with a Pomeroy 40x2.5 cm core barrel. The unoxidised state of the samples was later confirmed by their abundant organic matter and

pyrite contents. White to light-colored, weathered surfaces were removed by trenching (to a maximum depth of about 5 m) prior to drilling for samples. A few samples from the underlying and overlying formations were also collected for examination. The samples are designated by abbreviations related to their localities (Fig. 3.1), e.g., PAT for Prince Albert, LAG for Laingsburg, MAJ for Matjiesfontein, CAL for Calvinia, NUW for Nuwelande, LOE for Loeriesfontein, VAK for Vanwyksvlei, BTT for Britstown, STY for Strydenburg, HPT for Hopetown, and CST for Christiana. The samples have been studied recently by Chukwuma and Bordy (2016) and the description of the lithology and stratigraphy is provided.

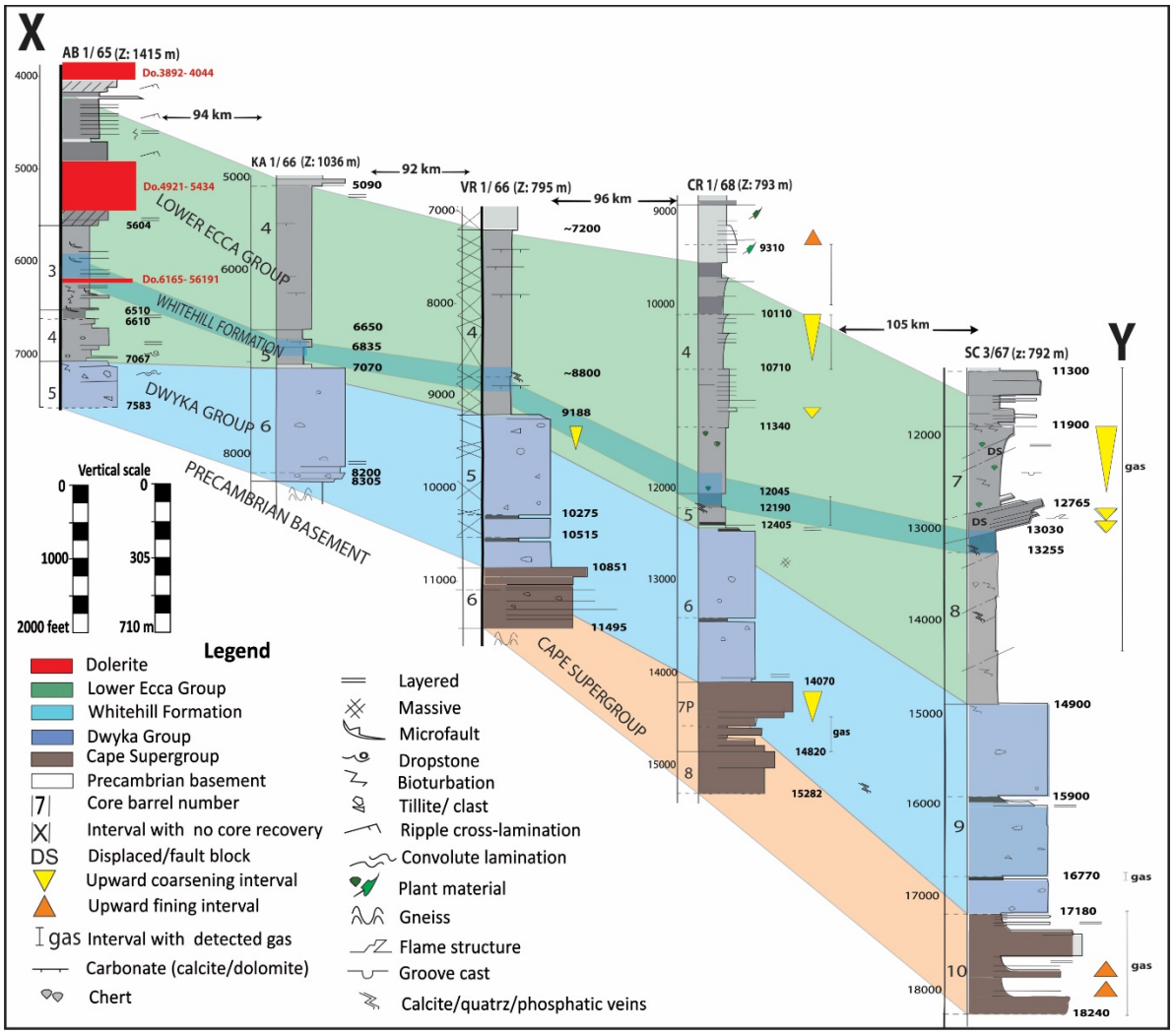

Fig. 3.2. Borehole stratigraphic logs of the lower the Ecca Group and the underlying strata in the southwestern portion of the Karoo Basin. The Karoo Basin is only about 5000 m deep and the maximum thickness of its sediment ranges between ~5500 to 6000 m. The WHF reaches a depth of about 4050 m. The Cape Supergroup pinches out beneath the Karoo Basin at about 32.5° S.

3.3.2. Methods

3.3.2.1. Elemental and organic compositions

The chemical compositions of 120 powdered samples were determined using standard X-ray Fluorescence (XRF) procedure in the Department of Geological Sciences at the University of Cape Town (UCT). Total carbon, nitrogen and sulfur as well as stable isotopic compositions of organic carbon and nitrogen were analysed for 30 selected samples using Costech Elemental Analyzer (EA) with zero-blank autosampler coupled to a ThermoFinnigan Delta Plus XL isotope ratio mass spectrometer (IRMS) at the Stable Isotope Laboratory of Iowa State University. International isotopic standards (acetanilide, caffeine, cellulose, IAEA-N2) were analysed with samples in each run. The stable isotopic compositions are reported in the conventional delta-notation with respect to the Vienna Peedee Belemnite (VPDB) standard for carbon whereas the $\delta^{15}N$ of each sample is expressed relative to atmospheric dinitrogen. Analytical reproducibility is about ±0.1‰ for both $\delta^{13}C_{org}$ and $\delta^{15}N$. The samples are low in organic sulfur (S_{org}; maximum of 2.07%), hence total sulfur (S_T) is assumed to be equal to pyritic sulfur (S_{pyr}). Rock-Eval pyrolysis was performed on 68 WHF samples and 6 samples from under- and overlying units using Rock-Eval 6 instruments, while total organic carbon was measured using an LECO CS-244 carbon analyzer. Carbon steel rings (1g, nominal carbon content of 0.8%) were used as internal standard verified against the acceptable range using a certified reference material (CRM) provided by the laboratory at the Indian Institute of Technology, Bombay. Thermal maturity (in vitrinite reflectance unit [%Ro]) was derived from T_{max} (°C) values using the method described by Jarvie et al. (2001, 2007): %Ro (calculated) = 0.0180 x T_{max} – 7.16. The calculated %Ro values were largely in agreement with those measured from the reflectance of vitrinite by previous authors (e.g., Rowsell and De Swardt, 1976, p. 107; Cole and Mclachlan, 1994; pers. comm with Dr D.I. Cole, 2016). We used the classification nomenclature for fine-grained sedimentary rocks proposed by Lazar et al. (2015). Redox terms used - oxic, dysoxic, and anoxic- are in accordance with those of Tyson and Pearson (1991); euxinic is as defined by Raiswell (1987). Diagenesis, which causes the present elemental and organic carbon concentrations in sediments to differ from those originally deposited, can cause strong geochemical bias, resulting in misinformation (e.g., Calvert and Pederson, 1993; Meyers, 1997). In this study, the effect of diagenetic alteration on geochemical proxies is compensated by the use of multiple geochemical indicators, thereby improving interpretations.

3.3.2.2. FE-SEM sample preparation and limitations

One hundred-and-forty-eight (148) pieces of whole rock with diameters of less than 10 cm provided sample base for optical petrographic and field emission scanning electron microscopy studies. A set these samples were prepared into thin slabs, while another set was prepared into 2x3 cm uncovered ultrathin sections (UTS; 10-20 µm thick). Prior to sectioning, the samples were impregnated with a mixture of low viscosity epoxy-resin and hardener in order to minimise mechanical impact. Hardening was performed at a moderate temperature (< 60 °C) and for a few minutes to avoid altering fine details of the organic macerals within the samples. Two sets of thin sections, one oriented perpendicular and the other parallel to bedding-plane, were ground using successive finer abrasives and then air-polished with fine (0.05 µm) silicon powder. Images of the slabs were captured under variable light imaging using Panasonic Lumix-TZ60 digital camera at x5, x10 and x20 magnifications. The slabs and UTS were also observed under the conventional petrographic microscope in both reflected and transmitted polarised light at the in the Department of Geological Sciences at the UCT. Lightly carbon/diamond-coated UTS were examined with a Zeiss MERLIN field emission scanning microscope (FE-SEM) at the Stellenbosch University Central Analytical Facilities under secondary electron (SE1), back-scattered electron (BSE), and cathodoluminescence (CL) detector. Cryo-energy-dispersive X-ray detector (cryo-EDS) provided identification and characterization of components. A swath of 10 images was captured at 20-10 µm horizontal field width, corresponding to machine magnification of 15 000x to 10 000x and pixel resolution of 20 nm/pixel and 10 nm/pixel using both SE and BSED detectors. Over 200 point counts were made to establish and quantify the overall abundance, nature, and distribution structured and amorphous OM, and mineral matrix and pores within the shale matrix. In order to avoid nonrepresentation, samples analysed were uniformly selected, however, preference was given to samples from intervals with higher organic carbon contents so that sufficient organic particles and macerals can be imaged for comparison. A subset of the samples was solvent extracted using the method of Radke et al. (1986) in order to differentiate bitumen from kerogen, using a solvent mixture comprised of 90% dichloromethane and 10% methanol in the Chemistry Department at the University of Cape Town for 68 hours. The samples were air-dried and subsequently prepared into UTS and FE-SEM imaged. All samples for FE-SEM studies were observed on surfaces both perpendicular and parallel to bedding.

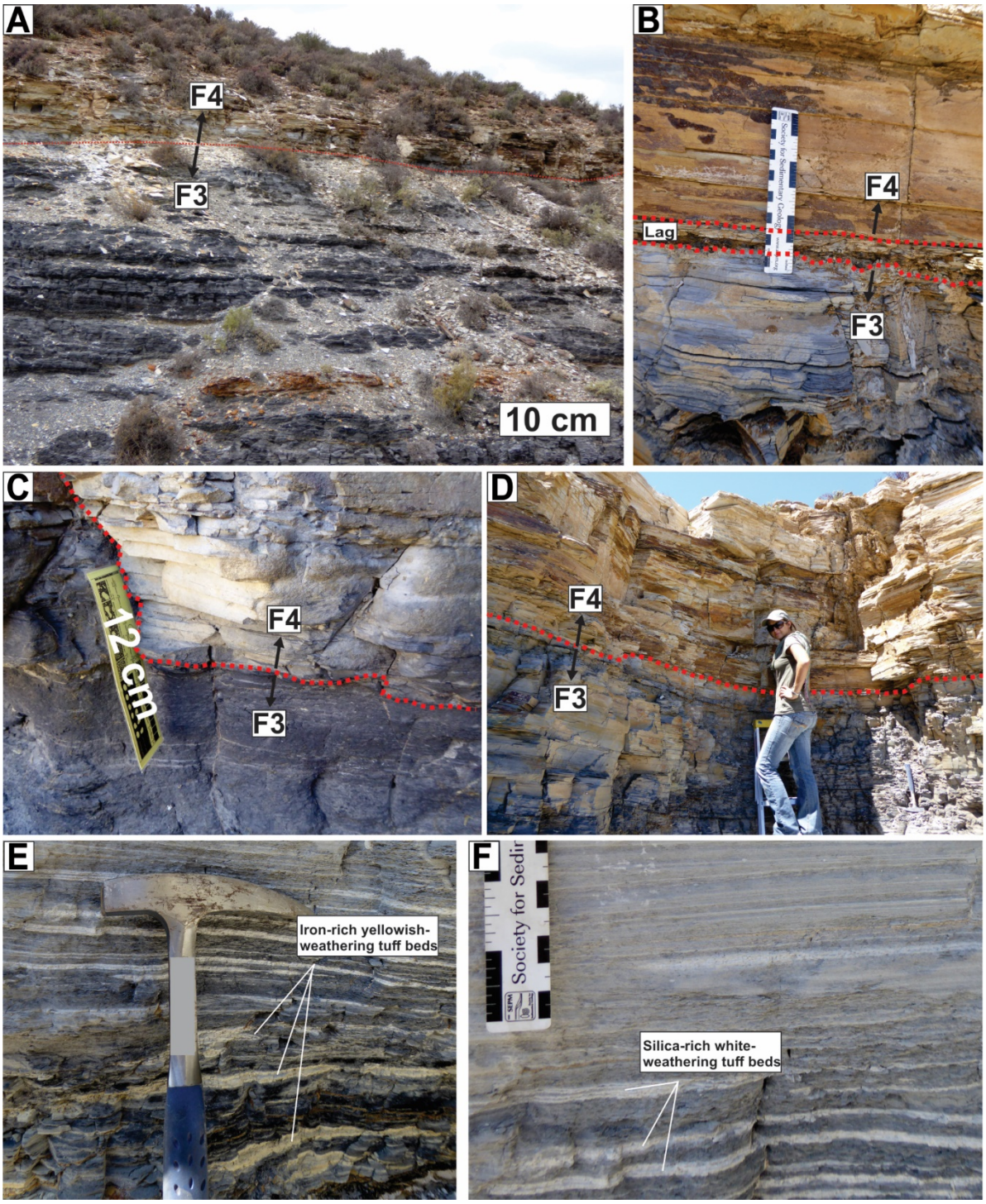

Fig. 3.3. **A-D**: Outcrop images of the contacts between the facies of the Whitehill Formation. **E** and **F:** Well-defined tuffaceous layers in the upper section of the Whitehill Formation. E shows yellowish-weathering of organic matter- and iron-sulfide-rich tuffaceous layers while the tuffaceous material in F is organic-matter poor, silica-richer and weathers white to light grey.

3.3.2.3. FE-SEM identification of sample constituents

The composition of samples, including mineralogy, OM, grain/crystal and their boundaries were distinguished using back-scattered electron detector (BSE), which has the ability to record variations in composition using the mean atomic number. Material with a low atomic number such as carbon exhibit low BSE intensity and are scaled as darker regions; whereas a material with higher mean atomic number exhibit high BSE intensity and are scaled lighter region. Energy-dispersive X-ray point measurements and mapping of larger areas taken across multiple images allowed identification of various minerals matrix, grain/crystals (Fig. 3.6).

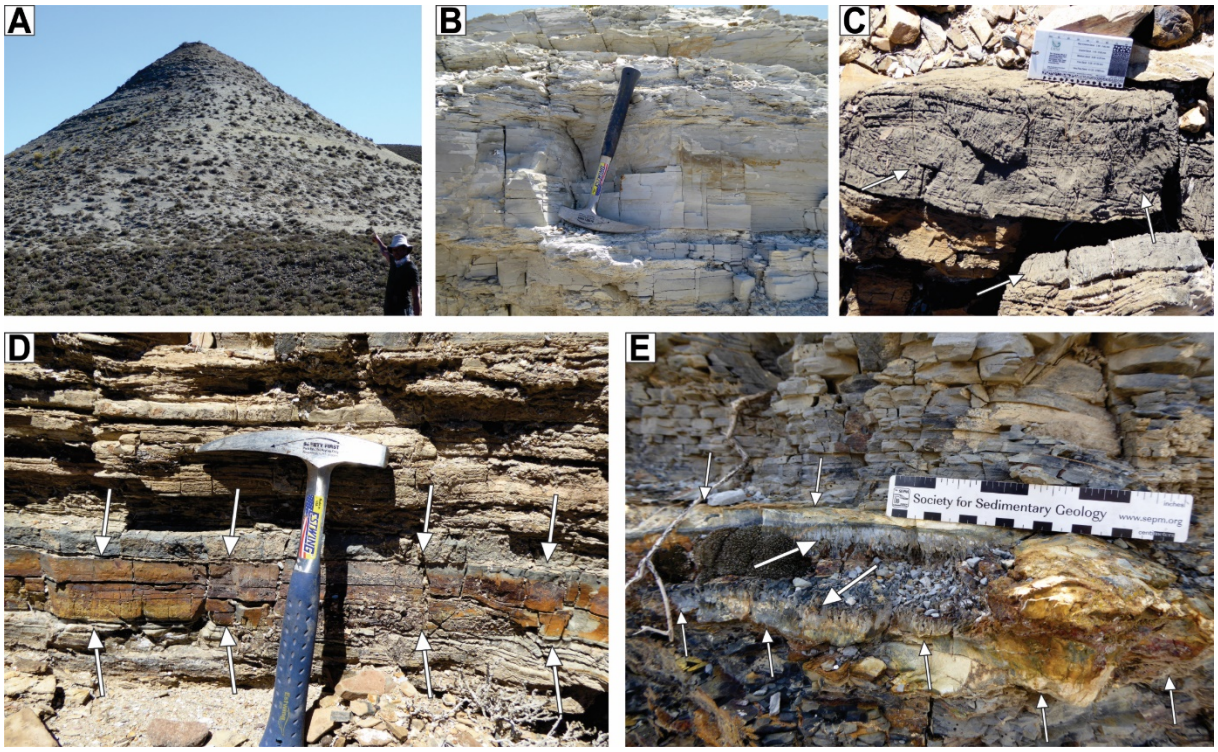

Fig. 3.4. Outcrop images that summarise some stratigraphic characteristics of the Whitehill Formation. **A-B**: A hill exposure showing white-weathering Whitehill Formation. Little white hills of the weathered Whitehill Formation are common in the central areas of Karoo Basin and earned the formation its famous name "Whitehill". The hills are mostly capped by dolerite which make them relatively stable and resistant. **C:** Dolomitic beds and nodules are common in the Whitehill Formation, particular at the F2-F3 boundary. The black color of the dolomite is due to the presence of OM (see text for details). **D-E**: Large amounts of iron sulfides accumulation (mostly in form of marcasite) at the boundary between F2 and F3 in form of a sequence boundary lag (up to 6 cm thick, in between arrows in D) with marcasite cement and nodules in stratiform horizon (E). Observe differential compaction indicating early diagenetic origin of these nodules. Rims of large bladed marcasite (the bigger arrows in E) are partly reddish due to oxidation. See text for details. For scale: the sedimentary field ruler in C is 10 cm.

3.4. Borehole logs and data

Borehole logs and other data (lithologic description, sketches, and reports) from the Karoo borehole database were made available for this study by Dr D.I. Cole of South African Council for Geoscience (CGS), Bellville. Data on newer boreholes that are not yet included on the CGS database, including those of the recent Karoo Research Initiative (KARIN) Drilling Project at Ceres were accessed online at KARIN's web page. Borehole data were used to constrain additional details of the WHF, particularly thickness and depth-to-surface variations. These data were valuable and complemented outcrop data especially in localities where outcrops are poorly exposed. The measured sections of the WHF in the boreholes were digitised using vector-based graphics software (CorelDraw®) and integrated with outcrop data (see Appendix 3.1).

3.5. Results

3.5.1. Stratigraphic and lithologic framework

Based on lithologic and stratigraphic characteristics, a related study (Chukwuma and Bordy, 2016) identified five lithofacies unit (Fig. 3.1): (1) black pyritic shale, F1; (2) black-dark grey carbonaceous shale, F2; (3) dark-light grey calcareous shale, F3; (4) medium-light gray siliceous-calcareous silty shale, F4; and (5) light grey siliceous massive-looking sandy shale, F5. The contacts of the first three facies are largely transitional, indicating no break in deposition. The most distinctive feature of these intervals is prominent laminations, although samples from localities closer to the Cape Fold Belt show progressive obliteration of this primary sedimentary feature. The laminae are largely undisturbed and uniform, without any lenticular aspect, thus showing the complete absence of foraging and burrowing bottom-dwellers and any bottom current, except the upper part of the formation, in the last three facies (F3-F5) where some trails of a worm-like organism were observed (Fig. 3.5).

In the southern part of the basin, up to latitude 32°12' S, the WHF is comprised only F1-F3, however, north of this latitude, F4 and F5 are detected. This latitude roughly coincides with the zone in the basin (north of latitude 32°30' S; Viljoen, 1994) where the formation overlying the WHF changed from the Collingham Formation to Tierberg Formation. The contact between F3 and F4 is marked by thin (<2 cm) calcitic/dolomitic lags and in places by an erosional surface, indicating a possible winnowing (Fig 3.3A-D). The contact between F4 and F5 is transitional and

sometimes marked by a change from thickly laminated/thinly bedded F4 to more massive F5. The thickness of F4 and F5 increases northward up to the area between Vanwykvlei and Hopetown and then decreases sharply further north. Both facies contain diminutive cross-laminations, ripple marks, slump structures, inverse grading and loadcasts (Fig. 3.5; Chukwuma and Bordy, 2016), which were described by Cole and McLachlan,(1991, 1994) and Visser (1992). Some of the laminae appeared disturbed and with some lenticular aspects. Invertebrate burrows (e.g., worm trails, *Planolities*; Fig. 3.5) were observed in Loeriesfontein and Britstown localities.

3.5.2. Basinal distribution of stratigraphy and lithology

Outcrop data were used to construct the distribution of lithostratigraphic units of the WHF across the basin (Fig. 3.1), while borehole data (summarised in Appendix 3.1) aided the generation of the thickness variation map for the WHF (see the inset in Fig. 3.1). From these data, the WHF is deepest in the southwestern part, where it reaches a depth of about 5043 m (Fig. 3.2). Borehole data also indicated that the Cape Supergroup pinches out beneath the Karoo Basin at about 32.5 °S in borehole VR1/66. Although borehole data allowed fine-scale reconstruction of thickness variations, facies differentiation benefitted largely from outcrop, hand specimens, and thin section observations as well as geochemical analyses of outcrop samples. Lithologic descriptions from the original borehole logs were limited and could not allow the establishment of facies boundaries.

3.5.3. Elemental and mineralogic compositions

3.5.3.1. Elemental Composition

The average chemical composition of the shales was calculated from the XRF results of 120 powdered samples selected from the five stratigraphic intervals (Table 3.1). Mineralogic identification and quantification were based on SEM-imaging and EDS analyses of 148 representative thin sections. The results of the two datasets show that the mineralogic and elemental compositions of the five facies are similar but with a wide difference in their concentrations. Silicates (majorly quartz), phyllosilicates (majorly clay, minor mica and biotite), carbonates (dolomite and calcite), and pyrite (and other iron sulfides) were the principal constituents, whereas phosphates (apatite), gypsum, and metal (Ba, Ti) oxides were in lesser proportions.

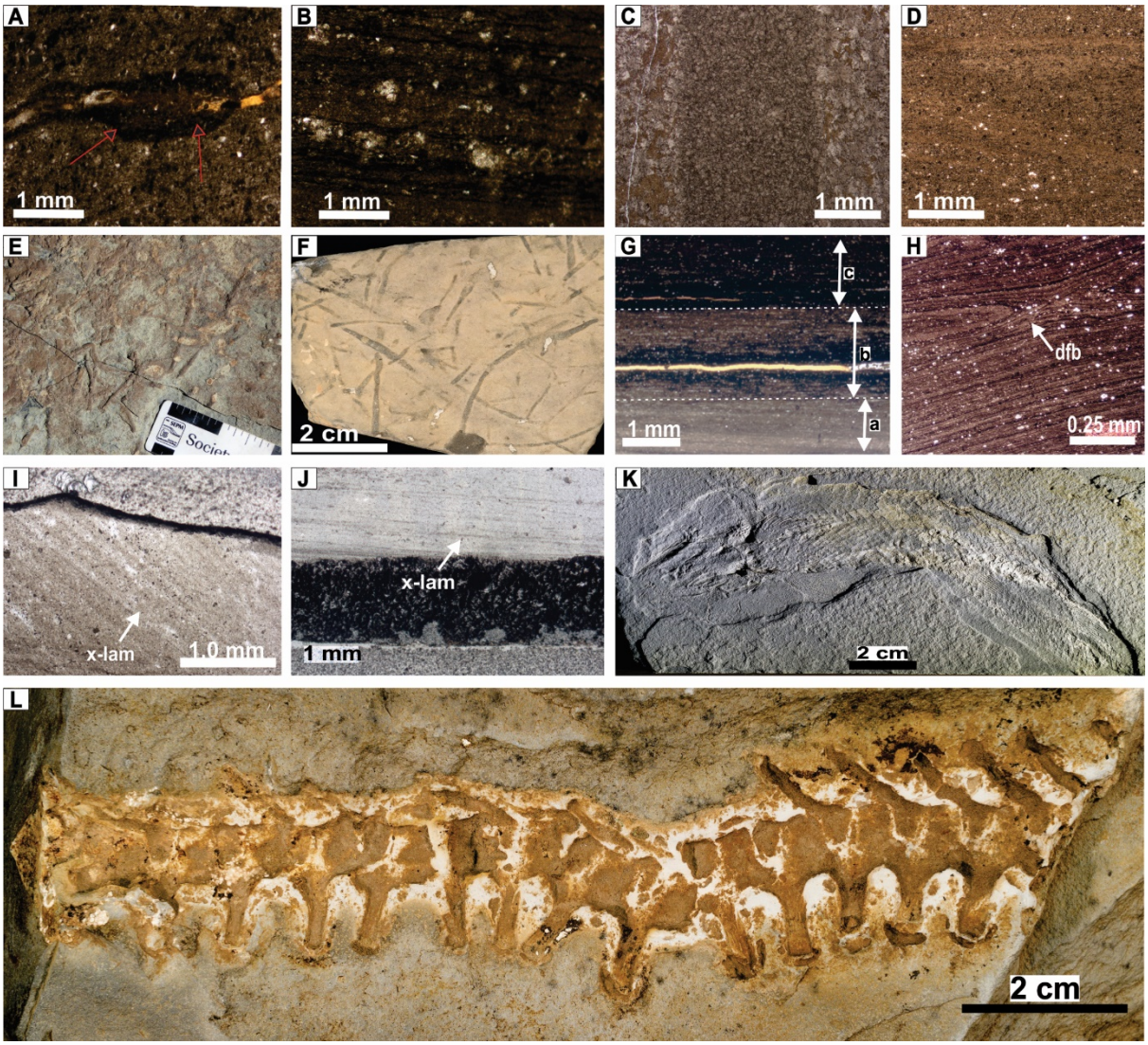

Fig. 3.5. Images that summarise the sedimentologic features of the upper (F3-F5) facies. **A**: Photomicrograph showing oxidised piece of woody material (arrow) in Hopetown. **B**: Photomicrograph of abundant dolomite nodules overprinting the original shale texture. **C:** vertical burrow (darker band) in F3. **D**: Bioturbation (BI=3) in some beds in Britstown. **E & F**: Trace fossils are common in the in middle WHF (near Britstwons and Nuwelande respectively; F3). **G**: Photomicrograph of triplet feature. Note the gradual increase in clay content (darker laminae). **H**: Photomicrographs of diffused bedding (dfb) and concave upward geometries. **I-J:** Diminutive ripple marks on a surface of F4 in Vanwyksvlei. **K**: Body fossil of palaeoniscid fish found in F4 near Nuwelande. **L:** Body fossil of mesosaurid reptile (dorsal spine) found in F4 near of Calvinia. Mesosaurids were endemic to SW Gondwana in the Early Permian.

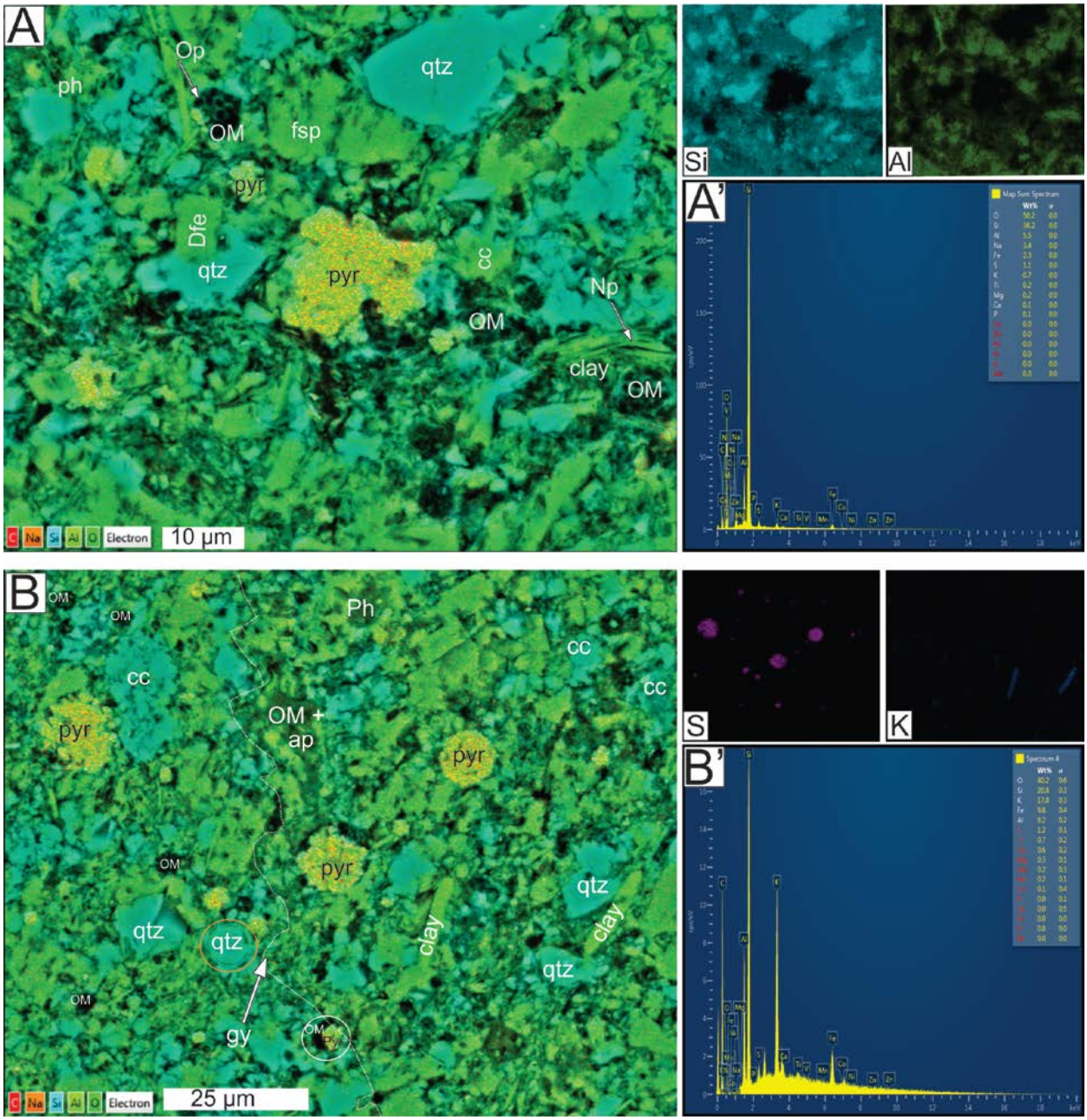

Fig 3.6. A-B: Back-scattered electron microscope images shale matrix and its constituents. Organic matter (OM) appears dark, mineral grains takes various light colors and shades of grey (see color legend at the base of the image). Ferroan dolomite (dfe), Feldspar (fsp), Quartz (qtz), Phosphate peloids (ph), organic pores (Op) and nonorganic pores (Np). A white dashed line in B emphasises a sinuous microchannel infilled with bitumen and gypsum (gy). **A'-B'**: EDS analyses.

3.5.3.2. Mineralogic composition

Silicates comprise about 60% of the bulk rock. Quartz (in form of single grain) is the chief component but significant amounts of chert and chalcedony were also present. Silicates occurred in two major forms: (1) as partial to complete replacement of certain microfossils (e.g., Tasmanites cysts and colonial algae cells; Fig. 3.8C) and other similar pores, and (2) as disseminated individual euhedral grains (Fig. 3.6). The former are of diagenetic origin - precipitated during early diagenesis, and occur mainly in F1 and F2 where they constitute at least 25% of the quartz budget. The latter constitutes close to 100% of the quartz budget in F3-F5 and about 50% in F1 and F2. BSE- and CL-SEM image analyses (Fig. 3.9) were useful in distinguishing the low temperature early diagenetic quartz grains from their detrital counterparts. Diagenetic quartz grains are finer-grained (>5-32 μm) and show irregular outline with embayments. They also show lobate-pointed grain edges, inclusions of pyrite, apatite, and OM, and growth zones (indicating successive developments of crystals - Fig. 3.9D). The detrital quartz grains are coarser (up to 64 μm) and show angular to rounded outlines (Fig. 3.9D'). On CL-SEM, diagenetic quartz grains showed weak and highly variable to none CL-SEM luminescence while their detrital equivalents showed strong and uniformly bright CL-SEM luminescence (Fig. 3.9).

Phyllosilicates (majorly clay minerals) comprise about 16% of the bulk rock. Smectite, illite, and chlorite were the chief components, while mica and biotite were minor. As expected, a steady increase from mixed-layer clays (MLC) containing smectite to mixed-layer clays containing illite and chlorite were documented with increasing proximity to the Cape Fold Belt. Textural features of the clays such as piercing, grains abutting against each other indicate compaction pressure (Fig. 3.7D-E) and were interpreted as diagnostic of detrital origin whereas finer-grained clays were seen bridging other shale components indicate diagenetic origin. Exfoliation observed in some mica indicate a detrital origin (Fig. 3.9D-E).

Iron sulfides (chiefly as pyrite) comprise up to 12% of the bulk rock and occurred various forms and majorly in F1 and F2. The two most common forms are: (1) partial to complete replacement of certain microfossils (colonial algae, few Tasmanites cysts, and similar pores) and (2) disseminated individual euhedral grains and framboidal/polyframboidal (bacterial) aggregates (Fig. 3.7A-C). Concretions (marcasitic) and thin laminae/lags cemented with marcasite were also

documented (Fig. 3.4E-F). Disseminated euhedral pyrite preferentially occur along bedding-planes (arrowed in Fig. 3.6B), while replacement pyrite and framboidal aggregates are disseminated within the shale matrix. In F3-F5, euhedral pyrite grains are rare and no framboidal aggregates were documented.

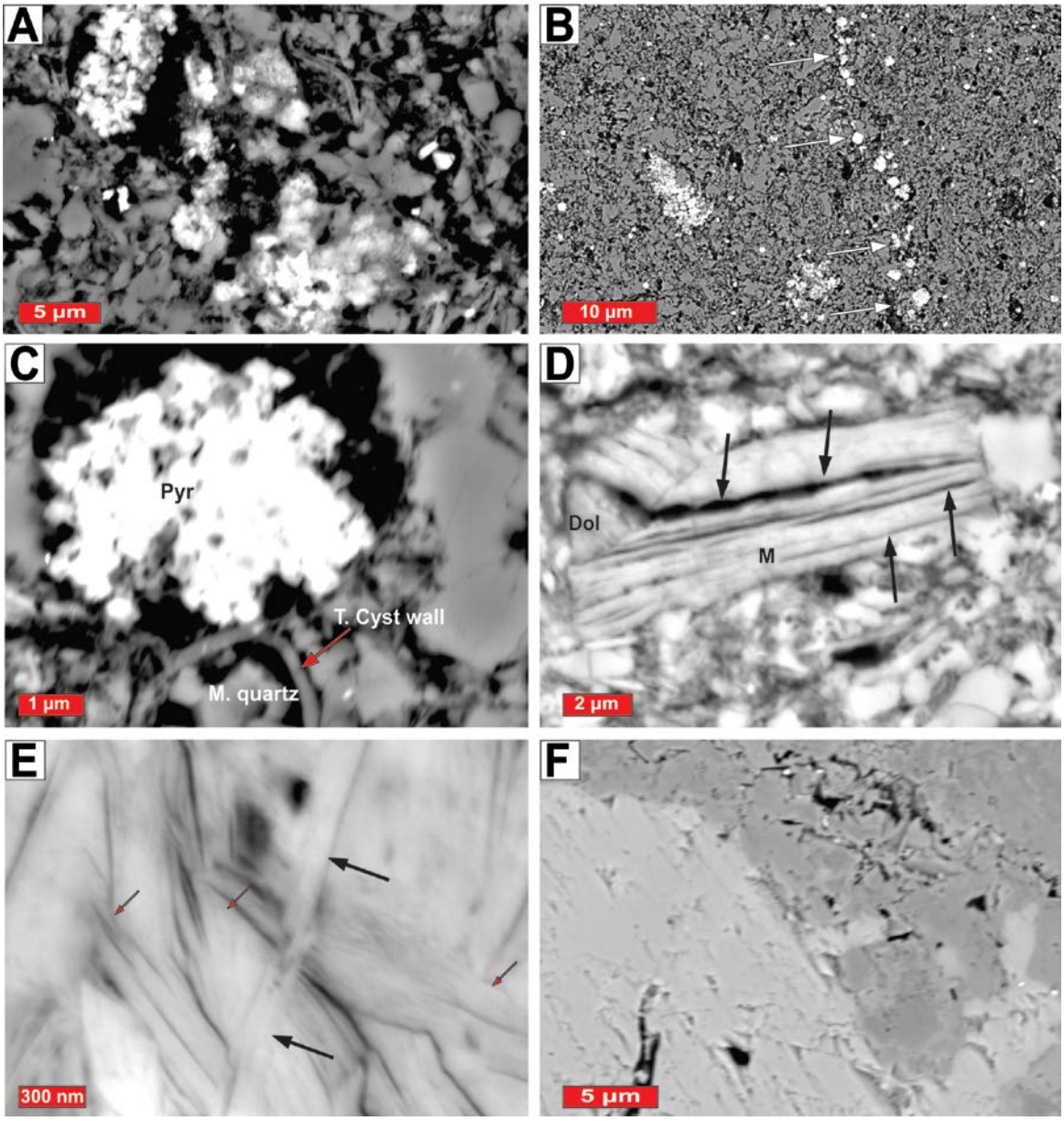

Fig. 3.7. Scanning electron microscope images of typical textures of major minerals and other matrix constituents in the WHF. **A-C**: various textures of pyrite (pyr) grains. **D-E**: Phyllosilicate textures. **F**: Zoned dolomite grain. T. cysts = Tasmanites cysts, m.quartz = microquartz, Dol = dolomite, M = mica. See text for details.

Carbonates (dolomite and calcite) comprised about 10% of the bulk rock and occurred in three forms: (1) as disseminated individual euhedral grains (Fig. 3.6); (2) as well-defined laminae (lenses, beds); and (3) as nodules (Fig. 3.4D). Carbonate grains within the organic-rich F1 and F2 were darker in color (due to associated OM) than those in organic-lean F3-F5. Some grains show color zonation indicating variations in iron content (Fig. 3.7F). Carbonate laminae were also reported in the F2-F3 boundary and were associated with primary gypsum crystal and lenticles common in Laingsburg, Nuwelande, Loeriesfontein, and Boshof localities. Dolomitic nodules were largely confined to F2. They are usually black in color and contain carbon-rich micro-laminations with gypsum crystals in between laminae. In addition to gypsum, which occurred mainly in association with carbonates, other minor constituents of the WHF include phosphorites and tuffaceous material/laminae. The phosphorites in WHF occur mainly in F2 and are closely associated with OM (Fig. 3.8E-F). EDS analyses indicate that they are made up of phosphorus, calcium, oxygen, and fluorine, indicating that the mineral is likely apatite (ap). This apatite has a botryoidal texture, suggesting its origin was associated with microbial processes. The large amount of fluorine required to effect the deposition of these phosphates (e.g., Strydom, 1950) were likely derived from air-borne volcanic ash (Visser, 1992; Viljoen, 1994). The latter occurred as disseminated volcaniclastic particles (e.g., glass shards) as well as in well-defined thin (up to 5 cm) laminae (Fig. 3.3E-F). These well-defined tuffaceous beds were only documented in F3-F5 and increased in both concentration and thickness in the central areas of the basin (Calvinia-Loeriesfontein).

3.5.4. Elemental enrichments and ratios

A common approach used by several workers (e.g., Calvert and Pederson, 1993; Rimmer, 2004; Brumsack, 2006) for evaluating elemental enrichment in modern and ancient sediments involves normalization of each elemental content to Al and then compare the ratio to that of an ‘average shale’ (AS; Wedepohl, 1971). Normalisation compensates for the influence of post-depositional processes and usually, Al is used because it is considered a conservative major element that is not significantly affected by early diagenetic processes and redox effects (Pederson and Calvert, 1993). The enrichment or depletion of each element relative to AS was calculated as follows (Brumsack, 1989; Piper and Perkins, 2004; Rimmer, 2004):

$$\text{Enrichment Factor (EF)} = (\text{element/Al})_{\text{sample}} / (\text{element/Al})_{\text{average shale}} \quad (3.1)$$

Based on EF values,
the magnitude of elemental enrichments within the five facies differed, with the order of enrichment relative to AS being: Mo>Pb>Cr>Th>Ba>Rb>Zr>Co>V>Nb>Y>Cu>Sr>Zn>Mn>Ni and Fe>Si>Na>P>K>Ti>Mg>Ca, for minor and major elements, respectively (Fig. 3.14; Table 3.2). F1 and F2 show the highest enrichment while F4 and F5 only show the lowest enrichment for most of the elements analysed. The enrichment of the shales relative to average black shale (Vine and Tourtelot, 1970), average South Africa shale (Danchin, 1970; Hofmeyer, 1971), and average Ecca shale (Danchin, 1970) was also calculated (Fig. 3.14; Table 3.2). Within the five facies, variations in elemental enrichment were most significant for Zn, Cu, and Co as well as Fe, Si, Na, and P. The enrichment patterns of Fe and P were similar (both peaked in F2). The enrichment of Ti and K varied in opposite directions (that is, negative covariation) such that the facies with higher contents of Ti had lower contents of K and vice versa. From F1 to F5, Mo concentrations decreased progressively while Si increased. Ni and Mn are significantly depleted in all facies while the concentration of V, Nb, Zr, Y, Rb, and Th in all five facies were relatively uniform.

3.5.5. Terrigenous influx

Al, Si, Ti, Th, and Zr are widely applied indicators of terrigenous influx (Arthur et al., 1985; Rimmer, 2004; Tribovillard et al., 2006). Ti occurs mainly in biogenic clay and heavy minerals (Kidder and Erwin, 2001), while Si occurs in both detrital and biogenic components (Schieber, 1996). Si/Al (that is, quartz to clay) ratio and Ti/Al ratio are widely applied detrital influx proxy (e.g., Rimmer, 2004; Scheffler et al., 2006), however where silica has been produced by post-depositional processes (diagenetic or biogenic), the Si/Al ratios are largely unreliable. The Ti/Al (Fig. 3.11; 3.13E) for the samples studied showed a general increase from F1 to F5, indicating a progressive increase in the detrital component from F1 to F5. The Al-normalized concentrations of K and Ti (Fig. 3.14) showed a similar trend, suggesting a general increase in detrital input from F1 to F5.

3.5.6. Redox flux

Molybdenum (Mo) content is considered as one of the most diagnostic indicators of anoxic conditions (e.g. Calvert and Pederson, 1993; Dean et al., 1997; Francois, 1998; Rimmer, 2004). According to these authors, modern sediments, such as the Black Sea sediments, deposited under reducing conditions are enriched in Mo relative to AS. All five lithofacies are enriched in Mo relative to AS. However, a notable progressive decrease in Mo was recorded from up to 14.43 ppm in F1 to less than 5.0 ppm in F5 (Table 3.1; 3.2; Fig. 3.11). This suggests a general decrease in redox condition from F1 to F5. Trace element ratios such as Ni/Co, V/Cr, V/(V+Ni) and Rb/K, are widely applied redox proxies (e.g., Ernst, 1970; Lewan, 1984; Jones and Manning, 1994; Piper, 1994; Rimmer, 2004; Scheffler et al., 2006). However, no relationship exist between the majority of these proxies and OM content (e.g. Scheffler et al., 2006). In addition, Ni concentrations in the shales were largely below the detection limit of the instrument used (< 5 ppm). As a result, the majority of these redox ratios were not applied in this study. Rb/K ratios provide an indication of fluctuations in palaeosalinity and are reported to be higher in marine shales (6.0×10^{-3}) than those in non-marine shales (4.0×10^{-3}). Rb/K of the samples ranges between 6.39×10^{-3} and 3.03×10^{-3} (Table 3.1). It decreased from F1 (average of 6.15×10^{-3}) to F5 (average of 4.05×10^{-3}).

The sharp difference in the geochemical properties between Sr and Ba makes the Sr/Ba ratio a good indicator of palaeosalinity where higher ratios indicate higher salinity, whereas lower ratios signal lower salinity (e.g., Jia et al., 2013 and references therein). The relative decrease in Sr/Ba ratios from F1 to F5 (Fig. 3.11; Table 3.1) are indicative of decreasing water salinity during the deposition of the WHF.

3.5.7. Organic carbon compositions

The Rock-Eval procedure is the most basic geochemical method for obtaining information on the amounts and types as well as thermal maturation of OM contained in sediments (Espitalié et al., 1985; Peters, 1986; Peters and Cassa, 1994). The results of Rock-Eval analyses and TOC measurements for the samples are shown in Table 3.3 and Fig. 3.10. TOC ranged between 0.72 and 16.5 wt.% (average of 5.15 ± 3.84 wt.% calculated from 48 samples). The pyrolysis S1, S2, and S3 were variable and ranged between <1.0-7.83 mg HC/g rock, 1.0-38.09 mg HC/g rock, and >1.0-3.0 mg CO_2/g rock, respectively. Hydrogen-index (HI) and Oxygen-index (OI) ranged

between 1.0-530.5 mg HC/g TOC and 1.0-425 mg CO_2/g TOC, respectively. Pyrolysis T_{max} ranged between <410 ˚C and 607 ˚C. On both HI versus OI (Peters, 1986) and HI versus T_{max} (Gorin and Feist-Burkhardt, 1990) pyrograms (Fig. 3.10), F1 and F2 plotted largely on Type II (with a few points on Type I and III) OM, while F3 and F4 plotted on Type III (with few scatter on Type II) OM. Type I and II OM are aquatic in origin and derived from aquatic matter, such as Tasmanites and *Botryococcus*, and other phyto- and zooplanktons. Type III is terrestrial OM sourced from higher land plants (Tissot and Welte, 1984). The Rock-eval data reported here are largely agreement with those of earlier investigators (e.g., Rowsell and De Swardt, 1976 [TOC range: 1.37-8.57 wt. %]; Cole and McLachlan, 1994 [TOC range: 0.44-14.75 wt.%]). However HI values for this study are slightly lower and the T_{max} values are higher than those of the Cole and McLachlan (1991; Appendix 3.2). This trend is expected because while samples for this study were taken across the entire basin (including the areas closer to the CFB where the shales are in the overmature stage), the samples studied by the previous authors were only taken from the relatively less mature area in the northern part of the basin between Hopetown and Hertzogville.

Within the five stratigraphic subunits of the WHF, organic carbon contents and other Rock-Eval data differed. The highest TOC was observed in F2, where TOC typically ranges between 4.2 and 16.5 wt.%. TOC spikes were recorded in few thin intervals within F2 in Loeriesfontein and Strydenburg areas. Apart from these spikes, there was a general upward increase in TOC from F1 to F2. However, TOC progressively declined from F3 to F4 with increasing silt and fine-sand contents. TOC in F3 range between about 1 and 3 wt.%. There is no distinct pattern to TOC distribution in F3 and F4, however, an outlier with TOC of 2.17 wt.% was recorded in Nuwelande for F4. The shale of F4 are generally light grey and silty; only a few samples were analyzed based on its obvious light color and high silt content, which were interpreted to mean poor organic contents. No sample from F5 was analysed for TOC because of its light color and high silt to fine-sand contents.

Organic particles (macerals) were observed in the WHF using FE-SEM and occurred in two forms: structured and amorphous matters. Identification of structured macerals was majorly based on the retained morphological features of the original organisms, and to a lesser extent, on inter-grain relationships between maceral and the other constituents of the shale matrix. Two structured macerals were identified: Tasmanites cysts and colonial algae cells (Fig. 3.8A-D). Tasmanites

cysts were identified based on their spherical to oval shape, thick cell walls, and textural features of their infilled materials (Fig. 3.8C; Tappan, 1980; Schieber, 1996; Telnova, 2012). Tasmanites is considered a cyst stage (phycomata) of a fossil algae with affinity to prasinophyta (i.e., modern planktonic green alga; Tappan, 1980; Schieber, 1996; Telnova, 2012). Colonial algae were identified based on their spherical to oval shape, thin cell wall, and their occurrence in clusters of closely associated cells (Fig. 3.8D). Both the Tasmanites cysts and the colonial algae cells occurred in F1 and F2, although a few remnants (poorly preserved) of colonial algae cells were documented in F3. A closer examination suggests that the colonial algae in F3 occurred in intraclast, and was likely those ripped from F2. These structured macerals constituted only a small fraction of the organic particles in the WHF, while the majority comprised amorphous OM, which are the unstructured organic particles disseminated within the shale matrix (e.g., Teerman et al., 1995) and are considered to have been derived from structured OM via bacterial degradation and biochemical alteration associated with compaction and burial diagenesis.

Organic macerals (structured and amorphous) occurred in two forms: (1) as disseminated particles throughout the shale matrix and closely aggregated with mineral grains in form of organo-mineral aggregates; and (2) as discrete laminae and organic domains with little mineral grains (Fig. 3.8A-B). The latter occurred mainly as elongated, wavy and discontinuous laminae composed of clusters of filamentous colonial algal cells, described here as lamalginites and as algal mats by previous authors (e.g., Cole and McLachlan, 1991; Faure and Cole, 1999; Fig. 3.8A-B).

3.5.8. Productivity flux and isotopic compositions

Most of the OM in sediments comes from biological productivity by autochthonous organisms, particularly phytoplankton (single-celled algae that reside in the euphotic zone). In addition to sunlight, the major limiting factor to planktonic productivity is the availability of mineral nutrients (phosphorus, nitrogen, barium, iron). Phosphorus (P) is the vital nutrient for growth of algae and its contents in organic-rich shales are linked to primary palaeoproductivity (e.g., Schoepfer et al., 2015). The presence of algae-derived OM in the WHF is revealed by SEM and Rock-Eval data. The majority of the OM were of Type II which is largely algae-derived. Within the shales, P contents are significantly enriched in F1 and F2 but depleted in F3-F5, relative to AS (Fig. 3.14; Table 3.1). P contents peaked in F2 (up to 1017 ppm) indicating highest level biological productivity. Barium (Ba) has also been used as a diagnostic indicator of palaeoproductivity (e.g.,

Brumsack, 2006). All the five lithofacies are enriched in Ba relative to AS indicating higher bioproductivity relative to AS (Fig. 3.14).

The $\delta^{13}C_{org}$ and $\delta^{15}N$ values, and C/N ratios for the shales are as summarised in Table 3.1 and Fig. 3.11. The $\delta^{13}C_{org}$ and $\delta^{15}N$ values ranged between -15.75 and -24.71‰ and 3.04 and 12.49 ‰, respectively, while C/N ratios ranged between 0.32 and 43.7. The $\delta^{13}C_{org}$ values for this study largely agree with those of Faure and Cole (1999) and Geel et al. (2015), which ranged between -24.1 and -18.5‰ and -18.9 and -24.7‰, respectively. The $\delta^{15}N$ values of the shales also concurred with those of the previous authors (7.7-10.1‰). F2 has the highest enrichments in $\delta^{13}C_{org}$ and $\delta^{15}N$, which ranged between -15.57 and -22.32‰ (average of -18.91‰) and 7.55 and 12.49‰ (average of 10.49‰), respectively and lowest C/N ratios that ranged between 2.48 and 0.77 (average of 1.50). F4 has the least enrichments with $\delta^{13}C_{org}$ values that ranged between -20.94 and -24.71‰ (average of -22.42‰) and $\delta^{15}N$ values that ranged between 3.04 and 6.15‰ (average of 4.93‰) but highest C/N ratios that ranged between 43.70 and 4.83 (average of 17.63).

3.5.9. Carbon-sulfur (C-S) relationships

The relationships between organic carbon and pyritic sulfur are few of the earliest and widely applied approaches for distinguishing depositional environments (e.g., Kaplan et al., 1863; Berner, 1967; 1984; Raiswell and Berner, 1983; Anderson et al., 1987; Ripley et al., 1990; Rimmer, 2004). According to Berner and Raiswell (1983), a cross-plot of S_{pyr} (in this study, the same as total sulfur, S_T) and C_{org} (TOC) for sediments deposited under anoxic to euxinic conditions usually show no positive correlation but with a positive (non-zero) sulfur intercept. Conversely, sediments deposited under oxygenated conditions show a positive correlation between S_{pyr} and TOC but with a zero intercept on a cross plot of the two variables. Significant differences were seen in the C/S ratios and C-S cross plot for the five stratigraphic subunits of the WHF (Fig. 3.12). F1 shows no correlation between carbon and sulfur. The correlation coefficient (r) for C_{org} versus S_T is 0.443 (n = 24). Using the methods outlined by Hair et al. (2006), only correlation coefficients greater than 0.488 are significant at the 1% level. Although a large scatter exist in the dataset, a linear regression line drawn through the data intercepted the sulfur axis at about 1.28. In F2, the correlation coefficient (r) for C_{org} versus S_T is 0.594, which is significant at 1% level, indicating that a positive correlation exists between organic carbon and sulfur. However, a low but positive sulfur intercept of about 0.2 also exist. The regression lines for C_{org} versus S_T in both F3 and F4 have a zero sulfur

intercept, however, the coefficient of correlation (r) for C_{org} versus S_T in F3 is 0.331, indicating that no significant correlation exists between C_{org} and S_T.

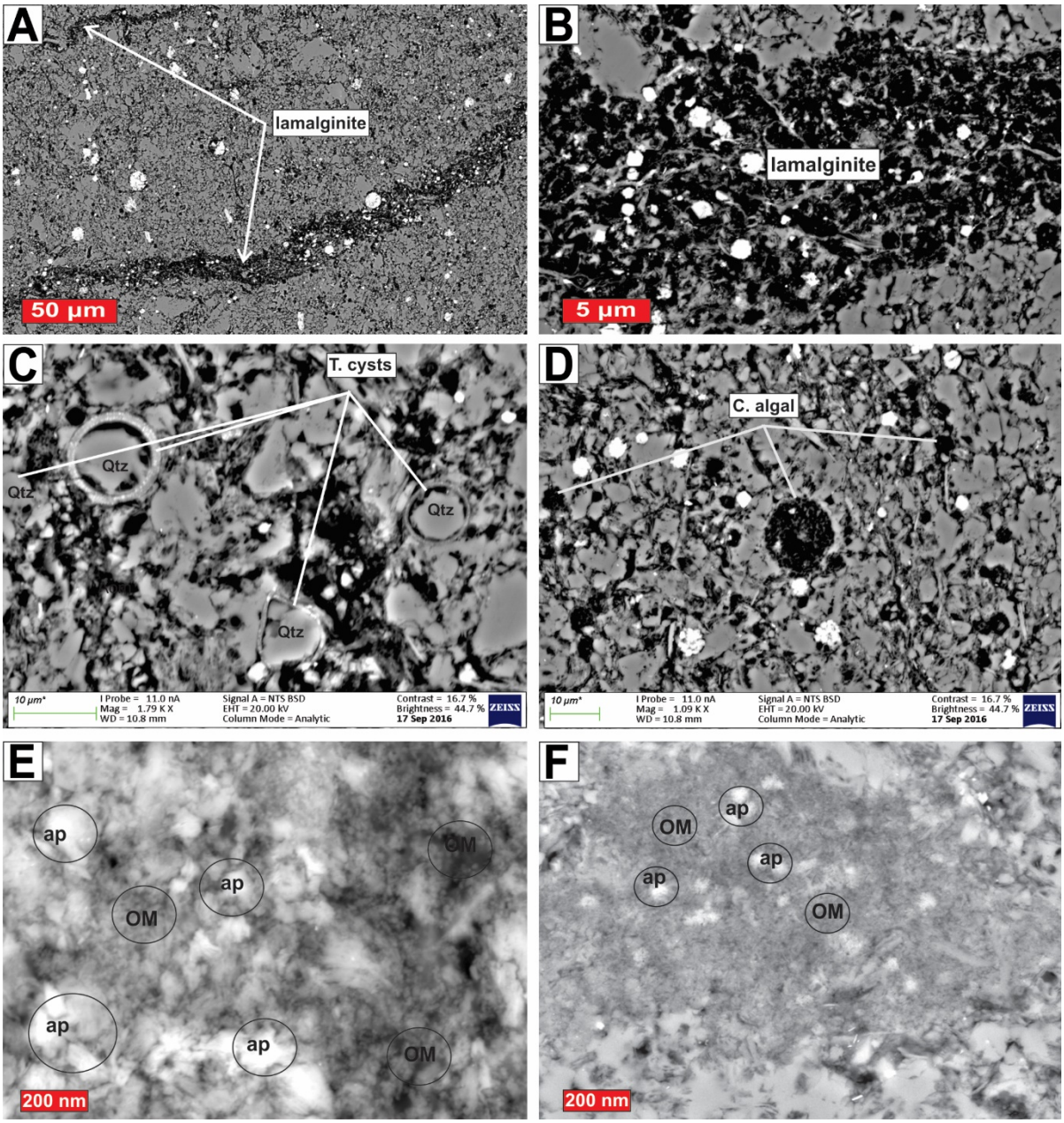

Fig. 3.8. Scanning electron microscope images of nature and occurrence of organic matter (OM) in the WHF. A-B: Dissemination and concentration of OM (lamalginites) within the shales matrix. C-D: Structured OM within the shale matrix. T.cyst = Tansamanites cysts, c.algal = colonial algal cells. E-F: A Binary mixture of OM and phosphates. Qtz = quartz, ap = apatite, T. cysts = Tasmanites cysts, c. algal = colonial algal. See text for details.

3.5.10. Climatic flux

Climate is one of the major controlling factors on both OM and detrital inputs. The chemical index of alteration (CIA; Nesbitt and Young, 1982), which is a measure of alumina versus labile oxides

is basically used to quantify the degree of weathering of fine-grained materials. Since weathering is primarily controlled by climate, CIA is a diagnostic indicator of climatic conditions during deposition. The CIA values of the samples (Fig. 3.11; Table 3.1) show a sharp and progressive increase from the lower (F1) to the upper (F5) subunits. The CIA in F1 ranged between 65.66 and 69.01 (average of 68.11). These values are indicative of cold condition with the possible presence of ice, likely in form of mountain ice-caps, to moderate climate condition in the source areas. Higher CIA values up to 83 in the upper F5 indicate warm and humid climate conditions. It is therefore likely that the sedimentation of the WHF witnessed systematic changes in climate conditions (from cold to warm conditions). Major element discrimination diagrams proposed by several workers (e.g. Suttner and Dutta, 1986; Ratcliffe et al., 2010) were also applied to reconstruct the climate conditions during the accumulation of the WHF. Based on the seminal binary SiO_2 versus (Al_2O_3 + K_2O + Na_2O) diagram proposed by Suttner and Dutta (1986; Fig. 3.13C), the sedimentation of the WHF coincided with a cold-temperate to semi-arid conditions that progressively became warmer.

3.6. Discussion

3.6.1. Input of organic matter and lithofacies sedimentary processes

OM contained in sediments and sedimentary rocks have two provenances: aquatic and terrestrial (e.g., Demaison and Moore, 1980; Tissot and Welte, 1984; Zonneveld et al., 2010). The majority of aquatic OM is derived from autochthonous organisms, such as phytoplankton (single-celled algae that live in the euphotic zone) and bacteria, whereas terrestrial OM is derived from vegetal and higher plants (woody material and waxes). The major limiting factors to planktonic productivity are sunlight and availability of mineral nutrients (P, N, Fe, Si). The latter are in short supply in the euphotic zone. Land plant productivity is dependent on the amount of rainfall on the supporting landmass.

Usually, to differentiate the sources of OM in sediments several methods, including elemental compositions, molecular biomarkers and polymers, or isotopic compositions can be used (e.g., Tissot and Welte, 1984; Peters and Cassa, 1994). Isotopic compositions of organic matter, particularly δ^{13}Corg, δ^{15}N, and C/N ratios, have been applied in a large number of studies (e.g., Peters et al., 1978; Meyers, 1997; Kuypers et al., 2004; Meyers and Bernasconi, 2006; Meyers, 2014; Könitzer et al., 2014) to identify sources of OM and their depositional processes. Stable

isotopes are relatively resistant to diagenetic alterations after organic matter is buried in sediments, and hence they preserve information about the original sources of OM as has been demonstrated in several studies (e.g., Carmack et al., 1976; Ertel and Hedges, 1985; Talbot and Johannessen, 1992; Meyers, 1997; 2014; Hodell and Schelske, 1998; Lehmann et al., 2002).

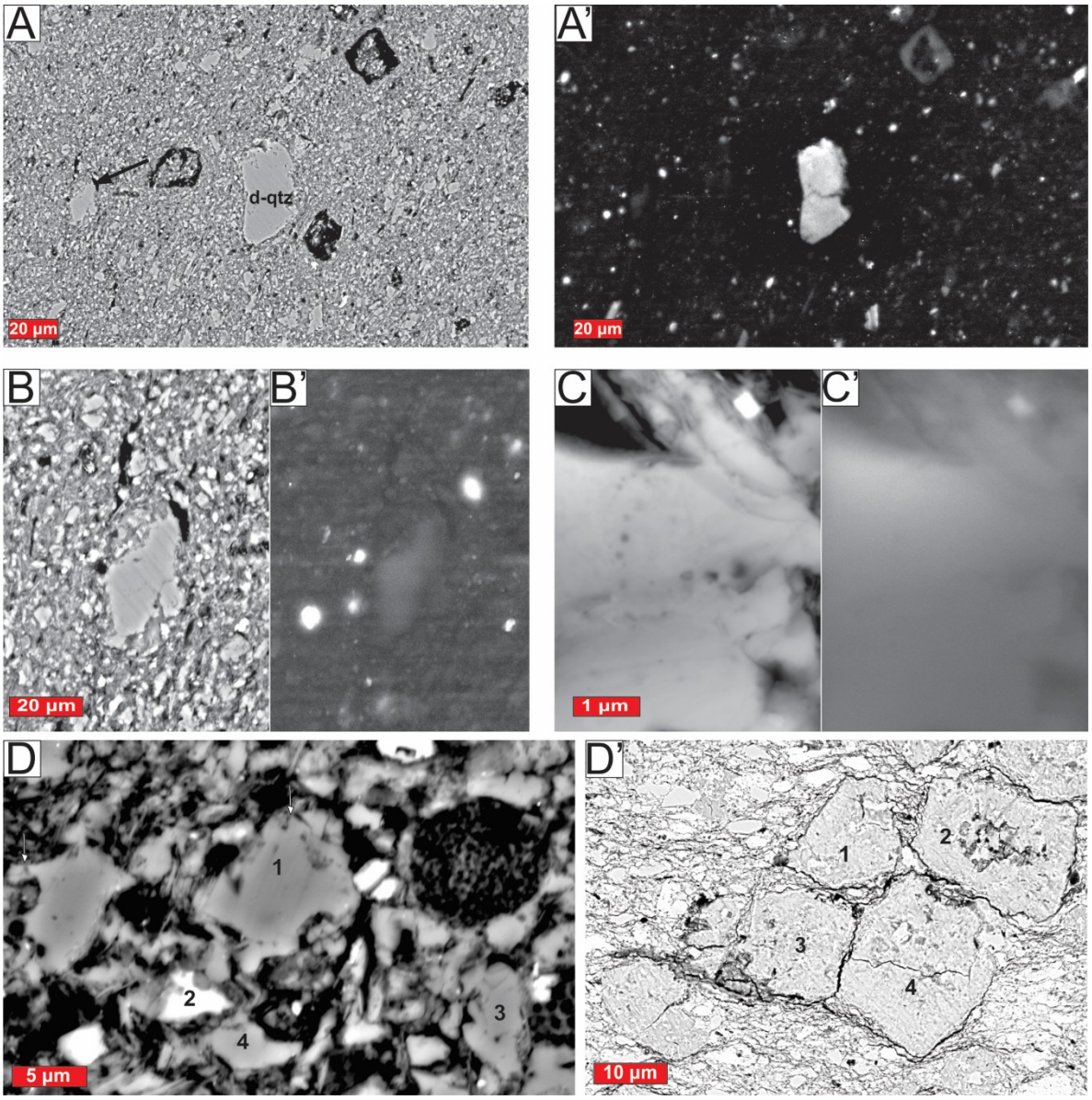

Fig. 3.9. Scanning electron microscope images of the variations in the intensity of luminescence between detrital and diagenetic quartz. Detrital quartz show uniformly bright and high cathodoluminescence (CL-SEM; A-A') whereas low-temperature diagenetic quartz show low and variable CL-SEM luminescence (B-B', C-C'). **D-D'**: Textural features of in situ quartz (Qtz) grains (1, 2, 3, and 4 in **D**) such irregular outline with indentations, embayments, and pointed to lobate projections sharply contrast those of detrital quartz (1, 2, 3, and 4 in **D'**).

According to Meyers (1997), variations in proportions of marine versus terrigenous OM sources can alter the δ^{13}Corg, δ^{15}N, and C/N ratios of OM. It was observed that alkanes produced by aquatic (lower) plants and animals (e.g., algae, bacteria) have shorter carbon chains ($\leq C_{21}$), whereas OM with longer carbon chains ($\geq C_{27}$) are attributed to higher, terrestrial plants and animals. Based on his observations, Meyers (1997) proposed that OM produced by land plants and marine algae have average $\delta^{13}C_{org}$ values of -27 and -21‰, δ^{15}N values of 0 and +8.5‰, and C/N ratios of >20 and <10, respectively. However, the $\delta^{13}C_{org}$ values of the Permian black shales of the southwestern Gondwana basins including the WHF (Karoo Basin), the Irati Formation (Paranà Basin), and the Black Rock Member (Falkland Islands), deviate from those of most Phanerozoic sequences (e.g., Dean et al., 1986; Faure and Cole, 1999). Generally, there is a positive shift of about 6‰ in their $\delta^{13}C_{org}$ compositions relative to other Phanerozoic successions (e.g., Rigby and Baths, 1986; Whiticar, 1996; Faure and Cole, 1999; Kuypers et al., 2004). The elevated $\delta^{13}C_{org}$ values for these Permian black shales is attributed to the greater availability of dissolved CO_2 to marine algae due to higher ρCO_2 of the Permian atmosphere (Dean et al., 1986). In addition, $\delta^{13}C_{org}$ values usually become more negative (that is smaller) as concentration of organic carbon increases (e.g., Hofmann et al., 2000), with the exception of periods (oceanic anoxic events) with greatly increased biological productivity (e.g., Sliter, 1989; Erbacher et al., 2005). Like $\delta^{13}C_{org}$ values, bulk δ^{15}N values for Permian black shales also show deviations from typical Phanerozoic shales (e.g., Kuypers et al., 2004), which is related to the widespread occurrence of cyanobacterial nitrogen fixation in southwestern Gondwana during the Permian (e.g., Faure and Cole, 1999).

The highest $\delta^{13}C_{org}$ values (up to -15.57‰, average of 18.91 ± 2.55‰), δ^{15}N values (average of 10.49 ±0.5‰), and the lowest C/N ratios (average of 1.50 ±0.75) are associated with highest detected TOC (up to 16.5 wt%) within the black-dark grey carbonaceous shales (F2; Fig. 3.11; ; Table 3.1). This suggests that the OM in this interval was sourced exclusively from lower aquatic organisms (phytoplankton and bacteria). From FE-SEM observations, Tasmanites cysts, colonial algae cells, and amorphous OM were the predominant contributor to the OM in this facies. These particles occur in thin uniform laminations composed of flattened but uncrushed Tasmanites cysts and colonial algae cells and few associated mineral grains in form of organo-minerallic composites (Fig. 3.8). The large size of these organo-minerallic aggregates suggests that flocculation was an effective mechanism for enhanced OM burial rates (e.g., Macquaker et al., 2010; Ghadeer and

Macquaker, 2012; Chukwuma and Bordy, 2016). These sedimentologic attributes suggest that these grains were directly produced in the overlying water column and delivered to the sediment surface via suspension settling (hemiplegic marine snow) and without any form of lateral transport. The near-absence of terrigenous input and the presence of phosphorites closely associated with OM (Fig. 3.8E-F) indicate sea-level highstand (Demaison and Moore, 1980; Cook, 1984; Visser, 1992). The presence and abundance of Tasmanites cysts suggest marine incursion (Tappan, 1980; Baceta and Nunez-Betelu, 1994; Schieber, 1996; Telnova, 2012). In addition, this facies lacks any sign of bioturbation, indicating that OM degradation may have been minor. These interpretations largely concurred with Rock-Eval data such as the HI-OI plot (Fig. 3.10), which indicate that this facies is largely composed of Type II kerogen. The major input of Type II OM is biological productivity by autochthonous organisms. Based on the above considerations, it is likely that the deposition of these facies coincided with a marine transgression. During transgressions, burial rates of organic carbon would be potentially favored by lowered clastic dilution. Reduced bioturbation indicates reduced oxygen in the bottom water (e.g., Calvert et al., 1996; Bohacs et al., 2005; Könitzer et al., 2014). Higher rates of biological productivity were likely fueled by an influx of nutrient-rich oceanic/marine waters (e.g., Littke et al., 1988; Piper and Calvert, 2009). A balance of these factors is likely to underpin the high TOC contents (up to 16.5 wt.%) observed in F1 and F2.

The relatively moderate to high $\delta^{13}C_{org}$ values (up to -21.52‰, average of 20.15 ± 1.15‰), $\delta^{15}N$ values (6.88‰, average of 5.24 ±1.13‰), and high C/N ratios (up to 12, average of 2.32 ±3.28), lower TOC values (average of 2.04 ±1.14 wt.%), lower HI and higher OI (plot major on Type II-III on Van Krevelen diagrams; Fig. 3.10), reduced populations of bioclastic material, laminae with few lenticular fabric indicate that F3 was likely deposited under reduced eutrophication. The absence of phosphorites, Tasmanites cysts, reduced populations and size of organo-minerallic aggregates, and increased terrigenous input suggests sea-level lowstand and desalination in the basin. The reduced fraction of marine OM was also due to significant dilution by coarser silt-grade material as indicated by higher Si/Al ratio. TOC:C/N cross plot (Fig. 3.13) reflect depositional mechanisms of interlinked but separate processes (a mixture of bioclastic and terrestrial materials). The presence of few bioturbation (Fig. 3.5) suggests periodic benthic colonisation of the seafloor, which contributed to OM mineralisation. Based on these considerations, it is likely that deposition of F3 occurred during a sea-level lowstand with fewer nutrients available to the

aquatic producers. During such reduced nutrient supply, nutrient recycling including OM oxidation could have been introduced, which adversely affected OM preservation. A balance of these conditions likely underpin the reduced TOC contents in F3.

The lowest $\delta^{13}C_{org}$ values (up to -24.71‰, average of 22.42 ± 1.92‰), $\delta^{15}N$ values (average of 4.93 ±1.62‰), and highest C/N ratios (up to 43.7, average of 17.62 ± 13.27‰) are associated with lowest TOC (1.03 wt.%; Fig 3.11; Table 3.1) within light grey siliceous massive-looking silty-sandy shale (F4 and F5). The texturally different and typically sharp contacts between the homogeneous and lenticular beds indicate a discontinuity in sedimentary processes during the deposition of this facies. The presence of knife-sharp contacts between layers, normal and inverse grading, loadcasts, cross-laminations indicate a more dynamic and active lateral transport that was influenced by storms and sea-level fluctuations and deposition from flows under relatively shallow setting (above storm-wave base; Wignall, 1989; Aigner and Reineck, 1982; Schieber, 1994). OM was composed entirely of Type III (Fig. 3.5) with low HI and higher OI indicating almost exclusively terrigenous sourced. Reduced organic productivity detected here also corresponds with reduced contents of P and Ba. Major element ratios, such as Si/Al and Rb/K concur with a terrestrial source for this facies.

3.6.2. Depositional processes from major element concentrations and ratios

Significant variability in major element concentrations and distribution (Fig. 3.13; 3.14) detected within the five stratigraphic subunits of the WHF suggest that detrital supply processes and depositional conditions were non-uniform during the deposition of the WHF. A progressive increase in quartz contents and size grade from F1 to F5 indicate a basinward shift of the shoreline, general fall in relative sea-level and progradation of the facies (e.g., Köntizer et al., 2014; Zavala et al., 2011; Zavala and Arcuri, 2016). The distribution of silt-grade quartz in mudstone and shales has been used in several studies to establish the distance to shoreline and palaeocurrents (e.g., Kolla and Biscaye, 1977; Blatt and Totten, 1981; Schieber, 1996; Schieber et al., 2000). However, in the WHF, a significant portion of the silt-size quartz, particularly in F1 and F2, are likely of early diagenetic origin. The presence of these *in situ* precipitated quartz grains limit their application as indicators of sediment supply direction and distance to palaeoshores (e.g., Schieber et al., 2000). However, the variations documented in detrital proxies, such as Si/Al and Ti/Al (Fig.

3.11) from F1 to F5 are, generally interpreted as indicative of differences in source areas, transport mechanisms, depositional and post-depositional conditions. The general increase in these detrital ratios indicate increasing shallower depositional profile (Potter et al., 1980; Ross and Bustin, 2009), and concomitant dilution of OM and seabed oxygenation.

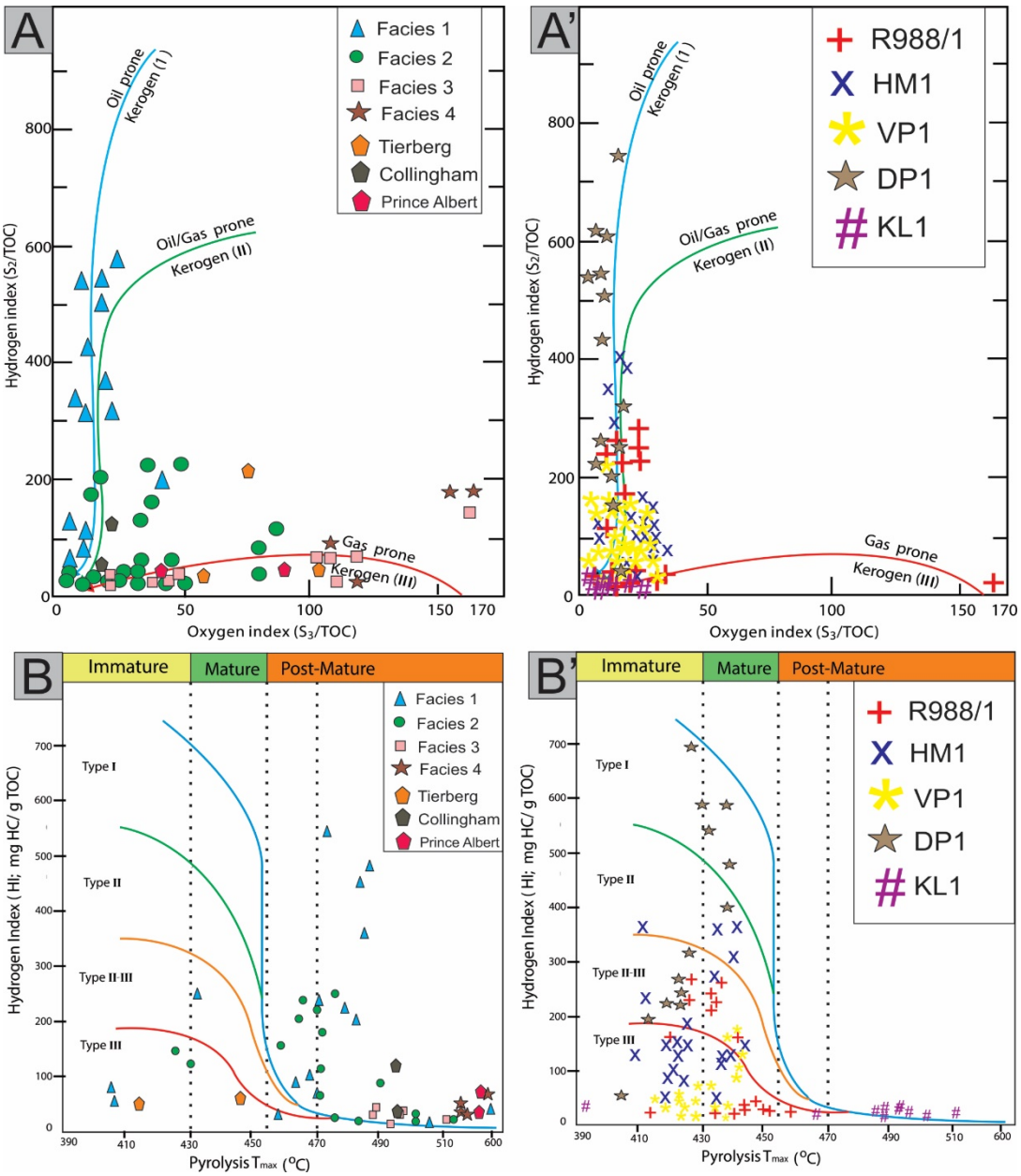

Fig. 3.10. Modified van Krevelen pyrograms of the nature and maturity of OM. **A**: Hydrogen index (HI) vs oxygen index (OI) of the facies of WHF (this study). **A'**: HI vs OI derived from the pyrolysis/TOC data of Rowsell and De Swardt (1976) and Cole and McLachlan (1991, 1994). **B**: HI vs T_{max} for this study. **B'** HI vs T_{max} derived from the pyrolysis/TOC data of Rowsell and De Swardt (1976) and Cole and McLachlan (1991, 1994). See text for details.

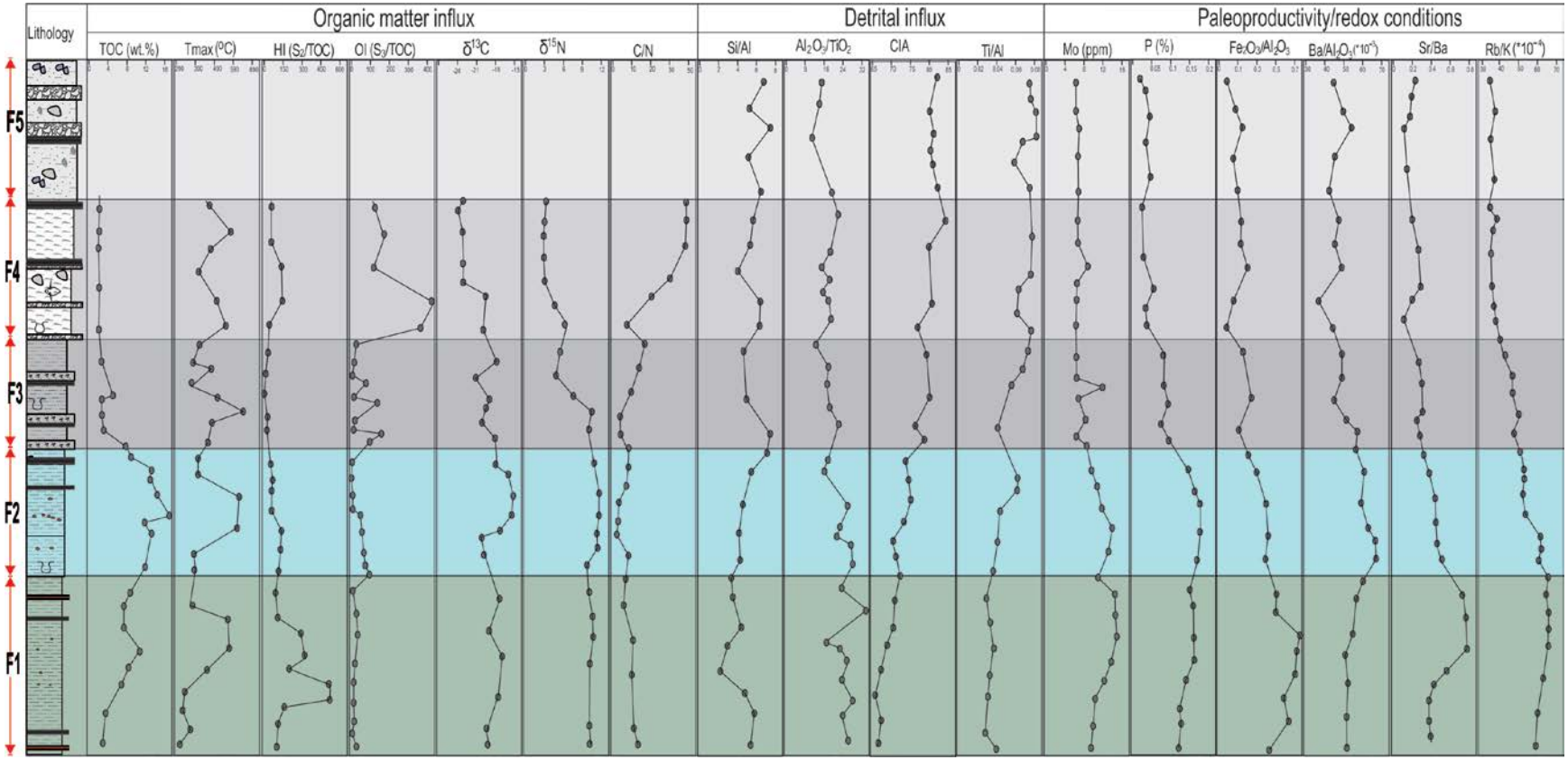

Fig. 3.11. Spatial variations of organic carbon contents, TOC pyrolysis data, stable isotope compositions, detrital influx proxies (major and trace element composition and ratios) across the five stratigraphic subunits of the WHF. See text for details.

3.6.3. Preservation of organic matter

The burial and preservation of OM are complex chemical processes closely related to redox conditions, particularly the development of anoxicity (e.g., Demaison and Moore, 1980; Katz, 2005; Zonneveld et al., 2010). The conditions that favored the accumulation of OM in the WHT shales are largely inferred from redox proxies.

3.6.3.1. Inference from trace element concentrations and redox ratios

The chemistry of a depositional environment often results in the enrichment or depletion of certain environment-sensitive transition elements and ratios, which have been widely applied in reconstructing palaeo-redox conditions (e.g., Jones and Manning, 1994; Piper and Perkins, 2004). However, for organic-rich sediments, it is usually difficult to differentiate the sources (terrigenous, biogenic, or diagenetic) of redox trace metals (e.g., Brumsack, 2006). The approach adopted in this study is to combine redox-proxies with background data provided by major element analyses and sedimentologic (lithologic, petrographic, SEM) observations. Also, because the preservation of organic carbon is favored under oxygen-limited (anoxic) conditions, the reliability of redox proxies was checked by their correlations with TOC (e.g., Scheffler et al., 2006).

Modern sulfate reducing (anoxic) sediments, such as Black Sea (e.g., Degens and Ross, 1974; Crusius et al., 1996), the Baltic Sea (Grasshoff, 1975), the Saanich Inlet of British Colombia (Nissenbaum et al., 1972) and Lake Tanganyika (Degens et al., 1971), show enrichments in Molybdenum (Mo). The Mo contents in AS is 2.6 ppm (Wedepohl, 1971) and that of North American black shale is 10 ppm (Vine and Tourtelot, 1970). In the WHF, all five lithofacies were enriched in Mo relative to AS, however, F1 is exceptionally enriched (up to 15 ppm). The actual mechanism and site of Mo enrichment, either within the water column or in the sediment, is controversial because several factors, such as redox conditions, OM type, sediment accumulation rates, and post-depositional (diagenetic) processes seem to influence Mo enrichment (e.g., Calvert and Pederson, 1993; Helz et al., 1996). As a result, no threshold has been established for anoxic versus oxic conditions. The enrichment of Mo in the five stratigraphic subunits of the WHF (3.15-15.03 ppm, average of 4.48) is close to those applied elsewhere as an indicator of anoxic to dysoxic environment (e.g., Rimmer, 2004).

The use of Rb/K ratio to differentiate sediments formed in fresh, brackish, or marine water was introduced by Campbell and Williams (1965) and is based on the knowledge that Rb content is higher in marine sediments because of higher concentration of Rb^+ in ocean water (0.12 ppm) than that in fresh water (0.0013 ppm; Scheffler et al., 2006). As a result of large contrast in Rb+ concentration in marine and freshwater settings, when fine-grained sediments are deposited in marine settings the K in detrital clay is readily replaced by Rb, resulting in higher Rb/K ratios (e.g., Wedepohl, 1978). However, Wedepohl (1978) cautioned that chemical weathering of clay and alteration of OM can result in desorption of K and a concomitant reduction of the Rb/K ratios. Rb/K values greater than $4.0x10^{-3}$ indicate marine conditions, whereas shale with Rb/K values less than this threshold are considered non-marine (e.g., Scheffler et al., 2006). Rb/K decreased progressively from $6.39x10^{-3}$ in F1 to $3.83x10^{-3}$ in F5, suggesting a gradual increase in freshwater clays or/and a switch from marine to non-marine conditions. The values for Rb/K for F1 and F2 are largely within the threshold for a marine to brackish water. This largely concurs with Rb/K ratios obtained in a previous study of the WHF by Geel and others (2015), however, Rb/K for F3-F5 are lower than those of these authors.

3.6.3.2. Inference from carbon-sulfur-iron relationships

Raiswell and Berner (1983) demonstrated that under oxygenated conditions, pyrite formation occurs below sediment-water interface and is limited by the availability of C_{org}, thus C_{org} and S_{pyr} show a strong positive correlation and on a plot of C_{org} versus S_{pyr}, a line of regressions passes through the origin. Whereas in sediments deposited under anoxic to euxinic environments, pyrite formation is not limited by the presence of C_{org} but iron availability, and a plot of C_{org} and S_{pyr} shows no correlation between organic carbon and pyritic sulfur but a non-zero sulfur intercept, thus, indicating higher contents of pyritic sulfur with low TOC (Berner and Raiswell, 1983; Lyons and Berner, 1992; Rimmser, 2004).

Marked differences were detected in the C-S plots of the samples (Fig. 3.12). For F1, there is no correlation between sulfur (S_T) and TOC (Fig 3.12A). Based on Berner (1984) and Berner and Raiswell (1983), the C-S relationships shown by F1 samples suggest anoxic to euxinic conditions. Positive intercept represents pyrite formations within the water column and at the sediment-water interface under anoxic to euxinic conditions, independent of organic carbon content. Conditions during the deposition of F2 were slightly different. A significant correlation exists between TOC

and sulfur, however, a linear regression line intercepted sulfur at about 0.2. This may indicate that conditions during the accumulation of F2 were not persistently anoxic, but were occasionally closer to normal conditions. The TOC versus sulfur regression line for F3 and F4 passed through the origin, however, there is no correlation between the two variables for F3 and with much scatter in the data. This may represent marked fluctuations in the supply of OM.

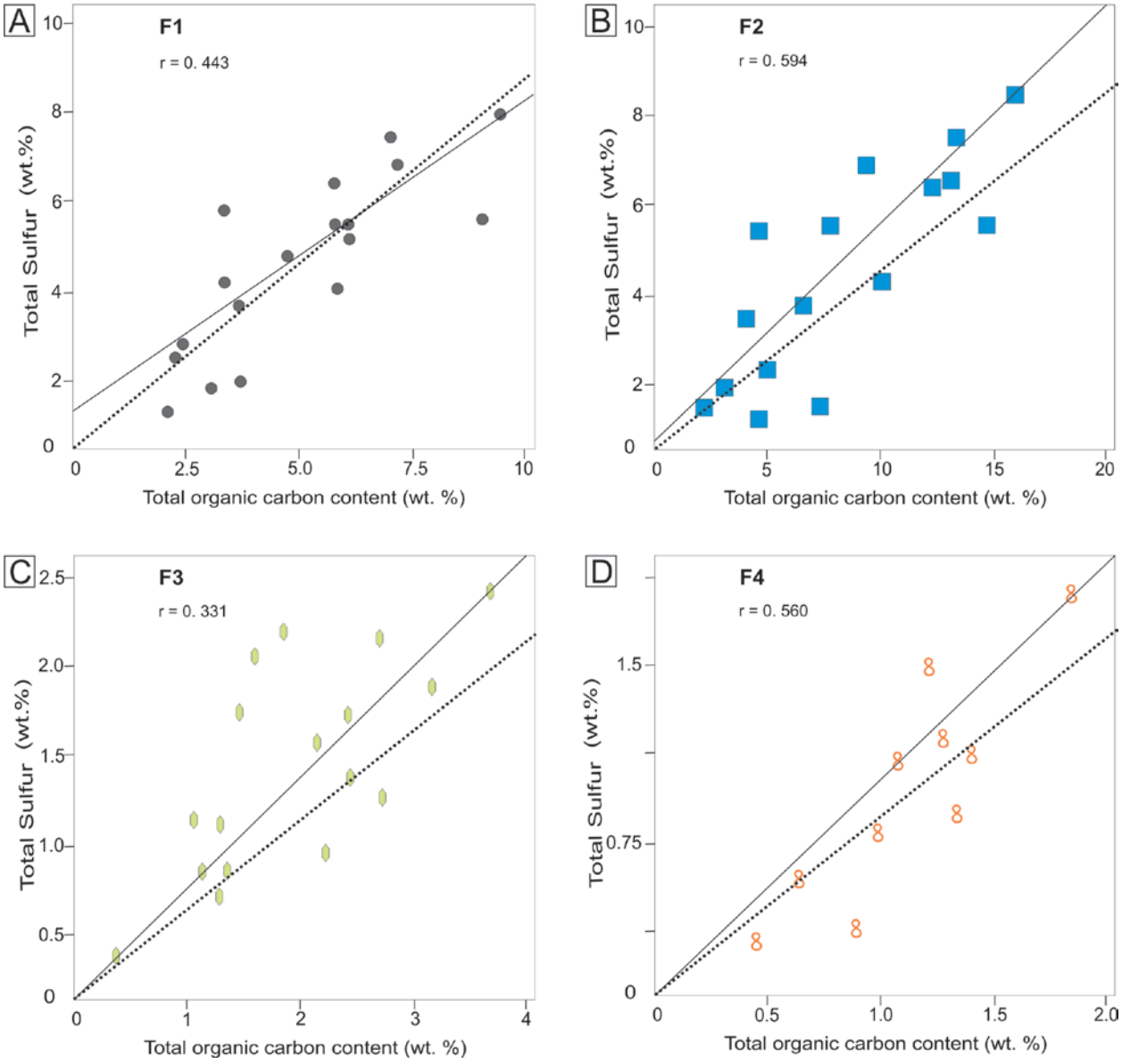

Fig. 3.12: Carbon-sulfur (C-S) relationships in the facies of the Whitehill Formation. Solid lines are linear regression lines for data from this study while dashed lines are typical S-C lines for oxic sediments based on Berner and Raiswell (1983). See text for details.

3.6.3.3. Inference from morphologies and microfabrics of iron sulfides

The bulk of sedimentary iron sulfides forms during early diagenesis by microbial reduction of seawater sulfate (Kaplan et al., 1963; Berner, 1970, 1984; Benning et al., 2000; Schieber, 2011). The mineral pyrite (FeS_2, cubic) and its metastable dimorph, marcasite (orthorhombic) are the most widespread sulfides within the WHF shales. The paragenesis of iron sulfides in sediments is presumed to proceed from acid volatile monosulfides, mackinawite (FeS_{1-X}) and greigite (Fe_3S_4) to pyrite (e.g., Wilkins and Barnes, 1966; Berner, 1970, Benning et al., 2000; Schieber, 2011), however recent studies (e.g., Rickard and Morse, 2005) have shown that there numerous pathways to pyrite formation and that majority of the pyrites in modern sediments formed without the precursory monosulfides. Regardless of how pyrite forms, the necessary elements are iron and sulfur. Iron is insoluble in presence of oxygen and its content in seawater is exceptionally low (Berner, 1970; Schieber, 2011). Therefore any iron that is available for FeS formation likely has to be a part of the particulate matter making up the sediment. However, majority of the iron in sediments require high temperatures of deep burial to be released and likely unavailable during early diagenesis when the bulk of sedimentary FeS form (Schieber, 1996, 2011). The likely iron that is available during early diagenesis is in form of colloidal/particulate iron oxyhydroxides (e.g., Canfield, 1989; Allard et al., 2004; Schieber, 1996). Sulfur is freely available in form of seawater sulfate, however, once it is below the sediment-water interface, downward diffusion is limited, making sulfur a limiting ingredient. In sediments, the H_2S required for FeS formation is derived by sulfate reducing bacteria (prokaryotes) that use sulfate to accept an electron donated by OM during chemosynthesis:

$$SO_4^{2-} + 2CH_2O \text{ =====> } H_2S + 2HCO_3^- \quad (3.2)$$

Where, CH_2O (carbohydrate) represents OM.

Thus, the abundance of sulfate in seawater notwithstanding, it is the contents of OM that limits sulfide production and ultimately the amount of iron that is converted to pyrite. The above considerations explain the correlation that usually exists between OM and pyrite contents in most sediments including the WHF shales (Fig.3.13).

Iron sulfides in sediments occur in various morphologies and textures. Pyrite (the most common iron sulfide) is cubic, thereby occurring in cubes and octahedral forms. Other textural patterns also exist, including, single grains, framboids and polyframboids, pore-filling cement, and concretions. The various textures of pyrite carry useful information about syn-depositional and early diagenetic conditions (e.g., Wilkins et al., 1996; Wignall and Newton, 1998; Schieber, 2011). Single grains (up to 10's of μm in size) usually show multi-stage growth patterns that are useful for reconstructing diagenetic history. Concretionary pyrite indicates decomposition of OM during sediment accumulation and is a proxy for the occurrence of high organic content and intervals of slow deposition (Schieber, 2011). The size of framboids is indicative of the degree of bottom water oxygenation (e.g. Wilkins et al., 1996; Wignall and Newton, 1998; Schieber, 2011). In euxinic basins, the lower portion of the water column is usually anoxic and sulfidic, which allows framboids to grow and then settle and become part of accumulating sediments (e.g., Wilkin et al., 1996). Framboids that formed in that way are reported to be smaller in size (mean framboid diameters of <5 μm) and with narrow size distribution compared to those that formed in sediment underlying dysoxic and oxic waters with mean framboid diameters of 5-10 μm and broad size range (e.g., Wilkin et al., 1997; Wignall and Newton, 1998).

The predominance of framboids with mean diameters between 8 and 15 μm in F1 and F2 indicate that they were formed largely within sediments underlying largely oxygenated (dysoxic to oxic) waters. This observation overrules the likely existence of euxinic conditions during the deposition F1 as could be inferred from the strict application of the C-S relationships. The predominance of framboids and polyframboids in F2 (Fig. 3.7A-C) suggest anoxic condition. The large amounts of iron sulfides mostly in form of marcasite cemented lags and nodules (Fig. 3.4E-F) in the upper section of F2 and at the boundary between F2 and F3 suggest that the redox interface stayed in those positions for a relatively long time. This is probably a reflection of zero to very low sedimentation rates.

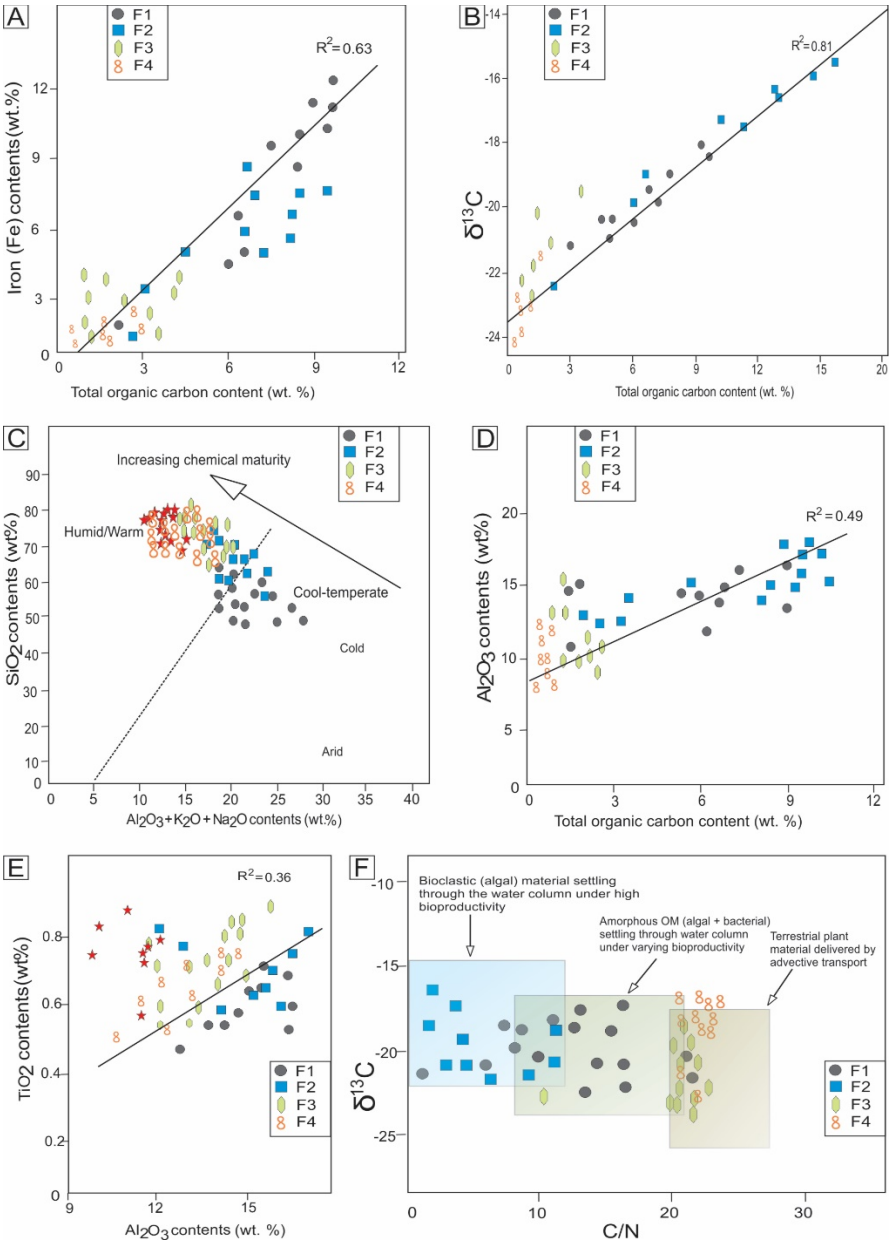

Fig. 3.13. Cross-plots of major and trace elements and ratios and isotopic compositions. **A**: Relationship between Fe_2O_3 and TOC contents. The correlation coefficient of 0.63 at the 1% level is considered significant. **B**: Relationship between $\delta^{13}C_{org}$ and TOC contents. The correlation coefficient of >0.8 at the 1% level is considered very significant. **C**: Binary SiO_2 vs (Al_2O_3 + K_2O + N_2O) diagram indicating the paleoclimate conditions during the sedimentation of the different stratigraphic intervals of the WHF (after Suttner and Dutta, 1986). **D**: Relationship between Al_2O_3 and TOC contents. The correlation coefficient of is less than 0.5, indicating a weak covariance between the two data. **E**: Relationship between Al_2O_3 and TiO_2 contents. The correlation coefficient of greater than 0.5 indicates a strong coupling between the two parameters. See text for details. **F**: C/N ratios and $\delta^{13}C_{org}$ values of the facies highlighting the various provenances and dispersal of OM in the facies of the Whitehill Formation.

3.6.3.4. Inference from excess silica content and distribution of volcanogenic tuffs

The silica content of the WHF is considerably high. All five stratigraphic subunits of the WHF were enriched in silica relative to AS (Fig. 3.14) and Ecca shale (Fig. 3.14; Table 3.2; Danchin, 1970). Excess silica content is defined by SiO_2 content above the AS background and is calculated as follows:

$$Si_{excess} = Si_{sample} - [(Si/Al)_{background} \times Al_{sample}] \quad (3.3)$$

The value of $(Si/Al)_{background}$ is 3.11 (Wedepohl, 1971). According to Eq. (3.3), between 12 and 33% (average of 26%) of the SiO_2 in F1 and F2 do not exist in aluminosilicate phase. Generally, this fraction (excess silica) represent input from coarse detrital grains, such as quartz and feldspar (e.g., Bertrand et al., 1996). However, SEM observation of the textural attributes of these grains suggests that the majority of the quartz grains in these facies in the silt-size range (4-32 µm; Fig. 3.9) were likely derived from infilling of Tasmanites cysts during early diagenesis (Fig. 3.8). This early diagenetic silica is spherical to ellipsoidal and range in size between 4 and 32 µm and comprised chalcedony (radiating fibers of quartz crystals), microquartz (crystal size < 0.02 mm) megaquatrz (crystal size >0.02 mm) and single quartz grains. Other diagnostic attributes are colloform textures, lobate-to-pointed and irregular grain margins, embayments, and pyrite, phosphorites, and OM inclusions. These features suggest that these silica grains originated from early diagenetic precipitation of dissolved silica. CL-SEM observation of these grains show them to contain growth bands with variable levels of luminescence that clearly distinguished them from extrabasinal detrital quartz (e.g., Milliken, 1994; Schieber et al., 2000; Fig 3.9).

Early diagenetic silica deposition in algal cysts requires a source of dissolved silica. In absence of diatomaceous opal and other siliceous tests in these shales, the likely source of dissolved silica in pore water was sourced from alteration of volcanogenic tuffaceous materials (e.g., Surdam and Boles, 1979; Inoue et al., 1988, 2005; Compton, 1991; Schieber, 1996). Air-fall volcanic ash beds are known to occur throughout the Permian Ecca and Beaufort Groups in the main Karoo Basin and are generally considered to have originated in the late Paleozoic Gondwana magmatic arc (Visser, 1992; Viljoen, 1994; López-Gamundi et al., 2013). The close association among the silica deposits, OM, pyrite, and phosphorites testify to an environment with bacteria sulfate reduction

and concomitant reduction of iron oxyhydroxides. Under such scenarios, the dissolution of iron oxyhydroxides, which requires oxygen-free pore water (e.g. Schieber, 2011) and a concomitant increase in the pH of the system, thereby enhancing silica dissolution (e.g., Canfield and Raiswell, 1991; Blatt, 1992). From thermodynamic studies (e.g., Goldhaber, 2003), the relationship between silica dissolution and pH is inelastic such that a small decrease in pH can cause a drastic decrease in silica solubility. Since silica solubility is bacterial mediated (e.g., Birnbaum and Wireman, 1984), a possible connection is suspected between the early diagenetic silica deposition in cysts and bacterial sulfate reduction. Previous authors (e.g., Wells, 1983; Schieber, 1996) share a similar opinion. From these considerations, it seems likely that the decomposition of volcanic ash and its subsequent precipitation in form of cyst-filled silica deposits explain the absence of well-defined tuffaceous beds in the lower WHF and not the absence of volcanic tuffs in the atmosphere over the basin. Therefore, the distribution of tuff bed within the WHF is a paleoenvironmental proxy for syn-sedimentary volcanic activity, because its absence (F1 and F2) may be apparent and signifies the presence of bacterial sulfate under reducing (anoxic) conditions, whereas its presence (F3-F5) largely indicate dysoxic to oxic depositional conditions.

3.6.3.5. Inference from white-weathering black shales

One of the conspicuous characteristics of the WHF, apart from lamination, is white-weathering of its dark grey to black shales under surface conditions. As a matter of fact, the formation derived its famous name “Whitehill” from this property (Fig. 3.4C). The under- and overlying Karoo Supergroup strata (e.g., Prince Albert Formation, Collingham Formation), in spite of their abundance in dark grey to locally black shales, notably do not weather white (Fig. 3.4A). White-weathering of the WHF is a diagnostic chemical characteristic that carries useful information about environmental conditions during and after deposition. The dark grey to black color of the unweathered WHF is largely due to the presence of iron monosulfide, which is generally presumed to be metastable and is subsequently transformed to pyrite (Berner, 1970, 1984; Shieber, 2011). The transformation of black unweathered shale into a white-weathered equivalent is a consequence of pyrite oxidation by the action of anaerobic bacteria, which results in the production of sulfate and sulfuric acid. The reaction of the latter with carbonate (calcite and dolomite) results in gypsum precipitation. The following equations summarise the reactions:

$$Fe_2S + 3.5O_2 + H_20 \text{ =====> } Fe^{2+} + 2SO_4^{2-} + 2H^+ \quad (3.4)$$

Additional oxidation of iron produces iron hydroxide:

$$Fe^{2+} + 0.25O_2 + 2.5H_2O \text{ =====> } Fe(OH)_3 + 2H^+ \quad (3.5)$$

Depending on the availability of carbonates (calcite and dolomite), the latter reaction may results in lowering of pore water pH, thereby enhancing the concentrations of F^{2+}.

$$CaCO_3 + 2H^+ \text{ =====> } Ca^{2+} + H_2O + CO_2 \quad (3.6)$$

$$CaMg(CO_3)_2 + 4H^+ \text{ =====> } Ca^{2+} + Mg^{2+} + 2H_2O + 2CO_2 \quad (3.7)$$

The reaction of sulfuric acid with carbonate results in production of gypsum:

$$CaCO_3 + 2H^+ + SO_4^{2-} + H_2O \text{ =====> } CaSO_4.2H_2O + CO_2 \quad (3.8)$$

From equation (3.4), the rate of pyrite oxidation (that is, whitening of the black shales) is dependent on the concentration of oxygen, particularly in the subsurface. According to McKibben and Barnes (1986) and Ritsema and Groenenberg (1993), oxygen concentrations at a specific depth is dependent on its rate of diffusion and consumption. The former has not been researched widely, whereas oxygen consumption occurs majorly by decomposition of OM and oxidation of pyrite.

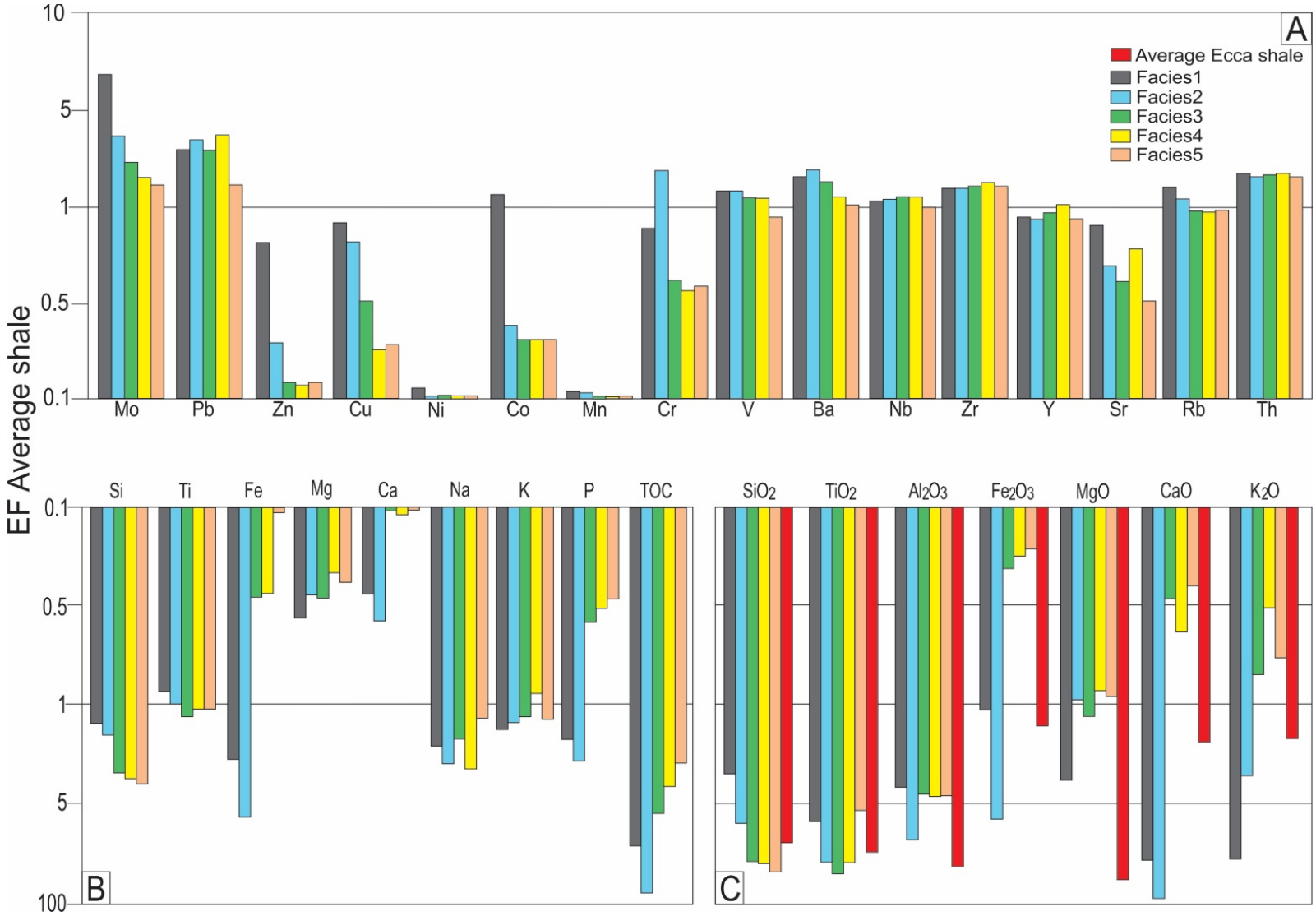

Fig. 3.14. A-B: Enrichment factor (EF) of major and trace elements in the five facies of the Whitehill Formation in comparison to average shale (AS) of Wedepohl (1971). A horizontal line represented $EF_{average\ shale} = 1$ is used to emphasise enrichment or depletion. **C**: Major oxides composition of the five facies of the Whitehill Formation in comparison to average Ecca shale (Danchin, 1970).

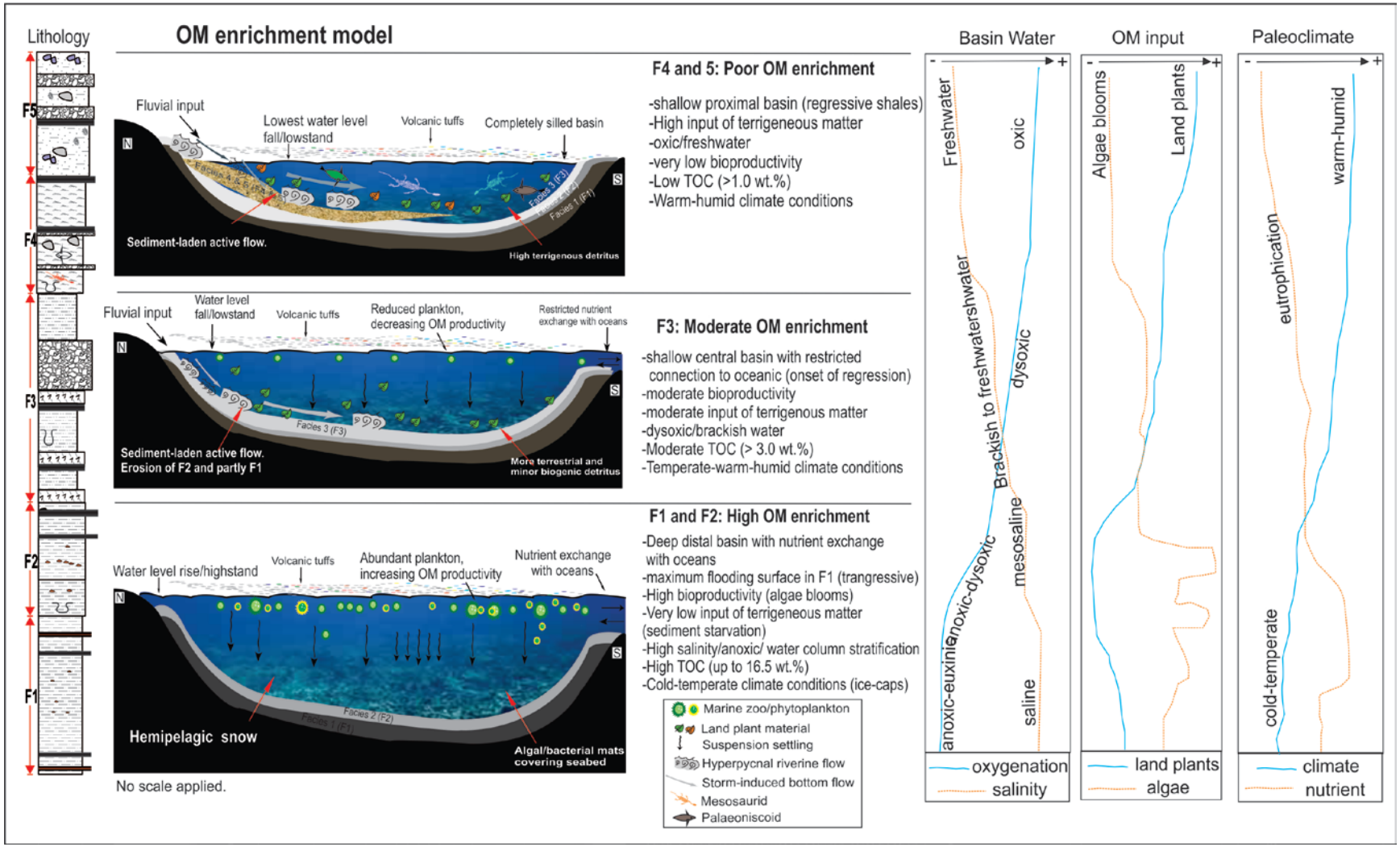

Fig. 3.15. Simplified sedimentological model of the WHF encompassing genetically-related sedimentologic controls that contributed spatial and temporal variability stratigraphy and composition.

Table 3.1. Enrichment factor (EF) for selected trace elements of the Whitehill Formation. Mean Al contents: F1: 7.53%; F2: 7.96%; F3: 7.63%; F4: 7.67%; F5: 7.73%. Trace element data are reported as ppm. [a] Average shale data from Wedepohl (1971) with mean Al content of 8.84%. [b]Average black shale data from Vine and Tourtelot (1970) with average Al content of 7.00%. [c]Average South African shale of Danchin (1970) with average Al content of 9.58%.[c]Average Ecca shale of Danchin (1970) with average Al content of 9.49% (n= number of samples analysed, min = minimum value, max = maximum value, SD = standard deviation)

Oxide/element/ ratio	Facies 1 (n = 24)				Facies 2 (n = 24)				Facies 3 (n = 24)				Facies 4 (n = 24)				Facies 5 (n = 24)				Average Shale[a]	Av. Ecca Shale[b]
	Min	Max	Mean	SD	Min	Max	Mean	SD	Min	Max	Mean	SD	Min	Max	Mean	SD	Min	Max	Mean	SD		
SiO2 (%)	46.34	64.50	56.37	7.00	56.40	73.53	63.85	5.03	63.32	75.89	69.01	3.97	66.58	76.20	70.77	3.15	69.79	80.26	73.46	4.65	58.90	67.30
TiO2 (%)	0.51	0.77	0.62	0.09	0.57	0.81	0.67	0.10	0.58	0.81	0.72	0.07	0.54	0.77	0.67	0.07	0.26	0.82	0.61	0.24	0.78	0.70
Al2O3 (%)	12.35	15.72	14.20	1.23	12.85	17.05	15.02	1.40	10.39	16.96	14.40	1.87	11.27	17.93	14.67	2.09	10.77	17.12	14.58	2.73	16.70	17.90
Fe2O3 (%)	1.25	9.79	5.03	4.90	5.70	12.82	7.51	2.40	0.38	3.67	1.09	0.94	0.24	2.11	1.04	0.60	0.38	1.22	0.71	0.41	2.80	6.00
MgO (%)	0.77	2.48	1.31	0.64	0.59	1.20	0.96	0.24	0.62	2.40	1.07	0.50	0.40	1.27	0.87	0.27	0.47	1.35	0.95	0.36	2.60	1.70
CaO (%)	0.78	1.02	0.92	0.49	0.89	1.34	1.13	0.24	0.06	0.57	0.20	0.15	0.08	0.94	0.33	0.29	0.14	0.26	0.18	0.06	2.20	0.65
Na2O (%)	1.99	2.22	1.86	0.38	0.88	2.37	2.01	0.58	0.38	2.56	1.81	0.77	1.13	2.49	1.95	1.14	0.59	1.96	1.50	0.62	1.60	
K2O (%)	3.69	3.82	3.87	0.16	2.64	4.47	3.43	0.56	2.40	4.02	3.28	0.49	1.08	3.64	3.05	0.77	2.55	4.42	3.41	0.77	3.60	3.60
P2O5 (%)	0.05	0.49	0.19	0.20	0.14	0.39	0.21	0.11	0.05	0.13	0.09	0.04	0.05	0.16	0.08	0.03	0.04	0.08	0.06	0.20	0.16	
Mo (ppm)	4.77	14.43	6.02	3.15	5.00	8.89	6.95	-	5.00	7.78	7.78	-	5.00	6.32	5.13	0.42	5.00	5.00	5.00	-	2.60	
Pb (ppm)	28.10	46.11	41.40	6.75	24.26	88.86	45.85	18.44	29.77	59.62	41.93	11.11	33.55	64.74	45.07	10.22	15.56	47.32	31.64	12.98	20.00	30.25
Zn (ppm)	8.21	123.98	60.69	49.92	9.33	43.88	19.79	15.05	10.17	17.28	13.41	3.58	7.21	14.32	9.69	2.70	8.96	19.76	12.07	5.28	95.00	80.55
Cu (ppm)	12.33	46.07	32.04	13.67	1.51	107.76	30.14	31.21	1.70	41.77	19.52	13.55	1.82	17.01	8.23	4.69	4.68	17.26	9.48	7.43	45.00	27.75
Ni (ppm)	5.00	20.73	9.26	5.96	5.00	5.00	5.00	-	5.00	5.00	5.00	-	5.00	5.00	5.00	-	5.00	5.00	5.00	-	68.00	26.70
Co (ppm)	5.00	34.89	20.23	19.76	5.00	17.09	6.68	3.95	5.00	5.00	5.00	-	5.00	5.00	5.00	-	5.00	5.00	5.00	-	19.00	12.30
Mn (ppm)	34.40	283.33	125.59	101.31	12.84	708.27	111.72	211.95	19.64	78.88	45.32	20.10	20.54	38.00	30.44	6.34	22.56	50.04	34.20	11.95		
Cr (ppm)	51.08	99.78	66.03	17.71	47.85	970.43	177.00	284.19	41.34	72.37	52.36	10.00	21.93	74.65	46.36	15.94	22.23	78.23	49.67	24.29	90.00	65.65
V (ppm)	105.13	158.40	126.40	18.78	111.19	174.36	133.19	19.37	101.93	142.90	118.66	12.15	61.17	179.16	119.70	40.88	35.65	154.69	106.28	55.59	130.00	92.30
Ba (ppm)	523.90	838.80	701.68	111.08	678.40	1017.00	820.75	120.55	431.00	628.70	533.67	86.66	389.80	786.40	523.88	84.30	355.30	521.60	426.13	40.73	580.00	
Nb (ppm)	13.46	19.39	15.85	2.30	12.78	22.23	16.98	3.92	15.20	21.38	17.64	2.64	14.75	21.28	17.32	2.45	8.93	18.59	15.78	4.61	18.00	
Zr (ppm)	134.63	228.70	165.37	33.65	133.80	227.13	174.97	30.77	154.57	224.79	175.87	19.56	149.54	243.36	189.25	37.29	128.78	203.58	174.05	35.36	41.00	
Y (ppm)	23.69	47.62	33.20	8.21	22.94	47.03	34.20	9.09	22.28	53.15	34.09	8.87	26.16	50.99	35.93	9.30	16.67	46.33	29.95	12.49		
Sr (ppm)	184.62	564.29	218.14	109.66	163.06	415.97	121.92	83.62	90.62	291.78	148.11	38.84	62.88	282.79	138.73	89.05	83.16	148.75	119.92	21.29	140.00	
Rb (ppm)	133.63	166.31	157.94	12.31	88.59	171.66	136.26	30.13	65.79	163.07	111.39	29.00	31.88	143.61	97.05	42.68	64.17	148.71	112.09	55.06	12.00	
Th (ppm)	14.38	19.72	17.04	1.76	9.03	24.87	16.79	3.99	9.99	23.16	16.45	3.40	13.19	21.18	16.96	2.99	13.04	19.65	16.23	2.84		18.30
ST (wt.%)	0.81	7.88	3.24	1.72	0.68	8.22	3.83	2.08	0.25	2.40	0.71	0.73	0.17	1.48	0.72	0.44						
TOC (wt.%)	2.06	9.61	6.15	2.92	1.67	16.50	6.22	3.31	0.30	3.91	2.04	1.14	0.48	1.80	1.03	0.67	-	-	-			
Fe2O3/TOC	0.98	1.65	0.82		3.41	0.78	1.21		0.13	0.49	0.35		0.27	0.03	0.14							
SiO2/Al2O3	3.75	4.10	3.97		4.39	4.31	4.25		6.09	4.47	4.79		5.91	4.25	4.82		6.48	4.69	5.04			
Al2O3/TiO2	24.22	20.42	22.90	13.67	22.54	21.05	22.42	14.00	17.91	20.94	20.00	26.71	20.87	23.29	21.90	29.86	41.42	20.88	23.90			
Ba/Al2O3	42.42	53.36	49.41		52.79	59.65	54.64		41.48	37.07	37.06		34.59	43.86	35.71		32.99	30.47	29.23			
Fe2O3/Al2O3	0.10	0.62	0.35		0.44	0.75	0.50		0.04	0.22	0.08		0.02	0.12	0.07		0.04	0.07	0.05			
P2O5/Al2O3	0.0040	0.0312	0.0134		0.0109	0.0229	0.0140		0.0048	0.0077	0.0063		0.0044	0.0089	0.0055		0.0037	0.0047	0.0041			
CIA	65.66	69.01	68.11		74.45	67.58	69.57		78.53	70.34	73.13		83.11	71.72	73.35		76.65	72.05	74.12			
Rb/K (x10-3)	5.45	6.56	6.15		5.25	5.78	5.98		3.30	4.89	4.09		3.56	4.40	3.83		3.03	4.05	3.96			
Sr/Ba	0.35	0.67	0.51		0.24	0.57	0.41		0.21	0.46	0.33		0.16	0.36	0.26		0.23	0.29	0.24			
Ni/Co	1.00	0.59	0.46		1.00	0.29	0.75		1.00	1.00	1.00		1.00	1.00	1.00		1.00	1.00	1.00			
V/Cr	2.06	1.59	1.91		2.32	0.18	0.75		2.47	1.97	2.27		2.79	2.40	2.58		1.60	1.98	2.14			
V/(V+Ni)	0.95	0.88	0.93		0.96	0.97	0.96		0.95	0.97	0.96		0.92	0.97	0.96		0.88	0.97	0.96			
δ13Corg (n=30)	-20.22	-18.57	-19.50	0.65	-22.32	-15.57	-18.91	2.55	-21.52	-18.30	-20.15	1.15	-24.71	-20.94	-22.42	1.92	n.a	n.a	n.a	n.a		
δ15N (n=30)	9.52	11.88	10.92	0.79	7.55	12.49	10.49	1.78	4.30	6.88	5.24	1.13	3.04	6.15	4.93	1.62	n.a	n.a	n.a	n.a		
C/N	2.13	16.47	9.54	5.73	0.77	2.48	1.50	0.75	0.32	12.38	2.32	3.28	4.83	43.70	17.62	13.27	n.a	n.a	n.a	n.a		

Table 3.2. Enrichment factor (EF) for selected trace elements of the Whitehill Formation. Mean Al contents: F1: 7.53%; F2: 7.96%; F3: 7.63%; F4: 7.67%; F5: 7.73%. Trace element data are reported as ppm. [a] Average shale data from Wedepohl (1971) with mean Al content of 8.84%. [b]Average black shale data from Vine and Tourtelot (1970) with average Al content of 7.00%. [c]Average South African shale of Danchin (1970) with average Al content of 9.58%.[c]Average Ecca shale of Danchin (1970) with average Al content of 9.49%.

Element	Average Shale[a]	Avergae Black Shale[b]	Average SA Shale[c]	Average Ecca Shale[c]	Facies 1 (n=24)	Facies 2 (n=24)	Facies 3 (n=24)	Facies 4 (n=24)	Facies 5 (n=24)	Average WHF
Mo	2.60	10.00	n.a	n.a	14.43	8.89	7.78	6.32	5.00	8.48
(Mo/Al)*10^4	0.30	1.40			1.88	1.17	1.03	0.79	0.65	1.10
EF		4.67			6.27	3.88	3.44	2.65	2.16	3.68
Pb	20.00	20.00	28.50	33.50	41.40	45.85	41.93	45.07	31.64	41.18
(Pb/Al)*10^4	2.30	2.90	2.97	3.53	5.50	5.76	5.50	5.88	4.09	5.34
EF		1.26	1.29	1.53	2.39	2.50	2.39	2.55	1.78	2.32
Zn	95.00	300.00	83.90	88.80	60.69	19.79	13.41	9.69	12.07	23.13
(Zn/Al)*10^4	10.70	42.90	8.76	9.36	8.06	2.49	1.76	1.26	1.56	3.03
EF		4.01	0.82	0.87	0.75	0.23	0.16	0.12	0.15	0.28
Cu	45.00	70.00	27.70	28.20	32.04	30.14	19.52	8.23	9.48	19.88
(Cu/Al)*10^4	5.10	10.00	2.89	2.97	4.25	3.79	2.56	1.07	1.23	2.58
EF		1.96	0.57	0.58	0.83	0.74	0.50	0.21	0.24	0.51
Ni	68.00	50.00	34.40	39.70	9.26	5.00	5.00	5.00	5.00	5.85
(Ni/Al)*10^4	7.70	7.10	3.59	4.18	1.23	0.63	0.66	0.65	0.65	0.76
EF		0.92	0.47	0.54	0.16	0.08	0.09	0.08	0.08	0.10
Co	19.00	10.00	15.90	16.10	20.23	6.58	5.00	5.00	5.00	8.36
(Co/Al)*10^4	2.10	1.40	1.66	1.70	2.69	0.83	0.66	0.65	0.65	1.09
EF		0.67	0.79	0.81	1.28	0.39	0.31	0.31	0.31	0.52
Mn	850.00	150.00	n.a	n.a	125.59	111.70	45.32	30.44	34.20	69.45
(Mn/Al)*10^4	96.15	21.43			16.68	14.03	5.94	3.97	4.42	9.01
EF		0.22			0.17	0.15	0.06	0.04	0.05	0.09
Cr	90.00	100.00	99.20	118.00	66.03	177.00	52.36	46.36	49.67	78.28
(Cr/Al)*10^4	10.20	14.30	10.35	12.43	8.77	22.24	6.86	6.04	6.43	10.07
EF		1.40	1.02	1.22	0.86	2.18	0.67	0.59	0.63	0.99
V	130.00	100.00	103.00	98.70	126.00	133.19	118.66	119.70	106.28	120.77
(V/Al)*10^4	14.70	21.40	10.75	10.40	16.73	16.73	15.55	15.61	13.75	15.67
EF		1.46	0.73	0.71	1.14	1.14	1.06	1.06	0.94	1.07
Ba	580.00	300.00	n.a	n.a	701.68	820.75	733.67	723.88	626.13	721.22
(Ba/Al)*10^4	65.61	42.86			93.18	103.11	96.16	94.38	81.00	93.57
EF		0.65			1.42	1.57	1.47	1.44	1.23	1.43
Nb	18.00	n.a	15.70	19.90	15.85	16.98	17.64	17.32	15.78	16.71
(Nb/Al)*10^4	2.04		1.64	2.10	2.10	2.13	2.31	2.26	2.04	2.17
EF			0.80	1.03	1.03	1.05	1.13	1.11	1.00	1.06
Zr	160.00	70.00	215.00	255.00	165.37	174.97	175.87	189.25	174.05	175.90
(Zr/Al)*10^4	18.10	10.00	22.44	26.87	21.96	21.98	23.05	24.67	22.52	22.84
EF		0.55	1.24	1.48	1.21	1.21	1.27	1.36	1.24	1.26
Y	41.00	30.00	43.60	47.40	33.20	34.20	34.09	35.93	29.95	33.47
(Y/Al)*10^4	4.64	4.29	4.55	4.99	4.41	4.30	4.47	4.68	3.87	4.35
EF		0.92	0.98	1.08	0.95	0.93	0.96	1.01	0.84	0.94
Sr	300.00	200.00	n.a	130.00	208.00	191.02	168.11	198.73	129.92	179.16
(Sr/Al)*10^4	33.94	28.57		13.70	27.62	24.00	22.03	25.91	16.81	23.27
EF		0.84	0.00	0.40	0.81	0.71	0.65	0.76	0.50	0.69
Rb	140.00	n.a	n.a	125.00	157.94	136.26	111.39	97.05	112.07	122.94
(Rb/Al)*10^4	15.84			13.17	20.97	17.12	14.60	12.65	14.50	15.97
EF				0.83	1.32	1.08	0.92	0.80	0.92	1.01
Th	12.00	n.a	17.80	21.20	17.04	16.79	16.45	16.96	16.23	16.69
(Th/Al)*10^4	1.36		1.86	2.23	2.26	2.11	2.16	2.21	2.10	2.17
EF			1.37	1.64	1.66	1.55	1.59	1.63	1.54	1.59

Table 3.3. Summary of Rock-Eval/TOC pyrolysis data of the five facies of the Whitehill Formation (See text for details).

Location												
Latitude (dms)	Longitude (dms)	Facies Code	Sample Code	Tmax (°C)	Maturity (%Ro)	S1 - (mg/g)	S2 - (mg/g)	S3 - (mg/g)	TOC (wt.%)	HI (S2/TOC)	OI (S3/TOC)	PI S1/(S1+S2)
33 14 31	21 51 26	F1	PAT1A	607	3.77	0.47	0.24	0.81	5.90	4.07	13.73	0.66
33 08 22	20 21 08	F1	MAJ1A	433	1.65	7.83	6.14	0.58	2.58	238.00	22.00	0.56
33 08 22	20 21 08	F1	MAJ1B	481	1.50	3.15	4.56	0.83	2.34	195.00	35.00	0.41
30 56 49	19 25 39	F1	LOE1A	454	1.01	0.30	3.40	0.24	9.27	37.00	3.00	0.08
30 56 49	19 25 39	F1	LOE1B	450	0.94	0.24	4.13	0.62	6.78	60.91	9.00	0.06
33 08 22	20 21 08	F1	MAJ2A	503	1.89	2.93	38.09	0.39	7.18	530.50	5.43	0.07
33 08 22	20 21 08	F1	MAJ2B	488	1.62	2.82	26.33	0.35	6.36	413.99	5.50	0.10
30 56 49	19 25 39	F1	LOE2A	447	0.89	0.46	4.80	0.33	9.27	51.78	3.56	0.08
30 56 49	19 25 39	F1	LOE2B	464	1.19	0.61	5.12	0.56	6.03	84.91	9.29	0.06
29 56 50	23 40 11	F1	STY 1A	488	1.62	4.72	7.18	0.39	2.06	348.54	18.93	0.41
30 56 49	19 25 39	F1	LOE2/H	402	1.02	6.52	6.43	0.65	9.61	67.00	7.00	0.50
33 13 51	21 42 10	F2	PAT2A	586	3.39	1.26	0.88	1.17	3.53	24.93	33.14	0.59
33 11 06	20 48 33	F2	LAG1A	595	3.55	1.80	1.37	2.25	5.23	26.00	43.00	0.57
33 14 20	20 51 58	F2	LAG2A	488	1.62	0.17	0.35	2.51	5.58	6.00	45.00	0.32
33 14 20	20 51 58	F2	LAG2B	526	2.31	0.06	0.15	2.72	8.44	2.00	32.00	0.27
33 14 20	20 51 58	F2	LAG2C	601	3.66	0.14	0.43	0.87	7.88	5.00	11.00	0.25
31 06 01	19 29 06	F2	LOE4A	428	1.67	0.15	0.93	0.64	0.72	129.00	89.00	0.14
31 06 01	19 29 06	F2	LOE4B	477	1.43	0.04	0.49	0.51	0.72	68.00	71.00	0.07
33 11 06	20 48 33	F2	LAG3A	526	2.31	0.03	0.14	1.75	3.90	3.59	45.00	0.19
33 11 03	20 48 45	F2	LAG5A	604	3.71	0.05	0.11	1.03	2.93	4.00	35.00	0.32
33 08 17	20 21 07	F2	MAJ5A	526	2.31	0.06	0.11	0.88	1.26	9.00	70.00	0.34
31 14 25	19 42 49	F2	NUW1H	443	0.81	0.10	0.45	0.31	0.67	67.00	46.00	0.18
31 14 25	19 42 49	F2	NUW1V	448	0.90	1.13	3.53	0.47	2.62	134.73	17.94	0.24
30 56 49	19 25 39	F2	LOE5B	454	1.01	0.03	0.13	0.10	9.13	1.00	1.00	0.19
30 56 49	19 25 39	F2	LOE6A	458	1.08	0.06	0.13	0.41	9.26	1.00	4.00	0.32
30 56 49	19 25 39	F2	LOE6B	404	0.11	0.06	0.14	0.16	8.83	2.00	2.00	0.30
30 56 49	19 25 39	F2	LOE-C2	405	0.13	0.87	0.29	2.28	16.51	2.00	14.00	0.75
30 56 49	19 25 39	F2	LOE-C1	417	0.35	0.30	0.98	0.59	9.87	10.00	6.00	0.23
30 56 49	19 25 39	F2	LOE3A	458	1.08	0.40	1.35	0.19	9.51	14.00	2.00	0.23
30 56 49	19 25 39	F2	LOE3B	495	1.75	0.10	0.58	0.22	8.92	7.00	2.00	0.15
33 06 17	20 35 53	F3	SUN1	453	0.99	0.07	0.15	0.16	0.15	100.00	107.00	0.30
33 11 41	20 39 54	F3	LAG7	425	0.49	0.07	0.10	0.08	0.05	200.00	160.00	0.43
31 14 25	19 42 46	F3	NUW2A	432	0.62	0.11	0.48	0.43	2.11	23.00	20.00	0.19
31 14 25	19 42 46	F3	NUW2B	449	0.92	0.10	0.48	0.68	1.67	29.00	41.00	0.17
31 06 45	19 28 52	F3	NAR2A	607	3.77	0.04	0.17	1.75	1.46	12.00	120.00	0.20
31 06 45	19 28 52	F3	NAR2B	494	1.73	0.10	1.02	0.82	0.93	110.00	88.00	0.09
30 34 14	23 28 28	F3	HPT1A	432	0.62	0.13	0.17	0.44	3.91	4.00	11.00	0.43
31 14 25	19 42 49	F3	CAL2A	455	1.03	0.06	0.15	0.40	3.70	4.00	11.00	0.29
31 14 25	19 42 49	F3	CAL2B	439	0.74	0.14	0.33	0.26	1.35	24.00	19.00	0.30
31 14 25	19 42 49	F3	CAL3A	441	0.78	0.33	0.49	0.23	1.21	40.00	19.00	0.40
31 14 25	19 42 46	F4	NUW4	422	0.44	0.13	0.49	0.61	2.17	18.00	47.00	0.43
31 09 53	19 40 35	F4	NAM2A	546	2.67	0.47	1.35	2.51	0.59	229.00	425.00	0.26
30 20 29	21 49 20	F4	VAK2	453	0.99	0.07	0.15	0.16	0.55	27.27	29.09	0.32
30 30 39	20 36 43	F4	BTT2B	465	1.21	0.07	0.10	0.08	0.65	15.38	12.31	0.41
28 06 19	25 28 49	F4	CST3B	495	1.75	0.05	0.16	0.33	0.29	55.00	114.00	0.24
31 06 45	19 28 52	TBF	TBF1	447	0.89	0.12	0.94	1.63	1.51	62.25	107.95	0.11
31 09 53	19 40 35		TBF2	419	0.38	0.11	0.54	0.63	1.11	48.65	56.76	0.17
31 06 01	19 29 06	CHF	CHF1	499	1.82	1.41	0.85	0.22	0.69	123.19	31.88	0.62
33 14 25	20 53 49		CHF2	492	1.70	0.11	0.48	0.43	2.11	22.75	20.38	0.19
31 06 01	19 29 06	PAT	PAF1	583	3.33	0.08	0.21	0.38	0.47	44.68	80.85	0.28
31 06 45	19 28 52		PAF2	561	2.94	0.05	0.16	0.33	0.73	21.92	45.21	0.24

3.6.4. The relative role of anoxia versus productivity in organic carbon accumulation

The conditions required for accumulation of organic matter-rich sediments has been a subject of a fascinating debate with models suggesting bottom-water oxygen levels (Demaison and Moore, 1980) or primary productivity (Pederson and Calvert, 1990) or combinations of these (Tyson and

Pearson, 1991). One reason for examining productivity and redox proxies in this study was to determine the relative role of organic productivity versus anoxia in the accumulation of this organic carbon-rich unit. Examination of the cross plot of C_{org} and redox sensitive elements versus C_{org} and productivity proxies (Fig. 3.13) provided clues as to the relative role of anoxia versus productivity in OM accumulation in the WHF.

A cross plot for C_{org} and pyrite contents (Fig. 3.13A; r = 0.63) show that a coupling exists between the two elements, and this suggests that redox condition during sedimentation influenced the accumulation of OM. However, a positive C_{org} intercept of about 1.2 indicates that higher C_{org} is associated with lower pyrite contents. This generally means that other factors such as productivity or changes in OM type may have also influenced OM sequestration in addition to anoxia. Also, from several redox proxies, such as C-S relationships, Mo contents, and Rb/K ratios, anoxia probably peaked during the deposition of F1, whereas the highest C_{org} contents were detected in F2. This observation also suggests that anoxia was not the primary control on OM accumulation. A cross plot for C_{org} and $\delta^{13}C_{org}$ values (which represents organic matter productivity; Fig. 3.13B) show a stronger coupling (r = 0.81) than that of C_{org} vs. pyrite, indicating that productivity had a stronger influence on OM accumulation than anoxia. The positive covariation detected between C_{org} and $\delta^{13}C_{org}$ also agree with the observation that both productivity and TOC peaked in F2. The highest C_{org} of up to 16.5 wt.% was detected within thin intervals in F2. It was also within the same intervals that the highest productivity proxies, such P and Ba contents and $\delta^{13}C_{org}$ were documented. However, in the cross plot for C_{org} and $\delta^{13}C_{org}$ larger scatter exists for values of C_{org} and $\delta^{13}C_{org}$ for F3 and F4 relative to F1 and F2 (Fig. 3.13B). A possible explanation for this observation is that there is no strong correlation between C_{org} and $\delta^{13}C_{org}$ values for F3 and F4. This means that OM in these two upper facies was largely derived from sources in addition to bioproductivity. From Rock-Eval data (Fig. 3.10), the OM of F3 and F4 has largely comprised type III OM, which is largely derived from terrestrial sources. Therefore, a large portion of the OM in F3 and F4 were produced on land and transported into the depository. The above considerations suggest that although both anoxia and productivity influenced OM accumulation, neither of the two factors nor their combinations completely accounts for organic carbon sequestrations in the WHF shales.

3.6.5. Other factors that controlled OM accumulation

3.6.5.1. Basin tectonics and climate conditions

In order to relate basin tectonics and climate conditions to the accumulation of OM in the WHF, aspects of the evolution of the main Karoo Basin are briefly reviewed. The Karoo Basin formed part of a long-lived (>100 Ma), much larger depression in southwestern Gondwana (Johnson et al., 1996). During the Permian, this depression covered most of southwestern South Africa, Namibia and southwestern Botswana (Johnson et al., 1996). In South America, the Permian Karoo-equivalents are mainly preserved in the Paraná Basin of Brazil, Paraguay and Uruguay as well as the Sauce Grande Basin of central-eastern Argentina (e.g., Visser & Praekelt, 1996, 1998; Visser, 1997; Faure & Cole, 1999; Stollhofen, 1999; Werner, 2006). In addition, the Falkland-Malvinas Islands, which in the Permian, were positioned close to the southeastern coast of South Africa, formed part of these depositional areas. Towards the east, Karoo-age deposits can be found in the Ellsworth and Transantarctic Mountains of Antarctica (Miller & Collinson, 1994; Veevers, 2000 & 2001). In addition, several authors (e.g., Oelofsen & Araújo, 1987; Williams, 1995; Stollhofen, 1999) suggested that the Paraná Basin area was possibly connected to the north with the Parnaiba Basin and possibly even with the Solimões-Amazonas Basin during maximum sea-level highstand in the Early Permian.

The origin of the main Karoo Basin is somewhat controversial with both thick-skinned vs thin-skinned models, advocated by Catuneanu et al. (1998, 2005) and Tankard et al. (2009, 2012), respectively, being used to explain the basin genesis. However, the development of the basin is generally viewed to have started in Late Carboniferous (~335 Ma ago -Bangert et al., 1999; McKay et al., 2015).

The onset of Karoo sedimentation coincided with active plate movements and development of a broad orogenic belt (the Cape Fold Belt or CFB). Episodes of tectonic activities (e.g., thrusting, folding) in the developing and growing CFB increasingly restricted the connection between the incipient Karoo Basin and the oceans (Lock, 1980; De Wit and Ransome, 1992). According to Hälbich (1983), the first evidence of a major compressional event in the southern margin of the basin occurred at ca 278 Ma, whereas the tectonic belt only became emergent at ~258 Ma, as evidenced by major sediment input from the growing thrust belt. Undoubtedly the seaway existed up to the deposition of the Prince Albert Formation as evidenced by the remains of a shark, sponge

spicules, foraminifera, acritarch, and other marine invertebrates (e.g., McLachlan and Anderson, 1973; Oelofsen, 1987; Visser, 1992). Previously, the absence of these marine species in the WHF has been interpreted by some workers as proof that the seaway was nonexistent during its sedimentation (e.g. Cole and McLachlan, 1991). From the observations made in this study, it is likely that the seaway indeed existed during deposition of the lower half of the WHF (F1, F2 times). This implies that the tectonic belt was only sufficiently developed to restrict contact with seawater after the deposition of the lower WHF (F3, F4, F5 times).

In addition, following the deposition of the Prince Albert Formation under warm climate conditions, the onset of the deposition of the WHF coincided with a temporal return of cold climate as seen by a drastic drop in CIA from 77 in Prince Albert to 67 in lower WHF (Visser and Young, 1990). In this study, average CIA of 68.11 was recorded for the lower WHF (F1), which progressively increases to 69.70 and 73.13 in F2 and F3, respectively (Fig. 3.12; Table 3.1). This implies the deposition of the WHF was marked by a possible systematic climatic warm-up. Cold climate during the onset of deposition likely restricted weathering concomitant with low input of coarser clastic materials, resulting in sediment starvation and a depositional system marked by the accumulation of almost exclusively mud size particles. During this period, it is likely that the basin had a sea connection (Fig. 3.15). The binary mixture of OM and phosphorites observed in F1 and F2 (Fig. 3.8E-F) attest to a marine environment with nutrient-upwelling, and minimal input of terrigenous sediment (e.g., Strydom, 1950; Cook, 1984; Brasier, 1992; Visser, 1992) and a possible marine incursion (e.g., Demaison and Moore, 1980). In such semi-enclosed (inland) basins with positive water balance, strong salinity contrast is usually created due to the outflowing of fresher surface water and the inflowing of denser saline and nutrient-rich oceanic water (e.g., Demaison and Moore, 1980). Such salinity contrast does not only initiate water column stratification and anoxia but also act as nutrient-trap, thus enhancing both productivity and preservation of OM. The phosphorites contain apatite grains with botryoidal texture suggesting microbial reduction and concomitant anoxic condition. This view largely contradicts the opinion of Faure and Cole (1999), who suggested a brackish water body with no oceanic connection and uninhabitable for the mesosaurid reptiles. In the comprehensive biostratigraphic reconstruction of the WHF by Oelofsen (1981, 1987), the mesosaurid reptiles are also shown to have only been preserved in the upper part of the WHF (i.e., subunits F3, F4, F5 of this study) with CIA data indicative of moderate to warm climate conditions. However, because the behavior of the mesosaurid reptiles and the preservation

of their skeletal remains (i.e., taphonomic conditions) in the Permian are poorly known, considering the spatiotemporal distribution of the mesosaurid fossils as diagnostic of warm conditions in the basin where WHF and its correlatives (Irati and Huab formations) formed would be premature at this stage.

Two upward-coarsening sequences in the stratigraphic sections of the WHF (Fig. 3.3A-D, Fig. 3.4E-F) are interpreted as evidence for progradation and linked to a fall in the relative sea-level within the basin. This assertion largely agrees with the observations of previous workers (e.g., Visser, 1990, 1992; Werner, 2006; Smithard et al., 2015). The first drop in the relative sea level occurred at the F2-F3 boundary and was marked by a stratiform horizon with large amounts of iron sulfides, mostly in form of marcasite-cemented lags and nodules (Fig. 3.4E-F) as well as dolomitic nodules and lags (Fig. 3.4D). These features suggest that the redox interface stayed at that particular level for a long period probably due to very low or zero sediment input (e.g., Schieber, 2011; Lazar et al., 2015). This horizon is documented across the basin but is particularly prominent near Willowmore, Prince Albert, Laingsburg, and Nuwelande localities. Geochemical evidence (e.g., C-S relationships, isotopic compositions, Mo content, Rb/K ratios) suggests that this horizon, which roughly separates the WHF into two sections (i.e., lower and upper WHF), is a key stratigraphic surface that can be linked to an important system highstand. It marked the end of persistent anoxia and high biological productivity as indicated by redox and productivity proxies (Fig. 3.11, 3.12). Above this surface, the first bioturbations, trace fossils and fossil plant material in the OM were documented in WHF. It also corresponds to the descriptions of the intervals from where tiny primary halite crystals were documented (e.g., Van der Westhuzien, 1979; Oelofsen, 1981). In addition, above this horizon CIA values increase to about those of normal shale (about 73.13), thus reflecting the return of normal geochemical conditions. These observations suggest that changes in climate from cold-temperate to warm-humid likely coincided with changes in the configuration of the basin. Therefore, it is likely that higher rates of evaporation and tectonic development in the CFB, which restricted oceanic connection, resulted in a negative water balance in the basin (Fig. 3.15). Typically, for inland basins with negative water balance, as shallow water flows in, the hypersaline water sinks downward and either flow out as density undercurrent into the ocean where a connection exists, or accumulate as hypersaline, oxygenated, nutrient-depleted water on the bottom of the basin. Under such conditions, the basin is both oxygenated and nutrient depleted. This scenario agrees with the observed bioturbations, various fossils, and lower organic

carbon content documented in F3-F5. It also likely that the halite crystals observed in this interval precipitated from the bottom brine overlain by fresher surface water. Based on this scenario, the basin does not necessarily need to be subaerially exposed for such evaporate crystal to form. Thus the presence of primary evaporites may be proxies for shallower water depth as suggested by Cole and McLachlan (1991) but not necessarily indicative of partial or complete drying out (zero water depth).

The second 3rd-order sea-level fall in the WHF is interpreted to coincide with the F3-F4 boundary. It is marked by thin (<2 cm) calcitic/dolomitic lags and in places by the erosional surface, indicating a possible winnowing (Fig. 3.3A-D), albeit in the central and northern areas of the basin. The drastically reduced organic carbon content and the predominance of Type III OM in F4 indicate drastically reduced biological productivity. Stable isotope data, including $\delta^{13}C_{org}$ and $\delta^{15}N$ value of up to -24.71 and 3.04, respectively, and C/N ratios of up to 43.7 indicate that F4 is dominated by land-produced OM likely transported into the basin (Fig. 3.15). The decreased HI of this facies indicates increasing distance to continental areas. This trend is also in agreement with increasing Si/Al and Ti/Al recorded for F4 and F5. Redox indices such as C-S relationships, iron sulfide contents, Rb/K as well as sedimentologic features such as high silt contents, normal and inverse grading, cross laminations, loadcasts, concur with these trends and are indicative of largely oxic conditions (e.g., Aigner and Reineck, 1982; Wignall, 1989; Shieber, 1994; Fig. 3.5). The complete absence of marine features (e.g., Tasmanites cysts and phosphorites) and reduced sea-level detected in F4 and F5 imply that CFB by that time was sufficiently developed to cut-off contact with the open oceans as previous studies (e.g., Vissser, 1990; 1992; Faure and Cole, 1999; Scheffler et al., 2006) predicted. These data also indicate that change from cold to warmer climate conditions coincided with these changes in the configuration of the basin.

3.6.6. Paleoenvironmental conditions: marine versus non-marine

Usually, the $\delta^{13}C_{org}$ values of sediments decrease (i.e., become more negative) as the concentration of C_{org} increases (e.g., Hofmann et al., 2000), with the exception of oceanic anoxic events where shift to less negative values with increasing organic carbon contents represents the greatly amplified marine productivity at those times (e.g., Meyers, 1997; Bowman and Bralower, 2005; Erbacher et al., 2005; Meyers and Bernasconi, 2006; Meyers, 2014). Oceanic anoxia usually parallels climatic warm-ups and large-scale transgressions (e.g., Berry and Wilde, 1978; Meyers,

2014). The stable isotope data collated for this study indicate that $\delta^{13}C_{org}$ values increased (i.e., become less negative) as C_{org} increased (Fig. 3.13B). In particular, thin intervals within F2 where highest TOC of 16.5 wt.% were documented corresponded with the highest $\delta^{13}C_{org}$ values of up to -15.57‰, whereas the silty interval in F4 where the least TOC of <1.0 wt.% also marked the least $\delta^{13}C_{org}$ value of 24.71‰. In addition, increase in CIA from 65% in F1 to over 80% in F5 indicates a possible climatic warm-up. The inferred minimal input of terrigenous sediments in F1 and F2 also corroborate a sea-level rise for this time. These geochemical data, therefore, suggest that the deposition of the WHF was analogous, on a reduced scale, to oceanic anoxic events. The striking similarities between the WHF and its correlative in Paranà and Huab basins indicate that the marine incursion and climatic warm-up that dictated their deposition were likely not a local but a regional event. Although the major constituent of the OM in F1 and F2 is an amorphous material, Tasmanites cysts (phycomata; Fig. 3.8C) and colonial algae cells (Fig. 3.8D) constitutes an ecologically notable fraction. The former is endemic to marine waters, whereas the latter can be found in both fresh and marine waters (e.g., Tappan, 1980; Baceta and Nunez-Betelu, 1994). Fossil Tasmanites cysts usually mark sedimentary intervals with maximum flooding and sediment starvation (Lazar et al., 2015) in marine settings (Tappan, 1980; Baceta and Nunez-Betelu, 1994; Schieber, 1996; Telnova, 2012), although some extant freshwater species do exist (Tappan, 1980; Martin, 1993). Enrichment of Tasmanites in Paleozoic deposits have been reported by Revill (1994) and interpreted as marine species. Therefore the occurrence of Tasmanites cysts indicates the prevalence of marine conditions during the accumulation of F1 and F2. The presence of phosphorites closely associated with OM (Fig. 3.8E-F) in F1 and F2 is also an indicative of marine conditions. According to several authors (e.g., Strydom, 1950; Cook, 1984; Visser, 1992), the presence of phosphorites indicate a marine environment associated with sea-level rise and minimal input of terrigenous sediment. The phosphorites observed in these WHF shales have a botryoidal texture, suggesting that their formation was associated with microbial sulfate reduction processes. These considerations, as well as the Rb/K ratios of these two lower WHF subunits, are strong evidence for marine transgression. On the contrary, the absence of these features and sharp contrast in Rb/K ratios between the upper and lower sections suggest largely non-marine conditions during the deposition of the upper WHF subunits (F3, F4, F5). In addition, the omnipresence of framboidal pyrites, clearly formed from the activities of sulfate-reducing bacteria, as well as large accumulations of other forms of iron sulfides clearly indicate that uniform reducing (anoxic)

conditions were persistent during the accumulation of the lower WHF subunits (F1, F2). Within the upper WHF subunits, evidence from animal-sediment interactions (i.e., invertebrate ichnofossils linked to different burrow styles and intensities) not only indicate progressive colonisation of the sediment by invertebrates but also different phases in the oxygenation of the sediment-water interface (Gibert et al., 2000; Bordy et al., 2001). It is therefore likely that during the accumulation of the upper WHF subunits, the progressive changes in the basin configuration from distal to proximal setting restricted connections with the open ocean and resulted in a progressive change from marine and anoxic to brackish and dysoxic and to oxic conditions in a lacustrine setting.

3.7. Conclusions

In this study, the spatiotemporal variations in the composition, particularly the distribution of organic carbon content, of the Lower Permian WHF in the main Karoo Basin has been quantified and the sedimentological controls responsible for the variability have been explained. The major findings of this study are as follows:

(1) The WHF comprises five vertically and laterally contiguous and genetically-related stratigraphic subunits, namely: black pyritic shale (F1), black to dark grey carbonaceous shale (F2), dark to light grey calcareous shale (F3), medium to light grey siliceous-calcareous silty shale (F4), and light grey siliceous massive sandy shale (F5). Although these five subunits in the WHF share similar sedimentologic characteristics at outcrop scale, such as prominent laminations and white-weathering, they are distinctive in their overall geochemical signatures including nature and amount of OM (amorphous, structured, plant-material dominated), isotopic compositions, and elemental enrichments, indicating variations in their provenances, dispersal mechanisms, depositional conditions, and post-depositional pathways.

(2) A sea-level highstand, high biological productivity, low terrigenous input and anoxic seafloor contributed to high organic carbon preservation during the deposition of subunits F1 and F2. Evidence in support of marine conditions during the accumulation of these lower subunits in the WHF include the presence of marine microfossils (e.g., Tasmanites

cysts and colonial algae cells) and the presence of phosphorites closely associated with OM. The $\delta^{13}C_{org}$ values increase with increasing organic matter content and indicate that the deposition of these subunits coincided with a climatic warm-up and sea-level highstand and are thus typical oceanic-anoxic deposits. A combination of these factors resulted in sea-level highstand coeval with the less-restricted oceanic connection. Moderate to warm climate conditions enhanced the supply of mineral nutrients and phytoplankton growth, resulting in increased OM input and development of anoxia as shown by increased TOC content and C-S relationships.

(3) The occurrence of large amounts of iron sulfides, including 5-10 cm marcasitic lags and nodules of various sizes, at the interface separating F2 and F3 suggests that the deposition of F2 was followed by an extended period of very low to zero deposition, during which desalination of the basin and a drop in relative sea-level occurred. The desalination and falling relative sea-level were possibly related to changes in the geometry of the basin that resulted from the basin-ward shift of the shoreline and concomitant change in depositional sub-environments from distal to more proximal as the fold-thrust belt (CFB) become more emergent. In addition, increasingly warmer climate as indicated by the CIA values could have resulted in higher evaporation levels.

(4) Accumulation of subunits F3-F5 occurred after cessation of deep-water flow and upwelling. Stable isotopes compositions and Rock-Eval data indicate that the greater part of the OM in F3 was sourced from terrestrial plants. A few solitary algae were observed supporting our opinion that primary productivity was minimal. CIA values of up to 80 suggest normal conditions. The presence and variations in bioturbation styles and intensities in these facies indicate that colonisation by invertebrates is related to the different phases in the oxygenation of the sediment-water interface. It is therefore likely that the progressive changes in the basin configuration from distal to proximal settings during later depositional stages of the WHF restricted connections with the ocean, resulting in a progressive change from brackish to oxic conditions in a lacustrine setting.

References

Aigner, T., and H.E. Reineck, 1982, Proximality trends in modern storm sands from the Helgoland Bight (North Sea) and their implications for basin analysis: Senckenbergiana Maritima, 14, 183-215.

Allard, T., M. Menguy, J. Solomon, T. Calligaro, T. Weber, G. Calas, and M.F. Benedetti, 2004, Revealing forms of iron in river-borne material from major tropical rivers of Amazon Basin (Brazil): Geochimica et Cosmochimica Acta, 68, 3079-3094.

Alldredge, A.L, and M.W. Silver, 1988, Characteristics, dynamics, and significance of marine snow: Progress in Oceanography, 20, 41-82.

Almond, J.E., 1996, Whitehill Formation, Western Cape: Joint Paleontological Research, October 1996: Unpublished report, Council for Geoscience, Pretoria, 17p.

Anderson, A.M., and I.R. McLachlan, 1979, The oil-shale potential of the Early Permian White Band Formation in southern Africa, 83-89, *in*, A.M. Anderson and W.J. van Biljon, eds, Some sedimentary basin and associated ore deposits of South Africa: Special Publication of the Geological Society of South Africa, 6, 228p.

Anderson, T.F., J. Kruger, and R. Raiswell, 1987, C-S-Fe relationships and the isotopic composition of pyrite in the New Albany Shale of the Illinois Basin, USA: Geochimica et Cosmochimica Acta, 51, 2795-2805.

Arnaboldi, M., and P.A. Meyers, 2006, Patterns of carbon and nitrogen stable isotopic compositions of latest Pliocene sapropels from six locations across the Mediterranean: Palaeogeography, Palaeoclimatology, Palaeoecology, 235, 149-167.

Arthur, M.A., and B.B. Sageman, 1994, Marine Black Shales: Depositional Mechanisms and Environments of Ancient Deposits: Earth and Planetary Science Letters, 22, 499-551.

Arthur, M.A., W.E. Dean, R.M. Pollastro, G.E. Claypool, and P.A. Scholle, 1985, Comparative geochemical and mineralogical studies of two cyclic transgressive pelagic limestone units, Cretaceous Western Interior Basin, U.S., *in*, L.M. Pratt, E.G. Kauffman, and F.B. Zelt, eds, Fine-grained Deposits and Biofacies of the Western Interior Seaway: Evidence of Cyclic Sedimentary Processes: Society of Economic Paleontologists and Mineralogists, 1985 Midyear Meeting, Golden, Colorado, Field Trip Guidebook No. 4, 16-27.

Baceta, J.I., and L. Nunez-Betelu, 1994, Basics and Application of Rock- Eval/TOC Pyrolysis:

an example from the uppermost Paleocene/lowermost Eocene, in, The Basque Basin, Western Pyrenees: Department of Geology and Geophysics, The University of Calgary, Ciencias Naturales-Natur Zientziak, 46, 43-62.

Bangert, B., H. Stollhofen, V. Lorenz, and R. Armstrong, 1999, The geochronology and significance of ash-fall tuffs in the glaciogenic Carboniferous-Permian Dwyka Group of Namibia and South Africa: Journal of African Earth Sciences, 29(1), 33-49.

Batten, D.J., 1983, Identification of amorphous sedimentary organic matter by transmitted light microscopy, in J. Brooks, ed., Petroleum Geochemistry and Exploration of Europe: Geological Society of London, Special Publication 12, 275-287.

Benning, L.G., R.T. Wilkins, and H.L. Barnes, 2000, Reaction pathways in the Fe-S system below 100^{o} C: Chemical Geology, 167, 25-51.

Berner, R.A., 1967, Thermodynamic stabilities of sedimentary iron sulfides: American Journal of Science, 265, 773-785.

Berner, R.A., 1970, Sedimentary pyrite formation: American Journal of Science, 268, 1-23.

Berner R. A., 1980, Early Diagenesis: A Theoretical Approach: Princeton University Press, Princeton, 241p.

Berner, R.A., 1984, Sedimentary pyrite formation: An update, Geochimica et Cosmochimica Acta, 48, 143-149.

Berner, R.A., and R. Raiswell, 1983, Burial of organic carbon and pyrite sulfur in sediments over Phanerozoic time: a new theory: Geochimica et Cosmochimica Acta, 47, 855-862.

Berner, R.A., and R. Raiswell, 1984, C-S method for distinguishing freshwater from marine sedimentary rocks: Geology 12, 365–368.

Berry, W.B., and P. Wilde, 1978, Progressive ventilation of the oceans: American Journal of Sciences, 278, 257-275.

Bertrand, P., G. Shimmield, P. Martinez, F. Grousset, F. Jorissen, M. Paterne, C. Pujol, I. Bouloubassi, P. Buat Menard, J.P. Peypouquet, L. Beaufort, M.A. Sicre, E. Lallier-Verges, J.M. Foster, and Y. Ternois, 1996, The glacial ocean productivity hypothesis: the Importance of regional temporal and spatial studies: Marine Geology, 130, 1-9.

Birnbaum, S.J., and J.W., Wireman, 1985, Bacteria sulfate-reduction and pH: implications for early diagenesis: Chemical Geology, 43, 143-149.

Blatt, H., 1992, Sedimentary Petrology: W.H. Freeman and Co., New York, 514p.

Blatt, H., and M.W. Totten, 1981, Detrital quartz as an indicator of distance from the shore in marine mudrocks: Journal of Sedimentary Petrology, 51, 1259-1266.

Bohacs, K.M., G.J. Grabowski, A.R. Carroll, P.J. Mankiewicz, K.J. Miskellgerhardt, J.R. Schwalbach, M.B. Wegner, and J.A. Simo, 2005, Production, destruction, and dilution: the many paths to source-rock development, in N.B. Harris, ed., The Deposition of Organic-Carbon-Rich Sediments: Models, Mechanisms, and Consequences: SEPM Special Publication 82, 61-101.

Bordy, E.M., S Linkermann, and R Prevec, 2001, Palaeoecological aspects of some invertebrate fossils from Mid- to Upper Permian Middleton Formation (Adelaide Supergroup, Beaufort Group, Karoo Supergroup), Eastern Cape, South Africa: African Earth Sciences, 61, 238-244.

Bowman, A.R., and T.J. Bralower, 2005, Paleoceanographic significance of high-resolution carbon isotope records across the Cenomanian-Turonian boundary in the western interior and New Jersey coastal plain, USA. Marine geology, 217, 305–321, doi:10.1016/j.margeo.2005.02.010.

Bralower, T. J., E. CoBabe, B. Clement, W.V. Sliter, C.L. Osburn, and J. Longoria, 1999, The record of global change in mid-Cretaceous (Barremian- Albian) sections from Sierra Madre, northeastern Mexico: Journal of Foraminiferal Research, 29, 418–437.

Brasier, M.D., 1992, Nutrient-enriched waters and the early skeletal fossil record: Journal of the Geological Society of London, 149, 621-629.

Broom, R., 1913, On some fishes from the Lower and Middle Karroo Beds: Annals of the South African Museum, 12, 1-5.

Brumsack, H.J., 1989, Geochemistry of recent TOC-rich sediments from Gulf of California and the Black Sea: Geolgishe Rundschau, 78, 851-882.

Brumsack, H.J., 2006, The trace metal content of recent organic carbon-rich sediments: Implication for Cretaceous black shale formation: Palaeogeography, Palaeoclimatology, Palaeoecology, 232, 344-361.

Calvert, S.E., and T.F. Pedersen, 1993, Geochemistry of recent oxic and anoxic marine sediments: implications for the geological record: Marine Geology, 113, 67-88.

Calvert, S.E., R.M Bustin, and E.D. Ingall, 1996, Influence of water column anoxia and sediment supply on the burial and preservation of organic carbon in marine shales: Geochimica et

Cosmochimica Acta, 60, 1577-1593.

Campbell, F.A., and G.D. Williams, 1965, Chemical composition of shales of Mannville Group Lower Cretaceous of Central Alberta, Canada: AAPG Bulletin 49, 81-87.

Canfield, D.E., 1989, Reactive iron in marine sediments: Geochimica et Cosmochimica Acta, 53, 619-632.

Canfield, D.E., and R. Raiswell, 1991, Pyrite formation and fossil preservation, in, P.A. Allison and D.E. Briggs, eds, Taphonomy: Releasing the data locked in the fossil record, Plenum Press, New York, 337-387.

Canfield, D.E., 1994, Factors influencing organic carbon preservation in marine sediments: Chemical Geology, 114, 315-29.

Carmack, C. L., J. D. Weete, and W. D. Kelley, 1976, Hydrocarbons, fatty-acids and sterols of cronartium-fusiforme aeciospores: Physiological Plant Pathology, 8, 43-49.

Catuneanu, O., P.J. Hancox, and B.S. Rubidge, 1998, Reciprocal flexural behaviour and contrasting stratigraphies: a new basin development model for the Karoo retroarc foreland system, South Africa: Basin Research, 10, 417-439.

Catuneanu, O., H. Wopfner, P.G. Eriksson, B. Cairncross, B.S. Rubidge, R.M.H. Smith, and P.J Hancox, 2005, The Karoo basins of south-central Africa: Journal of African Earth Sciences, 43, 211-253.

Christie, A.D.M., 1990, Origin, classification and utilization of oil shales in South Africa: South African Journal of Science, 86, 9-15.

Chukwuma, K., and E.M. Bordy, 2016, Spatiotemporal sedimentary facies variations in the Permian Whitehill Formation, main Karoo Basin, *in* B. Linol and M. de Wit, eds., Origin and Evolution of the Cape Mountains and Karoo Basin: Geo-biohistory in a terrain with shale gas resources and need for conservation, Part of the series Regional Geology Reviews 8643: Springer Verlag, 101-110, doi 10.1007/978-3-319-40859-0_10.

Cole, D.I., 1978, Preliminary report on the oil potential of the Whitehill Formation between Strydenburg (Cape Province) and Hertzogville (Orange Free State): Report of the Geological Survey of South Africa, 1978-0304, (open file report).

Cole, D.I., 2014, Geology of Karoo shale gas and how this can influence economic gas recovery, *in*, Presentation, Gas-The game changer for southern Africa?: Fossil Fuel Foundation, Glen Hove, Johannesburg, 21 May 2014, abstracts, 11-12.

Cole, D.I., and W.A. Basson, 1991, Whitehill Formation: Catalogue of South African Lithostratigraphic Units, M.R. Johnson, ed., 3, 3.51-3.52.

Cole, D.I., and I.R. McLachlan, 1991, Oil Potential of the Permian Whitehill Shale Formation in the Main Karoo Basin, South Africa, *in*, H. Ulbrich, and A.C. Rocha Campos, eds, Proceedings and Papers of the Seventh Gondwana Symposium, Sao Paulo Instituto de Geosciences: Universidade de Sao Paulo: 379-390.

Cole, D.I. and I.R. McLachlan, 1994, Oil shale potential and depositional environment of the Permian Whitehill Shale Formation in the main Karoo Basin: Open file report, Geological Survey of South Africa, 1994-0213, 1 & 2, 145p.

Compton, J.S., 1991, Origin and diagenesis of clay minerals in the Monterey Formation, Santa Maria Basin Area, California: Clays and Clay Minerals, 39, 449-466.

Cook, P.J., 1984, Spatial and temporal controls on the formation of phosphate deposits-a review, *in*, J.O. Nriagu, and P.B. Moore, eds, Phosphate minerals: Springer-verlag, New York, 242-274.

Crusius, J., S. Calvert, T. Pedersen, and D. Sage, 1996, Rhenium and molybdenum enrichments in sediments as indicators of oxic, suboxic, and sulfidic conditions of deposition: Earth Planetary Science Letters, 145, 65-78.

Danchin, R.V., 1970, Aspects of the geochemistry of some selected South African fine-grained sediments: unpublished Ph.D. thesis, University of Cape Town, 215p.

de Gibert, J.M., M.A. Fregenal-Martínez, L.A. Buatois, and M.G. Mángano, 2000, Trace fossils and their palaeoecological significance in Lower Cretaceous lacustrine conservation deposits, El Montsec, Spain: Palaeogeography, Palaeoclimatology, Palaeoecology 156, 89-101.

Dean, W.E., M.A. Arthur, 1989, Iron-sulfur-carbon relationships in organic carbon-rich sequences: I. Cretaceous Western Interior Seaway: American Journal of Science, 289, 708-743.

Dean, W.E., M.A. Arthur, and G.E. Claypool, 1986, Depletion of ^{13}C in Cretaceous marine organic matter: Source, diagenetic, or environmental signal? Marine Geology, 70, 19-157, doi:10.1016/0025-3227(86)90092-7.

Dean, W. E., J.V. Gardner, and D.Z. Piper, 1997, Inorganic geochemical indicators of glacial-

interglacial changes in productivity and anoxia on the California continental margin: Geochimica et Cosmochimica Acta, 61, 4507-4518.

Degens, E.T., and D.A. Ross, 1974, The Black Sea-geology, chemistry, and biology: AAPG Memoir 20, 633p.

Degens, E.T., R.P. Von Herzen, and H.-K. Wong, 1971, Lake Tanganyika: water chemistry, sediments, and geological structure: Naturwissenschften, 58, 224-291.

Demaison, G.J. and G.T. Moore, 1980, Anoxic environments and oil source bed genesis: AAPG Bulletin, 64, 1179-1209.

De Wit, M.J., and I.G.D. Ransome, 1992, Regional inversion tectonics along the southern margin of Gondwana, in, M.J. De Wit and I.G.D. Ransome, eds, Inversion tectonics of the Cape Fold Belt, Karoo and Cretaceous Basins of Southern Africa: Balkema, Rotterdam, Netherlands, 15-20.

Decker, J., and J. Marot, 2012, Investigation of hydraulic fracturing in the Karoo of South Africa: Annexure A, Resource Assessment, Petroleum Agency SA, Available at: <http://www.dmr.gov.za/publications/ viewdownload/ 182/854.html> (last viewed 07-02-17).

Du Toit, A.L., 1927, A geological comparison of South America and South Africa: Carnegie Institution, Washington, Publication No 381, 158p.

Erbacher, J., O. Friedrich, P.A. Wilson, H. Birch, and J. Mutterlose, 2005, Stable organic carbon isotope stratigraphy across oceanic anoxic Event 2 of Demerara Rise, western tropical Atlantic: Geochemistry, Geophysics, Geosystem, 6(6), Q06010, doi:10.1029/2004GC000850.

Ernst, W., 1970, Geochemical facies analysis, *in*, Methods in Geochemistry and Geophysics, Elsevier, Amsterdam, 152p.

Ertel, J. R., and J. I. Hedges, 1985, Sources of Sedimentary Humic Substances-Vascular Plant Debris: Geochimica et Cosmochimica Acta, 49, 2097-2107.

Espitalié, J., G. Deroo, and F. Marquis, 1985, Rock-Eval pyrolysis and its applications: Institut Français du Pétrole, Preprint no. 27299.

Faure, K., and D.I. Cole, 1999, Geochemical evidence for lacustrine microbial blooms in the vast Permian main Karoo, Paraná, Falkland Islands and Huab basins of southwestern Gondwana: Palaeogeography, Palaeoclimatology, Palaeoecology, 152, 189-213.

Flügel, E., 2004, Microfacies of carbonate rocks: Springer, Berlin, 976 p.

Francois, R., 1988, A study on the regulation of the concentrations of some trace elements (Rb, Sr, Zn, Pb, Cu, V, Cr, Ni, Mn and Mo) in Saanich Inlet sediments, British Columbia, Canada: Marine Geology, 83, 285-308.

Geel, C., M. de Wit, P. Booth, H-M. Schulz, and B Horsfield, 2015, Palaeo-environment, diagenesis and characteristics of Permian black shales in the lower Karoo Supergroup flanking the Cape Fold Belt near Jansenville, Eastern Cape, South Africa: Implications for the shale gas potential of the Karoo Basin: South African Journal of Geology, 118, 248–274.

Gervais, M.P., 1864, Description de *Mesosaurus tenuidens,* reptile fossile de l'Afrique Australe: Mem Acad. Mont. Pellier, Sec Sci., 169-175.

Ghadeer, S.G., and J.H.S. Macquaker, 2012, The role of event beds in the preservation of organic carbon in fine-grained sediments: analyses of the sedimentological processes operating during deposition of the Whitby Mudstone Formation (Toarcian, Lower Jurassic) preserved in northeast England: Marine and Petroleum Geology, 35, 309-320.

Goldhaber, M.B., 2003, Sulfur-rich sediments, in, F.T. Mackenzie, ed., Treatise in Geochemistry, vol. 7, Sediment, Diagenesis, and Sedimentary Rocks, Elsevier, Amsterdam, 257-288.

Gorin, G.E., and S. Feist-Brukhardt, 1990, Organic facies of Lower to Middle Jurassic sediments in the Jura Mountains, Switzerland: Review of Paleobotany and Palynology, 65, 349-355.

Hair, J.F., W.C. Black, B.J. Babin, R.E. Anderson, and R.L. Tatham, 2006, Multivariate Data Analysis-6th edition: Pearson Prentice Hall, Upper Saddle River, New Jersey, 928p.

Hälbich, I.W., 1983, A tectogenesis of the Cape Fold Belt (CFB), in, A.P.G. Söhnge, and I.W. Hälbich, eds, Geodynamics of the Cape Fold Belt: Special Publications of the Geological Society of South Africa, 12, 165-175.

Helz, G.R., C.V. Miller, J.M. Charnock, J.F.W. Mosselmans, R.A.D. Pattrick, C.D. Garner, D.J. Vaughan, 1996, Mechanisms of molybdenum removal from the sea and its concentration in black shales- EXAFS evidence: Geochimica et Cosmochimica Acta, 60, 3631–3642.

Hodell, D. A., C. L. Schelske, G. L. Fahnenstiel, and L. L. Robbins, 1998, Biologically induced calcite and its isotopic composition in Lake Ontario: Limnology and Oceanography, 43,

187-199.

Hofmann, P., W. Ricken, L. Schwark, and D. Leythaeuser, 2000, Carbon-sulfur-iron relationships and $\delta^{13}C$ of organic matter for late Albian sedimentary rocks from the North Atlantic Ocean: paleoceanographic implications: Palaeogeography, Palaeoclimatology, Palaeoecology, 163, 97-113, doi:10.1016/S0031-0182(00)00147-4

Hofmeyr, P.K., 1971, The abundances and distribution of some trace elements in some selected South African shales: Unpublished Ph.D. thesis, University of Cape Town, 218p.

Hollander, D. J., and J. A. McKenzie, 1991, CO_2 control on carbon isotope fractionation during aqueous photosynthesis: A paleo-CO_2 barometer: Geology, 19, 929-932.

Inoue, A., B. Velde, A. Meunier, and G. Touchard, 1988, Mechanism of illite formation during smectite-to-illite conversion in a hydrothermal system: American Mineralogist, 73, 1325-1334.

Inoue, A., B. Lanson, M. Marques Fernandes, B.A. Sakharov, T. Murakami, A. Meunier, and D. Beaufort, 2005, Illite-smectite mixed-layer minerals in the hydrothermal alteration of volcanic rocks: I. One-dimensional XRD structure analysis and characterization of component layers: Clays and Clay Minerals, 53, 423-439.

Isbell, J.L., D.I. Cole, D.I., and O. Catuneanu, O., 2008. Carboniferous-Permian glaciation in the main Karoo basin, South Africa: stratigraphy, depositional controls, and glacial dynamics, in, C.R. Fielding, T.D. Frank, and J.L. Isbell, eds, Resolving the Late Paleozoic Ice Age in Time and Space: Geological Society of America, Special Paper 441, 71-82.

Jarvie, D.M., B.L. Claxton, F. Henk, J.T. Breyer, 2001, Oil and Shale Gas from the Barnett Shale, Ft. Worth Basin, Texas: Talk presented at the AAPG National Convention, June 3-6, 2001, Denver, CO, AAPG Bulletin, p. A100.

Jarvie, D. M., R. J. Hill, T. E. Ruble, and R. M. Pollastro, 2007, Unconventional shale-gas systems: The Mississippian Barnett Shale of north-central Texas as one model for thermogenic shale gas assessment: AAPG Bulletin, 91, no. 4, 475-499.

Jia, J., A. Bechtel, Z. Liu, A.I. Susanne, P.S. Strobl, and F.S. Reinhard, 2013, Oil shale formation in the Upper Cretaceous Nenjiang formation of the Songliao Basin (NE China): Implications from organic and inorganic geochemical analyses: Int. Journal of Coal Geology, 113, 11-26.

Johnson, M. R., C.J. Van Vuuren, J.N.J. Visser, D.I. Cole, H. DeV Wickens, A.D.M Christie, and D.L. Roberts, 1997, The Foreland Karoo Basin, South Africa, in K.J. Hsü. Series ed., R.C. Selley, ed., Sedimentary basins of the world-African Basins: Elsevier, 269-317.

Johnson, M. R., C.J. Van Vuuren, J.N.J. Visser, D.I. Cole, H. DeV Wickens, A.D.M Christie, D.L. Roberts, and G. Brandl, 2006, Sedimentary rocks of the Karoo Supergroup, *in*, M.R. Johnson, C.R. Anhaeusser, and R.J. Thomas, eds., The Geology of South Africa: Geological Society of South Africa/Council for Geoscience, 461-499.

Jones, B., and D.A.C Manning, 1994, Comparison of geochemical indices used for the interpretation of palaeoredox conditions in ancient mudstones: Chemical Geology 111, 111-129.

Kaplan, I.R., K.O. Emery, and S.C. Rittenberg, 1963, The distribution and isotopic abundance of sulfur in recent marine sediments off southern California: Geochimica et Cosmochimica Acta, 27, 297-331.

Katz, B.J., 2005, Controlling factors on source rock development-a review of productivity, preservation and sedimentation rate, in N.B. Harris, ed., The Deposition of Organic-carbon-rich Sediments: Models, Mechanisms, and Consequences: SEPM Special Publication, 82, 7-16.

Kensley, B., 1975, Taxonomic status of the pygocephalomorphic crustacea from the Dwyka 'White Band' (Permo-Carboniferous) of South Africa: Annals of the South African Museum 67, 25-33.

Kidder, D.L., and D.H. Erwin, 2001, Secular distribution of biogenic silica through the Phanerozoic: comparison of silica-replaced fossils and bedded cherts at the series level: Geology, 109, 509-522.

Kolla, V., and P.E. Biscaye, 1977, Distribution of quartz in sediments of the Indian Ocean: Journal of Sedimentary Petrology, 47, 642-649.

Könitzer, S.F., S.J. Davies, M.H. Stephenson, and M.J. Leng, 2014, Depositional controls on mudstone lithofacies in a basinal setting: Implications for the delivery of sedimentary organic matter: Journal of Sedimentary Research, 84, 198-214.

Kuypers, M.M.M., Y. van Breugel, S. Schouten, E. Erba, and J.S. Sinninghe Damsté, 2004, N2-fixing cyanobacteria supplied nutrient N for Cretaceous oceanic anoxic events, Geology, 32, 853-856, doi:10.1130/G20458.1

Lazar, O.R., K.M. Bohacs, J. Schieber, J.H.S. Macquaker, and T.M. Demko, 2015, Mudstone Primer: Lithofacies variations, diagnostic criteria, and sedimentologic implications at lamina to bedset scale: nomenclature and description guidelines: SEPM Concepts in Sedimentology and Paleontology, 12, 198p.

Lehmann, M. F., S. M. Bernasconi, A. Barbieri, and J. A. Mckenzie, 2002, Preservation of organic matter and alteration of its carbon and nitrogen isotope composition during simulated and in situ early sedimentary diagenesis: Geochimica et Cosmochimica Acta, 66, 3573-3584.

Lewan, M.D., 1984, Factors controlling the proportionality of vanadium to nickel in crude oils: Geochimca et Cosmochimica Acta, 48, 2231-2238.

Littke, R., D.R. Baker, and D. Leythaeuser, 1988, Microscopic and sedimentologic evidence for the generation and migration of hydrocarbons in Toarcian source rocks of different maturities: Organic Geochemistry, 13, 549-559.

Lock, B. E., 1980, Flat-plate subduction and the Cape Fold Belt of South Africa: Geology, 8, 35-39.

López-Gamundí, O., A. Fildani, A. Weislogel, and E. Rossello, 2013, The age of the Tunas formation in the Sauce Grande basin-Ventana foldbelt (Argentina): Implications for the Permian evolution of the southwestern margin of Gondwana: Journal of South American Earth Sciences, no. 45, 250–258, doi:10.1016/j.jsames.2013.03.011

Lyons, T.W., and R.A. Berner, 1992, Carbon-sulfur-iron systematics of the uppermost deep-water sediments of the Black Sea: Chemical Geology, 99, 1-27.

Macquaker, J.H.S., and A.E. Adams, 2003, Maximizing information from fine-grained sedimentary rocks: an inclusive nomenclature for Mudstones: Journal of Sedimentary Research, 73, 735-744.

Macquaker, J.H.S., M.A. Keller, and S.J. Davies, 2010, Algal blooms and ‘‘marine snow’’: mechanisms that enhance preservation of organic carbon in ancient fine-grained sediments: Journal of Sedimentary Research, 80, 934-942.

McLachlan, I. R., and A. Anderson, 1973, A review of the evidence for marine conditions in southern Africa during Dwyka times: Palaeontologica Africana, 15, 37-64.

McLachlan, I. R., and A. Anderson, 1977, Carbonates, "stromatolites" and tuffs in the Lower

Permian White Band Formation: South African Journal of Science, 73, 92-94.

McKay, M.P., A.L Weislogel, A. Fildani, L. Rufus, R.L. Brunt, M. David, D.M. Hodgson, and S.S. Flint, 2015, U-PB zircon tuff geochronology from the Karoo Basin, South Africa: implications of zircon recycling on stratigraphic age controls: International Geology Review, 57, 393-410.

McKibben, M.A., and H.L. Barnes, 1986, Oxidation of pyrite in low temperature acidic solutions: Rates laws and surface textures: Geochimica Cosmochimica Acta, 50, 1509-1520.

Meyers, P.A., 1997, Organic geochemical proxies of paleoceanographic, paleolimnologic, and paleoclimatic processes: Organic Geochemistry, 276, no. 5/6, 213-250.

Meyers, P.A., 2014, Why are the $\delta^{13}C_{org}$ values in Phanerozoic black shales more negative than in modern marine organic matter?: Geochemistry Geophysics Geosystem, 15, 3085-3106, doi:10.1002/2014GC005305.

Meyers, P.A., and S.M. Bernasconi, 2006, Data report: organic carbon, total nitrogen, carbonate carbon, and carbonate oxygen isotopic compositions of Albian to Santonian black shales from Sites 1257-1261 on the Demerara Rise. In, D.C. Mosher, J. Erbacher, and M.J. Malone, eds, Proc. ODP, Sci. Results, 207, College Station, TX (Ocean Drilling Program), 1-13, doi:10.2973/ odp.proc.sr.207.106.2006.

Milliken, K. L., 1994, Cathodoluminescent textures and the origin of quartz silt in Oligocene mudrocks, South Texas: Journal of Sedimentary Research, A64, 567-571.

Nesbitt, H.W., and G.M. Young, 1982, Early Proterozoic climates and plate motions inferred from major element chemistry of lutites: Nature 299, 715-717.

Nissenbaum, A., M.J. Baedecker, and I.R. Kapian, 1972, Dissolved organic matter from interstitial organic water of a reducing fjord, in, Advances in organic geochemistry 1971: International Series Monographic Earth Sciences, 33, 117-120.

Oelofsen, B.W., 1981, An anatomical and systematic study of the family Mesosauridae (Reptilia, Proganosauria) with special reference to its associated fauna and palaeoecological environment in the Whitehill Sea: Unpublished Ph.D. thesis, University of Stellenbosch, 163p.

Oelofsen, B.W., 1987, The biostratigraphy and fossils of the Whitehill and Iratí Shale Formations of the Karoo and Paraná Basins, in, C.D. McKenzie, ed., Gondwana Six:

stratigraphy, sedimentology and paleontology: Geophysical Monograph, American Geophysical Union, 41,131-138.

Oelofsen, B.W. and D.C. Araújo, 1987, Palaeoecological implications of the distribution of mesosaurid reptiles in the Permian Irati sea (Paraná Basin), South America: Rev. Bras. Geociêc., 13, 1-6.

Pankhurst, R.J., C.W. Rapela, C.M. Fanning, and M. Ma´rquez, 2006, Gondwanide continental collision and the origin of Patagonia: Earth Science Reviews, 76, 235-257.

Passey, Q.R., K.M. Bohacs, W.L. Esch, R. Klimentidis, and S. Sinha, 2010, From oil-prone source rock to gas-producing shale reservoir: geologic and petrophysical characterization of unconventional shale-gas reservoirs: Society of Petroleum Engineers, no. 131350, 29p.

Pedersen, T.F., and S.E. Calvert, 1990, Anoxia versus productivity: what controls the formation of organic carbon rich sediments and sedimentary rocks?: AAPG Bulletin 74, 454–466.

Peters, K. E., 1986, Guidelines for evaluating petroleum source rock using programmed pyrolysis: AAPG Bulletin, 70, 318-329.

Peters, K.E., and M.R. Cassa, 1994, Applied source rock geochemistry, in L.B. Magoon, and W.G. Dow, eds, The petroleum system-from source to trap: AAPG Memoir 60, 93-120.

Peters, K.E., R.E. Sweeney, and I.R. Kaplan, 1978, Correlation of carbon and nitrogen stable isotopes rations in sedimentary organic matter: Limnology and Oceanography, 23, 598-604

Pickford, M., 1995, Karoo Supergroup palaeontology of Namibia and brief description of a The conodont from Omingonde: Palaeontolology Africana, 32, 51-66.

Piper, D.Z., 1994, Seawater as the source of minor elements in black shales, phosphorites and other sedimentary rocks: Chemical Geology, 114, 95-114.

Piper, D.Z., and R.B. Perkins, 1994, A modern vs. Permian black shale-the hydrography, primary productivity, and water-column chemistry of deposition: Chemical Geology, 206, 177-197.

Piper, D.Z., and S.E. Calvert, 2009, A marine biogeochemical perspective on black shale deposition: Earth Sciences Reviews, 95, 63-96.

Potter, P. E., J.B. Maynard, and W.A. Pryor, 1980, Sedimentology of Shale: Springer Verlag, New York, 310p.

Radke M., D.H. WeRe, and H. Willscli, 1986, Maturity parameters based on aromatic hydrocarbons: Influence of the organic matter type, *in*, D. Leythaeuser, and J. Rullktter, eds, Advances in Organic Geochemistry 1985, Pergamon Press, Oxford: Organic Geochemistry, 10, 51-64.

Raiswell, R., and R.A. Berner, 1985, Pyrite formation in euxinic and semi-euxinic sediments: American Journal of Science, 285, 710-724.

Raiswell, R., 1987, Non-steady state microbiological diagenesis and the origin of concretions and nodular limestones, in J.D. Marshall, ed., Diagenesis of Sedimentary Sequences: Geological Society of London, Special Publication 36, 41-54.

Ratcliffe, K.T., A.M. Wright, P. Montgomery, A. Palfrey, A. Vonk, J. Vermeulen, and M. Barrett, 2010, Application of chemostratigraphy to the Mungaroo Formation, the Gorgon field, offshore northwest Australia: Aust. Pet. Prod. Explor. Assoc. Jour., 50th Anniversary Issue, 371-388.

Revill, A.T., J.K. Volkman, T. O'Leary, R.E. Summons, C.J. Boreham, M.R. Banks, and K. Denwer, 1994, Hydrocarbon biomarkers, thermal maturity and depositional setting of Tasmanite oil shales from Tasmania, Australia: Geochimica et Cosmochimica Acta, 58, 3803-3822.

Richard, D., and J.W. Morse, 2005, Acid volatile sulfides (AVS): Marine Chemistry, 97, 141-198.

Rigby, D., and B.D. Batts, 1986, The isotopic composition of nitrogen in Australian coals and oil shales: Chemical Geology, 58, 273-282, doi:10.1016/0168- 9622(86)90016-3.

Rimmer, S.M., 2004, Geochemical paleoredox indicators in Devonian- Mississippian black shales, Central Appalachian Basin (USA): Journal of Chemical Geology, 206, 373-391.

Ripley, E.M., N.R. Shaffer, and M.S. Gilstrap, 1990, Distribution and geochemical characteristics of metal enrichment in the New Albany shale (Devonian– Mississippian): Indiana. Econ. Geol., 85, 1790-2807.

Ritsema, C.J., and J.E. Groenenberg, 1993, Pyrite oxidation, carbonate weathering, and gypsum formation in a drained potential acid soil: Soil Science Society of America, 57, 968-976.

Rogers, A.W., and Schwarz, E.H.L., 1901, Report on a survey of parts of the Beaufort West, Prince Albert, and Sutherland Divisions: Ann. Rep. Geol. Comm. C. G. H., 100-106.

Rogers, A.W., and Du Toit, A.L., 1903, Geological surveys of parts of the Divisions of Ceres,

Sutherland and Calvinia: Ann. Rep. Geol. Comm. C. G. H., 25-32.

Ross, D.J.K., and R.M. Bustin, 2009, Investigating the use of sedimentary geochemical proxies for paleoenvironment interpretation of the thermally mature organic rich strata: Examples from the Devonian and Mississippian shales, Western Canadian Sedimentary Basin: Journal of Chemical Geology, 260, 1-19.

Rowsell, D.M., and A.M.J. De Swart, 1976, Diagenesis in Cape and Karroo sediments, South Africa, and its bearing on their hydrocarbon potential: Transactions of the Geology Society of South Africa, 79, 81-145.

Russel, W.L., 1939, The stratigraphy of the Upper Witteberg, Dwyka, Ecca and Beaufort Formations in the Laingsburg region, Cape Province, Union of South Africa: Unpublished Report of the Geological Survey of South Africa, 56p.

SACS (South African Committee for Stratigraphy), 1980, Stratigraphy of South Africa, Part 1, L.E. Kent, compiler: Handbook Geological Survey of South Africa, Pretoria, 8, 690p.

Sakan, M.S., D.S. Dorđević, and S.S. Trifunović, 2011, Geochemical and statistical methods in the evaluation f trace elements combinations: an application on canal sediments: Polish Journal of Environmental Studies, 20, no 1, 187-199.

Scheffler, K., D. Bühmann, and L. Schwark, 2006, Analysis of late Palaeozoic glacial to postglacial sedimentary succession in South Africa by geochemical proxies-Response to climate evolution and sedimentary environment: Palaeogeography, Palaeoclimatology, Palaeoecology, 240, 184-203.

Schieber, J., 1994, Evidence for high-energy events and shallow-water deposition in the Chattanooga Shale, Devonian, central Tennessee, U.S.A: Sedimentary Geology, 93, 193-208.

Schieber, J., 1996, Early diagenetic silica deposition in algal cysts and spores: A source of sand in black shales?: Journal of Sedimentary Research, 66, 175-183.

Schieber, J., 2007, Oxidation of detrital pyrite as a cause for marcasitic formation in marine lag deposits from the Devonian of the eastern US: Deep Sea Research II, 54, 1312-1326.

Schieber, J, 2011, Iron sulfide formation, in, J. Reitner and V. Thiel, eds, Encyclopedia of Geobiology: Springer-Verlag, 486-502.

Shieber, J., D. Krinsley, and L. Riciputi, 2000, Diagenetic origin of quartz silt in mudstone and implication for silica cycling: Nature, 406, 981-985.

Schieber, J., J.B. Southard, and A. Schimmelmann, 2010, Lenticular shale fabrics resulting from intermittent erosion of water-rich muds: interpreting the rock record in the light of recent flume experiments: Journal of Sedimentary Research, 80, 119-128.

Schoepfer, S.D., J. Shen, H. Wei, R.V. Tyson, E. Ingall, and T.J. Algeo, 2015, Total organic carbon, organic phosphorous, and biogenic barium fluxes as proxies for paleomarine productivity: Earth Science Reviews, 149, 23-52.

Sliter, W.V., 1989, Aptian anoxia in the Pacific Basin: Geology, 17, 909-912.

Smith, R.M.H., 1990, A review of stratigraphy and sedimentary environments of the Karoo basin of South Africa: Journal of African Earth Science, 10, 117-137.

Smithard, T., E.M. Bordy, and D. Reid, 2015, The effect of dolerite intrusions on the hydrocarbon potential of the lower Permian WHF Formation (Karoo Supergroup) in South Africa and southern Namibia: A preliminary study: South African Journal of Geology, 118, 489-510.

Soyinka, O.A., and R.M. Slatt, 2008, Identification and micro-stratigraphy of hyperpycnites and turbidites in Cretaceous Lewis Shale, Wyoming: Sedimentology, 55, 1117-1133.

Stollhofen, H., I.G. Stanistreet, B. Bangert, and H. Grill, 2000, Tuffs, tectonism and glacially related sea-level changes, Carboniferous-Permian, southern Namibia: Palaeogeography, Palaeoclimatology, Palaeoecology, 161, 127-150, doi:10.1016/S0031-0182(00)00120-6.

Strydom, H.C., 1950, The geology and chemistry of the Laingsburg Phosphorites: Annals of the University of Stellenbosch, 26A, 267-285.

Surdam, R.C., and J.R. Boles, 1979, Diagenesis of volcanic sandstones, in P.A. Scholle and P.R. Schluger, eds, Aspects of diagenesis: Society for Economic Paleontologists and Mineralogists Special Publication, 26, 227-242.

Suttner, L.J., and P.K Dutta, 1986, Alluvial sandstone composition and palaeoclimate 1, Framework mineralogy: Journal of Sedimentary Research, 56, 329-345.

Talbot, M. R., and T. Johannessen, 1992, A high-resolution paleoclimatic record for the last 27,500 years in tropical West Africa from the carbon and nitrogen isotopic composition of lacustrine organic-matter: Earth and Planetary Science Letters, 110, 23-37.

Tankard, A., H. Welsink, P. Aukes, R. Newtond, and E. Stettlere, 2009, Tectonic evolution of the Cape and Karoo basins of South Africa: Journal of Marine and Petroleum Geology, 26 (8), 1379-1412.

Tankard, A., H. Welsink, P. Aukes, R. Newtond, and E. Stettlere, 2012, Geodynamic interpretation of the Cape and the Karoo basins, South Africa-Phanerozoic Passive Margins, Cratonic Basins and Global Tectonics Maps, USA and UK: Elsevier, 869p.

Tappan, H., 1980, The paleobiology of plant protists: W.H. Freeman and Co., San Francisco, 1028p.

Teerman, S. C., B. J. Cardott, R. W. Harding, M. J. Lemos De Sousa, D. R. Logan, H. J. Pinheiro, M. Reinhardt, C. L. Thompson-Rizer, and R. A. Woods, 1995, Source rock/dispersed organic matter characterization: TSOP research subcommittee results: Organic Geochemistry, 22, 11-25, doi:10.1016/0146-6380(95)90004-7.

Teichert, C., 1974, Marine sedimentary environments and their faunas in Gondwana area: AAPG Memoir 23, 43-145.

Telnova, O.P., 2012, Morphology and ultrastructure of Devonian prasinophycean algae (Chlorophyta): Paleontological Journal, 46, 543-548.

Tissot, B. P., and D.H. Welte, 1984, Petroleum formation and occurrence: Springer-Verlag, New York, 699p.

Tribovillard, N.P., A. Desprairies, E. Lallier-Verges, P. Bertrand, N. Moureau, A. Ramdani, and L. Ramanamposoa, 1994, Geochemical study of organic-matter rich cycles from the Kimmeridge clay formation of Yorkshire (UK): productivity versus anoxia: Palaeogeography Palaeoclimatology Palaeoecology, 108, 165-181.

Tribovillard, N., T.J. Algeo, T. Lyons, and A. Riboulleau, 2006, Trace metals as paleoredox and paleoproductivity proxies: an update: Chemical Geology, 232, 12-32.

Tyson, R.V., and T.H. Pearson, 1991, Modern and ancient continental shelf anoxia: an overview, *in*, R.V. Tyson, and T.H. Pearson, eds, Modern and Ancient Continental Shelf Anoxia: Special Publication of the Geological Society, 58, 1-24.

Van der Westhuizen, W.A., J.C. Loock, and D. Strydom, 1981, Halite imprints in the Whitehill Formation, Ecca Group, Carnarvon District: Annals of Geological Survey of South Africa, 15, 43-46.

Veevers, J.J., 1994, Case for the Gamburtsev subglacial mountains of East Antarctica originating by mid-Carboniferous shortening of an intracratonic basin: Geology, 22, 593-596.

Veevers, J.J., D.I. Cole, and E.J. Cowan, 1994, Southern Africa: Karoo Basin and Cape Fold

Belt, *in*, J.J. Veevers, C. Powell, and McA, eds, Permian-Triassic Pangean Basins and Foldbelts along the Panthalassan Margin of Gondwanaland: Memoir of the Geological Society of America, 184, 223-278.

Viljoen, J.H.A, 1994, Sedimentology of the Collingham Formation, Karoo Supergroup: South African Journal of Geology, 97, 167-183.

Vine, J.D., and E.B. Tourtelot, 1970, Geochemistry of black shale deposits-A summary report: Economic Geology, 65, 253-272.

Visser, J.N.J., 1990, The age of the late Palaeozoic glacigene deposits in southern Africa: South Africa Journal of Geology, 93, 366-375.

Visser, J.N.J., 1992, Sea-level changes in a back-arc-foreland transition: the late Carboniferous-Permian Karoo Basin of South Africa: Sedimentary Geology, 83, 115-131.

Visser, J.N.J., 1994, A Permian argillaceous syn- to post-glacial foreland sequence in the Karoo Basin, South Africa, *in* M. Deynoux, J.M.G. Miller, E.W. Domack, N. Eyles, I.J. Fairchild, and G.M. Young, eds, Earth´s glacial record: Cambridge University Press, Cambridge, 193-203.

Visser, J.N.J., 1995, Post-glacial Permian stratigraphy and geography of southern and central Africa, Boundary conditions for climatic modelling: Palaeogeography, Palaeoclimatology, Palaeoecology, 118, 213-243.

Visser, J.N.J., 1997, Deglaciation sequences in the Permo-Carboniferous Karoo and Kalahari basins of southern Africa: a tool in the analysis of cyclic glacio-marine basin fills: Sedimentology, 44, 507-521.

Visser, J.N.J., and G.M. Young, 1990, Major element geochemistry and paleoclimatology of the Permo-Carboniferous glacigene Dwyka Formation and post-glacial mudrocks in southern Africa: Palaeogeography, Palaeoclimatology, Palaeoecology 81, 49-57.

Visser, J.N.J., and H.E. Praekelt, 1996, Subduction, mega-shear systems and Late Palaeozoic basin development in the African segment of Gondwana: Geol. Rundsch., 85, 632-646.

Visser, N.J., and H.E. Praekelt, 1998, Late Palaeozoic crustal block rotations within the Gondwana sector of Pangaea: Tectonophysics, 287, 201-212.

Wedepohl, K.H., 1971, Environmental influences on the chemical composition of shales and clays, *in* L.H. Ahrens, F. Press, S.K. Runcorn, and H.C. Urey, eds, Physics and Chemistry of the Earth: Pergamon, Oxford, 8, 307-331.

Wedepohl, K.H., ed., 1978, Handbook of Geochemistry, vol. I–IV: Springer-Verlag, Berlin.

Wells, N.A., 1983, Carbonate deposition, physical limnology, and environmentally controlled chert formation in Paleocene-Eocene Lake Flagstaffe, central Utah: Sedimentary Geology, 35, 263-296.

Werner, M., 2006, The stratigraphy, sedimentology, and age of the Late Palaeozoic Mesosaurus Inland Sea. SW-Gondwana: new implications from studies on sediments and altered pyroclastic layers of the Dwyka and Ecca Group (lower Karoo Supergroup) in southern Namibia: Unpublished PhD thesis, University of Würzburg, Germany, 428p.

Wignall, P.B., 1989, Sedimentary dynamics of the Kimmeridge Clay: tempests and earthquakes: Geological Society of London, 146, 273-284.

Wilkin, R.T, and H.L Barnes, 1996, Formation processes of framboidal pyrite: Geochimica et Cosmochimica Acta, 61, 323-339.

Wilkin, R.T., M.A. Arthur, and W.E. Dean, 1997, History of water-column anoxia in the Black Sea indicated by pyrite framboid size distributions: Earth and Planetary Science Letters, 148, 517-525.

Whiticar, M.J., 1996, Stable isotope geochemistry of coals, humic kerogens and related gases: Int. Journal of Coal Geology, 32, 191-215.

Zavala, C., and M. Arcuri, 2016, Interbasinal and extrabasinal turbidites: origin and distinctive characteristics: Sedimentary Geology, 337, 36-54.

Zavala, C., M. Arcuri, M.D. Meglio, H.G. Diaz, and C. Contreras, 2011, A genetic facies tract for the analysis of sustained hyperpycnal flow deposits, *in*, R.M. Slatt, and C. Zavala, C., eds., Sediment Transfer from Shelf to Deep Water: Revisiting the Delivery System: AAPG Studies in Geology, 61, 31-51.

Zies, E.G., 1929, The Valley of Ten Thousand Smokes: I. The fumarolic incrustations and their bearing on ore deposition. II. The acid gases contributed to the sea during volcanic activity: National Geographic Society, Contributed Technical Papers, Katmai Series, 1, no. 4, 1-79.

Zhao, J., Z. Jin, Z. Jin, Y. Geng, and X. Wen, 2016, Applying sedimentary geochemical proxies for paleoenvironment interpretation of organic-rich shales deposition the Sichuan Basin, China: Int. Journal of Coal Geology, 163, 52-71.

Zonneveld, K.A.F., G.M.J. Versteegh, S. Kasten, T.I. Eglinton, K.-C. Emeis, C. Huguet, B.P.

Koch, G.J. de Lange, J.W. de Leeuw, J.J. Middelburg, G. Mollenhauer, F.G. Prahl, J. Rethemeyer, and S.G. Wakeham, 2010, Selective preservation of organic matter in marine environments: processes and impact on the sedimentary record: Biogeosciences 7, 483-511.

Chapter 4

Evolution of porosity and pore geometry in the Permian Whitehill Formation of South Africa – a FE-SEM image analysis study

4.1. Abstract

Since the technologically efficient exploitation of economic hydrocarbon reservoirs in shales, increasingly more research has been devoted to identifying and characterising pore systems within shales. However, only a handful of these studies focused on the development of porosity in thermally mature unconventional reservoirs. In this study, the evolution of porosity and pore geometry in the Permian Whitehill Formation is addressed with the aid of ultrathin sections (2x3 cm, 10-20 µm thick) and field emission scanning electron microscopy (FE-SEM) on samples with mean random vitrinite reflectance values ranging from 1.03 to 4.07% Ro. We document a positive covariation of thermal maturity and porosity for vitrinite reflectance values between 0.92% Ro and 2.58% Ro in samples with total organic content (TOC) greater than 2.03 wt.%. In samples with vitrinite reflectance value >2.58% Ro, a strong negative covariation of thermal maturity and porosity was detected, such that for every one unit increase in vitrinite reflectance, porosity decreased by about 4.5 vol.%. The positive covariation of thermal maturity and total porosity recorded here is unsurprising and have been documented previously in many gas shales. However, the dramatic decrease in porosity restricted to samples from localities that experienced advanced maturation (Ro > 2.58%) is viewed as an evidence that porosity decrease is directly related late thermal decarboxylation of organic matter. This opinion is supported by the presence of pores and micro-fractures infilled by fibrous mineral grains and residual fluid inclusions generated from re-precipitation of framework grains, including carbonates, clays, silicates, and phosphates previously dissolved by organic acids (carboxylic, phenolic) generated during thermochemical decarboxylation of sulfur-rich OM. Our findings do not only fill important gaps in the understanding of organic pore development, including processes that create, preserve, and destroy porosity, but the porosities described here are also key to gas transfer from shale matrix to induced fractures during fracture stimulation programs.

Keywords: gas shale, hydraulic fracturing, thermal maturation, thermochemical decarboxylation, carbonate dissolution.

4.2. Introduction

Traditionally, hydrocarbons (oil and gas) are generated within organic matter-rich shales (i.e., source rocks) and then migrate into more porous units (i.e., reservoir rocks such as sandstone, conglomerates or limestone and other naturally fractured rocks types (e.g., Demaison and Huizinga, 1991; Klemme and Ulmisheck, 1991; Magoon and Dow, 1994). However, appreciable hydrocarbons formed in some source rocks are retained after their formation, especially where the source rocks are highly impermeable or "tight", resulting in an unconventional situation where source rocks also serve as reservoirs for hydrocarbons (e.g., US-NPC, 2007; Boyer et al., 2011; Wright et al., 2015). A gas shale is a peculiar type of unconventional gas hosting rock that can only release its gas content by fracture permeability, either via artificial hydraulic fracturing (fracking) or via natural fractures (e.g., Jarvie et al., 2007; US-EIA, 2011). The cost effective exploitation of economic hydrocarbon reservoirs in shale successions has resulted in a significant paradigm shift in our knowledge of pore structures in shales (e.g., Loucks et al., 2009; Bernard et al., 2013; Milliken et al., 2013). The capability of shales to act as economically viable hydrocarbon reservoirs and their potential for fracture stimulation are largely dependent on their pore systems. Predicting the controls on porosity development in shales (e.g., Loucks et al., 2012; Bernard et al., 2013) has been a rather difficult task, largely because of the small pore sizes of these rocks, much smaller than those in conventional reservoirs (Schieber and Zimmerle, 1998; Camp et al., 2013). In addition, shales are dramatically heterogeneous with multi-level (from macro- down to nanoscale) variations in their structures and compositions (e.g., Curtis et al., 2012; Lazar et al., 2015). This means that each shale play is unique in several geological aspects and cannot be used with ease to evaluate another play, not even those in the same shale unit.

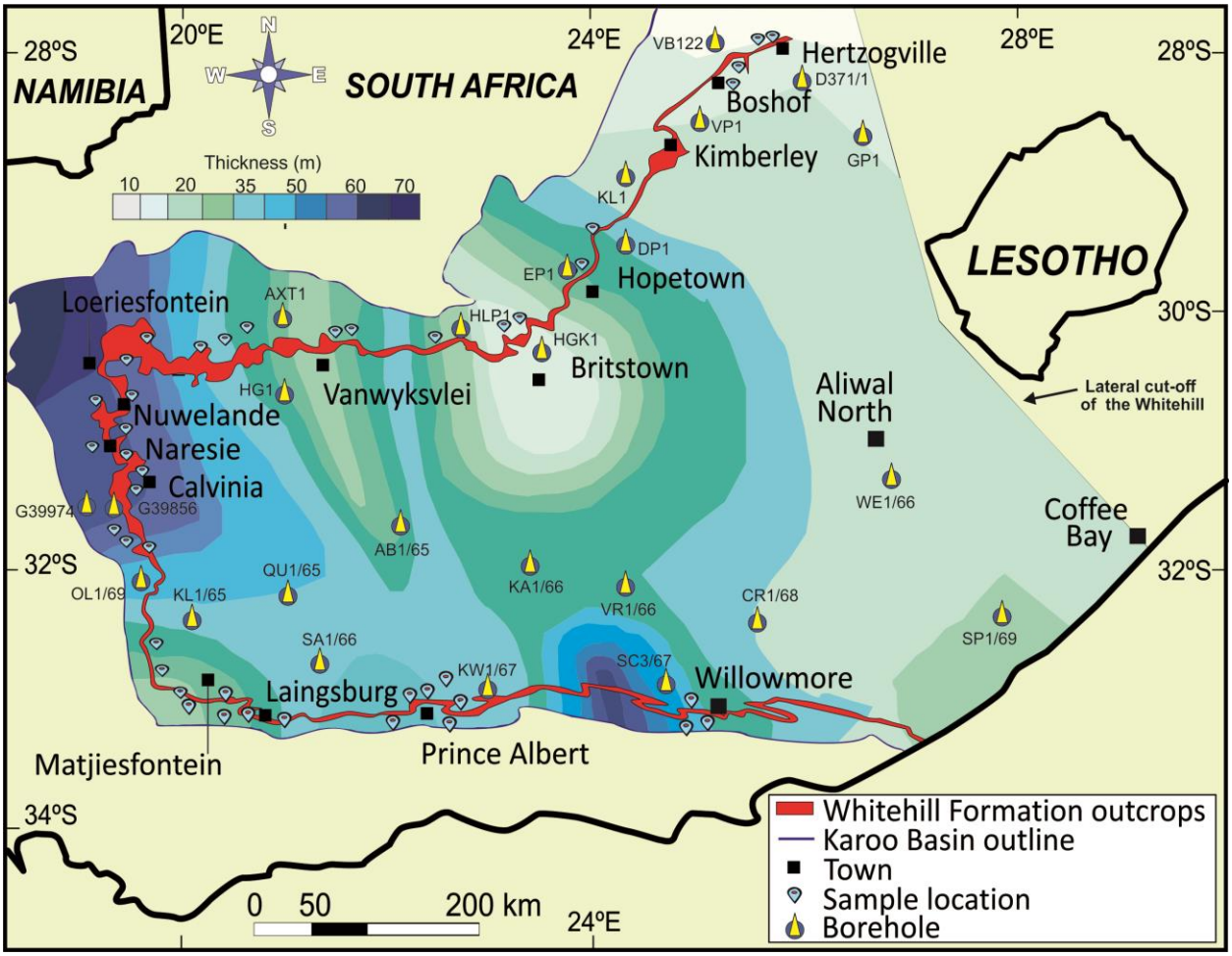

Fig. 4.1: Map of the southern main Karoo Basin and the semi-continuous outcrop belt of the WHF. The thickness of the WHF was constructed from borehole data. The location of some of the boreholes and samples analysed for this study are shown.

In addition, from a scientific standpoint, porosity is a multifaceted subject and is approached differently among disciplines. For instance, petroleum engineers and reservoir scientists quantify porosity using petrophysical methods, such as mercury porosimetry, gas induction, and low-pressure isotherm analysis (e.g., Cui et al., 2004; Ross and Bustin, 2007; Mastalerz et al., 2013; Bahadur et al., 2015). While these bulk characterization techniques effectively provide quantitation of pore throat dimensions and permeability (e.g., Dewhurst et al., 1999), they do not measure of total porosity, which is critical for estimating the capacity of reservoirs. On the other hand, shale petrographers approach porosity development in shale successions by providing both quantitative and visual qualitative analyses of porosity. It is based on direct petrographic examinations of pores through the application of scanning electron microscopy and its auxiliary

technologies (e.g., Loucks et al., 2009; Keller et al., 2011; Klaver et al., 2012; Camp et al., 2013; Milliken et al., 2013; Löhr et al., 2015). Direct observation of pores has a unique advantage of distinguishing pores within organic particles from those within the inorganic matrix of the shale sample. Although it is not clear if water- and hydrocarbon saturation vary by organic and nonorganic pore, such distinction allows porosity evolution to be related to factors closely associated with depositional, diagenetic, and catalytic processes (e.g., Curtis et al., 2012; Bernard et al., 2013; Schieber, 2013).

Pore networks within most gas shales are largely dominated by nanometer-size pores (e.g., Ross and Bustin, 2007; Curtis et al., 2012; Loucks et al., 2012; Milliken et al., 2013). IUPAC (1994) subdivided materials with nanometer-size pores into three categories: macropores (>50 nm), mesopores (2-50 nm), and micropores (<2 nm). Characterising nanometer-size pores is challenging because conventional transmitted and reflected optical microscopy cannot image meso- and micropores due to the low power of magnification of these standard methods. While FE-SEM and its auxiliary technologies have the suitable resolution (Loucks et al., 2009; Curtis et al., 2012; Camp et al., 2013), this method is however not suitable for rock chips because of their irregular surface topography (Loucks, 2009; Keller et al., 2011; Schieber, 2013). Mechanically polished thin sections often contain artefacts such as abrasion marks and grinding debris (Schieber, 2013; Kaufhold et al., 2016), which can influence the detection of delicate features in SEM images. Ion-milling techniques, including those that involve the use of either a focused ion beam (FIB) or a broad ion-beam (BIB) of Ar+ or Ga+ to remove a small amount of material, generates an ultra-smooth surface (Loucks et al., 2009; Keller et al., 2011; Camp et al., 2013; Schieber, 2013), has greatly enhanced the understanding of shale features with SEM. However, ion-milling only allows a small area of the sample (about 40x30 µm) to be imaged at one time (Curtis et al., 2012; Kaufhold et al., 2016).

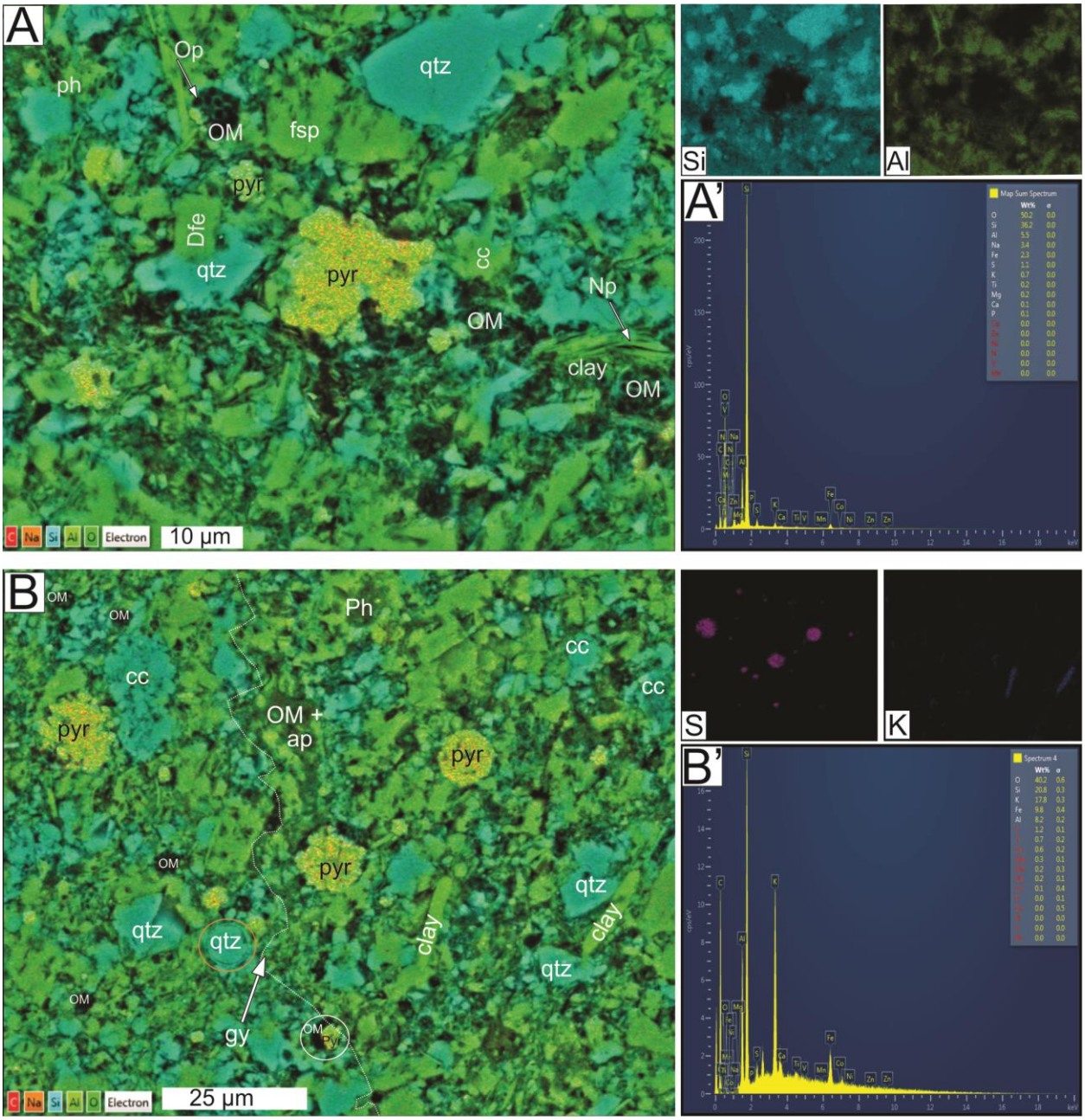

Fig. 4.2. **A-B**: Back-scattered scanning electron microscope images of shale matrix and its constituents. Organic matter (OM) appears dark, mineral grains takes various light colors and shades of grey (see color legend at the base of image). Ferroan dolomite (dfe), Feldspar (fsp), Quartz (qtz), Phosphate peloids (ph), organic pores (Op) and nonorganic pores (Np). A white dashed line in B emphasizes a sinuous microchannel infilled with bitumen and gypsum (gy). **A'-B'**: EDS analyses.

To date, the link between porosity and thermal maturity is inferred from studies that used samples with low thermal maturity range and where thermal maturity had been achieved through burial

diagenesis (e.g., Cui et al., 2004; Ross and Bustin, 2007; Keller et al., 2011; Chalmers et al., 2012; Curtis et al., 2012; Bernard et al. 2013). Studies are rare in the development of porosity with increasing thermal maturity using samples with a wider range of thermal maturity and where thermal maturities were achieved through tectonic burial and thermal devolatilization during igneous intrusion. Samples from the Permian Whitehill Formation (WHF) in the main Karoo Basin of South Africa have thermal maturities that range between ~1.0 and >4.0% Ro (Rowsell and De Swardt, 1976; Cole and McLachlan, 1991). Work by Oelofsen (1981), Visser (1992) and Chukwuma and Bordy (2016) have shown that the WHF consists of subunits with remarkably uniform primary lithologic and sedimentologic characters across the Karoo Basin. In particular, the omnipresence of pyrites in both euhedral and framboidal forms, that appear to have formed due to the activity of sulfate-reducing bacteria at or near the depositional interface, is a strong evidence that uniform reducing (anoxic) conditions were persistent at all localities across the basin during the deposition of the lower two subunits (F1 and F2). Also, the 'consistency in the thickness of the biozones' (Oelofsen, 1981, p. 24) in the upper WHF subunits (F3, F4, F5) indicates that the depositional conditions were seemingly the same over the entire basin floor. There is, therefore, no evidence that depositional conditions varied significantly across the basin during the deposition of any of the five subunits of the WHF. This inference is important because it gives weight to the assumption that initially, each subunit of the WHF was identical in overall properties and that significant differences observed in composition, organic matter content and structures, and pore systems are directly related to post-depositional (diagenetic and thermal maturation) processes, which were majorly controlled by the relative distance of each locality from the presumed heat source, the Cape Fold Belt (CFB). Rowsell and De Swardt (1976) and Cole and McLachlan (1991) observed that degree of thermal maturity (measured with reflectance of vitrinite, [%Ro]) show a progressive decrease from the south-west (heat source) to the northeast. In the study by the latter authors, samples localities within about latitude 29 °S and more southerly were within late dry gas window (%Ro > 2.3) whereas those within latitude 31.5 °S and more northerly were within oil to the wet gas window (%Ro< 2.3).

In order to provide both visual qualitative and quantitative analyses of the pore systems in the WHF, we examined two-dimensional (2-D) FE-SEM images of ultrathin sections (2x3 cm, 10-20 µm thick) from samples taken from three subunits (F1-F3) of the WHF (Chukwuma and Bordy, 2016). X-ray fluorescence spectroscopy, Rock-Eval pyrolysis, and stable isotope analyses

provided data on the compositional geochemistry of the shale samples. Our results show that a positive covariation of thermal maturity (% Ro) and total porosity (volume %) exist for vitrinite reflectance values between 0.92 and 2.58% Ro in samples with total organic content (TOC) greater than 2.03 wt.%. Above vitrinite reflectance value of 2.58 % Ro, a strong negative covariation of thermal maturity and porosity was detected, such that for every one unit increase in vitrinite reflectance, porosity decreased by about 4.5 vol%. The geology of the Karoo Basin and the WHF has been explained in detail in other parts of this thesis and in the literature [e.g. by SACS (1980), Cole and Basson (1991), Visser (1992), Catuneanu et al. (1998, 2005), Tankard et al. (2009, 2012), Geel et al. (2015)], and are not repeated here. In this chapter, some sections on methodology are in blue in order to notify readers that it is similar to those presented in Chapter 3. This overlap is to allow each chapter to be independent and organised for publication.

4.3. Samples, methods, and analytical limitations

4.3.1. Samples

Ten sampling localities were selected along the semi-continuous exposure belt of the WHF in the main Karoo Basin (Fig. 4.1), and they were targeted because they expose the same stratigraphic subunits of the WHT but at different distances from the CFB (Rowsell and De Swardt, 1976; Cole and McLachlan, 1991). The largely unweathered samples were taken with a STIHL E-Z Core Rock Drill fitted with a Pomeroy 40x2.5 cm core barrel. The samples are designated by abbreviations related to their localities (Fig. 4.1), e.g., PAT for Prince Albert, LAG for Laingsburg, MAJ for Matjiesfontein, CAL for Calvinia, NUW for Nuwelande, LOE for Loeriesfontein, VAK for Vanwyksvlei, BTT for Britstown, STY for Strydenburg, HPT for Hopetown, and CST for Christiana. The description of the lithology and sedimentary structures of the samples is provided by Chukwuma and Bordy (2016).

4.3.2. Whole-rock and organic composition

The chemical composition of powdered samples was determined using standard X-ray Fluorescence (XRF) procedure in the Department of Geological Sciences at the University of Cape Town. Stable isotopes of organic carbon and nitrogen were analysed for 30 samples using Costech Elemental Analyzer (EA) with zero-blank autosampler coupled to a ThermoFinnigan Delta Plus

XL isotope ratio mass spectrometer (IRMS) at the Stable Isotope Laboratory of Iowa State University. International isotopic standards (acetanilide, caffeine, cellulose, IAEA-N2) were analyzed with samples in each run. The stable isotopic compositions are reported in the conventional delta-notation with respect to the Vienna Peedee Belemnite (VPDB) standard for carbon, whereas the $\delta^{15}N$ of each sample is expressed relative to atmospheric dinitrogen. Analytical reproducibility is better than ±0.1‰ for both $\delta^{13}C$ and $\delta^{15}N$. Rock-Eval pyrolysis was performed on 68 samples using Rock-Eval 6 instruments, while total organic carbon was measured using a LECO CS-244 carbon analyser. Carbon steel rings (1g, nominal carbon content of 0.8%) were used as internal standard verified against the acceptable range using a certified reference material (CRM) provided by the laboratory at the Indian Institute of Technology, Bombay. Thermal maturity (in vitrinite reflectance unit [%Ro]) was derived from T_{max} (°C) using the method described by Jarvie et al. (2001, 2007): %Ro (calculated) = 0.0180 x T_{max} – 7.16. The calculated %Ro values were largely in agreement with those measured from the reflectance of vitrinite by previous authors (e.g., Rowsell and De Swardt, 1976, p. 107).

4.3.3. FE-SEM sample preparation and limitations

One-hundred-and-forty-eight (148) pieces of whole rock with diameters of less than 10 cm selected from the ten localities (Fig. 4.1) provided the sample base for the porosity study. These were prepared into 2x3 cm uncovered ultrathin sections (UTS; 10-20 µm thick). The samples were impregnated with a mixture of low viscosity epoxy-resin and hardener in order to minimise mechanical impact. Hardening was performed at a moderate temperature (< 60 °C) and for a few minutes to avoid altering the fine organic details within the samples. Two sides of the samples, one oriented perpendicular and the other parallel to bedding-plane, were ground using successive finer abrasives and then air-polished with fine (0.05 µm) silicon powder. Although this method does not produce the same level of ultra-smooth surfaces and resolution of less than 5 nm available with focused ion-beam (FIB) milling, its unique advantage over FIB is that it exposes a larger area of observation, up to 500 000x more than that available in most FIB systems, while still retaining a crisp resolution of shale features up to 8 nm without the usual artifacts associated with conventional (mechanically polished) thin sections. The larger area of examination does not only save cost and time but also provided adequate exposure and representation of features in the shale

matrix larger than 40 µm which is also unavailable with FIB method. Lightly carbon/diamond-coated UTS were examined using a Zeiss MERLIN FE-SEM at the Stellenbosch University Central Analytical Facilities operated with secondary electron (SE), back-scattered electron (BSE), and cathodoluminescence (CL) detectors. Cryo-energy-dispersive X-ray detector (cryo-EDS) provided identification and characterization of components. A swath of 10 images was captured at 20-10 µm horizontal field width, corresponding to machine magnification of 15 000x to 10 000x and pixel resolution of 20 nm/pixel and 10 nm/pixel using both SE, BSED, and CL detectors. Over 200 point counts were made to establish and quantify the overall abundance, nature, and distribution structured and amorphous OM, and mineral matrix and pores. Pores were assessed using images captured at 1.5-2.0 µm horizontal field width, at a magnification of 150 000x to 200 000x and pixel resolution between 1.5 to 2 nm/pixel. In order to avoid nonrepresentation, samples were uniformly selected, however, preference was given to areas with higher pore concentration so that a sufficient number of pores can be imaged for comparison. A subset of the samples was solvent extracted to assess whether pores are clogged by bitumen and to differentiate bitumen from kerogen, using a solvent mixture comprised of 90% dichloromethane and 10% methanol in the Chemistry Department at the University of Cape Town for 68 hours. The samples were air-dried and subsequently prepared into UTS and FE-SEM imaged. In this pore analysis, all samples were observed on surfaces perpendicular to bedding.

4.3.4. FE-SEM identification of shale constituents

The composition of samples including, mineralogy, OM, grain/crystal boundaries were distinguished using back-scattered electron detector (BSE), which has the ability to record variations in composition using the mean atomic number. Material with a low atomic number such as carbon exhibit low BSE intensity and are scaled as darker regions; whereas a material with a high mean atomic number exhibits high BSE intensity and are scaled lighter region. Energy-dispersive X-ray measurements and maps taken across multiple images allowed identification of various minerals matrix, grain/crystals, especially those adjacent to pore structures (Fig. 4.2).

4.3.5. FE-SEM pore identification and classification

Secondary electron (SE) are generated at shallow depths (few nanometers) within the samples and their strength is dependent on the number of electrons that escapes from the surface to reach a detector. Areas emitting more SE appears bright. Edges and angles on surfaces have a shorter distance to the detector, hence SE is suitable for identifying slight topographic variations (pores and textural features) which appear brighter relative to the flat and uniform areas in a sample.

Table 4.1: Distribution of mineralogic and organic compositions, total porosity and pore sizes in the Whitehill Formation compared with some selected gas shales units. Carbs = carbonates, T_{max} = temperature at peak evolution of S2 hydrocarbons (in ^{o}C), S2 = products that crack during Rock-Eval pyrolysis temperatures at 300^{o} C (in mg HC/g rock), TOC = total organic carbon present in rock samples (wt.%), Ro = vitrinite reflectance (in %), POS = Posidonia Shale, HAY = Haynesville Shale, MAR = Marcellus Shale, WOO = Woodford Shale, BAR = Barnett Shale, DOI = Doig (siltstone) Formation, 1 (superscript) = values after Kaufhold et al. (2016), 2 (superscript) = values after Chalmers et al. (2012), 3 (superscript) = values after Milliken et al. (2013)

Mineral and organic composition												Porosity		
Sample ID (wt%)	Silicates (wt%)	Clays (wt%)	Carbs (wt%)	Pyrite (wt%)	Tmax (^{o}C)	OM (Vol%)	TOC_P (wt%)	S2 (mg/g)	Maturity (%Ro)	$\delta^{13}C$ (‰)	$\delta^{15}N$ (‰)	Macro (vol %)	Meso (vol%)	Total (vol%)
PAT1	64.55	11.82	4.71	3.4	607	25	5.90	0.24	3.77	-18.3	10.59	5.41	3.24	8.65
PAT2	66.7	11.27	3.13	2.01	586	10	3.53	0.21	3.39	-21.52	9.59	2.2	1.68	3.88
LAG1	65.91	15.44	4.97	2.14	604	25	5.34	1.37	3.35	-19.5	11.01	5.77	3.53	7.72
LAG2	58.42	14.5	6.3	5.98	488	10	6.63	1.43	3.18	-18.21	11.69	1.99	1.73	4.80
LAG3	59.84	13.7	4.32	4.68	526	6	2.26	0.43	3.20	-19.13	11.88	0.64	0.38	1.02
MAJ1	61.28	13.25	4.85	4.95	403	25	8.83	26.33	2.52	22.42	8.93	8.3	4.5	12.80
MAJ2	46.34	12.35	2.54	10.79	394	15	4.16	38.09	2.60	-20.22	9.5	3.13	1.97	5.10
CAL2	65.2	17.1	3.2	2.3	494	5	1.46	1.02	1.73	-19.46	11.14	0.61	0.63	1.24
CAL3	69.62	13.89	2.24	3.06	607	5	0.93	0.17	3.81	-18.3	10.59	0.94	0.78	1.72
NUW2	62.6	15.7	3.25	2.52	385	12	3.91	3.53	1.03	-24.17	6.2	2.8	1.1	3.90
NUW3	64.12	12.8	2.83	1.57	455	12	3.70	0.45	1.03	-21.86	11.2	1.94	1.56	3.50
LOE1	52.5	15.2	3.92	6.87	388	20	9.33	6.42	1.96	-19.46	11.36	4.9	2.47	7.37
LOE2	64.3	14.4	5.56	2.5	385	25	16.51	0.29	2.17	-24.71	3.04	8.27	6.81	14.97
LOE3	66.5	12.85	2.64	4.54	417	10	9.87	5.12	1.65	-19.02	11.36	2.45	0.81	8.26
VAK3	72.18	16.36	2.83	0.55	393	5	0.65	0.45	1.81	-20.44	11.57	0.5	0.3	0.80
HPT3	75.89	10.39	4.3	0.86	432	5	3.43	0.21	1.40	-22.08	7.42	1.3	0.7	2.00
STY1	51.5	15.3	2.88	12.3	461	15	6.11	6.02	1.40	-18.6	10.8	5.75	2.65	7.40
STY2	56.3	12.8	4.03	2.45	448	15	2.21	0.75	1.37	-21.3	9.96	3.93	2.37	2.30
CST1	70.64	15.38	4.3	2.26	394	5	1.72	0.49	1.08	-20.4	9.92	0.72	0.55	1.27
Other gas shales														
POS[1]	18.00	6.00	29.00	4.00			8.50		0.49					15.00
HAY[2]	24.1	44.7	20.9	2.5			4.20		2.37					6.20
MAR[2]	28.7	43	6.5	2.1			3.80		1.56					3.70
MAR (31)[3]	38.81	37.97	4.98	6.98		14.6	8.10		1-2.1					6.70
MAR (36)[3]	56.05	22.25	6.03	2.67		16.1	10.70		1-2.1					9.12
WOO[2]	32	45.8	10.1	3.1			2.00		1.51					4.70
BAR[2]	46.7	36.3	7.8	3			3.20		2.25					3.00
DOI[2]	58.5	5.5	19.1	0.6			0.70		1.45					6.60

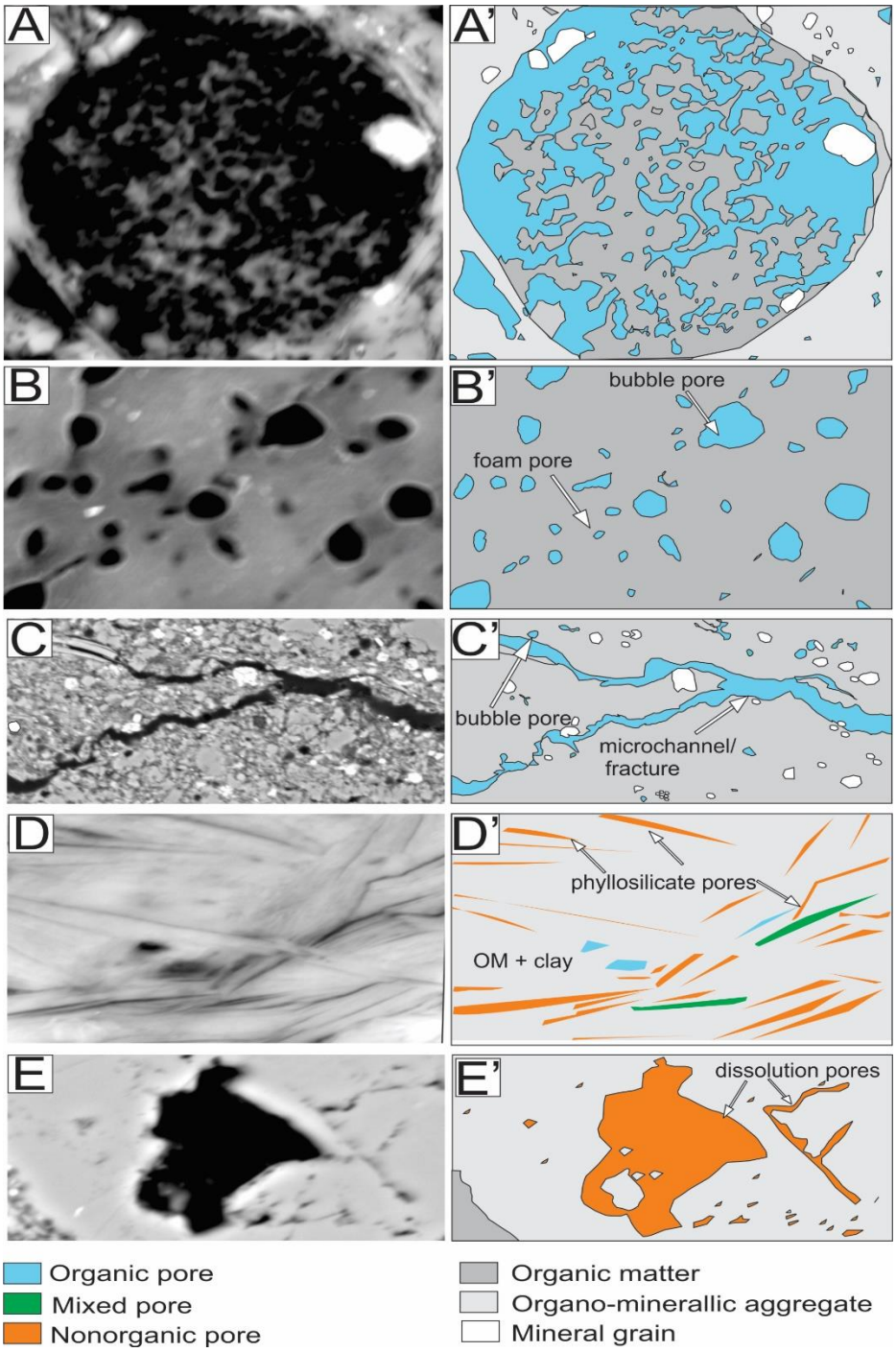

Fig.4.3: Scanning electron microscope images (**A-E**) and their interpreted line drawings (A'-E') illustrating the pore categorization scheme applied in this study. No scale applied because each form of pore type illustrated was captured across a range of scales. See text for details.

The pore classification scheme presented here (Fig. 4.3) is based on observations made in this study, and therefore it is ad-hoc and exclusive to this study, although it is hoped that the approach can be used, with relevant alterations, in other studies as well. Pores were classified according to the nature (organic/nonorganic) of particles they were associated with. Distinguishing organic- from nonorganic pores was necessary in order to relate porosity, pore size distribution, and other shale characteristics to mechanical and geochemical processes. The three types of pores observed are (Fig. 4.3):

1. Organic pores: defined based on the presence of OM along at least three sides of the pores or for >75% of the diameter of the pore (in the case of circular pores).
2. Nonorganic pores: are surrounded by >75% of the nonorganic material.
3. Mixed organic/nonorganic pores: are surrounded by mixed organic and nonorganic materials. They occur where one or two sides of the pores or less than 75% (in the case of circular pores) abut OM or nonorganic grain.

Organic pores are divided into three subcategories based on their size and shape (Fig. 4.3; Walls and Sinclair, 2011):

1. Bubble pores: are rounded to irregular shaped and are predominantly associated with intergranular OM and grain contact areas. They can occur singly or within one clearly visible principal area with several subparts in form of alveolar networks. They range in size from about 100 nm to a few microns in diameter (Fig. 4.3B).
2. Foam pores: are similar to bubble pores (though generally more abundant) and tend to occur mostly in clusters and range in size from a few to about 100 nm (Fig. 4.3B).
3. Microchannels and fractures (Fig. 4.3C): Narrow cracks characterised by irregular fracture faces and occur mostly along bedding-planes (horizontal), although a few inclined to vertical fractures, mostly inter-connected to the horizontally-oriented ones, were also documented.

Nonorganic pores occur majorly in two form: phyllosilicate platelet pores (usually created by volume change associated clay minerals transformation and/or splitting of mica books due to compaction; Fig 4.3D) and dissolution pores (commonly associated with carbonate grains; Fig. 4.3E).

A few of the pores detected in the shales were not intrinsic part of the shales but were likely induced by a number processes such as cooling and degassing during core retrieval, grain and fabric shrinkage during sample storage, abrasion and mechanical defects inflicted on samples during sample preparation. Fig. 4.9B show pores that developed due to grain shrinkage on exposure to surface condition.

4.3.6. FE-SEM pore analyses

Outline of pores was hand-digitized using CorelDraw® and subsequently colored in with a designated color for each pore type. A total of 618 images displaying a total of 84 608 pores were then processed using ImageJ, a public domain image-processing and analysis software available from United States Institute of Health (http://rebweb.nih.gov/ij/index.html).

4.4 FE-SEM and EDS observations

4.4.1. Nature and occurrence of mineral grains

The results from the bulk composition and total organic carbon of the shales (Table 4.1.) show that despite a sharp decrease in thermal maturation with increasing distance from the CFB, mineralogic compositions of the shales (Fig. 4.2) from the same stratigraphic subunit of the WHF are similar across the basin. Energy-dispersive X-ray measurements taken across several samples indicate that the shales are principally composed of silicates (majorly quartz), clays, carbonates, iron sulfides (majorly pyrite) as well as lesser volumes of phosphates and metals (Ti, Ba) oxide. Quartz (in form of single grain) is the chief component but significant amounts of chert and chalcedony were also present. Silicates occurred in two major forms: (1) as partial to complete replacement of certain microfossils (e.g., Tasmanites cysts and colonial algae cells; Fig. 4.6) and other similar pores; and (2) as disseminated individual euhedral grains (Fig. 4.2). Smectite, illite, mixed-layer, and chlorite were the chief phyllosilicate components while mica and biotite were minor. Iron sulfides (chiefly as pyrite) occurred in various forms and majorly in lower two subunits (F1, F2). The two most common forms are: (1) partial to complete replacement of certain microfossils (colonial algae, few Tasmanites cysts, and similar pores); and (2) disseminated individual euhedral grains and framboidal/polyframboidal (bacterial) aggregates (Fig. 4.10). Carbonates (dolomite and calcite) occur largely as disseminated individual euhedral grains (Fig. 4.9). Some grains show color

zonation indicating variations in iron content (Fig. 4.9). Gypsum (Fig. 4.9A), which usually occur in association with carbonates, and phosphorites (Fig. 4.12C) are also documented. EDS analyses indicate that the latter are made up of are phosphorus, calcium, oxygen, and fluorine, indicating that the mineral is likely apatite (ap). This apatite has a botryoidal texture, suggesting its origin was associated with microbial processes.

4.4.2. Nature and occurrence of organic matter

Two forms of organic matter (OM) are observed:

1) Structured organic matter (SOM) is identified mainly based on the retained morphological features of the ancient organisms to which the organic matter may be linked to and to a lesser extent on differences in relief and texture between the organic matter and the other shale constituents. Two structured organic macerals can be identified: Tasmanites cysts and colonial algae cells. The former can be identified based on its spherical to oval shape, thick cell walls, and relief/textural features of their infilled materials. The materials that infilled the walls of the Tasmanites cysts are usually different from those that fill their internal membrane (Fig. 4.4D). The cyst wall is composed of lipoid-like substance (algenan) which is very resistant to chemical alteration and bacterial degradation (e.g., Tappan, 1980; Schieber et al., 2000). Infilling of the cysts usually starts from the inner wall and grew inward, retaining the original lipoid-like material of the walls. In scanning electron and optical microscopy, the appearance of this material is distinct and sharply contract those of the cyst interior and can be used to identify cysts (Fig 4.4E-F; Schieber et al., 2000). Colonial algae can be identified based on their spherical to oval shape, thin cell wall, and their occurrence in clusters (Fig. 4.4E-F, 4.5A-C).

2) Amorphous (unstructured) organic particles (AOM) occur as disseminated, often irregular patches that fill the spaces between mineral grains and can be described amorphinite (e.g., Teerman et al., 1995).

Structured and amorphous organic particles are disseminated throughout the shale matrix and closely aggregated with mineral grains in form of organo-minerallic aggregates (Fig. 4.4). They also occur in discrete laminae and organic domains with small mineral grains. Elongate, wavy and continuous laminae (lamalginite) composed of clusters of filamentous colonial algal cells (Fig

4.5A-C), interpreted as algal mats by previous authors (e.g., Cole and McLachlan, 1991 and Faure and Cole, 1999), are also common.

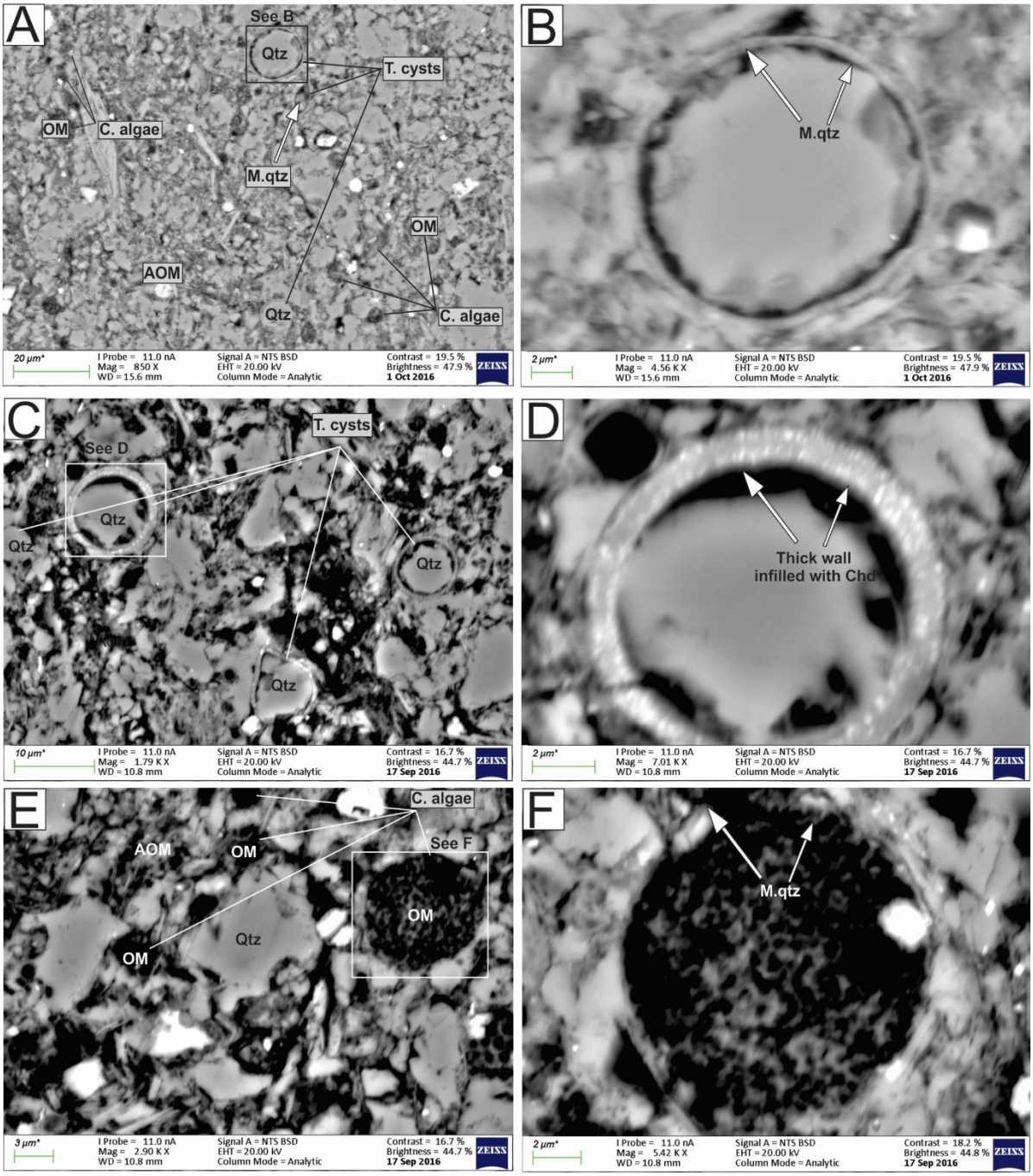

Fig. 4.4: BSE scanning electron microscope images of structured and amorphous organic matter (OM). B-D: Tasmanites cysts (T. cysts), E-F: Colonial algal cells (c. algae). chd = chalcedony, qtz = quartz, m. qtz = microquartz, aom = amorphous organic matter. See text for details.

4.5. Porosity and pores size distributions

4.5.1. Prince Albert samples

Based on SEM images (e.g., Fig. 4.6), the samples taken at the Prince Albert locality contain 15-30 vol.% of OM, whereas the TOC values indicate an average of 4.42 wt.% organic content. Samples from the lower subunits of the WHF are dominated by amorphous OM that is disseminated throughout the shale matrix and in few laminae (interpreted as lamalginites based on their shape; e.g., Löhr et al., 2015). The observed Tasmanites cysts are preferentially infilled with quartz grains and non-porous, whereas the colonial algae cells are largely unfilled and retained pores, although a few are partially filled with pyrites framboids and some occasional quartz (Fig. 4.6C-D). The organo-minerallic matrix and the lamalginites were notably porous, comprising a complex network of equant, circular to angular pores in two size ranges: foam pores with a diameter of up to 50 nm and bubble pores with diameters ranging between 100 and 500 nm. Few pores with diameter/long dimensions more 1 μm are also present (Fig. 4.6A-B). Horizontal to sub-horizontal microfractures are also abundant. A few of these organic pores are empty, while the majority are partially filled with pyrite, carbonate, quartz, OM, and fibrous apatite. The lamalginite contain abundant pores located between adjacent cells of colonial algae and within the single cell membrane of the individual cell (Fig. 4.6D). This suggests partial compaction and collapse of the individual cells that makeup the colony. The pores within individual cells are homogeneous in shape and size (circular with diameters of <50-125 nm). Dissolution of carbonate and other frameworks created irregular/vuggy mesopores around carbonate and few quartz grains. These pores are preferentially oriented horizontal to sub-horizontal, parallel to laminae and were interconnected. The majority of the elongate vuggy dissolution pores are connected with the organic pores and are completely infilled by fibrous carbonate, chert and few phosphate grains and cement (Fig. 4.7). Carbonate and phosphatic filled microchannels (veins) are abundant in samples taken east of Prince Albert (Fig. 4.7A, D, E-F).

In the upper subunits of the WHF, the shale matrix is not dominated by pervasive organo-minerallic aggregation, rather OM occurs in patches of various sizes surrounded by the inorganic grains (Fig. 4.7A). No Tasmanites cysts are recorded and number of colonial algae has reduced considerably. Several horizontal microchannels and fractures (Mf), mostly filled with fibrous

crystals (carbonate, chert, phosphate) are observed (Fig. 4.7). Few sponge-like, porous residual pyrobitumen are also recorded (Fig 4.7B). Nonorganic pores are dominated by carbonate dissolution pores.

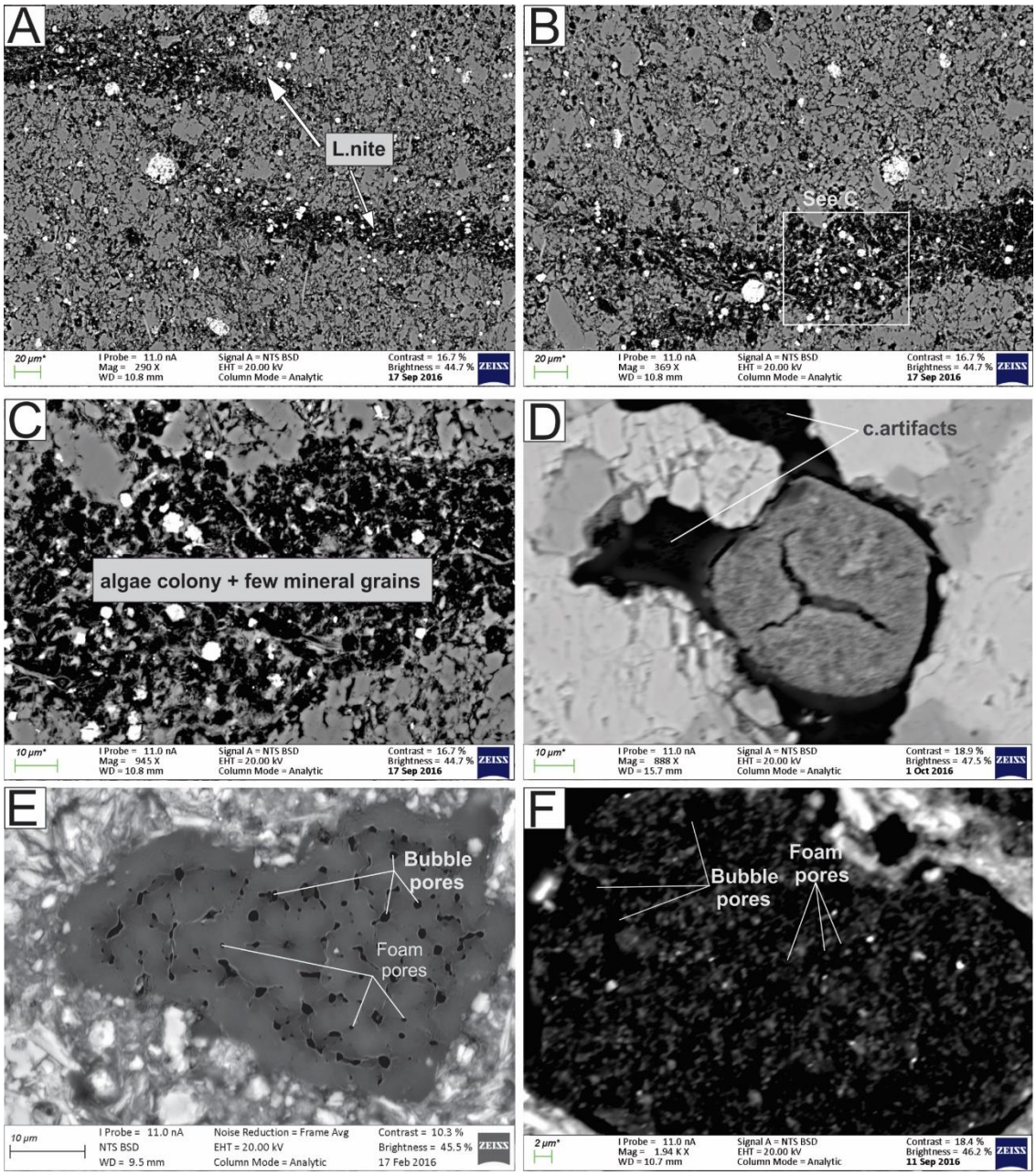

Fig. 4.5: Scanning electron microscope images of nature and occurrence of organic matter (OM) in the WHF. A-C: lamalginite (l.mite). D-F: Small organic domains. See text for details.

4.5.2. Laingsburg samples

OM represented about 15-20 vol.% of the samples based on SEM images, which is consistent with TOC of up to 9 wt.% (average of 4.88 wt.%). The lower subunits of the WHF in Laingsburg, similar to samples from Prince Albert, are dominated by AOM and SOM disseminated through the shale matrix and closely associated with mineral matter and lamalginites, however, the samples here contain more colonial algae cells, and fewer Tasmanites cysts. The organic pores observed here are similar to those in Prince Albert samples, however they contain more foam pores and less bubble pores. Another set of larger pores with diameters of 1-3 μm are also common (Fig. 4.8). Pores are observed between pyrite framboids and between clay minerals (Fig. 4.8D-H). The latter consists of a network of randomly oriented triangular platelet pores. Dissolved margins on carbonates grains are common and of larger dimension than those observed in Prince Albert and are connected with other pores. In the lower subunits of the WHF, the majority of the pores contain kerogen residue and are filled with quartz, carbonate, and apatite peloids (Fig. 4.9A-B). Microcracks infilled by carbonates and quartz are abundant. Sub-horizontal fractures (bedding plane parting) are seen cutting through the kerogen-mineral aggregates and are filled with carbonate and gypsum. From several FE-SEM images, samples have a porosity of up to 7.72 vol.%. Organic pores in the upper section have a wider size distribution, ranging from 400 nm to 3 μm and are irregular in shape. Nonorganic pores are developed with clay mineral aggregates and range in size between 20-80 nm. A total porosity of about 4.8 vol.% is recorded. Pore within the silt-rich upper subunits of the WHF occurs within carbonate grains and show evidence of dissolution and reprecipitation (Fig. 4.9C-D).

4.5.3. Matjiesfontein samples

OM represented about 15-20% of the sample volume. The samples here are less dense, weighing only 1.14 g/cm3. Colonial algae occur in long wavy lamalginites and discrete patches within the matrix (Fig. 4.10A-B). Tasmanites cysts are few and partially filled with microquartz while colonial algal cells are more in number and are partially filled with pyrite and quartz grains. Both are seen disseminated within the matrix. In the upper subunits of the WHF, OM occurs in discontinuous laminae and irregular patches. Elongated microfractures occur beneath the OM

domains. Pores within the membrane of algal cells are homogeneous in shape (equant, circular) and size (range between 40-130 nm), whereas pores within organo-minerallic aggregates occur in various shapes and sizes (Fig. 4.10). Elongate microfractures (bedding-plane partings) are interconnected with pores within the matrix (Fig. 4.10E). Carbonate dissolution pores and microchannels are similar to those observed in Laingsburg but are less common. Triangular phyllosilicate platelet pores containing kerogen residue are also noted.

4.5.4. Calvinia and Nuwelande samples

OM represented 5-10% and 10-15 v% of Calvinia and Nuwelande sample volume, based on FE-SEM images, and is consistent with reported average TOC values of about 2% and 4%, respectively. Calvinia samples are not characterized by abundant organo-minerallic aggregates, rather OM occurs in few discrete patches. Organic particles in sample taken closer to dolerite sills are nonporous and denser (1.38 g/cm^3), appear baked, and with high thermal maturity (%Ro > 3.8). These are interpreted as pyrobitumen, and not kerogen maceral (Fig. 4.12E-F). Nuwelande samples contain a few large porous organic domains, which are likely preserved where compaction sheltered areas provided by the presence of rigid framework grains (Fig. 4.12A). The pores within the organic domain are heterogeneous with some associated with euhedral pyrite grains (Fig. 4.12C). Pores within phyllosilicates are also observed (Fig. 4.12B).

4.5.5. Loeriesfontein and Strydenburg samples

OM represent about 20-30 vol.% of the samples based on SEM images, which is consistent with TOC of up to 16.5 wt.% (average of 8.3 wt.%). In the lower subunits of the WHF, OM occurs in disseminations and in lamalginites (Fig. 4.11A-B). Recognisable organic detritus includes silt-sized Tasmanites cysts, colonial algal cells and macerals with a smooth-textured and defined outline (Fig. 4.11E). The organo-minerallic matrix and the distinct organic domains are notably porous, comprising a complex network of pores, which ranges between >50 and 1 µm. The pores occur in various shapes: equant, circular, angular, sub-angular and mostly empty with only a fraction partially to completely infill with pyrite, carbonate and quartz grains. Some organic maceral show some minor cracks (Fig. 4.11E). It is unclear whether these were intrinsic or artefacts, thus they were not included in the pore dimensioning.

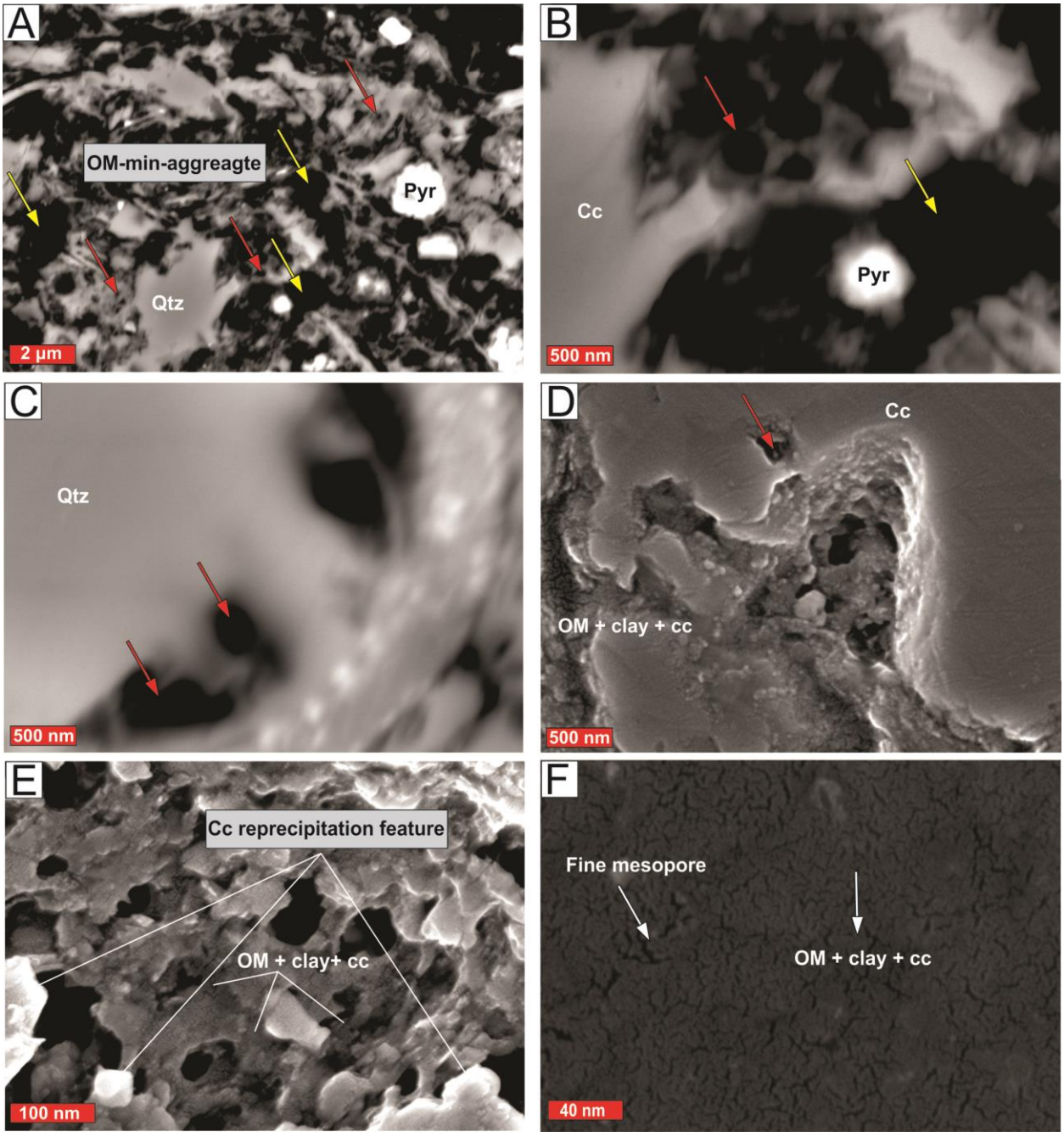

Fig. 4.6: Scanning electron microscope images of shale matrix pores in the lower section of the WHF in Prince Albert. Both organic pores (white arrow) and nonorganic pores (black arrow) in two size ranges: <10-120 nm and 100-1000 nm. cc = carbonate, dol = dolomite, OM = organic matter, qtz = quartz, pyr = pyrite. See text for details.

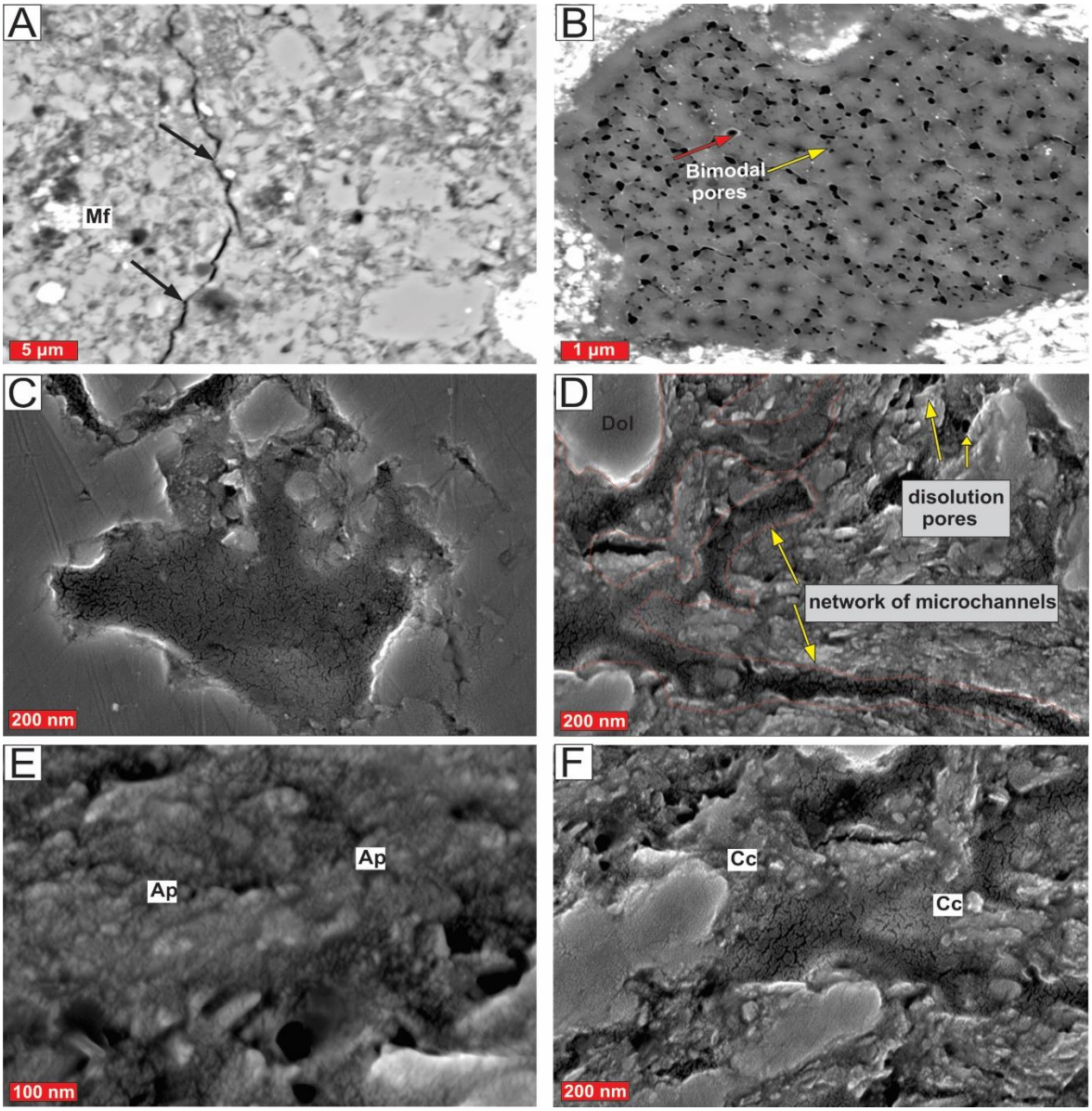

Fig. 4.7: Scanning electron microscope images of matrix pore sizes and geometries in the upper section of the Whitehill Formation in Prince Albert. Mf = microfracture, ap = apatite, cc = carbonate. See text for details.

4.6. Discussion

4.6.1. General trends

In general, the samples of the WHF represent a pore system that is strongly influenced by organic porosity. A strong positive covariation of TOC (wt.%) and total porosity (vol.%; measured with ImageJ using manually digitized FE-SEM images) exists in all localities (Fig. 4.13), however, the trend line for TOC versus porosity intersected a TOC of zero at a porosity of about 1.4 vol.%. This

indicates that nonorganic porosity contributed approximately a minimum of 1.4 vol.% of the total porosity documented. The positive covariation between OM and total porosity recorded here is unsurprising and predictable, given that these pores were presumably generated during thermal decomposition of OM and has been noted previously in several gas shales (e.g., Passey et al., 2010; Chalmers et al., 2012; Loucks et al., 2012; Bernard et al., 2013; Milliken et al., 2013). However, it was observed here that the positive covariation between TOC and total porosity only holds for values of TOC between 2.03 and 5.4 wt.%. From Fig. 4.13, at lower or higher TOC values, no systematic covariation was detected between TOC and porosity. At TOC of <2.03 wt.%, porosity either rises to as high as 1.8 vol.% or drops as low as less than 0.3 vol.%, whereas at TOC of >5.4 wt.%, porosity increased in an irregular fashion relative to TOC. In the organic matter-hosted pore system of the Marcellus Formation, Milliken et al. (2013) observed that shale samples with a TOC of less than 5.5 wt.% had a positive correlation with porosity, whereas samples with TOC greater 5.5 wt.% displayed little or no increase in porosity with more increase in TOC. Comparison of their results with this study shows some important similarities as well as marked differences. Most notable is the indirect proportional relationship between OM contents and porosity at TOC contents above 5.5 wt.%. However, in their study, a positive correlation exist in all values of TOC less than 5.5 wt%, whereas our results indicate that there was no such correlation for samples with TOC contents <2.03 wt.%. Also, while these authors recorded a general decline in porosity for TOC values above 5.5 wt.%, our results show that in some locations, samples with TOC values >5.5 wt.% show relative increase in porosity. These difference could be related to a number of factors, including levels of thermal maturation, nature of organic and inorganic matter as well as burial/diagenetic history. The trends recorded in this study suggest that organic porosities within the samples were not only influenced TOC contents.

The difference in levels of thermal maturation is another critical factor that affects porosity (e.g., Curtis et al., 2012; Bernard et al., 2013). A plot of thermal maturity versus TOC (Fig. 4.14) showed a strong positive covariation between thermal maturity and porosity. The trend line for maturity vs porosity intersect a porosity of zero at a thermal maturity of 0.88% Ro. This indicates that until the samples attained a thermal maturity of 0.88 % Ro, they were largely nonporous. This trend agrees with the general knowledge that appreciable organic maturation only starts after sediments attains temperature of about 60 °C (e.g., Tissot and Welte, 1984; Jarvie et al., 2007) and further

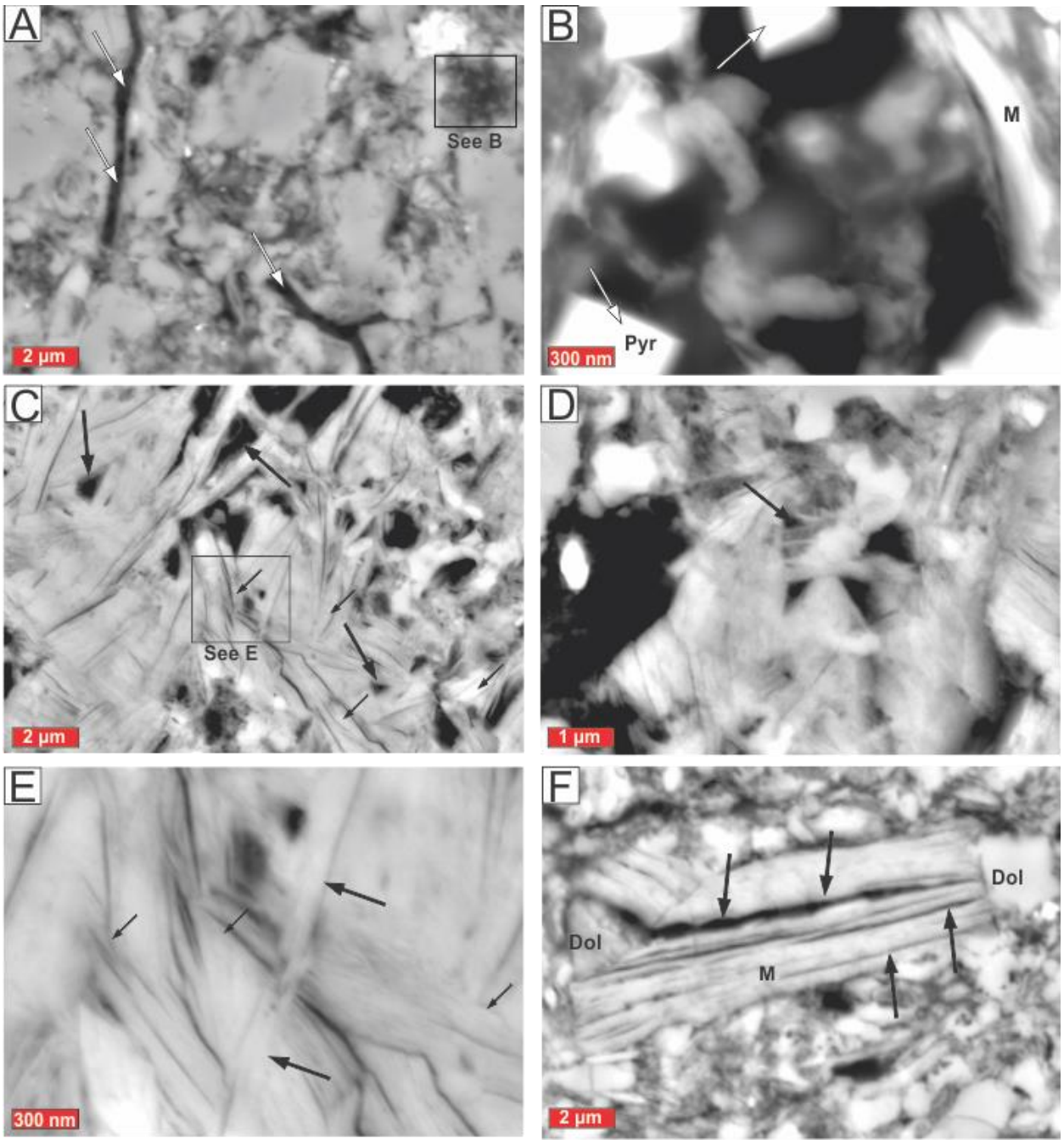

Fig. 4.8: Scanning electron microscope images of matrix pore sizes and geometries in the lower section of the WHF in Laingsburg. A: Bitumen-filled cracks were abundant (arrows) and homogeneous pores observed within algal cells. B: Degraded algal cell partly infilled with late diagenetic euhedral pyrite grains. C-E: Various pore structures created by phyllosilicate grains. F: Slit-shaped pores within an exfoliated mica book. Authigenic dolomite (dol) cement were seen infilling these pores. cc = Calcite, B = biotite, pyr = pyrite, qtz = quartz, sid = siderite, M = mica, K = kaolinite, dol = dolomite.

support our view that the pores within these samples were products of thermal decomposition. From Fig. 4.14, for vitrinite reflectance values between 0.88 and 2.58% Ro, a strong positive

correlation exist between thermal maturity and porosity. However, above approximately 2.58% Ro, porosity steeply declined with further increase in thermal maturity such that for every one unit increase in vitrinite reflectance, porosity decreased by about 4.5 vol%. Relating this trend to the earlier observed indirect proportional relationship between porosity and TOC, it is obvious that thermal maturity had a stronger influence on porosity than TOC.

4.6.2. Trends in development of organic porosity with increasing thermal maturation

The development of the pore system (pore sizes, pore shapes, pore orientations) observed in the shale investigated, comprising both organic and nonorganic pores, appeared to represent an integral part of the depositional and diagenetic history of the WHF. Studies of modern sediments suggest that freshly deposited muds are rich in water contents, up to 70-90% (e.g., Müller, 1967; Parthenaides, 1991; Schieber, 2013). Burial compaction results in expulsion of this excess pore water and concomitant collapse of the flocculated fabrics. With continued burial, the preservation potential of the latter is limited, unless where compaction is minimised by rigid grains. The abundance of partially compacted colonial algal cells and Tasmanites cysts (Fig. 4.4, 4.5, and 4.11B) preserved in pristine condition suggests that rigid silt-size grains offered protections during compaction. A likely source of the rigid grains that minimised compaction is the formation of early diagenetic cement and authigenic grains (e.g., Schieber, 1996; Schieber et al., 2000). Subject to local conditions, the bacterial-mediated precipitation of framboidal pyrite, carbonate and quartz grains can be triggered in the sediments during very early diagenesis by anaerobic microbial sulfate reduction (e.g., Berner, 1984; Blatt, 1992). In shales with high organic contents (TOC >5 wt.%) framework (primary) pores are completely filled with OM (kerogen) as the rock is compacted, whereas shales with low (TOC <5 wt.%), framework pores might be incompletely filled. As OM is buried, it experiences a progressive increase in temperature and pressure resulting from increasing overburden and geothermal gradient and a concomitant increase in specific volume of the pore-fluid (Tissot and Welte, 1984; Littke et al., 1988; Jarvie et al., 2007). The increase in volume of the pore-fluid is accompanied by an increase in pore-fluid pressure (e.g., Ungerer et al., 1983; Littke et al., 1988). Where pore-fluid pressures exceed the vertical load pressure, horizontal open fractures develops (e.g., Littke et al., 1988). It is conceivable that the horizontal microfractures and microchannels in these WHF samples developed in direct response to over-

pressuring caused by hydrocarbon generation. The alignment of the majority of the fractures along bedding-planes, which are most likely to yield to pressure, supports our opinion that their origin is related to over-pressuring. The absence of these fractures and channels in the organic-lean upper subunits of the WHF, where OM likely did not cover all available framework pores, is further evidence that these fractures are related to organic matter maturation. From this scenario, these pores were likely the first set of secondary porosity to be generated and their formation precedes significant hydrocarbon generation and thus they acted as conduits for the expulsion of generated hydrocarbon, as inferred from their bitumen infills (Fig 4.3C).

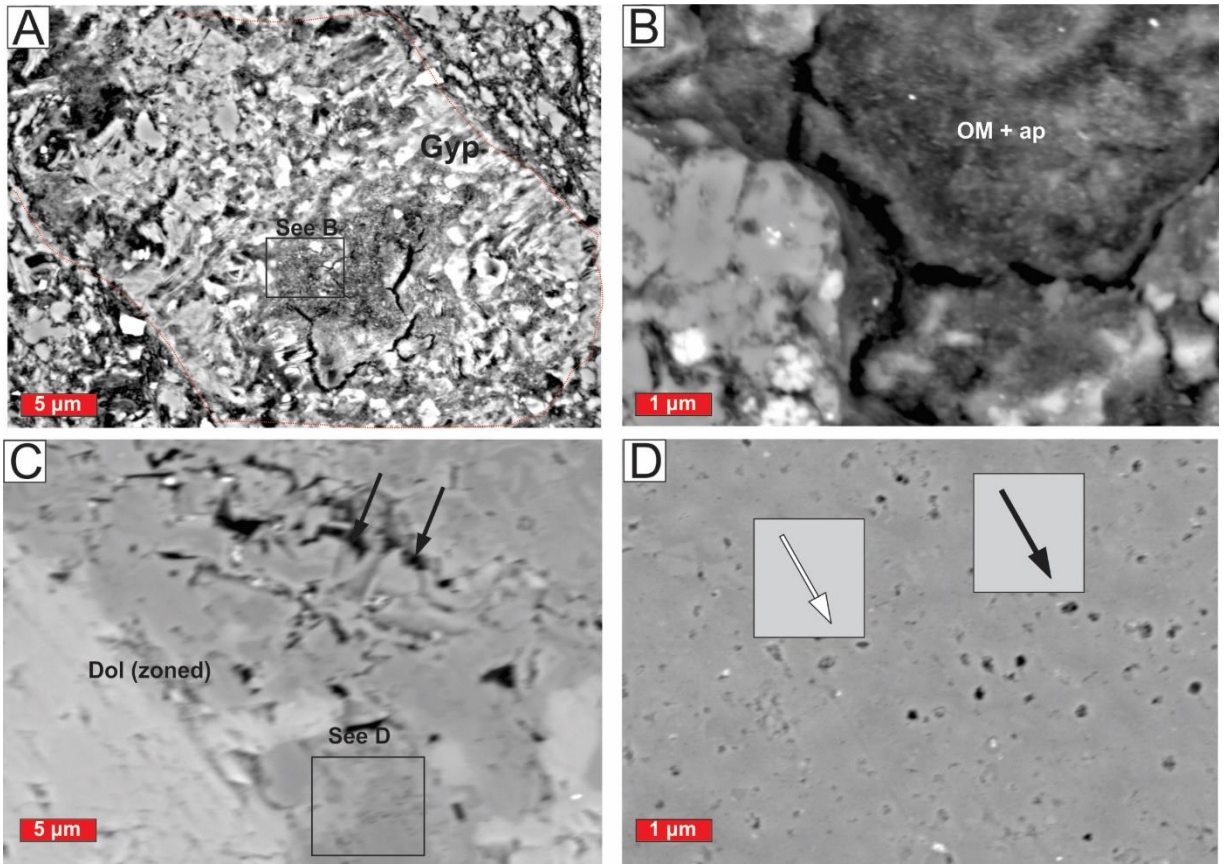

Fig. 4.9: Scanning electron microscope images of pore type and pore geometries in the upper section of the WHF in Laingsburg. A: Shale matrix and associated mineral grains. Note gypsum (gyp) mineralisation around organic debris (red dashed line). B: A close-up view from A showing organic matter (darker) and apatite (lighter) composites. C-D: Pervasive small-scale dissolution pores within a zoned dolomite (dol) crystal. Note the light and dark zoning of this grain which results from variation in iron contents, with lighter region containing elevated amounts of iron

The abundance of bubble and foam pores with spherical to oval cross-section suggests that their formation was related to fluid phase, presumably, conversion of OM to bitumen and hydrocarbons (Tissot and Wlete, 1984; Loucks et al., 2009; Passey et al., 2010). The close spatial association between bubble and foam pores suggests a common origin (e.g., Schieber, 2013).

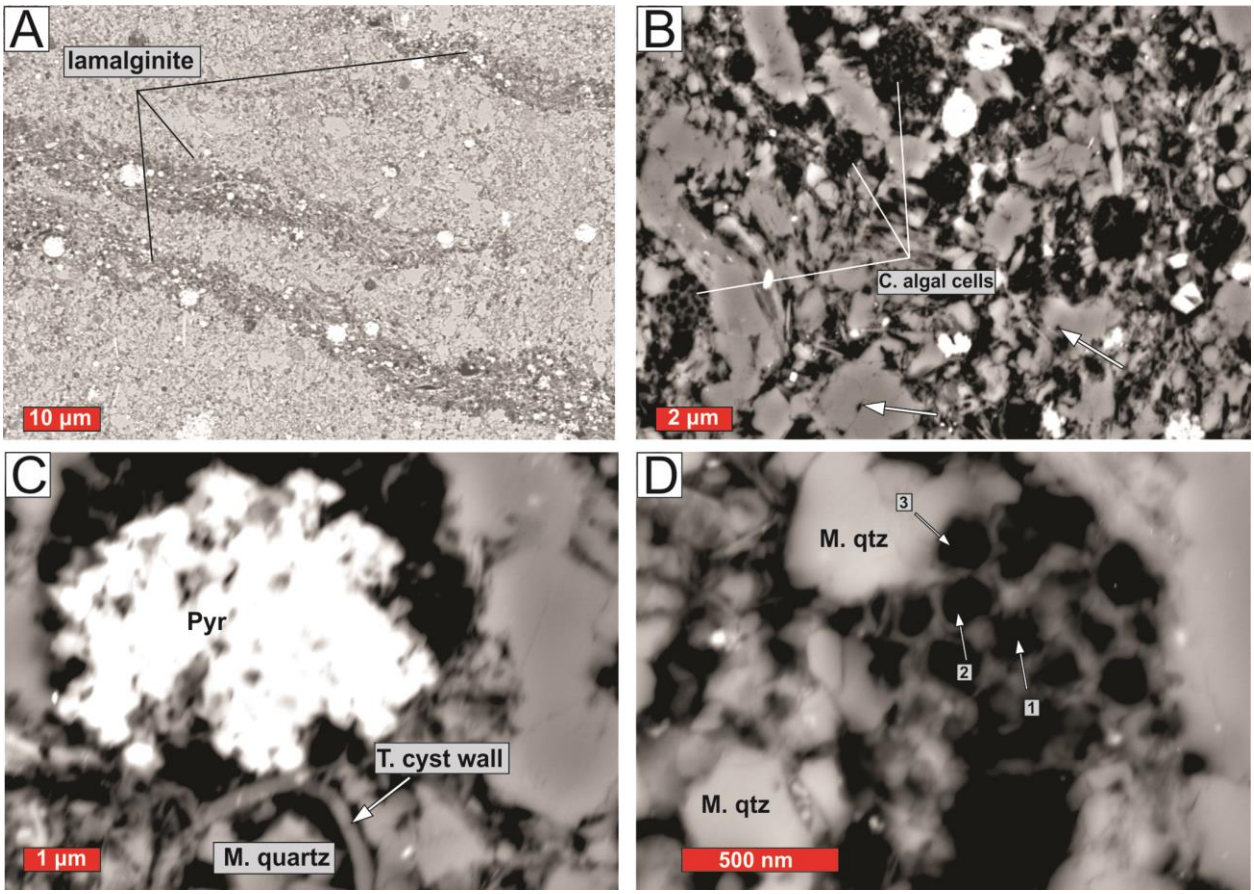

Fig. 4.10: Scanning electron microscope images of pore types and pore geometries in the WHF in Matjiesfontein. A-B: Pores located between adjacent algae cells and within the membrane of individual cells in lamalginite. C: Pores in algal cell partially infilled by pyrite (pyr) framboids. T. cyst =Tasmanites cyst. D: Unfilled algal cell with homogenous bubble pores. The long dimensions of the pores indicated by arrows are 117 nm (1), 125 nm (2), and 127 nm.

4.6.2. Trends in development of nonorganic porosity with increasing thermal maturation

The studied shales contain at least 10 and 3 vol.% of clays and carbonates, respectively (Table 4.1). Given this volume of clay, the phyllosilicate pores observed in the samples are typical of

shale successions that have been buried sufficiently to initiate the transformation of clay minerals (e.g., smectite-to-illite). The smectite-to-illite transformation is usually accompanied by volume change and the concomitant development of pores (e.g., Osborne and Swarbrick, 1999). The change in shale architecture (fabric and texture transformation) during the smectite-to-illite conversion thus is the likely source of the phyllosilicate pores observed. The smectite-to-illite conversion overlaps with or closely precedes the onset of kerogen (OM) transformation to bitumen (e.g., Schieber, 2013). This explains why most of the phyllosilicate pores were infilled with kerogen residue, particularly in samples with higher TOC. The majority of the phyllosilicate pores in TOC lean samples remain open even after deep burial.

Research on pore water evolution during burial (e.g., Hayes, 1991; Surdam et al., 1991; Spötl et al., 1999) suggests that smectite-to-illite transformation is closely followed by, and sometimes overlaps with, decarboxylation of kerogen, which results in accumulation of carboxylic and phenolic acids and concomitant destruction of carbonate and other framework grains. Where organic matter and its sulfur content is high, a reasonable amount of these organic acids is usually generated (Schieber, 2013), and can result in widespread corrosion and dissolution of framework grains, particularly carbonate grains and carbonate-rich clays. The dissolution pores observed in the samples (Figs. 4.6E-H, 4.7C-F, 4.9C-D) are similar in every aspect to those described by these previous authors. It, therefore, seems reasonable to conjecture that they were generated in a similar scenario. The occurrence of more complex dissolution pores in samples which experienced more advanced maturation, particularly in Prince Albert and Laingsburg localities are viewed as an evidence for their development is related to late diagenesis and advanced thermal maturation. This view is supported by the absence of diagenetic clays in these dissolution cavities, indicating that smectite-to-illite conversion must have been concluded by the time organic acid production peaked.

The dramatic reduction in porosity observed in the overmature samples (Ro > 2.58%) is inferred to related to the large-scale infilling of the previously generated pores and fractures by fibrous crystals/cement and residual fluid inclusions (Fig. 4.6C-F). The occurrence of these fibrous crystals/cement (majorly calcite and to a lesser extent silicates and phosphates) on the borders of the fractures and residual fluid inclusions trapped in the central portion indicate that the grains precipitated the organic-rich fluid inclusions (e.g., Littke et al., 1988; Bernard et al., 2013). Similar

hydrocarbon-bearing fluid inclusions have been reported in calcite-filling fractures at a temperature in excess of 180 °C (e.g., Bernard et al., 2012). These features differentiate the late diagenetic precipitates from their early diagenetic counterparts, which formed largely by the action of anaerobic microbial sulfate reduction (e.g., Berner, 1984; Shieber, 1996). The precipitation of these authigenic components and their subsequent filling pores created during hydrocarbon generation resulted in the loss of porosity in the overmature samples and the formation of complex networks of veins. These veins, which are preferentially oriented along bedding-planes were once fractures and channels that served as conduits for the expulsion of hydrocarbons. Similar calcite- and quartz-veining and fibrous cement have been documented in the WHF by previous authors in the area between Laingsburg and Prince Albert (e.g., Egle at al., 1998; Craddock et al., 2008). Geel and others (2015) documented an extensive bedding-plane-aligned quartz-calcite veining in the WHF in the Jansenville-Prince Albert areas with geothermometry data that showed trapping temperature between 230-260 °C at 2-3 kb. The shale matrix porosity described here represent a fundamental parameter for gas transfer from the rock matrix to induced (artificial) fractures during gas shale stimulation programs. It can strongly impact the potential for commercial gas production and is therefore of considerable economic importance.

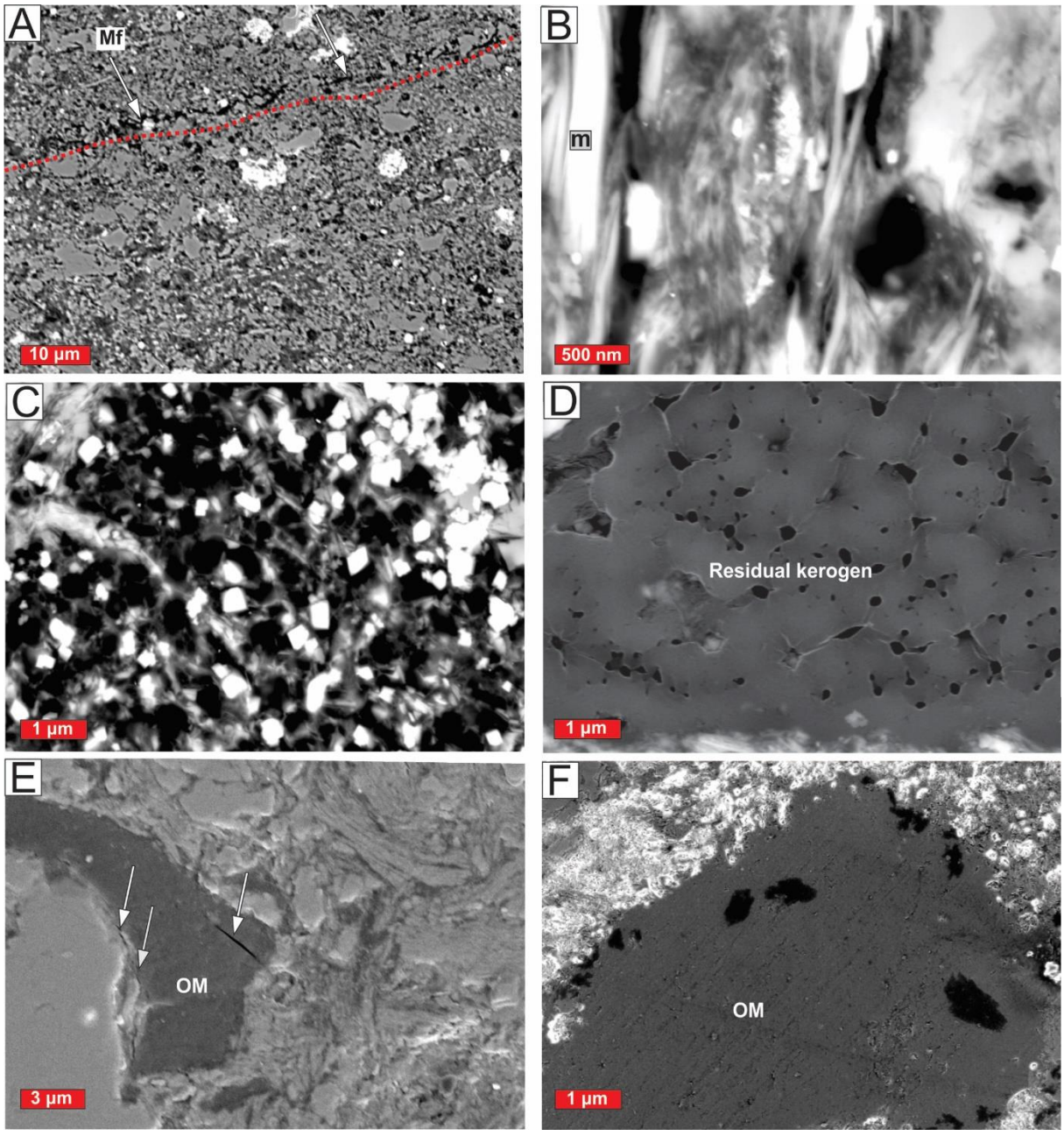

Fig. 4.11: Scanning electron microscope images of pore types and pore geometries in the WHF in Calvinia and Nuwelande. A: Shale fabric characterised by silt-size quartz grains, carbonate, clays, and patches of OM domains. Microfractures (Mf) can be seen running along beddings. B: Close-up view of closely associated OM and phyllosilicate grains. C: Porous discrete OM domains associated with pyrite and clay minerals. D: Porous sponge-

like residue of kerogen that presumably resulted from thermal maturation. E: Nonporous dolerite-impacted kerogen maceral in a matrix of dolomite and clays. F: Dolerite-impacted OM with micropores.

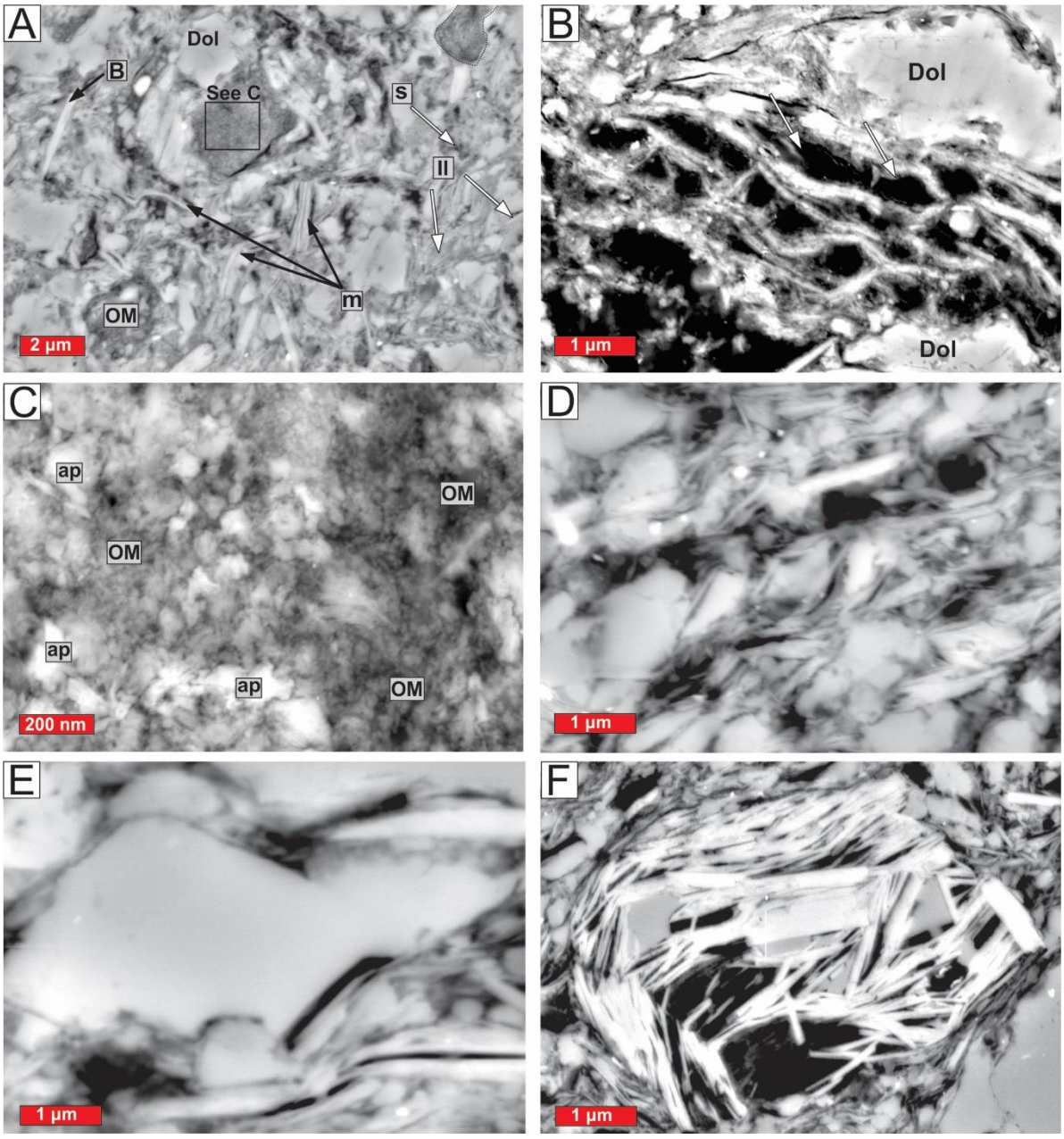

Fig. 4.12: Scanning electron microscope images of pore types and pore geometries in the WHF in Strydenburg. A: Low magnification image showing microlaminated shale fabric, characterised by subvertical orientation of elongated grains. Note the abundance of phyllosilicates, including mica (m), smectite (s), and illite (il). B: Phyllosilicate network pore created from exfoliation of elongated and subparallel oriented mica books; dol = dolomite. C: Close-up image of the rectangle area in A showing OM fabric.

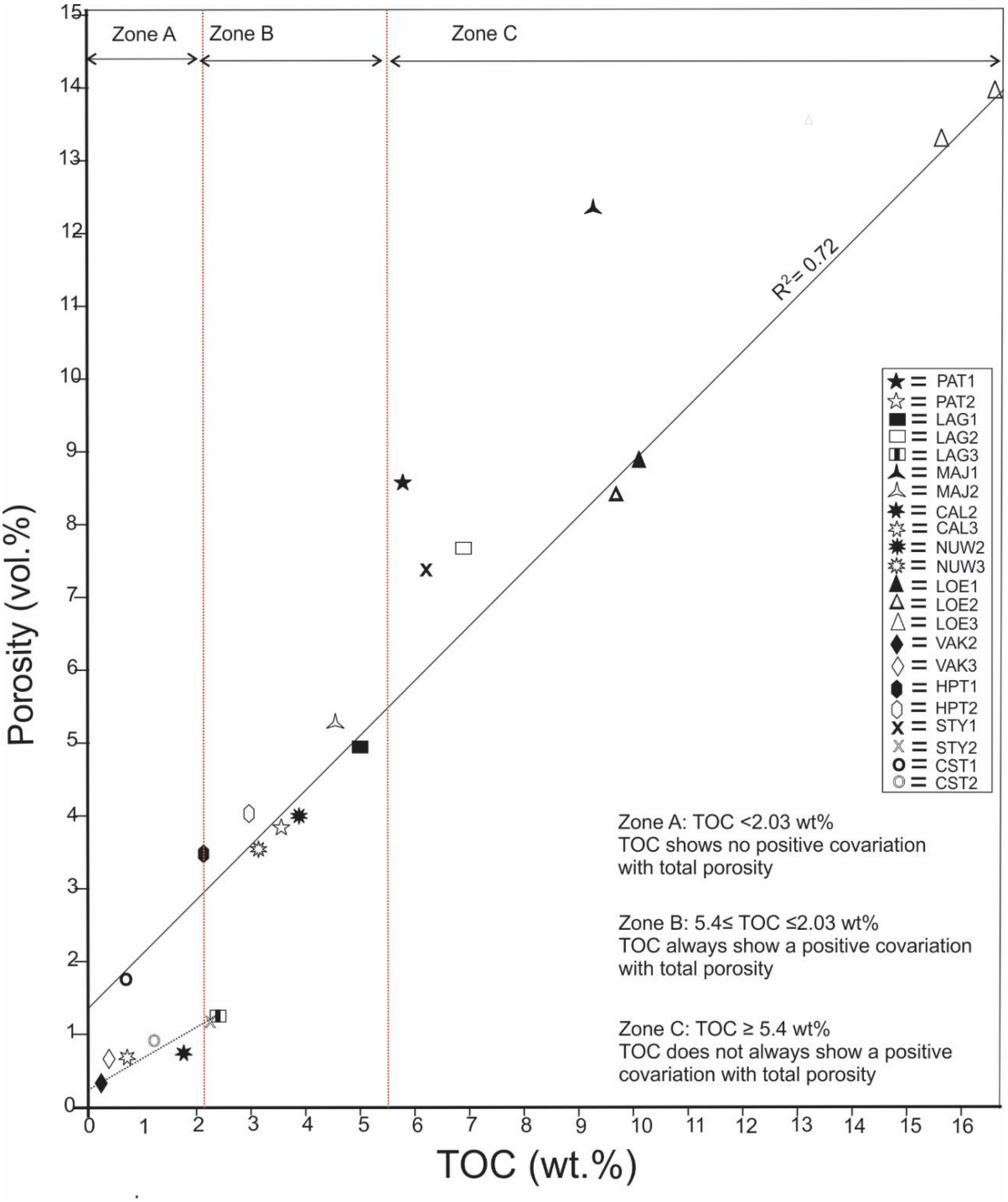

Fig. 4.13: Total organic carbon (TOC, wt.%) versus total porosity (vol.%). Values of TOC less than 2.03 wt% show no positive covariation with total porosity, values of TOC between 2.03 and 5.4 wt% a positive covariation with total porosity exists, TOC value of 5.4 wt%, covariation with total porosity does not always exist.

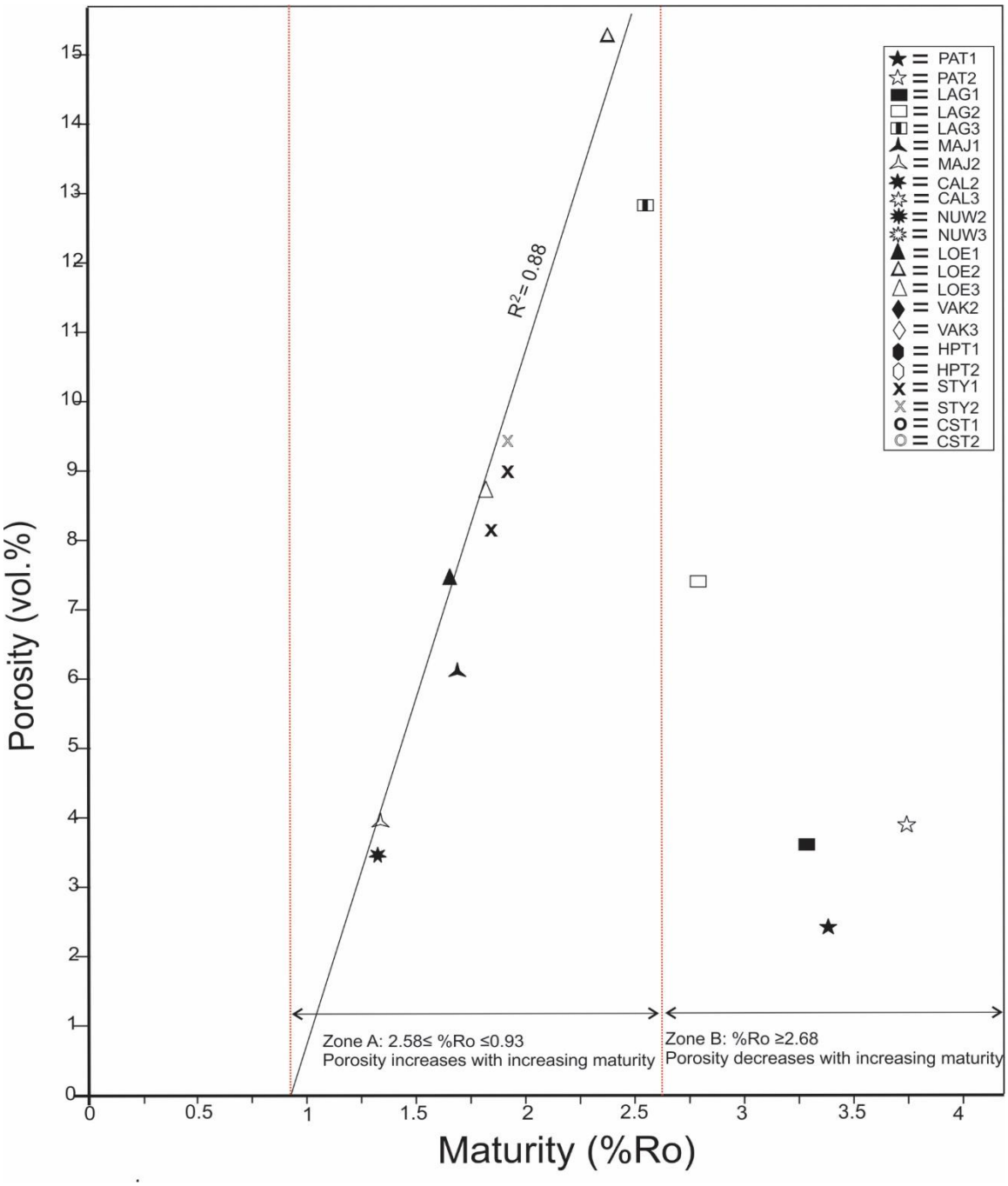

Fig. 4.14: Organic maturity (%Ro) versus measured total porosity. In samples with > 2.03 wt.% TOC, positive covariation exists between maturity and porosity for %Ro values between 0.88 and 2.58. Above 2.58 %Ro, maturity shows a negative covariation with porosity.

4.7. Conclusions

Two-dimensional (2-d) FE-SEM images of ultrathin section (2x3 cm, 10-20 µm thick) from outcrop core samples taken from three subunits of the WHF provided both visual qualitative and quantitative analyses of the pore system in the potential gas shale of the WHF. Two families of pores were identified: organic and nonorganic pores. Organic pores appeared to be associated with exsolution of hydrocarbons during thermal cracking of OM and are therefore more sensitive to mechanical (compaction) diagenesis. Nonorganic pores were sensitive to chemical diagenesis (dissolution, reprecipitation, authigenesis). The development of both pore types appeared to be an integral part of the depositional and diagenetic history of the WHF. The main findings of this study are as follows:

1. Samples with <2.03 wt.% TOC contain more nonorganic porosity than samples with >2.03 wt.% TOC. The latter are almost entirely dominated by organic porosity. This may imply that in samples with high OM content (>2.03 wt % TOC), primary pores were initially completely filled by nonporous OM (amorphous kerogen) that were converted to porous bitumen with organic maturation; whereas samples with lower OM content (<2.03 wt % TOC) preserved many of the primary pores.

2. A positive covariation between TOC and total porosity exist for values of TOC between 2.03 and 5.4 wt.%; whereas at lower or higher TOC values, no systematic covariation was detected between TOC and porosity.

3. A positive covariation between thermal maturity and porosity only exist at a thermal maturity 0.88 and 2.58% Ro. This indicates that until the samples attained a thermal maturity of 0.88 % Ro, they were largely nonporous and after being exposed to thermal maturation of 2.58% Ro, residual fluid inclusion and its mineral precipitates infill earlier created pores, thereby drastically reducing porosity.

References

Bahadur, J., A.P. Radlinski, Y.B. Melnichenko, M. Mastalerz, and A.Schimmelmann, 2015, Small-angle and ultrasmall-angle neutron scattering (SANS/USANS) study of New Albany Shale: a treatise on microporosity: Energy and Fuels, 29, 567-576.

Bernard, S., B. Horsfield, H. M. Schulz, R. Wirth, A. Schreiber, and N. Sherwood, 2012, Geochemical evolution of organic-rich shales with increasing maturity: A STXM and TEM study of the Posidonia Shale (Lower Toarcian, northern Germany): Marine and Petroleum Geology, 31, 70-89.

Bernard, S., R. Wirth, A. Schreiber, H-M., Schulz, and B. Horsfield, 2013, FIB-SEM and TEM investigation of organic-rich shale maturation series from the Lower Toarcian Posidonia Shale, Germany: Nanoscale pore system and fluid-rock interactions in Camp, W., Diaz, E., Wawak, B., eds., Electron Microscopy of Shale Hydrocarbon Reservoirs: AAPG Memoir, 102, 53-66.

Berner, 1984, Sedimentary pyrite formation: An update, Geochimica et Cosmochimica Acta, 48, 143-149

Bohacs, K.M., 1998, Contrasting expressions of depositional sequences in mudrocks from marine to non-marine environs, in J. Schieber, W. Zimmerle, and P. Sethi, eds., Shales and Mudstones, Volume I: Basin Studies, Sedimentology, and Paleontology: Stuttgart, E. Schweizerbart'sche Verlagsbuchhandlung (Nagele u. Obermiller), 33-78.

Boyer, C., B Clark, R. Lewis, and C.K. Miller, 2011, Gas shale: A global resource: Oil Field Review, Autumn 2011, 23, no. 3, 26-39.

Camp, W., E. Diaz, and B. Wawak, 2013, Introduction, *in* Camp, W., Diaz, E., Wawak, B., eds, Electron Microscopy of Shale Hydrocarbon Reservoirs: AAPG Memoir 102, p. ix-xi.

Catuneanu, O., H. Wopfner, P.G. Eriksson, B. Cairncross, B.S. Rubidge, R.M.H. Smith and P.J. Hancox, 2005, The Karoo basins of south-central Africa, Journal of African Earth Sciences, 43, 211-253.

Chalmers, G.R., M.R. Bustin, and I.M. Power, 2012, Characterization of gas shale pore systems by porosimetry, surface area, and field emission electron microscopy/transmission electron microscopy image analyses: Examples from Barnett, Woodford, Haynesville, Marcellus, and Doig units, AAPG Bulletin, 96, 6, 1099-1119.

Chukwuma, K., E.M. Bordy, 2016, Spatiotemporal sedimentary facies variations in the Permian Whitehill Formation, main Karoo Basin, *in* Linol B and de Wit M., eds., Origin and Evolution of the Cape Mountains and Karoo Basin: Geo-biohistory in a terrain with shale gas resources and need for conservation, Part of the series Regional Geology Reviews 8643: Springer Verlag, pp.101-110, doi 10.1007/978-3-319-40859-0_10.

Cole, D.I., and W.A. Basson, 1991, Whitehill Formation in Catalogue of South African Lithostratigraphic Units, M.R. Johnson, ed., 3, 3.51-3.52.

Cole, D.I. and I.R. McLachlan, 1991, Oil Potential of the Permian Whitehill Shale Formation in the Main Karoo Basin, South Africa, *in* Ulbrich, H. and Rocha Campos, A.C., eds., Proceedings and Papers of the Seventh Gondwana Symposium, Sao Paulo: Instituto de Geosciences, Universidade de Sao Paulo, 379-390.

Craddock, J.P., W. Alex, A.W. McKiernan, and M.J. de Wit, 2008, Calcite twin analysis in syntectonic calcite, Cape Fold Belt, South Africa: Implications for fold and cleavage formation within a shallow thrust front, Journal of Structural Geology, 29, 1100-1113.

Cui, Y., H. Kita, and K. Okamoto, 2004, Preparation and gas separation performance of zeolite T membrane: Journal of Materials Chemistry, 14, 924-932.

Curtis, J.B., 2002, Fractured shale gas systems: AAPG Bulletin, 86, 1921-1938.

Curtis, M.E., R.J. Ambrose, C.H. Sondergeld, and C.S. Rai, 2010, Structural characterization of gas shales on the micro- and nano-scales: Canadian Unconventional Resources and International Petroleum Conference, Society of Petroleum Engineers, Calgary, Alberta, Canada, p. 15. SPE 137693.

Curtis, M.E., B.J. Cardott, C.H. Sondergeld, and C.S. Rai, 2012, Development of organic porosity in the Woodford Shale with increasing thermal maturity, International Journal of Coal Geology, 103, 26-31.

Demaison, G., and B. J. Huizinga, 1991, Genetic classification of petroleum systems: AAPG Bulletin, 75, 1626-1643.

Egle, S., M.J. de Wit, and S. Hoernes, 1998, Gondwana fluids and subsurface palaeohydrology of the Cape Fold Belt and the Karoo Basin, South Africa, Journal of African Earth Sciences, 27, 63-64.

Faure, K. and D. Cole, 1999, Geochemical evidence for lacustrine microbial blooms in the vast

Permian Main Karoo, Parana, Falkland Islands and Haub basins of southwestern Gondwana, Palaeogeography, Palaeoclimatology, Palaeoecology, 152, 189-213.

Fisher D. St J., and J.D. Hudson, 1987, Pyrite formation in Jurassic shales of contrasting biofacies, *in* J. Brooks, and A.J. Fleet, eds, Marine Petroleum Source Rocks: Blackwell Scientific, Oxford, 69-78.

Geel, C., M. de Wit, P. Booth, H-M Schulz, B. Horsfield, 2015, Palaeo-environment, diagenesis and characteristics of Permian black shales in the lower Karoo Supergroup flanking the Cape Fold Belt near Jansenville, Eastern Cape, South Africa: Implications for the shale gas potential of the Karoo Basin, South African Journal of Geology, 118, 248-274.

Halbouty, M. T., R. T. King, H. D. Klemme, R. H. Dott, Sr., and A. A. Meyerhoff, 1970, World's giant oil and gas fields, geologic factors affecting their formation, and basin classification, Part II-factors affecting formation of giant oil and gas fields, and basin classification, M. T. Halbouty, ed., Geology of giant petroleum fields: AAPG Memoir, 14, 528-555.

Hamblin AP, 2006, The ‘‘Shale Gas’’ concept in Canada: a preliminary inventory of possibilities, in, Geological Survey of Canada, pp. Open File 5384.

Hayes, J.B., 1991, Porosity evolution of sandstones related to vitrinite reflectance: Organic Geochemistry, 17, 117-129.

IUPAC (International Union of Pure and Applied Chemistry), 1994, Physical Chemistry Division Commission on Colloid and Surface Chemistry, Subcommittee on Characterization of Porous Solids: Recommendations for the characterization of porous solids (Technical Report): Pure and Applied Chemistry, 66, no. 8, 1739-1758.

Jarvie, D.M., B.L. Claxton, F. Henk, J.T. Breyer, 2001, Oil and Shale Gas from the Barnett Shale, Ft. Worth Basin, Texas, Talk presented at the AAPG National Convention, June 3-6, 2001, AAPG Bulletin, p. A100.

Jarvie, D. M., R. J. Hill, T. E. Ruble, and R. M. Pollastro, 2007, Unconventional shale-gas systems: The Mississippian Barnett Shale of north-central Texas as one model for thermogenic shale gas assessment, AAPG Bulletin, 91, no. 4, 475-499.

Keller, L.M., L. Holzer, R. Wepf, and P. Gasser, 2011, 3D geometry and topology of pore pathways in Opalinus clay: Implications for mass transport: Applied Clay Science, 52, 85-95.

Klaver, J., G. Desbois, J.L. Urai, and R. Littke, 2012, BIB-SEM study of the pore space morphology in early mature Posidonia Shale from the Hils area, Germany: International Journal of Coal Geology, 103, 12-25.

Klemme, H.D., and G.F. Ulmisheck, 1991, Effective petroleum source rocks of the world: stratigraphic distribution and controlling factors: AAPG Bulletin, 75, 1809-1851.

Lazar, O.R., K.M. Bohacs, J.H.S. Macquaker, J. Schieber, and T.M. Demko, 2015, Capturing key attributes of fine-grained sedimentary rocks in outcrops, cores, and thin sections: nomenclature and description guidelines, Journal of Sedimentary Research, 85, 230-246.

Littke, R., D.R. Baker, and D. Leythaeuser, 1988, Microscopic and sedimentologic evidence for the generation and migration of hydrocarbons in Toarcian source rocks of different maturities: Organic Geochemistry, 13, 549-559.

Löhr, S.C., E.T. Baruch, P.A Hall, and M.J. Kennedy, 2015, Is organic pore development in gas shales influenced by primary porosity and structure of thermally immature organic matter?: Organic Geochemistry, 87, 119-132.

Loucks, R.G., R. M. Reed, S.C. Ruppel, and D.M. Jarvie, 2009, Morphology, genesis, and distribution of nanometer scale pores in mudstones of the Mississippian Barnett Shale: Journal of Sedimentary Research, 79, 848-861, doi:10.2110/jsr.2009.092.

Loucks, R.G., R.M. Reed, S.C. Ruppel, and U. Hammes, 2012, Spectrum of pore types and networks in mudrocks and a descriptive classification for matrix-related mudrock pores, AAPG Bulletin, 96, 1071-1098.

Magoon, L. B., 1988, The petroleum system-a classification scheme for research, exploration, and resource assessment, in L. B. Magoon, ed., Petroleum systems of the United States: USGS Bulletin, 1870, 2-15.

Magoon, L. B., 1989, Identified petroleum systems within the United States-1990, *in*, L. B. Magoon, ed., The petroleum system-status of research and methods, 1990: USGS Bulletin, 1912, 2-9.

Magoon, L. B, and W. G. Dow, eds., 1994, The petroleum system-from source to trap: AAPG Memoir, 60, 1-24.

Mastalerz, M., A. Schimmelmann, A. Drobniak, and Y. Chen, 2013, Porosity of Devonian and Mississippian New Albany Shale across a maturation gradient: insights from organic petrology, gas adsorption, and mercury intrusion, AAPG Bulletin, 97, 1621-1643.

Milliken, K.L., 1992, Chemical behavior of detrital feldspars in mudrocks versus sandstones, Frio Formation (Oligocene), South Texas, Journal of Sedimentary Petrology, 62, 790-801.

Milliken, K.L., M. Rudnicki, D.N. Awwiller, and T. Zhang, 2013, Organic matter-hosted pore system, Marcellus Formation (Devonian), Pennsylvania, AAPG Bulletin, 97, 177-200.

Müller, G., 1967, Diagenesis in argillaceous sediments, in, G. Larsen and G.U. Chilingar, eds, Diagenesis in sediments, Developments in Sedimentology 8: Elsevier, Amsterdam, 127-178.

Oelofsen, B.W., 1981, An anatomical and systematic study of the family Mesosauridae (Reptilia, Proganosauria) with special reference to its associated fauna and palaeoecological environment in the Whitehill Sea: Unpublished Ph.D. thesis, University of Stellenbosch, 163p.

Osborne M.J, and R.E. Swarbrick, 1997, Mechanisms for generating overpressure in sedimentary basins: a reevaluation: AAPG bulletin, 81, 1023-1041.

Passey, Q. R., K.M. Bohacs, W. L. Esch, R. Kimentidis, and S. Sinha, 2010, From oil-prone source rock to gas-producing shale reservoir: Geologic and petrophysical characterization in unconventional shale-gas reservoirs: Chinese Petroleum Society/Society of Petroleum Engineers International Oil & Gas Conference and Exhibition, Beijing, China, June 8-10, 2010, SPE Paper 121250, 29p., doi:102118/131350-MS.

Potter, P. E., J. B. Maynard, and P. J. Depetris, 2005, Mud and mudstones: Introduction and overview: Berlin, Germany, Springer, 304p.

Ross, D.J.K., and R.M. Bustin, 2007, Impact of mass balance calculations on adsorption capacities in microporous shale gas reservoirs: Fuel, 86, 2696-2706.

Rouchet J. du, 1981, Stress fields, a key to oil migration: AAPG Bulletin, 65, 74-85.

Rowsell, D.M., and A.M.J. De Swart, 1976, Diagenesis in Cape and Karroo sediments, South Africa, and its bearing on their hydrocarbon potential: Transactions of the Geology Society of South Africa, 79, 81-145.

Ruttenberg, K.C., and R.A Berner, 1993, Authigenic apatite formation and burial in sediments from non-upwelling, continental margin environments, Geochimica et Cosmochimica Acta, 57, 991-1007.

SACS (South African Committee for Stratigraphy), 1980. Stratigraphy of South Africa, Part 1, L.E. Kent, Compiler, Handbook Geol. Surv. S. Afr., Pretoria, 8, 690p.

Schieber, J., 1996, Early diagenetic silica deposition in algal cysts and spores: A source of sand in black shales?: Jornal of Sedimentary Research, 66, 175-183.

Schieber, J., 2011, Shale Microfabrics and Pore Development -An Overview with Emphasis on the Importance of Depositional Processes: Recovery-2011 CSPG CSEG CWLS Convention.

Schieber, J., 2013, SEM Observations on ion-milled samples of Devonian Black Shales from Indiana and New York: the petrographic context of multiple pore types, *in* Camp, W., Diaz, E., Wawak, B., eds., Electron Microscopy of Shale Hydrocarbon Reservoirs: AAPG Memoir, 102, 153-171.

Schieber, J., and W. Zimmerle, 1998, Introduction and overview: the history and promise of shale research, in J. Schieber, W. Zimmerle, and P. Sethi, eds., Shales and Mudstones, Volume I. Basin Studies, Sedimentology, and Paleontology: Stuttgart, E. Schweizerbart'sche Verlagsbuchhandlung (Nagele u. Obermiller), 1-10.

Shieber, J., D. Krinsley, and L. Riciputi, 2000, Diagenetic origin of quartz silt in mudstone and implication for silica cycling: Nature, 406, 981-985.

Spötl, C, F.J. Longstaffe, K. Ramseyer, and B. Rudinger, 1999, Authigenic albite in carbonate rocks-a tracer for deep-burial brine migration?: Sedimentology, 46, no. 4, 649-666.

Surdam, R. C., D. B. MacGowan, and T. L. Dunn, 1991, Predictive models for sandstone diagenesis: Organic Geochemistry, 17, 243-253.

Tankard, A., H. Welsink, P. Aukes, R. Newton, and E. Stettler, 2012, Geodynamic interpretation of the Cape and the Karoo basins, South Africa, Phanerozoic Passive Margins, Cratonic Basins and Global Tectonics Maps, USA and UK, Elsevier, 869p.

Tappan, H., 1980, The paleobiology of plant protists, San Francisco, W.H. Freeman and co., 1028p.

Teerman, S. C., B.J. Cardott, R.W. Harding, M.J. Lemos De Sousa, D.R. Logan, H.J. Pinheiro, M. Reinhardt, C.L. Thompson-Rizer, and R.A. Woods, 1995, Source rock/ dispersed organic matter characterization: TSOP research subcommittee results: Organic Geochemistry, 22, 11-25, doi:10.1016/0146-6380(95)90004-7.

Telnova, O.P., 2012, Morphology and ultrastructure of Devonian prasinophycean algae (Chlorophyta): Paleontological Journal 46, 543-548.

Tissot, B. P., and D. H. Welte, 1984, Petroleum formation and occurrence: Berlin, Germany, Springer Verlag, 699 p.

Ungerer, P., E. Behar, and D. Discamps, 1983, Tentative calculation of the overall volume expansion of organic matter during hydrocarbon genesis from geochemistry data: Implications for primary migration, *in*, Bjorøy, M, ed., Advances in organic geochemistry, 1981, Wiley, Chichester, 129-135.

US National Petroleum Council (NPC), 2007, Unconventional gas reservoirs- Tight ga, coal seams, shales: Working document of NPC Global Oil and Gas Supply, Topic paper no. 29, Washington, D.C.

US-EIA (V. Kuuskraa, S Stevens, T. Van Leeuwen, and K. Moodhe), 2011, World shale gas resources: An initial assessment of 14 regions outside of the United States, US DOE, EIA, open file, assessed March 2014.

Visser, J.N.J., 1992, Deposition of the Early to Late Permian Whitehill Formation during a sea-level highstand in a juvenile foreland basin, South African Journal of Geology, 95, 181-193.

Walls, J.D., and S.W. Sinclair, 2011, Eagle Ford shale reservoir properties from digital rock physics, First Break, 29, 97-101.

Wright, M.C., R.W. Court, F-C. A. Kafantris, F. Spathopoulos, and M.A. Sephton, 2015, A new rapid method for shale oil and shale gas assessment: Fuel, 153, 231-239.

Chapter 5

Fossil algal cysts and diagenetic quartz reveal a complex syn- and post-depositional history for the Permian carbonaceous shales of the Whitehill Formation (South Africa)

5.1. Abstract

Thinly laminated, carbonaceous shales of the Permian Whitehill Formation (WHF) are largely considered the result of suspension settling of organic matter-rich muds. The unit also contains high amounts of silt-size quartz, which ensures its rigidity, an attribute needed for hydraulic fracturing of unconventional gas reservoirs. New sedimentological and geochemical evidence shown here indicates that the majority of the quartz is not extrabasinal but rather *in situ*, sourced within the main Karoo Basin. Analyses of scanning electron microscope images captured with back-scatter and cathodoluminescence detectors allowed the distinction of the extra- and intrabasinal quartz based on textural and morphological attributes. The *in situ* quartz has: (1) radial fibrous and colloform textures; (2) irregular outlines, embayments, lobate-to-pointed margins; (3) monominerallic growth bands (zonation); (4) pyrite and bitumen inclusions; (5) low and highly variable CL-luminescence. Furthermore, the results revealed not only marine fossil algal cysts in form of Tasmanites but also the early diagenetic deposition of silica in these algal cysts. The potential source of the silica was felsic tuffs that were supplied to the basin from the adjacent active magmatic province. The precipitation of the silica from the altered tuffs started as fibrous chalcedony, which subsequently recrystallized into quartz of variable sizes and shapes. The ubiquity of marine Tasmanites cysts and early diagenetic *in situ* quartz show that the WHF, a potentially important shale gas resource unit in the main Karoo Basin, has a complex sedimentary history.

Keywords: diagenetic quartz, basin modelling, shale gas, non-marine, Gondwana felsic magmatism

5.2. Introduction

Shales - sedimentary rocks with a dominant grain size below 62.5 µm - contain the largest portion of quartz in the sedimentary record (e.g., Blatt and Schultz, 1976; Potter et al., 1980; Schieber, 1996; Boggs, 2011). The majority of the quartz in shales are thought to be detrital constituents, derived extrabasinally and carried into sedimentary basins by flowing water and/or winds chiefly from the mechanical weathering and erosion of older, quartz-rich rocks. Quartz can also precipitate (i.e., crystalize) in shale from silica-rich solutions that originate from: 1) post-depositional dissolution of detrital quartz and felsic tuffs 2) clay mineral diagenesis, (Compton, 1991); and 3) dissolution of biogenic opal (e.g., Kastner et al., 1977; Compton, 1991; Totten and Blatt, 1996; Schieber, 1996; Peter, 2008). Being physically and chemically resistant to alterations, quartz can preserve paragenetic evidence and provide provenance information, including sediment transport modes, types, intensities, etc. (Potter et al., 1980). For example, the detrital quartz in shales is used as a proxy for reconstructing palaeocurrents and distance to the shoreline, based on the common assumption that detrital quartz content decreases in an offshore direction (e.g., Schieber, 1996).

Compared to an average shale with quartz content of ~30% (e.g., Blatt and Schultz, 1976) and other organic matter-rich black shales with average quartz contents between 19 and 44% (e.g., Loucks et al., 2009, 2012; Curtis et al., 2012; Milliken et al., 2013), the thinly laminated, carbonaceous shales in the Permian Whitehill Formation (WHF) contain anomalous amount (up to 66%) and varieties of quartz that range in size from silt to fine-grained sand (Oelofesen, 1981; Cole and McLachlan, 1991, 1994; Visser, 1992). A high quartz content is an important petrological character of unconventional shale reservoirs because this attribute ensures a higher rigidity and thus a better hydraulic fracturability, which is key for the economic extraction of hydrocarbons (Bohacs et al., 2013; Bryndzia and Braunsdorf, 2014).

The source and mechanism of deposition of the quartz in the organic carbon-rich lower subunits of the WHF in the main Karoo Basin remain unknown and largely under-researched to date with consequences for the interpretation of the palaeoenvironments of the WHF and the overall depositional model of the main Karoo Basin during the Permian. Generally, the majority of the WHF quartz in the upper subunits occurs in association with herbaceous/woody organic material

(e.g., Cole and McLachlan, 1991; Visser, 1992), is assumed to be detrital in origin and sourced from peat-swamps via freshwater plumes (e.g., Visser, 1992). However, the quartz in the lower subunits is associated with amorphous and structured organic macerals, which were produced within the basin (Cole and McLachlan, 1991; Faure and Cole, 1999).

In this study, we show that the majority of the quartz in the WHF is early diagenetic silica that precipitated, among others in algal cysts like Tasmanites. Furthermore, we demonstrate that *such* early diagenetic quartz can contribute significantly to the sedimentary quartz budget, particularly in distal shale successions. The occurrence of a high proportion of *in situ* precipitated quartz can completely offset some conventionally accepted sedimentation patterns, including the decrease in quartz content in an offshore direction. Therefore, the recognition of abundant *in situ* precipitated quartz in shales is crucial for the critical elucidation of depositional conditions of unconventional shale reservoirs and the accurate reconstruction of basin models, including palaeoproductivity, palaeoclimate and the global biogeochemical silica cycle.

5.3. Geological background

The WHF is generally interpreted to have been formed by continuous deposition of carbonaceous mud into an extensive basin that was a part of a much larger depository in southwestern Gondwana, the Permian sedimentary fill of which remnants are found in South America, Falkland Islands, and Antarctica (Fig. 1; Oelofsen, 1987; Cole and McLachlan, 1991; Visser, 1992). The WHF underlies an area of about 260,000 km^2 in the main Karoo Basin and is between 10 and 80 m thick (Cole and McLachlan, 1991). The geology of the main Karoo Basin and the WHF have been explained in detail previously [e.g. by SACS (1980), Cole and Basson (1991), Visser (1992), Catuneanu et al. (2005), Tankard et al. (2012), Geel et al. (2015)], and are not repeated here.

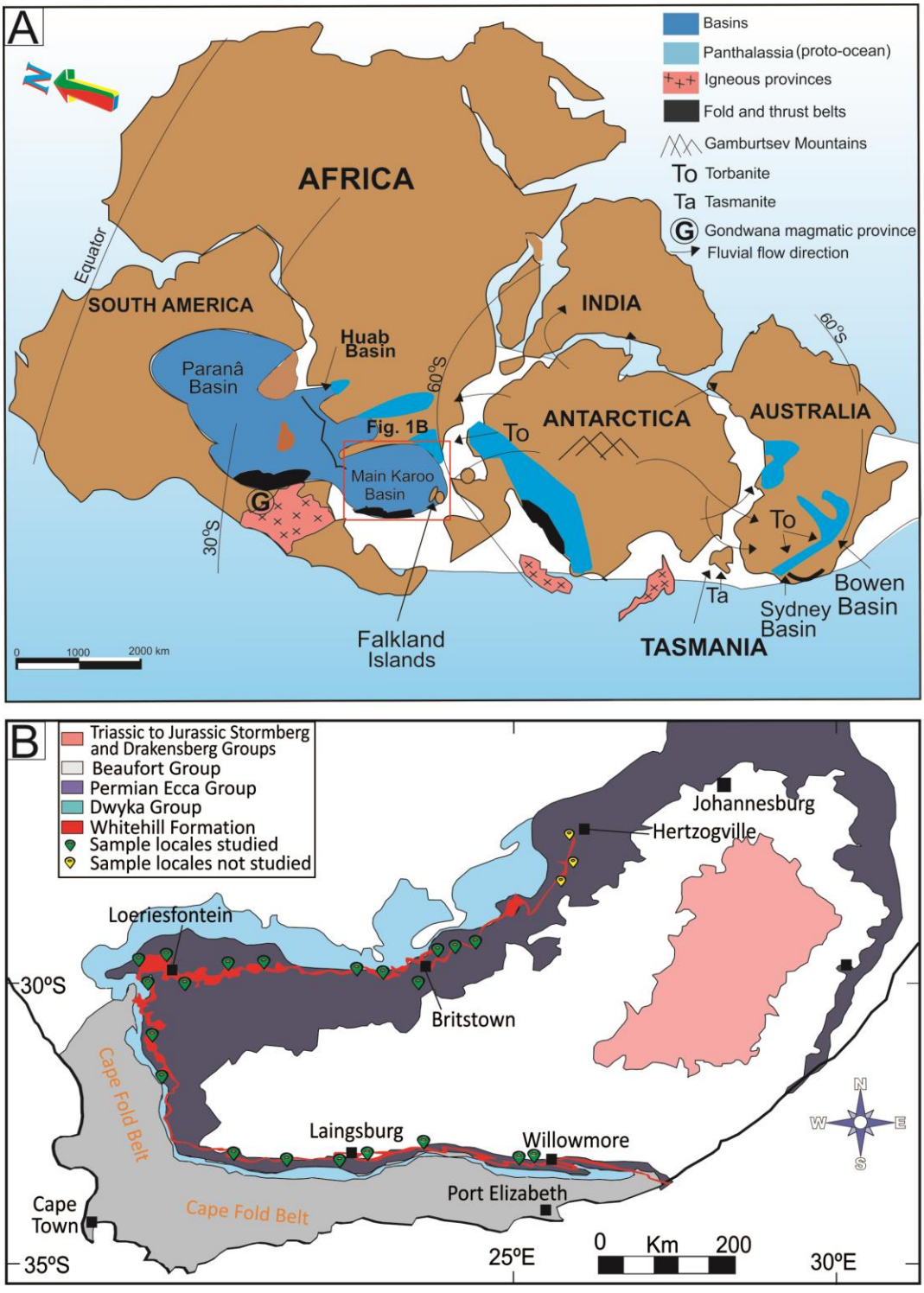

Fig. 5.1. **A**: Geology of southern Gondwana, the locations of southwestern Gondwana basins, magmatic provinces, and thrust belts during the Permian (modified from Visser, 1992; López-Gamundi and Rossello, 1998; Faure and Cole, 1999). **B**: Geologic map of South Africa (adapted from SACS, 1980). Locations of the samples analysed for this study and some towns are shown.

5.4. Methodology

This study, which forms part of a research program on the spatial and temporal variations in the geometry and internal composition of the WHF, was based on analyses of scanning electron microscope images of WHF samples taken from the main Karoo Basin (Fig. 5.1). Outcrop samples (cores and rock chips) were collected from the semi-continuous exposure belt of the WHF in the main Karoo Basin (Fig. 5.1B). In this study, only the lower two subunits (F1, F2) of the WHF, which make up over 80% and 60% of the formation in the southern and northern portions of the basin, respectively, were evaluated. The samples have been studied recently by Chukwuma and Bordy (2016) and the description of the lithology and stratigraphy is provided. Samples of the WHF from the uppermost and more northerly subunits (see Fig 1B) were not included in this study because the earlier study has shown that those stratigraphic intervals which contain less organic matter, are composed of materials (organic/inorganic) that were likely sourced from the northern basin margin and transported into the basin.

During sampling, care was taken to collect samples with limited subaerial weathering, and for this reason, up to 5 m deep trenches were dug (inset in Fig. 5.7A), from where cores were extracted with the aid of a STIHL E-Z Core Rock Drill fitted with a Pomeroy 40 x 2.5 cm core barrel. The unoxidised state of the core samples was later confirmed by their abundant organic matter and pyrite contents. Samples were prepared into 2x3 cm uncovered ultrathin sections (UTS; typically 10-20 µm thick) and ultrathin foils (UTF; typically 5x5 mm, 5 µm thick) polished with air using dry silicon powder. UTS were observed under conventional petrographic microscope in both reflected and transmitted polarised light in the Department of Geological Sciences at the University of Cape Town (UCT). Lightly carbon-coated UTS and uncoated UTF were examined at the Stellenbosch University Central Analytical Facilities using a Zeiss MERLIN field emission scanning electron microscope (FE-SEM) operated with secondary electron (SE), back-scattered electron (BSE), and cathodoluminescence (CL) detectors. Cryo-energy-dispersive X-ray detector (cryo-EDS) provided identification and characterization of components. The description of the core samples, in terms of their lithology, sedimentary structures, bulk and organic geochemical compositions, is provided by Chukwuma and Bordy (2016) and in the earlier chapters of this doctoral dissertation.

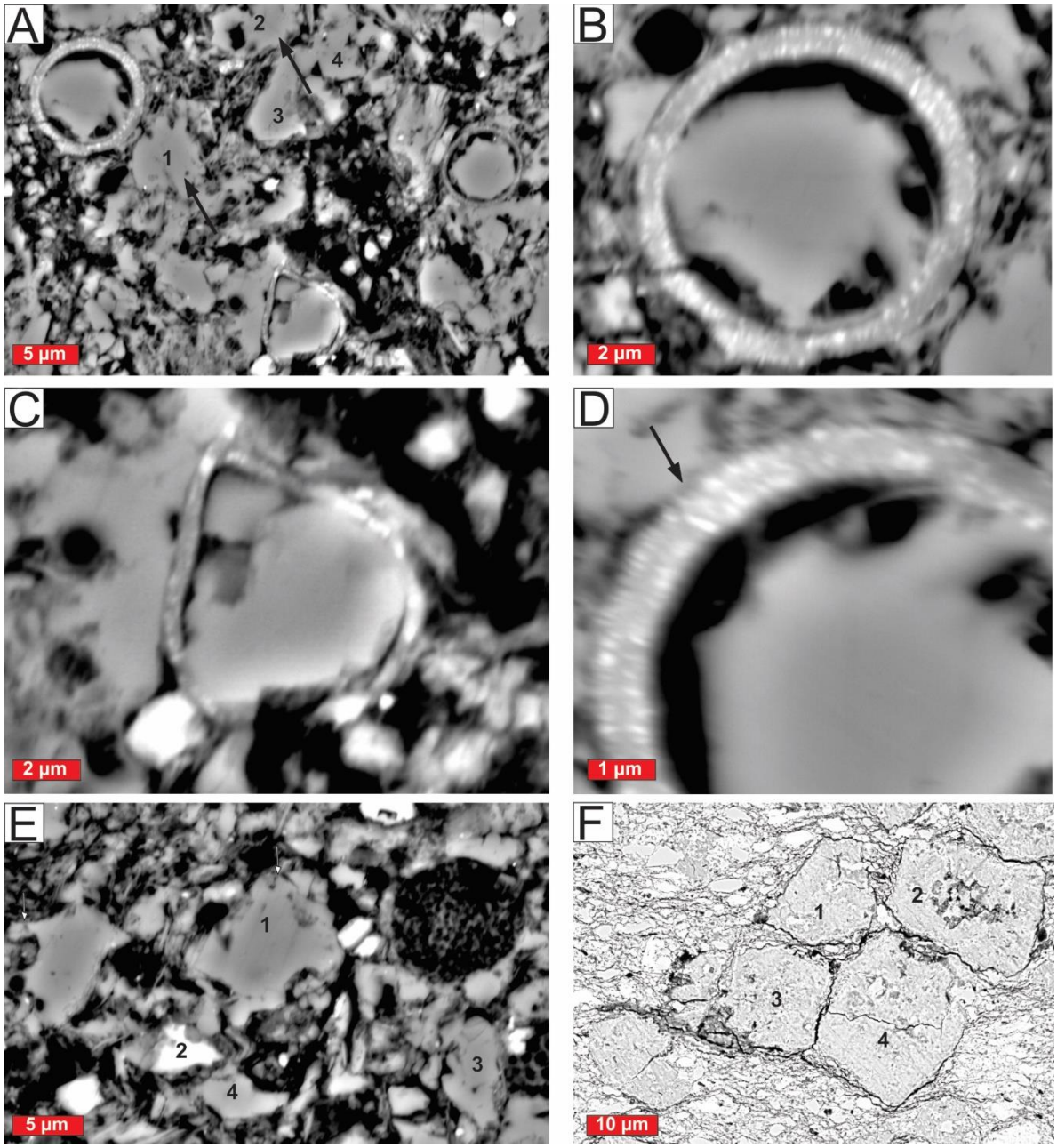

Fig. 5.2. Scanning electron microscope images of Tasmanites cysts infilled with various quartz textures with morphological features that are suggestive of early diagenetic origin. See text for details.

5.5. Observations

BSE- and CL-SEM images of UTS reveal that spore-like microfossils, commonly referred to as Tasmanites (Figs. 5.2-5.5; e.g., Tappan, 1980; Schieber, 1996, 2013; Telnova, 2012) occur throughout the black to dark grey organic-rich shales in the lower and middle stratigraphic sections

of the WHF. In most samples examined, the Tasmanites cysts are completely collapsed and flattened with oval to irregular outlines and are preferentially infilled with silica, a few cysts are, however, infilled with framboidal pyrite. The silica deposits in cysts show several different types of textures, including chalcedony (radial fibrous with colloform textures), microquartz (crystal size smaller and/or up to 20 μm), megaquartz (inter-grown crystals with size >20 μm), and single quartz (singular crystals larger than 20 μm) grains-Figs. 5.2-5.5. Because of the original oval to spherical shape of the Tasmanites cysts, the majority of the silica deposits have rounded to oval outlines and show good sphericity. Especially where the original cyst was preserved in pristine condition, their silica infills retained the morphological features of these microorganisms. In addition to round-to-spherical outline, some silica deposits are surrounded by a thin rim, representing the cysts wall (Figs. 5.2). This feature particularly facilitated the identification of these cysts infills and their original organisms because the difference in the texture of the silica that infilled the cyst walls from those that infilled the cyst internal membrane. This textural difference created a sharp contrast between the preserved cyst walls and the internal membranes. Some cysts deposits show indentations, lobate-to-pointed outlines and embayments (Figs. 5.2 and 5.3), which is interpreted as due to burial compaction. In some cases, the silica was seen to grow out of the cysts membrane and form spherical deposits with irregular outline, often with lobate-to-pointed projections. These features also assisted in the identification cysts silica deposits, where the cyst wall had been removed. These diagnostic features of the cyst silica deposits, particularly size, oval to irregular shape, and lobate-to-pointed grain margins, oval silica surrounded by a rim (more like Saturn and its ring!) clearly differentiate these quartz crystals from their detrital counterparts (Fig. 5.2E-F). The extrabasinally-derived detrital quartz grains are moderately rounded and rhombohedral in outline and are often interconnected by cryptocrystalline silica cement, while the majority occurred as isolated grains in the shale matrix (Fig. 5.2F).

From BSE-SEM image and EDS analyses, the silica deposits in cyst show several different types of textures, including chalcedony (radial fibrous with colloform textures), microquartz (crystal size smaller and/or up to 20 μm), megaquartz (crystal size >20 μm), and single quartz grains (often over 32 μm-Figs. 5.2-5.5). The cyst walls and rims are preferentially infilled with fibrous chalcedony with concentrically arranged colloform textures and growth bands (Fig. 5.2B, D; 5.3C) whereas the internal membranes are infilled with microquartz, megaquartz, and single quartz grains (Figs. 5.2-5.33). In some cysts, the silica deposits extend outside of the cysts to form a

spherical deposit with irregular outlines and lobate-to-pointed projections may conjoin other matrix grains (Figs. 5.2A, C).

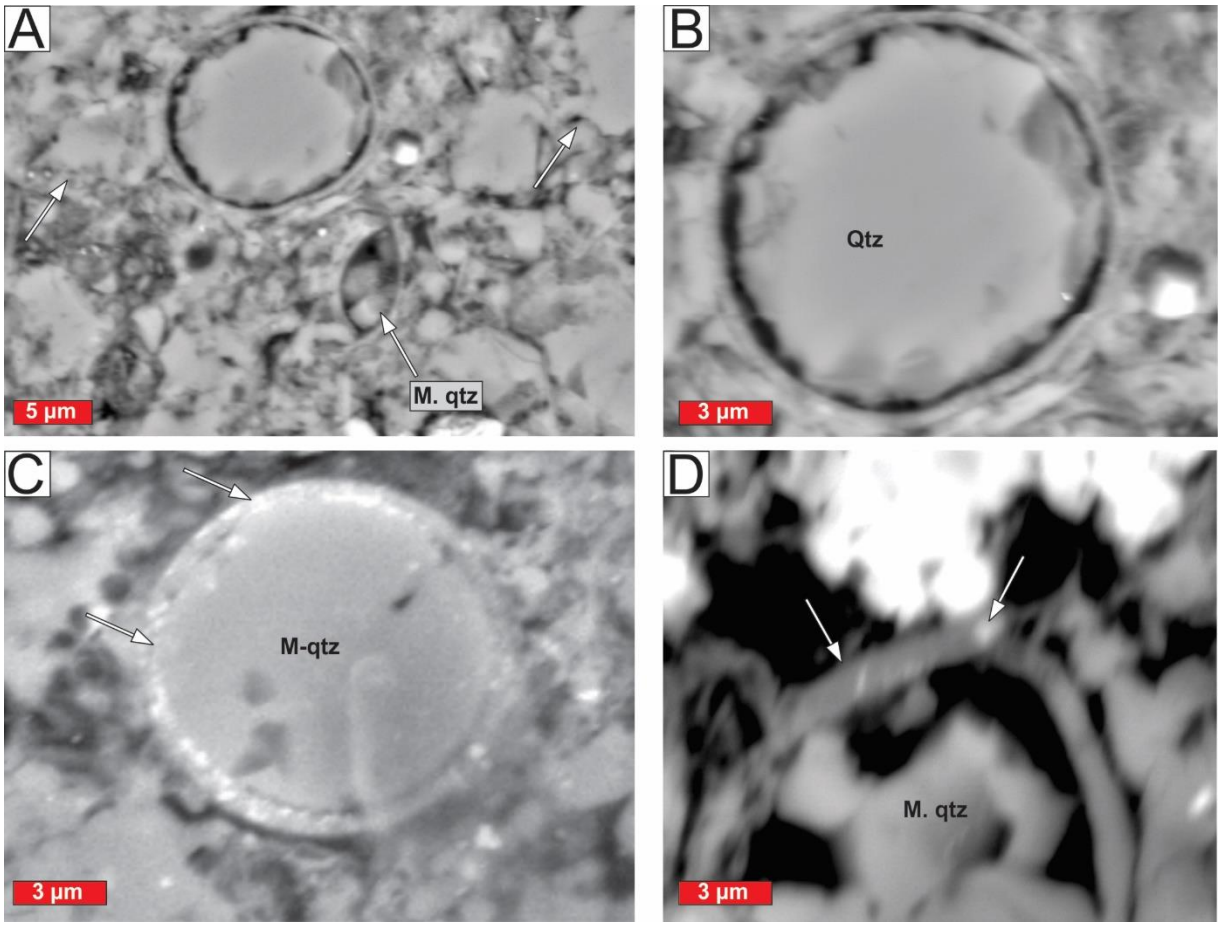

Fig. 5.3. Scanning electron microscope images Tasmanites cysts infilled with various quartz textures. The majority of cyst rims are preferentially filled with fibrous chalcedony (arrows in C, D) while the interior is filled with microquartz (m. qtz), megaquartz (m-qtz), and single quartz (qtz).

BSE- and CL-SEM images of UTF provided further clues on the spatial relationship of the quartz crystals within cysts. BSE-SEM images of UTF show that cysts quartz comprise several radial growth generations of crystals represented by concentric bands, typically starting from the outer cysts and building inwards (Figs. 5.4 -5.5). These concentric growth bands are considered evidence for sequential recrystallization of chalcedony into micro- and megaquartz, and eventually single quartz grains. CL-SEM images of the cyst quartz show that these growth zones display variable intensities of luminescence. While some are largely non-luminescent, others show variable levels

of luminescence. Although no systematic pattern is noticeable, crystals that contain more impurities, particularly pyrite and bitumen inclusions, are darker and least luminescent (Fig. 5.6). Detrital quartz grains displayed sharp and uniformly bright luminescence (Fig 5.6). The textural features observed in these cysts quartz are similar to those described in previous studies (e.g. Zinkernagel, 1978; Ramseyer and Mullis, 1990; Milliken, 1994; Pagel et al., 2000; Schieber et al., 2000) as indicators for a low-temperature authigenic origin.

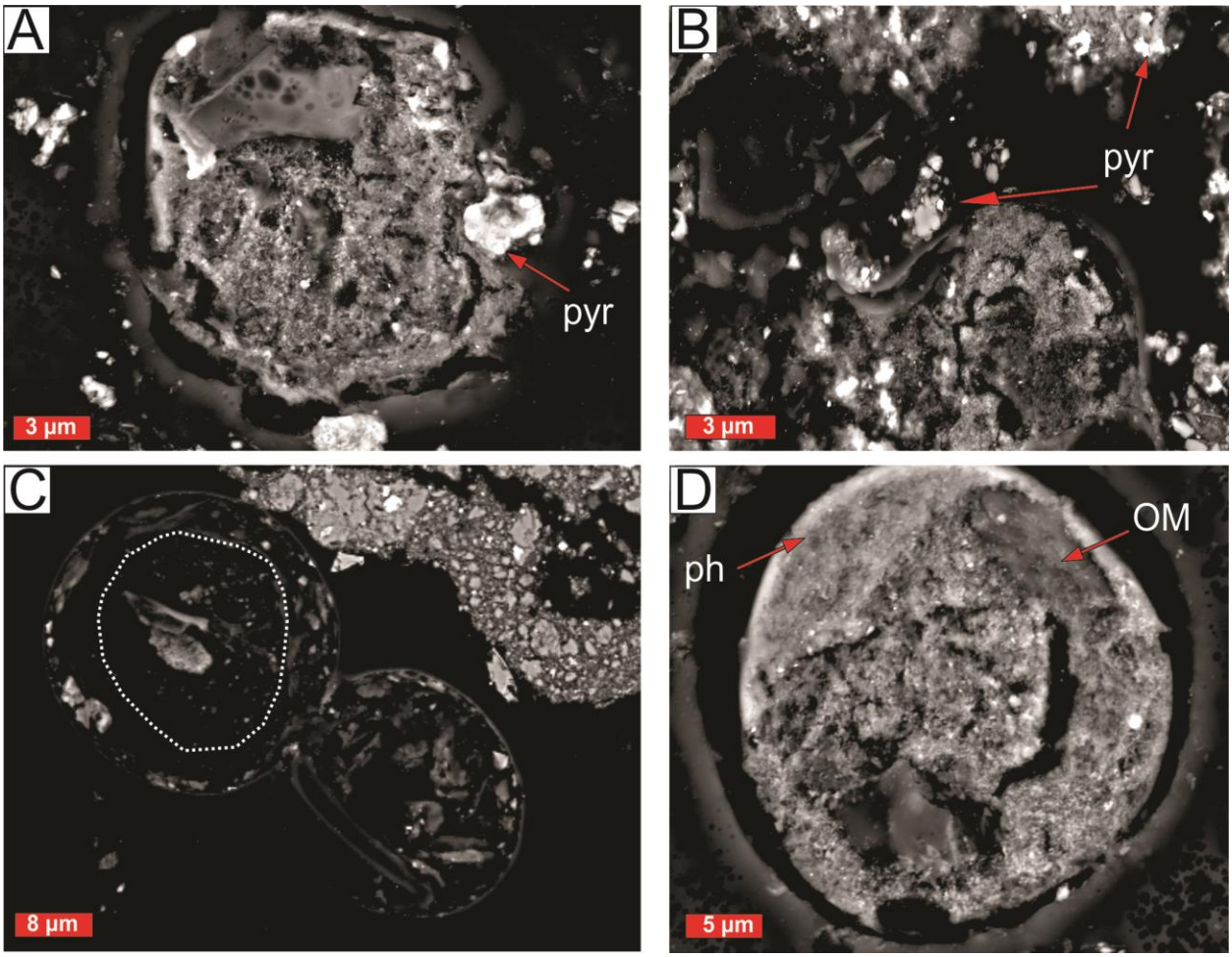

Fig. 5.4. Scanning electron microscope images of internal crystal arrangement in cyst filled quartz. The presence of colloform and hopper-like textures with inclusions of pyrite (pyt), organic matter (OM), and phosphates (ph) as well as monominerallic growth bands (C) suggests sequential growth of crystal.

5.6. Discussion

Tasmanites cyst is described by most authors (e.g., Tappan, 1980; Martin, 1993; Schieber, 1996; Hoek et al., 2006; Telnova, 2012) as the cyst stage (phycomata) of a fossil algae with affinity to *Prasinophyceae*, which is a group of modern planktonic, unicellular green algae. Fossil *Prasinophyceae*, like their extant counterparts, existed in two distinct forms during the course of their life cycle: the quadriflagellate cell stage (motile) and the cyst (resting/reproductive) stage (Tappan, 1980; Efremova, 1990; Telnova, 2012). The motile Tasmanites has no skeletal structure suitable for fossilization, whereas the cyst has a thick wall composed of algenan (lipoid material), which is resistant to degradation and extreme extraction procedures (e.g., acetolysis, which is a mixture of acetic anhydride and sulfuric acid), and is abundant in the Phanerozoic rock record (Tappan, 1980; Revill et al., 1994; Hemsley et al., 1996; Schieber, 1996; Telnova, 2012). Enrichment of Tasmanites in Paleozoic deposits of Gondwana have been reported by Revill (1994) and interpreted as an indication of algal blooms. Generally, fossil *Prasinophyceae* are indicative of marine conditions, although some freshwater extant species exist (e.g., Tappan, 1980; Baceta and Nunez-Betelu, 1994; Telnova, 2012). Abundance of fossil *Prasinophyceae* usually indicate maximum flooding events during transgression, when extreme low clastic sedimentation rates cause sediment starvation and allow the more labile OM to be effectively degraded by microbes in marine settings (e.g., Baceta and Nunez-Betelu, 1994; Schieber, 1996; Telnova, 2012; Lazar et al., 2015).

5.6.1. Timing of quartz deposition in cysts

Studies of modern sediments indicate that newly deposited muds contain up to 70-90% water by volume (e.g., Müller, 1967; Schimmelmann et al., 1990; Parthenaides, 1991). Major expulsion of this excess pore water concomitant with significant grain reorientation occur during initial compaction, typically at 10-20 cm of burial (e.g., Burst, 1976). The flattened algal cysts and their infilled silica deposits, as well as irregular outlines, embayments, lobate-to-pointed projections, indicate that silica precipitation predated significant expulsion of pore water and considerable grain realignment (also see section 5.6.3). In some instances (Figs. 5.2A-B and Fig. 5.3A-C), the cysts and their silica infills retained their original spherical shape, which suggests that silica precipitation sheltered the cysts from pervasive early diagenetic compaction and collapse, and by

extension, played a key part in cysts preservation. The above observations strongly suggest that deposition of silica in cysts occurred very close to the sediment-water interface and during very early diagenesis. However, some authors (e.g., Reineck and Signh, 1980; O'Brien and Slatt, 1990) maintain that cysts and other similar microfossils (e.g., foraminifera) are able to maintain their shape during early burial because gas bubbles resulting from decaying microorganisms, prevent the collapse of cells and halt compaction of the surrounding sediment. By comparison with their extant counterparts, cysts probably lost their internal content prior to settling to the seabed (e.g., Tappan, 1980; Schieber, 1996; Telnova, 2012), which makes it unlikely that their internal fluid pressure supported their original spherical shape upon burial. The presence of framboidal pyrite and phosphate peloids inclusions in some cyst silica deposits (Fig. 5.4) also support early diagenetic origin of the silica. Studies of modern sediments show that framboidal pyrite and phosphate peloids typically form immediately below the sediment-water interface, usually within 10-20 cm (e.g., Burnett, 1977; Berner, 1984; Schieber and Baird, 2001; Schieber, 2011).

5.6.2. Sources of silica

The study by Telnova (2012) shows that cyst wall is made up pores. Precipitation of quartz in algal cysts, therefore, requires silica in dissolved form. Silica in pore water can be derived from: (1) the dissolution of mainly detrital quartz and feldspars (e.g. Schott and Oelkers, 1995); (2) the transformation of clay minerals, particularly smectite illitization (e.g., Burst, 1957; Weaver, 1957; Pytte and Reynolds, 1989; Compton, 1991); (3) the dissolution of diatomaceous opal and other siliceous tests (e.g., Kastner et al., 1977; Schieber, 1996; Van Cappellen et al., 2000); and (4) the alteration of felsic volcanic tuffs (e.g., Cerling et al., 1985; Inoue et al., 1988, 2005; Compton, 1991). Dissolution of silicates and heavy minerals during diagenesis have also been reported to generate silica (e.g., Bernard et al., 2010) but not during early diagenesis and at the very shallow depths indicated by textural observations for the silica reported here. Therefore, dissolution of silicate and heavy minerals is a less likely potential source of silica that infilled the algal cysts in the WHF. Contingent on local conditions, all of the common clay minerals can be stable in the early stages of diagenesis (e.g., Powers, 1967; Burst, 1969). The transformation of most common clay minerals (e.g., smectite-to-illite), as discussed by Staplin et al. (1973) and Freed et al. (1989), involves the expulsion of pore- and interlayer water and concomitant release of silica. According

to these and several other workers, such transformation occurs over a temperature range of between ~60 and 180° C and requires at least some overburden. According to Burst (1969) and Dunoyer de Segonzac (1970), the expulsion of interstitial pore water occurs at ~1000 m of burial depth. Textural evidence suggests that the cyst silica deposits in the samples occurred at a shallower burial depth. The dissolution of diatomaceous opal and siliceous cysts is a less likely potential source of the dissolved silica that infilled the algal cysts in the WHF because remnants of siliceous fossil materials have not been identified in this succession.

Volcanic tuffs can be an important source of early diagenetic silica in shales (Cerling et al., 1985; Inoue et al., 1988, 2005; per. comm with Prof John Compton, 2016). Interbedded with the Permian strata of Ecca and Beaufort Group in the main Karoo Basin are numerous air-fall tuffs that are generally considered to have been produced in the late Paleozoic magmatic arc of Gondwana (Fig. 5.1.; Visser, 1992; Viljoen, 1994; López-Gamundi et al., 2013). Remnants of the magmatic arc are locally preserved as the Choyoi and Puesto Viejo magmatic suites in South America (López-Gamundi et al., 2013; Bordy and Abrahams, 2016). Based on the similarity in palaeogeography and geochemistry, the Choiyoi and Puesto Viejo magmatism (ca. 276-234 Ma; López-Gamundi et al., 2013) is likely responsible for air-fall tuff deposits in Pàrana, Cuyo, and main Karoo Basins (Rochas-Campos et al., 2011; Bordy and Abrahams, 2016). During this study, the volcanogenic material has been recorded within the upper, organic-lean subunits of the WHF as well as in discrete laterally extended, yellowish-weathering layers of up to 5 cm in Calvinia-Loeriesfontein locality (Fig. 5.7). The occurrence of laminations and thin lenses of tuffaceous material within the shale laminations is an evidence that these tuffs were water deposited. The presence of these well-defined tuffaceous beds, as well as disseminated volcaniclastic particles (e.g., Visser, 1992), suggest the presence of ash in the atmosphere over the basin during the deposition of the WHF. This study argues that, among the various potential sources of silica, the likely source of the silica that precipitated in the early diagenetic phase of the WHF sediment is from the alteration of the syn-sedimentary felsic volcanic ash layers. In addition to silica, the tuffs are enriched in iron and phosphorous (Visser, 1992; Viljoen, 1994) and therefore their syn-sedimentary alteration could have contributed significantly to the influx of nutrients into the waterbody and that powered (i.e., “fed”) algal growth.

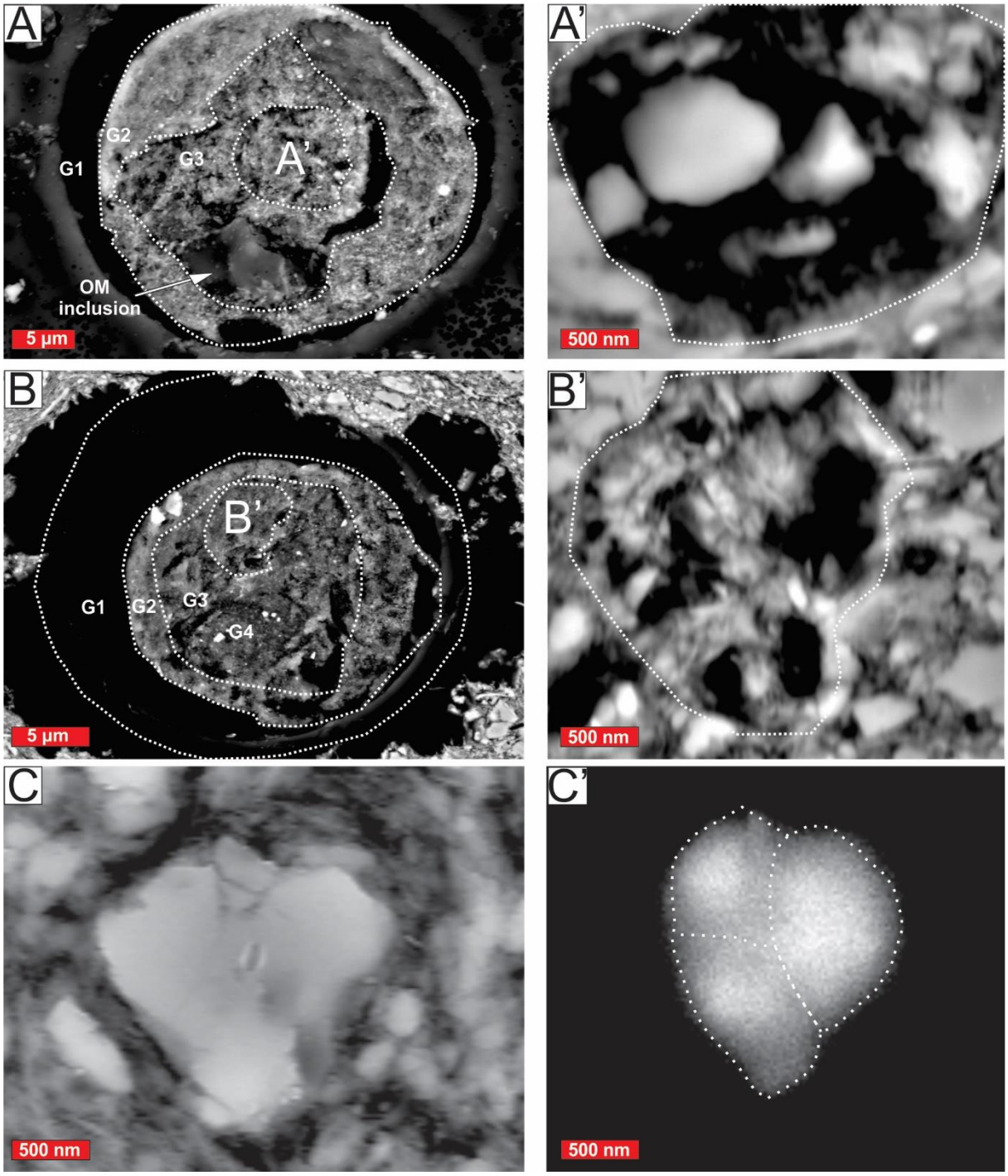

Fig 5.5. Scanning electron microscope images of the sequential arrangement of crystals in cyst filled quartz. The consecutive crystal growths represented by G1 to G4 indicate that the deposition of silica started from the inner cyst wall (G1) and grew inwardly (G4). These crystals exhibit a variable level of cathodoluminescence (C'). The quartz in C is composed of three crystals (dashed lines in C') identified based on their varying degree of cathodoluminescence.

5.6.3. Mechanism and sequence of silica precipitation

Several models describing the early diagenetic transformation of silica in fine-grained sediments are based on studies of sediments that are formed from siliceous oozes, such as diatomites and radiolarites (e.g., Schink et al., 1975; DeMaster et al., 1996; Van Cappellan et al., 2002). Generally, early diagenetic (eodiagenetic) processes occur at temperatures <30 °C, depths shallower than 1 km and in the upper few meters of the sediment on the seabed (Boggs, 2011). In these rocks, silica is precipitated by dissolution of silica-secreting organisms (diatoms, radiolarians) in form of opaline silica (opal-A). Opal-A is a highly disordered (nearly amorphous) form of silica and water (Hurd and Birduwhistell, 1983). During the initial stages of burial diagenesis, opal-A is transformed into opal-CT (a more ordered form of silica). Further diagenesis transforms opal-CT into chalcedony. Chalcedony occurs mainly as spherulitic (fiber/needle) quartz and is largely metastable but can exist for long periods (Rabouille and Gaillard, 1990; Dixit et al., 2001). However, if the concentration of silica is below the solubility of opal-CT, chalcedony can be precipitated directly from silica without the precursory opal-CT pathways (e.g., Kastner et al., 1977; Schieber, 1996). Considering that the silica deposition in the cysts was likely derived from alteration of volcanic tuffs and not from siliceous organisms, one may wonder how this may affect the silica synthetic pathways. A study by Compton (1991) indicates that the alteration of volcanic ash to clay minerals may constrain the opal-A to pal-CT transformation by removing pore-water Mg. Another factor capable of inhibiting the early diagenetic formation of opal-CT is high organic content (e.g., Hinman, 1990; Schieber, 1996). Hints et al. (1997) suggested that such alteration of volcanic ash to silica can occur during early diagenesis but is dependent on the composition of source magma, climate, and sedimentary conditions. Considering these factors and based on textural features described below, we suggest that dissolution of volcanic ash yielded silica that infilled the algal cysts and that the silica was directly transformed to chalcedony without the opal-CT precursor.

The occurrence of chalcedony with concentric and radially arranged fibrous and colloform textures and growth bands, preferentially along the rims of these silica deposits (Figs. 5.4 and 5.5) agree with the above interpretation that chalcedony was the first cyst infill. Chalcedony is common pore-filling deposit in sediments and has been documented in many studies (e.g., Meyers, 1977; Milliken, 1979; Schieber, 1996). Early diagenetic precipitation of chalcedony without the opal-CT precursor was likely favored by the high organic and clay contents in the WHF sediments (e.g.,

Hinman, 1990; Compton, 1991; Schieber, 1996). The presence and close association between the cyst quartz, OM, pyrite, and phosphate (Figs. 5.4 and 5.5) attest to an environment with anaerobic bacterial sulfate reduction (Berner, 1984), where the two distinct but closely related processes likely co-occurred. First, the deposition of microbial pyrite and phosphate by reduction of iron oxides and hydroxides present in the sea water. The latter usually results in lowered pore water acidity and a concomitant increase in the pH of the system. The higher pH would have enhanced dissolution of volcanic ash and its silica constituent (e.g., Hasse, 1986; Blatt, 1992; Schieber, 1996). When iron content in the seawater becomes reduced, microbial formation of pyrite resorts to the decomposition of OM (e.g., Schieber and Baird, 2001). Decomposition of OM results in lowering of pH and increasing of acidity (Hesse, 1986; Schieber, 1996). This would result in precipitation and deposition of earlier dissolved silica. The equilibrium between silica dissolution and pH is such that a small reduction in pH can cause a drastic reduction in solubility of silica (Hinman, 1990; Schieber, 1996). The association of OM, phosphate, and pyrite in the *in situ* precipitated quartz testify to their simultaneous precipitation.

Chalcedony-rimmed cysts walls that surround a megaquartz- and single quartz center (Figs. 5.2-5.5) suggest that chalcedony formed prior to megaquartz and single quartz. This precipitation sequence has been documented in several studies of cyst quartz and infilling of pore space by silica (e.g., Milliken, 1979; Schieber, 1996). Silica diagenesis, therefore, likely started as chalcedony which then recrystallized into mirco- and megaquartz and single quartz. A number of factors are capable of controlling the transformation in crystal habit from chalcedony to megaquartz and single quartz, including the chemistry of pore water, temperature, pressure, and time (Schieber, 1996). These factors do not work in isolation and since their resultant effect is similar, isolating the effect of one from another is hard and beyond the scope of this study. However, it is generally assumed that the change from chalcedony to megaquartz and single quartz grains are directly connected to a decrease in silica concentration (Milliken, 1979; Schieber, 1996).

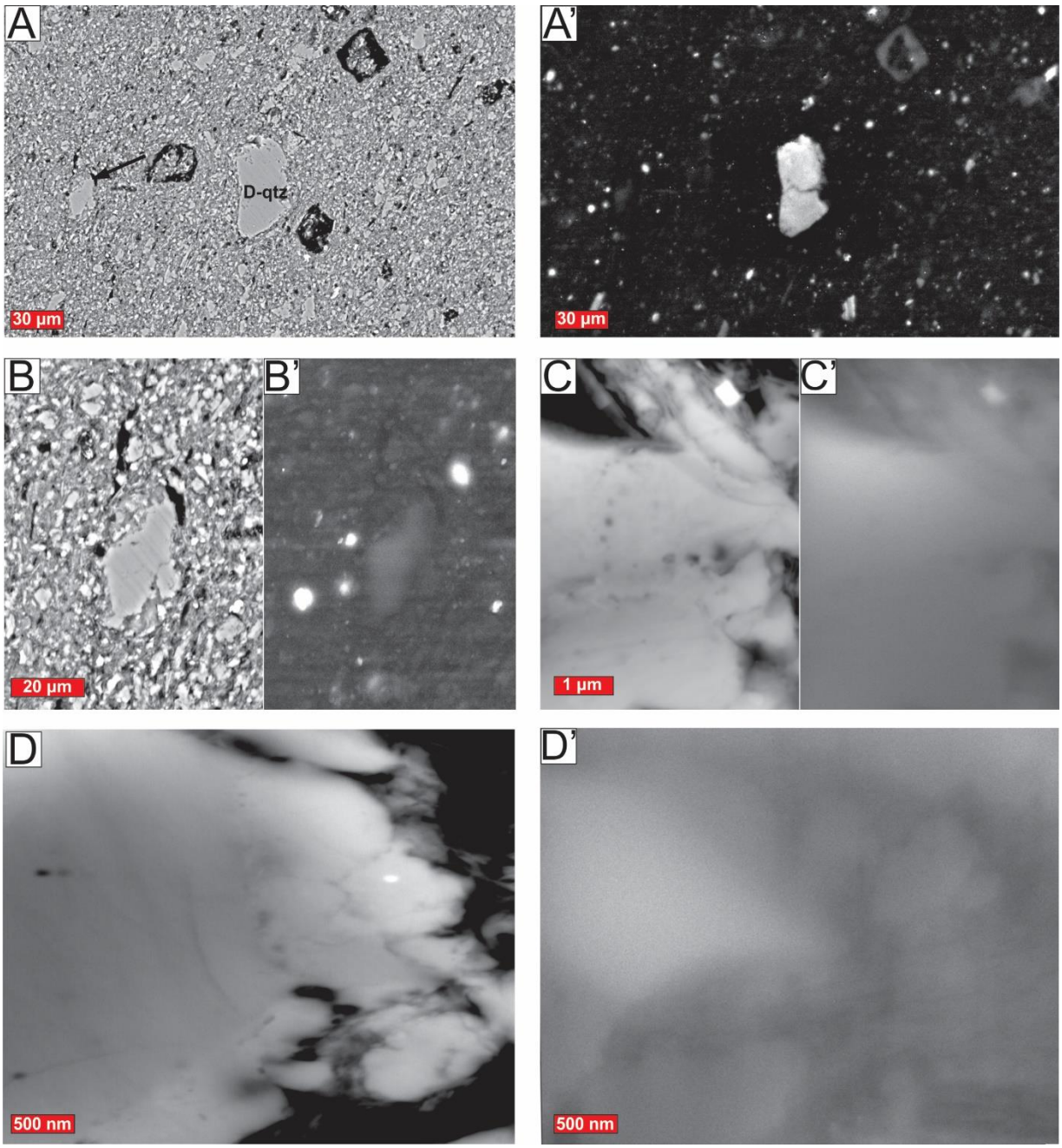

Fig. 5.6. Scanning electron microscope images of the variations in the intensity of luminescence between detrital and diagenetic quartz. Detrital quartz usually exhibits uniformly bright and high cathodoluminescence (A-A') whereas cysts quartz is of low and variable CL-SEM luminescence (B-B', C-C', D-D').

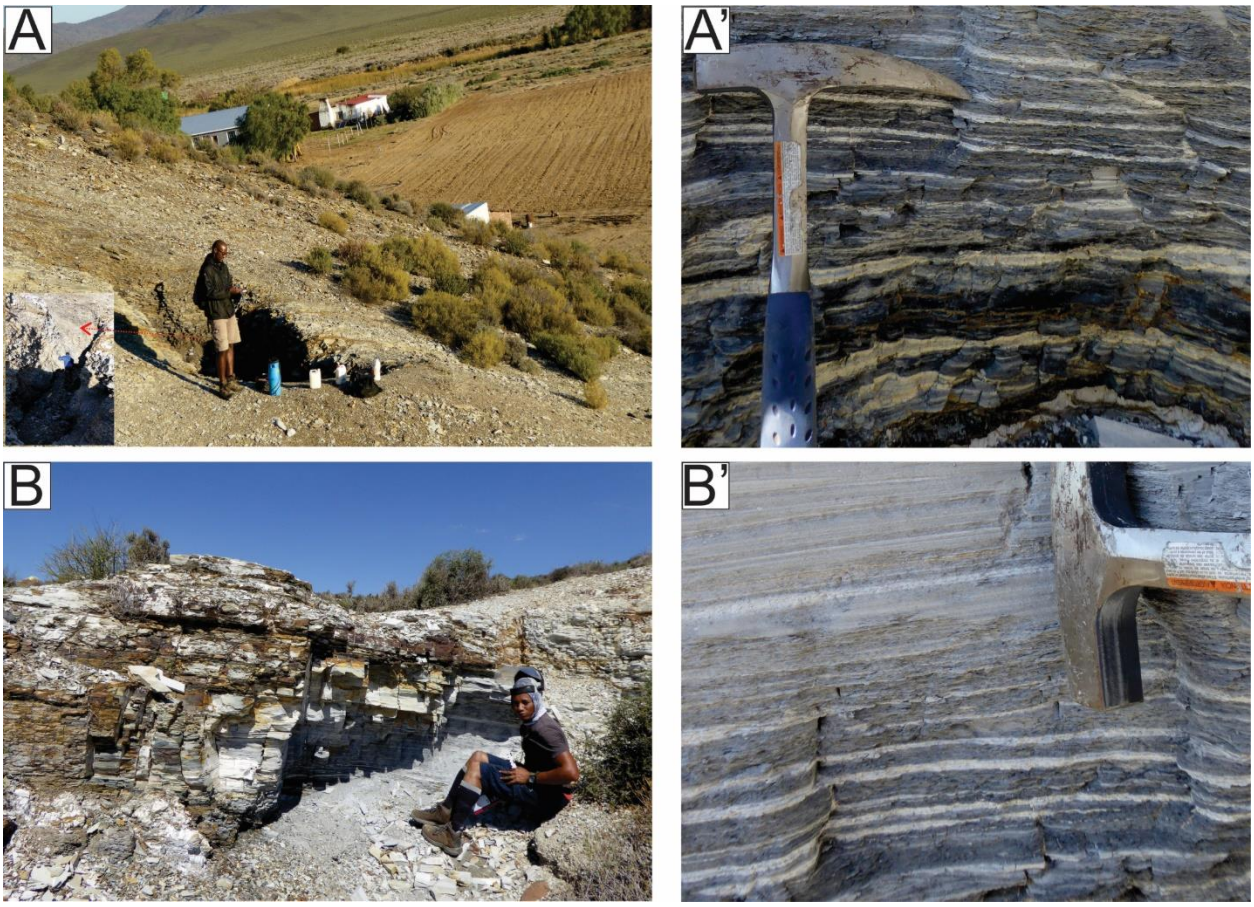

Fig. 5.7. Outcrop images of well-defined yellowish- to greyish-weathering tuffaceous layers in Matjiefontein-Sunderland locality (A) and Calvinia (B) district. A 4.8 m trench (inset in A) was made before relatively fresh samples were encountered.

5.6.4. Implications for depositional conditions

Early diagenetic mobilisation of silica from volcanic ash and its consequent precipitation in algal Tasmanites cysts likely provided the mechanism by which quartz crystals were being produced at a very low temperature and shallow depths within the carbonaceous sediments of the WHF. Recognition of algal Tasmanites cysts and a large proportion of *in situ* precipitated quartz that developed from silica infilling of the cysts have implications for our understanding of the depositional environment, palaeoproductivity, and palaeoclimate during the accumulation of the WHF. Based on textural features, such as thin laminations, high organic and pyrite contents, lack of bioturbations and reduced detrital grains, the WHF, especially its lower subunits, is interpreted by most authors to have been deposited under anoxic condition (Anderson and McLachlan, 1979; Oelofsen, 1981; Cole and McLachlan, 1991; Visser, 1992; Geel et al., 2015). However, the type

of environment (i.e., marine vs non-marine) remains largely unresolved, with most authors (e.g., Teichert, 1974; Kensley, 1975; Anderson and McLachlan, 1979; Oelofsen, 1981; Oelfosen and Araujo, 1987; Christie, 1990; Visser, 1992; Geel et al., 2015) suggesting a marine environment, whereas others (e.g., Cole and McLachlan, 1991; Veevers et al., 1994; Pickford, 1995) endorse a non-marine to brackish water body with no connection to the ocean. Although OM deposited in freshwater usually contain much less diagenetic pyrite than those found in the WHF samples, because of lower concentration of dissolved sulfate in freshwater (e.g., Berner and Raiswell, 1984), the absence of marine fossil had been a strong evidence in favor of non-marine conditions (Cole and McLachlan, 1991). The presence of Tasmanites cysts in sediments, and particularly in Paleozoic successions of Gondwana (e.g., Revill, 1994), has been interpreted as an indication of algal blooms in marine settings (e.g., Tappan, 1980; Baceta and Nunez-Betelu, 1994; Telnova, 2012). If the syn-depositional dissolution of volcanic ash, as argued above, indeed occurred, high pH and low sedimentation rates can be assumed, and these also have been interpreted as indirect signals of marine incursions (Schieber, 1996; Kiipli et al., 2007).

Previously, the presence of well-defined tuffaceous beds in the organic-lean upper subunits of the WHF (Fig. 5.7) and the overlying Collingham Formation, and absence of the same in the organic matter-rich, lower subunits were interpreted as an indication of higher levels of ash concentrations in the atmosphere over the basin during the deposition of the upper WHF and Collingham Formation (Viljoen, 1994, 1998; Visser, 1992). Based on this deduction, the climate conditions during the deposition of the WHF was understood to have changed to drier and windier conditions (Visser, 1992). We propose that considerable amounts of *in situ* precipitated quartz can be considered as an evidence of the vanished (diagenetically cannibalised) felsic tuffs and that the preservation of tuffs was controlled by depositional conditions (e.g., pH, the rate of sedimentation) during the deposition of the lower Ecca strata. Therefore the absence of the lowermost Ecca Group of well-defined tuffaceous beds and its presence in the upper portion is a possible proxy for change in depositional conditions, as it is essentially an indicator of change in paleoclimate conditions. Finally, if *in situ* precipitated/cyst quartz is an extensive, significant and widespread component in the WHF correlative units in southwestern Gondwana (e.g., Irati, Huab formations), our understanding of the Permian depositional conditions, palaeoproductivity, and palaeoclimate in this part of Gondwana can be improved.

5.7. Conclusions

The main concluding points of this study are the following:

1. The distinction between *in situ* and detrital quartz benefitted from BSE- and CL-SEM observations. BSE-SEM images allowed recognition of morphological features, while CL-SEM was based on luminescence and spectral properties.

2. The dominant quartz fraction in the WHF shales was *in situ* precipitated during early diagenesis, and among others, within algal Tasmanites cysts at very shallow depths within the distal part of the WHF.

3. Algal Tasmanites cysts and *in situ* precipitated silica suggest: i) elevated primary production (possible algae blooms), ii) low rate of sedimentation and iii) bacterial sulfate reduction and high pH during deposition.

4. The mobilisation of silica was from in situ, syn-sedimentary altering felsic volcanic ash, which was in part controlled by bacterial sulfate reduction and concomitant reduction of sea water iron oxides and hydroxides, resulting in the formation of pyrite and increased pH; whereas silica precipitation was favored by subsequent bacterial decomposition of OM concomitant with lowered pH.

5. Using the palaeoenvironmental clues of the fossil algal Tasmanites and other geochemical considerations, it is likely that marine condition existed during the deposition of the lower subunits of the WHF.

References

Altaner, S. P., R. F Ylagan, S.M. Savin, J.L. Aronson, H.E. Belkin, and A. Pozzuoli, 2003, Geothermometry, geochronology, and mass transfer associated with hydrothermal alteration of a rhyolitic hyaloclastite from Ponza Island, Italy: Geochimica Et Cosmochimica Acta, 67, 275-288.

Anderson, A.M., and I.R. McLachlan, 1979, The oil-shale potential of the Early Permian White Band Formation in southern Africa, 83-89, *in*, A.M. Anderson and W.J. van Biljon, eds, Some sedimentary basin and associated ore deposits of South Africa: Special Publication of the Geological Society of South Africa, 6, 228p.

Baceta, J.I. and Nunez-Betelu, L., 1994, Basics and Application of Rock-Eval/TOC Pyrolysis: an example from the uppermost Paleocene/lowermost Eocene, *in* The Basque Basin, Western Pyrenees: Department of Geology and Geophysics, The University of Calgary, Ciencias Naturales-Natur Zientziak, 46, 43-62.

Berner R. A., 1980, Early Diagenesis: A Theoretical Approach: Princeton University Press, Princeton, 241p.

Berner, R.A., 1984, Sedimentary pyrite formation: An update: Geochimica et Cosmochimica Acta, 48, 143-149.

Berner, R.A., and Raiswell, R., 1984, C-S method for distinguishing freshwater from marine sedimentary rocks: Geology 12, 365-368.

Blatt, H., 1987, Oxygen isotopes and the origin of quartz: Journal of Sedimentary Petrology, 57, 373-377.

Blatt, H., 1992, Sedimentary Petrology: W.H. Freeman and Co., New York, 514p.

Blatt, H., and D.J. Schultz, 1976, Size distribution of quartz in mudrocks: Sedimentology, 23, 857-866.

Blatt H., G. Middleton, and R. Murray, 1980, Origin of Sedimentary Rocks: Prentice-Hall, Englewood Cliffs, 782p.

Boggs, S., Jr., 2011. Principles of sedimentology and stratigraphy, Fifth Edition: Pearson Prentice Hall, Upper Saddle River, New Jersey, 585p.

Bohacs K.M., Q.R. Passey, M. Rudnicki, W.L. Esch, and O.R. Lazar, 2013, The spectrum of fine-grained reservoirs from ‘shale gas’ to ‘shale oil’/tight liquids: Essential attributes, key controls, practical characterization: International Petroleum Technology Conference,

IPTC 16676, 16p

Bordy, E.M., M. Abrahams, 2016, Geochemistry of the Pronksberg bentonite in the upper Elliot Formation (Early Jurassic), Eastern Cape, South Africa, *in*, Linol B and de Wit M, eds, Origin and Evolution of the Cape Mountains and Karoo Basin: Geo-biohistory in a terrain with shale gas resources and need for conservation, Part of the series Regional Geology Reviews 8643: Springer Verlag, 119-127, doi 10.1007/978-3-319-40859-0-12.

Botz R. and G. Bohrmann G, 1991, Low-temperature opal-CT precipitation in Antarctic deep-sea Sediments-evidence from oxygen isotopes: Earth Planet. Sci. Lett. 107, 612-617.

Bryndzia, L.T., and N.R. Braunsdorf, 2014, From source rock to reservoir: The evolution of self-sourced unconventional resource plays: Elements 14, 271-276.

Burnett, W.C., 1977, Geochemistry and origin of phosphorite deposits from off Peru and Chile: Geological Society of America Bulletin, 88, 813-823.

Burst, J. F., 1957, Post diagenetic clay mineral environmental relationships in the Gulf Coast Eocene: Clays and Clay Minerals, 6, 327-341.

Burst, J.F., 1969, Diagenesis of Gulf Coast clayey sediments, and its possible relation to petroleum migration: AAPG Bulletin, 53, no.1, 73-93.

Burst, J.F., 1976, Argillaceous sediment dewatering: Annual Review of Earth and Planetary Sciences, 4, 93-318, doi:10.1146/annurev.ea.04.50176.001453.

Cerling, T., E. Brown, and J. Bowman, 1985, Low-temperature alteration of volcanic glass: Hydration, Na, K, $^{18}0$ and Ar mobility. Chemical Geology, 52, 281-293.

Christie, A.D.M., 1990, Origin, classification and utilization of oil shales in South Africa: South African Journal of Science, 86, 9-15.

Chukwuma, K., E.M. Bordy, 2016, Spatiotemporal sedimentary facies variations in the Permian Whitehill Formation, main Karoo Basin, *in*, Linol B and de Wit M., eds., Origin and Evolution of the Cape Mountains and Karoo Basin: Geo-biohistory in a terrain with shale gas resources and need for conservation, Part of the series Regional Geology Reviews 8643: Springer Verlag, 101-110, doi 10.1007/978-3-319-40859-0_10.

Clarke, F.W., 1924, The data of geochemistry: U.S. Geological Survey Bulletin, vol., 770.

Cole, D.I. and McLachlan, I.R., 1991, Oil Potential of the Permian Whitehill Shale Formation in the Main Karoo Basin, South Africa, in, H. Ulbrich, and A.C. Rocha Campos, eds, Proceedings and Papers of the Seventh Gondwana Symposium, Sao Paulo: Instituto de

Geosciences, Universidade de Sao Paulo, 379-390.

Compton, J.S., 1991, Origin and diagenesis of clay minerals in the Monterey Formation, Santa Maria Basin Area, California: Clays and Clay Minerals, 39, 449-466.

Curtis, M.E., B.J. Cardott, C.H. Sondergeld, and C.S. Rai, 2012, Development of organic porosity in the Woodford Shale with increasing thermal maturity, International Journal of Coal Geology, 103, 26-31.

Demaison, G.J., and G.T. Moore, 1980, Anoxic environments and oil source bed genesis: Organic Geochemistry, 2, 9-31.

Dixit S., P. Van Cappellen, and A.J. Van Bennekom, 2001, Processes controlling solubility of biogenic silica and pore water build-up of silicic acid in marine sediments: Marine Chemistry, 73, 333-352.

Drits, V. A., Lindgreen, H., Sakharov, B. A., Jakobsen, H. J., Fallick, A. E., Salyn, A. L., Dainyak, L. G., Zviagina, B. B., and Barfod, D. N., 2007, Formation and transformation of mixed-layer minerals by tertiary intrusives in cretaceous mudstones, West Greenland: Clays and Clay Minerals, 55, 260-283.

Dunoyer de Segonzac, G., 1970, The transformation of clay minerals during diagenesis and low-grade metamorphism- a review: Sedimentology, 15, 281-346.

Efremova, G.D., 1990, The Upper Paleozoic Prasinophytes of the Eastern and Southeastern Russian Plate, in Stratigrafiya i paleontologiya Prikaspiiskoi vpadiny (Stratigraphy and Paleontology of the Caspian Sea Depression), Il', *in*, V.D. and T.K. Zamilatskaya, eds, Moscow: VNIGNI, 93-102.

Eisma D. and S.J. van der Gaast, 1971, Determination of opal in marine sediments by X-ray diffraction: Neth. J. Sea Res., 5, 382-389.

Faure, K. and D. Cole, 1999, Geochemical evidence for lacustrine microbial blooms in the vast Permian Main Karoo, Parana, Falkland Islands and Haub basins of southwestern Gondwana, Palaeogeography, Palaeoclimatology, Palaeoecology, 152, 189-213.

Freed, R.L., and D.R. Peacor, 1989, Variability in temperature of the smectite/illite reaction in Golf Coast sediments: Clay Minerals, 24, 171-180.

Geel, C., M. de Wit, P. Booth, H-M Schulz, B. Horsfield, 2015, Palaeo-environment, diagenesis and characteristics of Permian black shales in the lower Karoo Supergroup flanking the Cape Fold Belt near Jansenville, Eastern Cape, South Africa: Implications for the shale

gas potential of the Karoo Basin, South African Journal of Geology, 118, 248–274.

Guy_Ohlson, D. and G.T. Boalch, 1992, Comparative Morphology of the Genus Tasmanites (Pterospermales, Chlorophyta): Phycologia, 31, 523-528.

Hasse, R., 1986, Early diagenetic pore water/sediment interaction: Modern offshore basins: Geoscience Canada, 13, 165-196.

Hemsley, A.R., A.C. Scott, P.J. Barrie, and W.G. Chaloner, 1996, Studies of fossil and modern spore wall biomacromolecules using ^{13}C sold NMR: Annals of Botany, 78, 83-94.

Hinman, N.W., 1990, Chemical factors influencing the rates and sequences of silica phase transitions: effects of organic constituents: Geochimica et Cosmochimica Acta, 54, 563-1574.

Hints, O., T. Kallaste, and T. Kiipli, 1997, Mineralogy and micropalaeontology of the Kinnekulle altered volcanic ash bed (Ordovician) at Pääsküla, North Estonia: Proceedings of the Estonian Academy of Sciences, Geology, 46, 107-118.

Hoek, C., D.G. Mann, and H.M. Jahns, 1995, Algae: An Introduction to Phycology, Cambridge: Cambridge Univ. Press, 640p, ISBN 0-521-30419-9.

Hover, V.C., D.R. Peacor, and L.M. Walter, 1996, STEM/AEM evidence for preservation of burial diagenetic fabrics in Devonian shales: Journal of Sedimentary Research, 66, 519-530.

Hower J., E.Eslinger, M.E. Hower, and E.A. Perry EA, 1976, Mechanism of burial metamorphism of argillaceous sediment-1, Mineralogical and chemical evidence: Geological Society of America Bulletin, 87, 725-737.

Hurd D. C. and S. Birdwhistell, 1983, On producing a more general model for biogenic silica Dissolution: American Journal of Science, 283, 1-28.

Inoue, A., B. Velde, A. Meunier, and G. Touchard, 1988, Mechanism of illite formation during smectite-to-illite conversion in a hydrothermal system: American Mineralogist, 73, 1325-1334.

Inoue, A., B. Lanson, M. Marques Fernandes, B.A. Sakharov, T. Murakami, A. Meunier, and D. Beaufort, 2005, Illite-smectite mixed-layer minerals in the hydrothermal alteration of volcanic rocks-I, One-dimensional XRD structure analysis and characterization of component layers: Clays and Clay Minerals, 53, 423-439.

Isaacs, C. M., 1982, Influence of rock composition on kinetics of silica phase changes in the

Monterey Formation, Santa Barbara area, California: Geology 10, 304-308.

Johnson, M.R., C.J. Van Vuuren, J.N.J. Visser, D.I. Cole, H. DeV. Wickens, A.D.M. Christie, D.L. Roberts, and G. Brandl, 2006, Sedimentary rocks of the Karoo Supergroup, *in* M. R. Johnson, C. R. Anhaeusser and R. J. Thomas, eds., The Geology of South Africa: Geological Society of South Africa and Council for Geoscience, 669p.

Kastner, M., J.B. Keene, and J.M. Gieskes, 1977, Diagenesis of siliceous oozes- chemical controls on the opal-A to opal-CT transformation-an experimental study: Geochimica et Cosmochimica Acta, 41, 1041-1059.

Kensley, B., 1975, Taxonomic status of the pygocephalomorphic crustacea from the Dwyka 'White Band' (Permo-Carboniferous) of South Africa: Annals of the South African Museum, 67, 25-33.

Lazar, O.R., K.M. Bohacs, J.H.S. Macquaker, J. Schieber, and T.M. Demko, 2015, Capturing key attributes of fine-grained sedimentary rocks in outcrops, cores, and thin sections: nomenclature and description guidelines: Journal of Sedimentary Research, 85, 230-246.

López-Gamundí, O.R., and E.A. Rossello, 1998, Basin fill evolution and paleotectonic patterns along the Samfrau geosyncline: the Sauce Grande Basin-Ventana Foldbelt (Argentina) and Karoo Basin-Cape Fold Belt (South Africa) revisited: Geologische Rundschau, 86 (4), 819-834.

López-Gamundí, O., A. Fildani, A. Weislogel, and E. Rossello, 2013, The age of the Tunas formation in the Sauce Grande basin-Ventana foldbelt (Argentina): Implications for the Permian evolution of the southwestern margin of Gondwana: Journal of South American Earth Sciences, 45, 250-258, doi:10.1016/j.jsames.2013.03.011.

Loucks, R.G., R. M. Reed, S.C. Ruppel, and D.M. Jarvie, 2009, Morphology, genesis, and distribution of nanometerscale pores in mudstones of the Mississippian Barnett Shale: Journal of Sedimentary Research, 79, 848-861, doi:10.2110/jsr.2009.092.

Loucks, R.G., R.M. Reed, S.C. Ruppel, and U. Hammes, 2012, Spectrum of pore types and networks in mudrocks and a descriptive classification for matrix-related mudrock pores, AAPG Bulletin, 96, 1071-1098.

Martin, F., 1993, Acritarchs: A Review, Biological Review, Cambridge Philosophical Society, 1993, 68, no. 4, 475-538.

Meyers, W.J., 1977, Chertification of the Mississippian Lake Valley Formation, Sacramento

Mountains, New Mexico: Sedimentology, 24, 75-105.

Milliken, K. L., 1979, The silicified evaporate syndrome-two aspects of silicification of former evaporate nodules from southern Kentucky and northern Tennessee: Journal of Sedimentary Petrology, 49, 245-256.

Milliken, K. L., 1994, Cathodoluminescent textures and the origin of quartz silt in Oligocene mudrocks, South Texas: Journal. Sedimentary Research, A64, 567-571.

Milliken, K.L., M. Rudnicki, D.N. Awwiller, and T. Zhang, 2013, Organic matter-hosted pore system, Marcellus Formation (Devonian), Pennsylvania: AAPG Bulletin, 97, 177-200.

Müller, G., 1967, Diagenesis in argillaceous sediments, in, G. Larsen and G.U. Chilingar, eds, Diagenesis in sediments, Developments in Sedimentology 8: Elsevier, Amsterdam, 127-178.

Nesbitt, H.W., and G.M. Young, 1982, Early Proterozoic climates and plate motions inferred from major element chemistry of lutites: Nature 299, 715-717.

O'Brien, N.R., and R.M. Slatt, 1990, Argillaceous rock atlas: Springer Verlag, New York, 141p.

Oelofsen, B.W., 1987, The biostratigraphy and fossils of the Whitehill and Iratí Shale Formations of the Karoo and Paraná Basins. In: McKenzie, C.D., ed., Gondwana Six: stratigraphy, sedimentology and paleontology, Geophysical Monograph, American Geophysical Union, 41,131-138.

Pagel M, V. Barbin, P. Blanc, and D. Ohnenstetter, 2000, Cathodoluminescence in geosciences: Springer, Berlin, 514p.

Parthenaides, E., 1991, Effect of bed shear stresses on the deposition and strength of deposited cohesive muds, *in*, R. H. Bennett, W. R. Bryant, and M. H. Hulbert, eds, Microstructure of fine-grained sediments: Springer-Verlag, New York, 175-183.

Pedersen, T.F., and S.E. Calvert, 1990, Anoxia versus productivity: what controls the formation of organic carbon rich sediments and sedimentary rocks? AAPG Bulletin, 74, 454-466.

Peter C. van de Kamp, 2008, Smectite-Illite-Muscovite Transformations, Quartz Dissolution, and Silica Release in Shales: Clays and Clay Minerals, 56, 66-81, DOI: 10.1346/CCMN.2008.0560106.

Pickford, M., 1995, Karoo Supergroup palaeontology of Namibia and brief description of a the conodont from Omingonde: Palaeontolology Africana, 32, 51-66.

Potter, P. E., J.B. Maynard, and W.A. Pryor, 1980, Sedimentology of Shale: Springer Verlag, New York, 310p.

Powers, M.C., 1967, Fluid release mechanisms in compacting marine mudrocks and their importance in oil exploration: AAPG Bulletin, 51, 1240-1254.

Pytte, A. M., and Reynolds, R. C., 1989, The thermal transformation f smectite to illite, *in,* N.D. Naeser, and T.H. McCulloh, eds, Thermal history of sedimentary basins: New York, Springer, 133-140.

Rabouille C. and J.F. Gaillard, 1990, The validity of steady state flux calculations in early diagenesis: a computer simulation of deep-sea silica diagenesis: Deep-Sea Res. 37, 625-646.

Ramseyer, K., and J. Mullis, 1990, Factors influencing short-lived blue cathodoluminescence of a-quartz: American Mineralogist, 75, 791-800.

Ramseyer, K., J. Fischer, A. Matter, P. Eberhardt, P., and J. Geiss, 1989, A cathodoluminescence microscope for low intensity luminescence: Journal of Sedimentary Petrology, 59, 619-622.

Reineck, H.E., and I.B. Singh, 1980, Depositional sedimentary environments: Springer Verlag, Berlin, 549p.

Revill, A.T., J.K. Volkman, T. O'Leary, R.E. Summons, C.J. Boreham, M.R. Banks, and K. Denwer, 1994, Hydrocarbon biomarkers, thermal maturity and depositional setting of Tasmanite oil shales from Tasmania, Australia: Geochimica et Cosmochimica Acta, 58, 3803-3822.

Rocha-Campos, A.C., M. Basei, A. Nutman, L. Kleiman, R. Varela, E. Llambia, F. Canile, and C.R. Darosa, 2011, 30 million years of Permian volcanism recorded in the Choiyoi igneous province (W Argentina) and their source for younger ash fall deposits in the Paraná Basin: SHRIMP U–Pb zircon geochronology evidence: Gondwana Research, 9, 509-523, doi:10.1016/j.gr.2010.07.003.

Ruppert, L.F., C.B. Cecil, and R.W. Stanton, 1985, Authigenic quartz in the Upper Freeport coal bed, west-central Pennsylvania: Journal of Sedimentary Petrology, 55, 334-339.

SACS (South African Committee for Stratigraphy), 1980, Stratigraphy of South Africa, Part 1, L.E. Kent, Compiler, Handbook Geological Survey of South Africa, Pretoria, 8, 690p.

Schieber, J., 1998, Sedimentary features indicating erosion, condensation, and hiatuses in the

Chattanooga Shale, Central Tennessee: Relevance for sedimentary and stratigraphic evolution in Schieber, J., Zimmerle, W., & Sethi, P., eds, Shales and Mudstones: Schweizerbart, Stuttgart, 187-215.

Schieber, J., 1996, Early diagenetic silica deposition in algal cysts and spores: A source of sand in black shales?: Journal of Sedimentary Research, 66, 175-183.

Schieber, J, 2011, Iron sulfide formation, in, J. Reitner and V. Thiel, eds, Encyclopedia of Geobiology: Springer-Verlag, 486-502.

Schieber, J., 2013, SEM Observations on ion-milled samples of Devonian Black Shales from Indiana and New York: the petrographic context of multiple pore types, *in* Camp, W., Diaz, E., Wawak, B., eds., Electron Microscopy of Shale Hydrocarbon Reservoirs: AAPG Memoir 102, 153-171.

Schieber, J., and G. Baird, 2001, On the origin and significance of pyrite spheres in Devonian black shales of North America: Journal of Sedimentary Research, 71, 155-166.

Schieber, J., D. Krinsley, and L. Riciputi, 2000, Diagenetic origin of quartz silt in mudstone and implication for silica cycling: Nature, 406, 981-985.

Schimmelmann, A., C.B. Lange, and W.H. Berger, 1990, Climatically controlled marker layers in Santa Barbara basin sediments and fine-scale core-to-core correlation: Limnology and Oceanography, 35, 165-173.

Schink, D. R., N.L. Guinasso, Jr., and K.A. Fanning, 1975, Processes affecting the concentration of silica at the sediment-water interface of the Atlantic Ocean. J. Geophys. Res. 80, 3013-3031.

Schott, J., and E.H. Oelkers, 1995, Dissolution and crystallization of silicate minerals as a function of chemical affinity: Pure an Applied Chemistry, 67, 903-910.

Spalletti, L.A., C.M. Fanning, and C.W. Rapela, 2008, Dating the Triassic continental rift in the southern Andres: The Potrerillos formation, Cuyo basin, Argentina: Geologica Acta, 63, 267-283.

Staplin, F.L., N.J.L. Bailey, S.A.J. Pocock, and C.R. Evans, 1973, Diagenesis and metamorphism of sedimentary organic matter: AAPG Bulletin, 57, 806.

Tappan, H., 1980, The paleobiology of plant protists: W.H. Freeman and Co., San Francisco, 1028p.

Teichert, C., 1974, Marine sedimentary environments and their faunas in Gondwana area: AAPG

Memoir 23, 43-145.

Telnova, O.P., 2012, Morphology and ultrastructure of Devonian prasinophycean algae (Chlorophyta): Paleontological Journal, 46, 543-548.

Totten, M.W., and H. Blatt, 1993, Alterations in the non-clay mineral fraction of politic rocks across diagenetic to low-grade metamorphic transition, Ouachita Mountains, Oklahoma and Arkansas: Journal Sedimentary Petrology, 63, 899-908.

Van Cappellen, P., S. Dixit, and J. van Beusekom, 2002, Biogenic silica dissolution in the oceans: Reconciling experimental and field-based dissolution rates: Global Biogeochemical Cycles, 16, 1075, doi:10.1029/2001GB001431.

Veevers, J.J., D.I. Cole, and E.J. Cowan, 1994, Southern Africa: Karoo Basin and Cape Fold Belt, *in*, J.J. Veevers, and C. McA Powell, eds, Permian–Triassic Pangean Basins and Foldbelts along the Panthalassan Margin of Gondwanaland: Memoir of the Geological Society of America, 184, 223-278.

Viljoen, J.H.A, 1994, Sedimentology of the Collingham Formation, Karoo Supergroup: South African Journal of Geology, 97, 167-183.

Viljoen, J.H.A, 1998, Distribution of altered volcanic ash beds in the Dwyka and Ecca Groups of the main Karoo Basin, South Africa: Journal of African Earth Sciences Special Abstract Issue, Gondwana 10, Event Stratigraphy of Gondwana 27, 204-205.

Visser, J.N.J., 1992, Sea-level changes in a back-arc-foreland transition: the late Carboniferous-Permian Karoo Basin of South Africa: Sedimentary Geology, 83, 115-131.

Visser, J.N.J., and G.M. Young, 1990, Major element geochemistry and paleoclimatology of the Permo-Carboniferous glacigene Dwyka Formation and post-glacial mudrocks in southern Africa: Palaeogeography, Palaeoclimatology, Palaeoecology 81, 49-57.

Weaver, C. E., 1957, The clay petrology of sediments: Clays and Clay Minerals, 6, 154-187.

Wollast, R., and F.T. Mackenzie, 1983, The global cycle of silica, in, S.R. Aston, ed., Silicon geochemistry and biogeochemistry: Academic Press, 39-76.

Zinkernagel, U., 1978, Cathodoluminescence of quartz and its application to sandstone petrology: Contribution to Sedimentology, 8, 69p.

Chapter 6

Synthesis and recommendations for further study

This chapter provides a summary of the main findings of this study and shows how the understanding of the WHF in the main Karoo Basin has been advanced, with regards to the fundamental controls on the spatiotemporal variations in its stratigraphy and geochemistry. Finally, the remaining research challenges and possible future research questions are also presented.

6.1. Synthesis

The Lower Permian WHF exposed in the southwestern half of the main Karoo Basin in South Africa is a historic rock unit. The white-weathering black shale unit, which also occurs in the subsurface to depths of over 4000 m, is organic matter-rich, locally self-igniting and had been mined in small-scale operations in the pre-1940. During the energy crisis of the 1950s, the formation was also explored for shale oil, but the project was hampered, among other factors, by significant heterogeneities in its stratigraphy and uneven distribution of its organic carbon content. The recent global proliferation of unconventional hydrocarbon resources originating in organic matter-rich shale successions has resulted in a renewed interest in the WHF, which is seriously being considered for gas shale exploitation in South Africa. Consequently, this research was primarily motivated by the need to enhance our understanding of this heterogeneous rock unit, particularly of the depositional controls on the spatiotemporal variations in its stratigraphy and geochemical composition. In order to address this problem, four basic objectives were identified for this research, each of which is presented as a separate chapter of this dissertation, including: (1) to what extent does the WHF differ in terms of texture, bedding, and composition? Are these differences in rock attributes visible in the field, hand-specimen, optical microscope, and scanning electron microscope? Are these variations in stratigraphy genetically related, controlled by one process, or are they disconnected? (2) Why are some intervals particularly enriched in organic carbon relative to others? What physical and chemical processes/conditions controlled the

preservation of organic carbon? (3) What has changed in the organic matter and other rock components since deposition and what factors controlled these changes? (4) What environmental conditions existed in the basin during the formation of this rock unit and what role did they play in the distribution of organic matter?

To be able to answer these questions, a multidisciplinary approach that included a combined analyses of 37 major borehole logs, field observations, hand-specimen and thin section observations obtained at nanometer to decimeter scales using optical and electron optical microscopy as well as multiple whole rock geochemical methods on over 600 outcrop core samples. The integrated data collectively provided for the detailed assessment of key attributes and the heterogeneities in the WHF, and ultimately resulted in the recognition of five distinct but genetically-related sedimentary facies within the formation. These facies can be distinguished from one and another on the basis of different textural properties (e.g., fine to coarse-grained), bedding style (laminated, graded beds, starved ripples, intraclast-rich, bioturbated), composition (organic matter-, clay mineral-, silica-, carbonate-rich), and grain origin (clastic, bioclastic, diagenetic, authigenic). These five facies are: F1, a black pyrite-, chert-, nanoplankton-bearing, carbonaceous laminated fine shale in the lowermost WHF; F2, a black-dark grey, clay-, siliceous-nanoplankton-bearing, carbonaceous fine-medium laminated shale; F3, a dark-light grey calcareous intraclast-rich, well-bedded medium shale; F4, a medium-light grey siliceous-calcareous silty, occasionally bioturbated, well-bedded medium-coarse shale; and F5, a light grey siliceous, sandy, massive-bedded coarse shale in the uppermost WHF. The F1-F2 contact is gradational and marked by an increase in thickness of laminae, whereas the F2-F3 contact is marked by marcasite-cemented lags and nodules of both marcasite and carbonates (majorly dolomite). In the southern part of the basin, up to latitude 32°12’ S, the WHF is comprised only F1-F3, however, north of this latitude, F4 and F5 is increasingly more common. The F3-F4 contact is marked by thin (<2 cm) calcitic/dolomitic lags, and in places, by an erosional surface. The F4-F5 contact is transitional and sometimes marked by a change from thickly laminated/bedded F4 to massive-looking F5.

The five primary lithofacies show specific and systematic variations in nature and content of organic carbon, stable isotopic compositions (of $\delta^{13}C_{org}$ and $\delta^{15}N$), C/N ratios, major and trace

elements, nature and contents of iron sulfides and quartz grains, and CIA values. The lower black to dark grey pyritic, carbonaceous thinly laminated fine shales (F1 and F2) contain up to 16.5 % TOC, $\delta^{13}C_{org}$ of -15.57‰, $\delta^{15}N$ of 12.49‰, C/N ratio of 1.50, average CIA of 68.11, Rb/K ($x10^{-3}$) and Sr/Ba ratios of 6.56 and 0.67, respectively. Relative to average shale, this unit is up to 6.27 and 3.11 times richer in Mo and Fe, respectively. The organic macerals here comprise Tasmanites cysts and colonial algae cells in lamalginites and disseminations with amorphous macerals. At least 25% of the quartz grains are of early diagenetic origin, possibly derived from alteration of air-fall volcanic ash. Iron sulfides occur dominantly in form of framboidal aggregates of pyrite and marcasite-cemented lags and nodules. A binary mixture of OM and phosphorites with botryoidal textures is also documented. The upper medium to light grey calcareous-siliceous silty lenticular shale (F3-F5) contains up to 2.04% TOC, $\delta^{13}C_{org}$ of -24.71‰, $\delta^{15}N$ of 4.93‰, C/N ratio of 17.62, average CIA of 74.33, Rb/K ($x10^{-3}$) and Sr/Ba ratios of 3.83 and 0.36, respectively. Relative to average shale, this unit is up to 2.65 and 0.43 times richer in Mo and Fe, respectively. The organic macerals here comprise disarticulated plant remains and few amorphous maceral that are disseminated within the shale matrix. At least 85% of the quartz grains are of detrital origin likely derived from the basin margins and transported to the depository by the action of bottom currents. Iron sulfides occur dominantly in form of octa- and euhedral pyrite grains.

The observed facies variability indicates significant differences in the provenance of the components that make up the WHF. The lower two facies (F1 and F2) are dominated by sediments produced largely within the basin. The organic detritus was derived from biological production within the water column. The middle facies (F3) is dominated lithic grains derived from reworking of previously deposited sediments outside and inside the basin, while the upper facies (F4 and F5) is largely composed of siliciclastic and organic detritus derived from the surrounding hinterland. Apart marked differences in provenance, the processes that operated to deliver and disperse sediments as well as water-column energy levels among the facies were also diverse. The presence of laminations and organo-minerallic aggregates in the lower facies indicate sediment delivery to the seafloor by grain aggregation and continuous hemipelagic settling out of buoyant plumes whereas the presence of starved ripples, triplet fabrics, normally and inversely graded beds and sharp bases in the upper shales suggest discontinuous sediment delivery by repeated density flows on a reworked basin floor. The five facies also exhibit marked differences important geochemical

proxies, such as the degree of enrichment in major and trace elements relative to an average shale, redox ratios, and C-S relationships. The redox proxies in conjunction with an abundance of framboidal pyrites, apatite-rich phosphorites with botryoidal textures, and *in situ* precipitated quartz grains suggest that the deposition of F1 and F2 in the lower WHF was under predominantly anoxic conditions where the surficial sediments underwent microbially mediated processes. In contrast, the absence of these features and the presence of occasional bioturbation and various trace and body fossils in the upper subunits (F3 to F5), suggest an oxic basin floor and colonisation of the sediments and water by complex organisms (both invertebrates and vertebrates), and by extension, dysoxic/oxic pore waters.

Notable variability was also documented in the distribution of felsic tuffaceous sediment layers within the facies. Well-defined volcaniclastic layers, with laminations up to 5 cm thick, are documented in the upper subunits but are completely absent in the lower subunits. This study argues that the distribution of the volcanogenic constituent in the WHF was controlled by changes in depositional conditions. During the deposition of the lower subunits, bacterial-mediated sulfate reduction and concomitant reduction of sea-water iron oxides and hydroxides resulted in the formation of pyrite and increased pH. An interplay of these conditions resulted in cannibalization of the felsic tuffs and their subsequent reprecipitation in form of *in situ* quartz during the diagenesis of F1 and F2. This further demonstrates the complexity of the syn- and post-depositional processes that resulted in the heterogeneities observed in the WHF.

Although all samples from the same stratigraphic units are similar in overall sedimentological attributes, depending on their distance from the Cape Fold Belt (CFB), significant variations exit in their levels of thermal maturity and porosity (pore size and pore geometry). Particularly for samples with TOC of >2.03%, a sharp decrease in porosity was documented for thermal maturity values greater that are >2.58% Ro in the southwestern side of the basin up to Matjiefontein locality. This spatial variation in thermal maturity and porosity confirms earlier studies, which suggested that samples localities within about latitude 29 °S and more southerly were within late dry gas window (overmature; %Ro > 2.3) whereas those within latitude 31.5 °S and more northerly were within oil to the wet gas window (%Ro< 2.3).

Using the high-resolution data obtained in this study, the reconstruction of the environmental conditions prevalent during the deposition of the WHF can be refined. During the deposition of the lower subunits (F1 and F2), sea-level highstand, high biological productivity, low terrigenous input, and anoxic seafloor collectively contributed to the preservation of organic carbon. The presence of marine microfossils (e.g., Tasmanites cysts and colonial algae cells) and phosphorites closely associated with OM indicate marine conditions. The $\delta^{13}C_{org}$ values increase with increasing organic matter content and indicate that the deposition of these subunits coincided with a climatic warm-up, and thus F1 and F2 are similar to deposits that form during oceanic anoxic events. A combination of these factors resulted in sea-level highstand coeval with the less-restricted oceanic connection. Accumulation of subunits F3-F5 occurred after cessation of deep-water flow and upwelling. Stable isotopes compositions and Rock-eval data indicate that the greater part of the OM in F3 was sourced from terrestrial plants. The presence of intraclasts, starved ripples, triplet fabrics, normally graded beds, and sharp bases, in the upper subunits indicate deposition above the storm-wave base and in a relatively shallow water that possibly had restricted oceanic connection (i.e., was an inland lake).

It may be concluded from this work that the spatial and temporal variations in the geometry and geochemical composition of the WHF are systematic and controlled by the complex interplay several factors, including changes in the bioproductivity in the water column and at the sediment-water interface, bottom-water conditions (energy and oxygen concentration), burial and sediment accumulation rates, and early diagenetic overprints. These factors were, in turn, and as expected, broadly influenced by changes in climate, sea-level, and basin tectonics.

6.2. Recommendations for future studies

This study quantitatively and systematically documents the heterogeneity in the WHF and relates facies variability to changes in primary production, clastic dilution and bottom water anoxia. In order to clearly decipher the high-resolution stratigraphy of the WHF, particularly the duration of the deposition, the nature and rate of climate change, and the time relationship between the depositions of the lower and upper successions, absolute dating of the formation is recommended. This will, among others, not only facilitate the emergence of a higher resolution sequence of the

sedimentologic events that controlled the accumulation of the sediments but also allow the more detailed correlation of the unit across SW Gondwana to better understand and separate local from regional controlling factors. To date, no absolute date exit for this important rock unit in South Africa. The present age of the formation, Late Kungurian to Early Ufimian is based on palynology (Visser, 1992) and absolute dates from its correlative in Namibia (280.5 ± 2.1 Ma; Werner, 2006) and in Brazil (278.4 ±2.2 Ma; Santos et al., 2006).

This study has demonstrated that during the deposition of the WHF a dramatic change from marine to non-marine conditions occurred in the main Karoo Basin marked. To fully appreciate the development of the Karoo Basin during this critical change that among others impacted on the evolution of organisms in the region obtaining several absolute dates from the unit is crucial, especially for regional biogeographical studies.

Furthermore, this study has demonstrated, using textural and morphological features observed in images captured with back-scatter and cathodoluminescence detectors of scanning electron microscope that the significant amounts of the quartz in the lower subunits of the WHF are of early diagenetic origin. In order to gain further insights into the chemical conditions and the precise mechanisms that dictated their production additional studies, particularly the analysis of stable isotopes (Sr, O), is recommended.

References

Ghadeer, S.G., and J.H.S. Macquaker, 2012, The role of event beds in the preservation of organic carbon in fine-grained sediments: analyses of the sedimentological processes operating during deposition of the Whitby Mudstone Formation (Toarcian, Lower Jurassic) preserved in northeast England: Marine and Petroleum Geology, 35, 309-320.

McKay, M.P., A.L. Weislogel, A. Fildani, R.L. Brunt, D.M. Hodgson, and S.S. Flint, 2015, U-PB zircon tuff geochronology from the Karoo Basin, South Africa: implications of zircon recycling on stratigraphic age controls, International Geology Review, 57:4, 393-410, doi:10.1080/00206814.2015.1008592.

Sing, K. S. W., D. H. Everett, R. A. W. Haul., L. Moscou, R. A. Pierotti, J. Rouquerol, and T. Siemieniewska, 1985, Reporting physisorption data for gas/solid systems with special reference to the determination of surface area and porosity: Pure and Applied Chemistry, 57, 603-619.

Santos, R.V., P.A. Souza, C.J. de Alvarenga, E.L. Dantas, M.M. Pimentel, C. Gouveia de Oliverira, L. Medeiros de Araújo, 2006,Shrimp U-Pb zicon dating and palynology of bentonitic layers from the Permian Irati Formation, Paranà Basin, Brazil: Gondwana Research, 9, 456-463.

Visser, J.N.J., 1990, The age of the late Palaeozoic glacigene deposits in southern Africa: South Africa Journal of Geology, 93, 366-375.

Visser, J.N.J., 1992. Deposition of the Early to Late Permian Whitehill Formation during a sea-level highstand in a juvenile foreland basin. South African Journal of Geology, 95, 181-193.

Werner, M., 2006, The stratigraphy, sedimentology, and age of the Late Paleozoic Mesosaurus Inland Sea, SW-Gondwana: new implications from studies on sediments and altered pyroclastics layers of the Dwyka and Ecca Group (lower Karoo Supergroup) in southern Namibia: unpublished PhD thesis, University of Würzburg, Germany, 428p.

Appendices

Appdx 3.1. Extensive borehole data sets used to constrain the depths and boundaries between the Karoo stratigraphic units, top and base as well as stratigraphic descriptions and geometry of the WHF across the main Karoo Basin. Measured depths are converted from Cape feet to meters. These data include deep SOEKOR boreholes (Rowsell and De Swardt, 1976), Council for Geoscience, CGS, and industry boreholes (Cole and McLachlan, 1994) in the northeastern part of the basin and were supplied by CGS.

Borehole Name	Farm Name	Latitude dms (S)	Longitude dms (E)	Elevation (m)	Year Drilled	Borehole Owner	WHF Top (m)	WHF Base (m)	WHF Thickness (m)	Dolerite Thickness (m)	Borehole Total Depth (m)	Lithologic description
KL1/65	Klipdrift 156	32 37 00	20 27 15	729	1965	Soekor	1359	1391	32	None	3460	Layer III: (1359-1368 m) dark grey laminated to beded shales.
												Layer II: (1368- 1375 m) dark grey to slightly lbalck laminated to bedded shales.
												Layer I: (1359-1391 m) thinly laminated black shales.
OL1/69	Olyvenbosch	32 00 00	19 51 38	550	1969	Soekor						Obscured by dolerite
SA1/66	Hamel Kraal 16	32 40 10	21 19 45	738	1966	Soekor/Geo Sur.	2754	2789	35	None	4170	Layer II: (2105- 2083): dark grey laminated to bedded shale with silty uppermost part.
												Layer I: (2789-2768 m) dark grey to black laminated shales. Pyritie lenses and nodules observed.
QU1/65	Quagga's Fontein 357	31 49 35	21 26 20	1261	1965	Soekor	1653	1682	47	52	2530	Layer II: (1635- 1682): dark grey laminated to bedded shale with the uppermost part impacted by dolerite.
												Layer I: dark grey laminated dark grey to black laminated pyritic shales. Pyritie lenses and nodules observed.
AB1/65	Abrahams Skraal 206	31 48 05	22 37 05	1415	1965	Soekor	1881	1913	21	11	2282	Layer III: (1897-1881m) dark grey laminated to beded shales.
												Layer II: (1909-1897m) dark grey to slightly black laminated to bedded shales with carbonates beds.
												Layer I: (1916-1909 m) thinly laminated black shales with pyrite and carbonates lenses and chert at the base.
KW1/67	Spreeuw Fontein 26	32 59 03	22 20 12	969	1966	Soekor	4361	4404	44	None	5555	Layer III: (4373-4306m) silty light to dark grey shales with graphitic intervals.
												Layer II: (4373-4390 m) dark grey to slightly black bedded-laminated to bedded moderately indurated shales with more carbonates beds/concretions and few pyrite lenses.
												Layer I: (4404-4390 m) thinly laminated indurated dark grey to black shales with pyrite and carbonates lenses.
KA1/66	Karree Bosch 63	32 00 48	23 25 35	1006	1966	Soekor	2083	2126	43	None	2600	Layer II: (2105- 2083 m): dark grey laminated to bedded shale with silty uppermost part.
												Layer I: (2126-2105 m) dark grey to black laminated shales with pyritie lenses and nodules.
CR1/68	Drooge Rivier 34 (Cranemere)	32 29 07	25 00 33	793	1968	Soekor	3671	3716	44	None	4658	Layer II: (2682-2670 m) dark grey to slightly black laminated to bedded moderately indurated shales with carbonates beds and few pyrites. Upper portion consists of silty greyish silty shales.
												Layer I: (3716-2682 m) thinly laminated black shales with pyrite.
SC3/67	Schiet Fontein 209	32 46 25	24 18 00	791	1967	Soekor	3972	4042	44	None	5560	Layer III: (3992-3972 m) silty light to dark grey shaes with cherty intervals.
												Layer II: (4020-3992 m) dark grey to slightly black bedded-laminated to bedded moderately indurated shales with carbonates beds/concretions and few pyrite lenses.
												Layer I: (4042-4020 m) thinly laminated indurated dark grey to black shales with pyrite and carbonates lenses.

Appdx 3.1 continued

VR1/66 (VREDE)	De Vrede 286	32 15 30	24 15 00	870	1966	Soekor	2655	2719	40	None	3948	Layer II: (2683- 2655 m): dark grey laminated to bedded shale with TOC of 0.34 wt% and C1-C5 of 5650 microlitres/kg. Layer I: (2719-2683 m) Dark grey to black laminated shales. Pyritie lenses and nodules observed. TOC contents of 3.77 wt.% and total C1-C5 of 2830 microlitres/kg.
SP1/69	Spring Fontein 853	33 00 15	27 45 48	244	1969	Soekor	3668	3705	37	None	4557	Layer III: (3678-3668 m) silty light to dark grey shaes with silty intervals towards the uppermost portion. Layer II: (3694-3678 m) dark grey to slightly black bedded-laminated to bedded moderately less-indurated shales with carbonates beds/concretions and few pyrite lenses. Layer I: (3705-3694 m) thinly laminated indurated dark grey to black shales with pyrite and carbonates lenses?
WE1/66	Weltevreden 117	30 53 52	26 50 25	1532	1966	Soekor	3491	3520	30	129	3746	Layer III: (3494 m-dolerite?) silty light to dark grey dolerite-impacted shaes with silty intervals towards the uppermost portion that appear baked Layer II: (3507-3494 m) dark grey to slightly black bedded-laminated to bedded moderately less-indurated shales with carbonates beds/concretions and few pyrite lenses. Layer I: (3507-3521 m) thinly laminated indurated dark grey to black shales with pyrite.
EP1/78	Elans Berg 164	29 52 08	23 48 02	1189	1978	CGS	NR	58	6	52	100.45	Layer II: (51.1- 47.88 m): dark grey laminated to bedded grey shale interbedded with whitish carbonates with concretions and is underlain by dolerite. Layer I: (58.10-54.7 m) dark grey to black laminated shales.
DP1/78	Swinks Pan 170	29 24 06	24 26 09	1250	1978	CGS	76.84	90	13	None	112.01	Layer III: (80-76.84 m) bedded silty shales with buff layers. Layer II: (85-80 m) dark grey bedded-laminated moderately indurated shales interbedded in the upper section with grey calcareous beds/laminae Layer I: (89.53-85 m) dark grey to black bedded shales with no obvious pyrite
KL1/78	Klein Kareelaagte 168	29 22 44	24 27 04	1250	1978	CGS	66.99	93	11	15	139.60	Layer II: (72- 66 m): dark grey laminated to bedded grey shale interbedded with whitish carbonates and underlain by dolerite. Layer I: (92.15-87.33 m) dark grey to black laminated shales. Pyrite and carbonates lenses and nodules observed.
VP1/78	Boshof Townsland 432	28 29 50	25 12 43	1220	1978	CGS	48.39	67	18	None	107.15	Layer III: (55-48.39 m) bedded silty shales with larger clasts/particles. Layer II: (64.2-55 m) dark grey bedded-laminated moderately indurated shales interbedded in the upper section with grey calcareous beds. Layer I: (66.59-64.2 m) dark grey to black bedded shales with no obvious pyrite.
HM1/78	Hermon 8	28 21 47	25 19 24	1241	1978	CGS	31.95	43	11	None	110.78	Layer III: (34.5 31.95 m) silty light to dark grey interbeded with light grey rip-up clasts, predominatly carbonates. Layer II: (36.5-34.5 m) dark grey to slightly black bedded-laminated shales with carbonates beds/concretions. Grading observed. Layer I: (43.12-36.5 m) thinly laminated indurated dark grey to black shales that grades into the Prince Albert Formation.
GP1/78	Wilhelmsshohe 693	28 03 20	25 34 40	1271	1978	CGS	14.7	15	0	None	87.25	Dark grey to black shales.

Appendices

Appdx 3.1 continued

R988/1	NA	NA	NA	NA	NA	CGS	24	37	13	None	106.15	Layer III: (29.5-24 m) bedded silty grey shales with larger clasts/particles. Layer II: (29.5-36 m) dark grey bedded-laminated moderately indurated shales intercalated with softer laminae and carboantes. Layer I: (36-37.5 m) thinly laminated indurated dark grey to black shales with pyrite.
G39856	Kopoas Fontein 698	31 29 10	19 54 10	1056	1997	DWAF	392	439	47	14	755	The WHF is over- and underlain by dolerite which made it challenging to recognise individual intervals. Pyrite-rich finely bedded shales. The basal contact with the dolerite appeared baked and graphitic. The middle layer is bedded-laminated black to dark grey shales intercalated with pyrite lens and thin bed. The top layer is dark grey to grey bedded dolerite-impacted shales intercalated with grey dolomite and thin tuff beds.
G39974	Kopoas Fontein 698	31 29 25	19 53 52	1044	1997	DWAF	349	411	62	15	1016	The WHF is over- and underlain by dolerite which made it challenging to recognise individual intervals. Limited lithologic description in original borehole log.
D731/1	Die Vlakte 731	28 34 10	25 22 30	1242	1978	IDC	113.50	125	11	None	184.50	Layer III: (115-113.5 m) bedded silty grey shales with whitish rip-up clasts. Layer II: (118-115 m) dark grey bedded-laminated moderately indurated shales with few pyrite and interbedded in the upper section with grey calcareous beds/laminae. Layer I: (124.57-118 m) dark grey to black bedded shales with no obvious pyrite.
HG1/84	Hans gat	30 47 45	20 17 29	976	1984	Anglo-American	230.24	318	33	55	671	Layer II: (253.3- 230.5 m): bleached? to baked dark grey laminated to bedded shale in the lower section and pyrite and pyrrholite aligned along bedding planes and in thin masssive bands. Layer I: (318.5-253.3 m) dark grey to black laminated shale with pyrite and pyrrholite both as disseminated and in thin massive bands. Haircracks filled with carbonate observed.
AXT1	Annex Steeldam	30 36 45	22 36 35	1240	1985	Anglo-American	259.26	270	10	2	319.80	Layer II: (264.5- 259.5 m): laminated to bedded to massive grey to dark grey silty shales. Layer I: (269.8-264.5 m) dark grey to black laminated shale with pyrite as disseminated and in thin lenses and concretions. Tuff-like thin bed present.
BKP1	Bookport 8	30 40 40	22 48 16	1250	1984	Anglo-American	356	388	12	20	406.50	Layer III: (359.2-356.1 m) bedded silty grey shales with small-scale grading and two upward-coarsening units. Layer II: (384.3-381.8 m) dark grey bedded dolerite-impacted shales with intercalated silty intervals. Layer I: (387.8-384.3 m) dark grey to black bedded shales with pyrite aligned to laminae surfaces.
HLP1	Holpan 69	30 27 58	23 11 15	1095	1984	Anglo-American	87.8	137	18	31	313.50	Layer III: (87.8-93.5 m) bedded silty grey shales with small-scale grading. *Mesosaurus* rib observed. Layer II: (132.5-123 m) dark grey bedded dolerite-impacted graphitic shales with intercalated silty intervals. Layer I: (136.5-132.5 m) dark grey to black bedded graphitic shales that grades into the overlying dolerite sill.
HGK1	Hondeblaf 46	30 16 12	23 43 35	1112	1985	Anglo-American	107.9	134	7	19	269.50	Layer II: (110- 107.9 m): grey to black bedded silty shales. Layer I: (133.8-123 m) with a dolerite sill of about 4.8 m, consists of dark grey to black bedded shale with silty upper section.
VB122	Claremont 695	28 01 17	25 31 48	1301	1985	Anglo-American	86.5	93	7	None	162.62	Layer I: (93.49-86.5 m) grey to blak silty carbonaceous and miccaceous shale.

Appdx 3.2. Summary of rock-eval/TOC pyrolysis data of the Whitehill Formation from the studies of Cole and McLachlan (1994).

R988/1	Depth (m)	Tmax (°C)	S1	S2	S3	TOC	HI	OI	PI
	24.40	436	2.92	20.27	0.62	9.00	225.22	6.89	0.13
	24.90	420	2.40	9.57	0.73	7.80	122.69	9.36	0.20
	25.40	437	2.56	15.34	0.66	5.71	268.65	11.56	0.14
	25.90	434	1.43	7.39	0.61	3.49	211.75	17.48	0.16
	26.40	440	2.02	9.62	0.71	5.46	176.19	13.00	0.17
	26.90	437	1.90	10.65	0.64	4.67	228.05	13.70	0.15
	27.40	429	2.29	10.33	0.71	3.77	274.01	18.83	0.18
	27.90	428	2.18	7.34	0.53	3.24	226.54	16.36	0.23
	29.90	416	1.47	0.99	0.64	5.39	18.37	11.87	0.60
	30.40	432	0.39	0.54	0.91	3.16	17.09	28.80	0.42
	30.90	445	0.69	1.41	0.16	3.01	46.84	5.32	0.33
	31.40	450	0.29	0.70	0.30	2.58	27.13	11.63	0.29
	31.90	447	0.40	1.01	0.27	3.01	33.55	8.97	0.28
	32.40	448	0.45	1.19	0.27	3.06	38.89	8.82	0.27
	32.90	447	0.42	1.12	26.00	3.12	35.90	833.33	0.27
	33.40	429	0.58	0.62	0.28	2.78	22.30	10.07	0.48
	33.90	452	0.51	0.81	0.22	2.78	29.14	7.91	0.39

HM1	Depth	Tmax	S1	S2	S3	TOC	HI	OI	PI
	32.31	441	3.33	32.05	0.63	9.08	352.97	6.94	0.09
	33.10	443	2.33	24.71	0.53	6.17	400.49	8.59	0.09
	33.79	436	1.17	12.41	0.34	4.24	292.69	8.02	0.09
	34.35	433	2.51	20.71	0.57	5.33	388.56	10.69	0.11
	34.90	406	1.61	8.52	1.21	8.16	104.41	14.83	0.16
	32.52	419	1.66	8.53	0.54	4.13	206.54	13.08	0.16
	36.22	416	1.63	5.45	0.76	4.18	130.38	18.18	0.23
	36.70	415	0.77	1.49	0.54	3.07	48.53	17.59	0.34
	37.20	416	1.29	3.92	0.77	1.03	380.58	74.76	0.25
	37.68	415	1.05	2.50	0.38	4.98	50.20	7.63	0.30
	38.20	425	1.34	5.74	0.77	3.16	181.65	24.37	0.19
	38.70	421	1.01	3.33	0.72	3.03	109.90	23.76	0.23
	39.20	416	0.93	2.64	0.72	3.04	86.84	23.68	0.26
	39.80	431	0.62	2.01	0.80	4.97	40.44	16.10	0.24
	40.30	415	0.55	1.65	0.70	2.77	59.57	25.27	0.25
	40.80	416	1.20	3.41	0.88	3.38	100.89	26.04	0.26
	41.30	419	1.87	6.07	0.99	4.14	146.62	23.91	0.24
	41.68	242	1.65	4.69	1.00	3.87	121.19	25.84	0.26
	42.40	432	1.54	4.16	0.53	3.56	116.85	14.89	0.27
	43.07	437	1.94	8.01	0.59	7.70	104.03	7.66	0.19

Appdx 3.2 continued

VP1	Depth	Tmax	S1	S2	S3	TOC	HI	OI	PI
	48.74	433	3.17	4.45	0.77	7.51	59.25	10.25	0.42
	49.30	447	4.17	10.53	0.81	7.49	140.59	10.81	0.28
	49.89	443	2.85	3.57	0.67	5.66	63.07	11.84	0.44
	50.55	433	1.86	5.10	0.62	5.09	100.20	12.18	0.27
	51.20	439	2.50	4.33	0.70	5.22	82.95	13.41	0.37
	51.80	441	2.51	6.65	0.56	4.16	159.86	13.46	0.27
	52.40	436	2.14	5.20	0.55	3.94	131.98	13.96	0.29
	52.98	433	2.28	5.84	0.57	3.82	152.88	14.92	0.28
	53.60	427	1.72	2.21	0.56	3.65	60.55	15.34	0.44
	54.25	413	2.28	1.89	0.59	4.40	42.95	13.41	0.55
	54.85	427	2.19	2.52	0.65	3.95	63.80	16.46	0.46
	55.48	418	3.27	2.13	0.54	3.78	56.35	14.29	0.61
	56.60	438	7.73	15.17	0.64	10.14	149.61	6.31	0.34
	57.10	442	4.44	12.55	0.74	5.98	209.87	12.37	0.26
	57.60	437	2.31	3.72	0.77	4.57	81.40	16.85	0.38
	58.10	437	2.52	5.75	0.65	4.05	141.98	16.05	0.30
	58.60	429	2.81	3.35	0.55	3.84	87.24	14.32	0.46
	59.02	417	2.79	2.69	0.51	5.08	52.95	10.04	0.51
	59.50	447	1.43	4.51	0.27	3.44	131.10	7.85	0.24
	62.00	428	0.90	0.92	0.47	3.25	28.31	14.46	0.49
	63.00	428	1.49	2.71	0.48	3.23	83.90	14.86	0.35
	64.00	429	1.46	2.82	0.48	3.26	86.50	14.72	0.34
	65.50	438	1.79	4.78	0.64	4.96	96.37	12.90	0.27
	66.07	433	2.56	6.22	0.77	5.02	123.90	15.34	0.29
	66.56	423	1.23	2.04	0.96	7.70	26.49	12.47	0.38

DP1	Depth	Tmax	S1	S2	S3	TOC	HI	OI	PI
	77.35	440	2.76	62.95	1.01	14.73	427.36	6.86	0.04
	78.15	430	1.93	44.05	0.42	7.15	616.08	5.87	0.04
	78.60	439	3.03	44.22	0.39	7.18	615.88	5.43	0.06
	79.19	438	2.76	35.33	0.35	6.36	555.50	5.50	0.07
	80.50	429	2.62	29.07	0.44	3.96	734.09	11.11	0.08
	81.70	409	1.18	3.78	0.42	2.21	171.04	19.00	0.24
	82.49	430	1.78	46.06	0.26	8.24	558.98	3.16	0.04
	83.05	413	1.61	6.07	0.31	3.00	202.33	10.33	0.21
	84.20	435	2.66	17.25	0.31	3.42	504.39	9.06	0.13
	85.30	425	2.00	8.69	0.31	4.24	204.95	7.31	0.19
	86.35	429	3.32	10.84	0.39	4.45	243.60	8.76	0.23
	87.40	427	2.32	8.98	0.40	2.75	326.55	14.55	0.21
	88.40	424	2.35	7.15	0.33	2.74	260.95	12.04	0.25
	89.53	400	0.39	0.96	0.48	3.20	30.00	15.00	0.29

Appdx 3.2 continued

KL1	Depth	Tmax	S1	S2	S3	TOC	HI	OI	PI
	67.47	444	0.24	0.09	0.29	4.60	1.96	6.30	0.73
	68.00	486	0.12	0.14	0.16	3.15	4.44	5.08	0.46
	68.50	517	0.07	0.06	0.19	2.35	2.55	8.09	0.54
	69.00	515	0.09	0.16	0.27	3.00	5.33	9.00	0.36
	69.50	502	0.09	0.12	0.22	2.23	5.38	9.87	0.43
	70.10	489	0.06	0.04	0.23	1.98	2.02	11.62	0.60
	70.59	497	0.03	0.01	0.39	1.36	0.74	28.68	0.75
	88.35	487	0.08	0.11	0.16	1.17	9.40	13.68	0.42
	88.85	488	0.08	0.06	0.16	1.50	4.00	10.67	0.57
	89.35	491	0.13	0.10	0.07	1.66	6.02	4.22	0.57
	91.35	487	0.11	0.09	0.16	2.05	4.39	7.80	0.55
	92.40	463	0.47	0.19	0.22	4.36	4.36	5.05	0.71
	92.90	301	0.18	0.09	0.07	1.39	6.47	5.04	0.67
KL1/65	**Depth**	**Tmax**	**S1**	**S2**	**S3**	**TOC**	**HI**	**OI**	**PI**
	1361.03	432.00	0.17	0.20	0.22	5.57	3.59	3.95	0.46
	1365.61	318.00	0.12	0.13	0.24	5.05	2.57	4.75	0.48
	1367.13	314.00	0.07	0.03	0.26	5.20	0.58	5.00	0.70
	1368.55	309.00	0.38	0.59	0.14	2.86	20.63	4.90	0.39
	137.18	314.00	0.28	0.41	0.17	4.00	10.25	4.25	0.41
	1379.32	322.00	0.11	0.19	0.14	3.73	5.09	3.75	0.37
	1383.89	327.00	0.08	0.07	0.23	4.84	1.45	4.75	0.53
	1386.94	306.00	0.25	0.06	0.43	6.05	0.99	7.11	0.81